Edited by
Maksym Maksymov,
Pavlo Gultsov

SIMULATION MODELING OF ARTILLERY SYSTEMS FOR IMPROVING GAME SIMULATORS. FROM THEORY TO PRACTICE

Collective monograph

Scientific Route®

Tallinn

Published in May 2026
by Scientific Route OÜ®
Parda tn 4, Kontor 526, Tallinn, Harju maakond Estonia, 10151
www.route.ee

Simulation modeling of artillery systems for improving game simulators. From theory to practice
Maksym Maksymov, Pavlo Gultsov (Editors)

This book contains information obtained from authentic and highly regarded sources. Reasonable efforts have been made to publish reliable data and information, but the author and publisher cannot assume responsibility for the validity of all materials or the consequences of their use. The authors and publishers have attempted to trace the copyright holders of all material reproduced in this publication and apologize to copyright holders if permission to publish in this form has not been obtained. If any copyright material has not been acknowledged please write and let us know so we may rectify in any future reprint.

The publisher, the authors and the editors are safe to assume that the advice and information in this book are believed to be true and accurate at the date of publication. Neither the publisher nor the authors or the editors give a warranty, express or implied, with respect to the material contained herein or for any errors or omissions that may have been made.

The Open Access version of this book, available at monograph.route.ee, has been made available under a Creative Commons Attribution 4.0 International License.

Cover photo: "Artillery system with digital simulation and data visualization background" © Canva.com. The cover was created using a Canva's Content License.

Trademark Notice: Product or corporate names may be trademarks or registered trademarks, and are used only for identification and explanation without intent to infringe.

DOI: 10.21303/978-9908-8450-1-2
ISBN 978-9908-845-01-2 (eBook)
ISBN 978-9908-845-02-9 (ePub)

This publication has been peer reviewed.

ISBN 978-9908-845-01-2 (eBook)
ISBN 978-9908-845-02-9 (ePub)
© The Author(s) of individual chapters, 2026

This is an open access book under the Creative Commons Attribution 4.0 International License (CC BY 4.0)

AUTHORS

Chapter 1

Maksym Maksymov
Doctor of Technical Sciences, Professor,
Head of Department
Department of Software and Computer-Integration Technology
Odesa Polytechnic National University
ORCID: https://orcid.org/0000-0002-7536-2570

Pavlo Gultsov
Doctor of Philosophy (PhD), Senior Researcher
Department of Software and Computer-Integration Technology
Odesa Polytechnic National University
ORCID: https://orcid.org/0000-0001-5083-380X

Oleksandr Toshev
PhD Student
Department of Software and Computer-Integration Technology
Odesa Polytechnic National University
ORCID: https://orcid.org/0009-0000-4093-2556

Ruslan Riaboshapka
PhD Student
Department of Software and Computer-Integration Technology
Odesa Polytechnic National University
ORCID: https://orcid.org/0009-0004-2068-0290

Chapter 2

Maksym Maksymov
Doctor of Technical Sciences, Professor,
Head of Department
Department of Software and Computer-Integration Technology
Odesa Polytechnic National University
ORCID: https://orcid.org/0000-0002-7536-2570

Pavlo Gultsov
Doctor of Philosophy (PhD), Senior Researcher
Department of Software and Computer-Integration Technology
Odesa Polytechnic National University
ORCID: https://orcid.org/0000-0001-5083-380X

Volodymyr Demydenko
Doctor of Philosophy (PhD), Senior Researcher
Scientific Research Center of the Armed Forces of Ukraine "State Oceanarium"
Naval Institute of the National University "Odesa Maritime Academy"
ORCID: http://orcid.org/0000-0003-4127-9645

Valentin Davydov
Candidate of Technical Sciences,
Associate Professor
Department of Software and Computer-Integration Technology
Odesa Politechnic National University
ORCID: https://orcid.org/0000-0003-3099-7596

Chapter 3

Oleksandr Brunetkin
Doctor of Technical Sciences, Professor
Department of Software and Computer-Integration Technology
Odesa Polytechnic National University
ORCID: http://orcid.org/0000-0002-6701-8737

Pavlo Gultsov
Doctor of Philosophy (PhD), Senior Researcher
Department of Software and Computer-Integration Technology
Odesa Polytechnic National University
ORCID: https://orcid.org/0000-0001-5083-380X

Oleksandr Sidelnykov
PhD Student
Department of Software and Computer-Integration Technology
Odesa Polytechnic National University
ORCID: https://orcid.org/0009-0003-0657-0215

Chapter 4

Oksana Maksymova
Candidate of Technical Sciences,
Associate Professor, Head of Department
Department of Fundamental Sciences
Naval Institute of the National University "Odesa Maritime Academy"
ORCID: http://orcid.org/0000-0003-3986-0991

Pavlo Gultsov
Doctor of Philosophy (PhD), Senior Researcher
Department of Software and Computer-Integration Technology
Odesa Polytechnic National University
ORCID: https://orcid.org/0000-0001-5083-380X

Volodymyr Demydenko
Doctor of Philosophy (PhD), Senior Researcher
Scientific Research Center of the Armed Forces of Ukraine "State Oceanarium"
Naval Institute of the National University "Odesa Maritime Academy"
ORCID: http://orcid.org/0000-0003-4127-9645

Yevhenii Dobrynin
Candidate of Technical Sciences, Head of Faculty
Faculty of Armaments
Naval Institute of the National University "Odesa Maritime Academy"
ORCID: https://orcid.org/0000-0003-2777-3137

Chapter 5

Oleksandr Brunetkin
Doctor of Technical Sciences, Professor
Department of Software and Computer-Integration Technology
Odessa Polytechnic National University
ORCID: http://orcid.org/0000-0002-6701-8737

Oksana Maksymova
Candidate of Technical Sciences,
Associate Professor, Head of Department
Department of Fundamental Sciences
Naval Institute of the National University "Odesa Maritime Academy"
ORCID: http://orcid.org/0000-0003-3986-0991

Yevhenii Dobrynin
Candidate of Technical Sciences, Head of Faculty
Faculty of Armaments
Naval Institute of the National University "Odesa Maritime Academy"
ORCID: https://orcid.org/0000-0003-2777-3137

Oleksandr Sidelnykov
PhD Student
Department of Software and Computer-Integration Technology
Odessa Polytechnic National University
ORCID: https://orcid.org/0009-0003-0657-0215

Chapter 6

Pavlo Gultsov
Doctor of Philosophy (PhD), Senior Researcher
Department of Software and Computer-Integration Technology
Odesa Polytechnic National University
ORCID: https://orcid.org/0000-0001-5083-380X

Oksana Maksymova
Candidate of Technical Sciences,
Associate Professor, Head of Department
Department of Fundamental Sciences
Naval Institute of the National University "Odesa Maritime Academy"
ORCID: http://orcid.org/0000-0003-3986-0991

Yevhenii Dobrynin
Candidate of Technical Sciences, Head of Faculty
Faculty of Armaments
Naval Institute of the National University "Odesa Maritime Academy"
ORCID: https://orcid.org/0000-0003-2777-3137

Chapter 7

Volodymyr Demydenko
Doctor of Philosophy (PhD), Senior Researcher
Scientific Research Center of the Armed Forces of Ukraine "State Oceanarium"
Naval Institute of the National University "Odesa Maritime Academy"
ORCID: https://orcid.org/0000-0003-4127-9645

Yevhenii Dobrynin
Candidate of Technical Sciences, Head of Faculty
Faculty of Armaments
Naval Institute of the National University "Odesa Maritime Academy"
ORCID: https://orcid.org/0000-0003-2777-3137

Oleksii Maksymov
Doctor of Philosophy (PhD), Associate Professor
Department of Radio Engineering Armament, Communications, and Robotics
Naval Institute of the National University "Odesa Maritime Academy"
ORCID: https://orcid.org/0000-0003-2504-0853

Ruslan Riaboshapka
PhD Student
Department of Software and Computer-Integration Technology
Odesa Polytechnic National University
ORCID: https://orcid.org/0009-0004-2068-0290

Chapter 8

Pavlo Gultsov
Doctor of Philosophy (PhD), Senior Researcher
Department of Software and Computer-Integration Technology
Odesa Polytechnic National University
ORCID: https://orcid.org/0000-0001-5083-380X

Viktor Boltenkov
Candidate of Technical Sciences,
Associate Professor
Department of Information Systems
Institute of Computer Systems
Odesa Polytechnic National University
ORCID: https://orcid.org/0000-0003-3366-974X

Yevhenii Dobrynin
Candidate of Technical Sciences, Head of Faculty
Faculty of Armaments
Naval Institute of the National University "Odesa Maritime Academy"
ORCID: https://orcid.org/0000-0003-2777-3137

Oleksii Maksymov
Doctor of Philosophy (PhD), Associate Professor
Department of Radio Engineering Armament, Communications, and Robotics
Naval Institute of the National University "Odesa Maritime Academy"
ORCID: https://orcid.org/0000-0003-2504-0853

Chapter 9

Volodymyr Demydenko
Doctor of Philosophy (PhD), Senior Researcher
Scientific Research Center of the Armed Forces of Ukraine "State Oceanarium"
Naval Institute of the National University "Odesa Maritime Academy"
ORCID: http://orcid.org/0000-0003-4127-9645

Yevhenii Dobrynin
Candidate of Technical Sciences, Head of Faculty
Faculty of Armaments
Naval Institute of the National University "Odesa Maritime Academy"
ORCID: https://orcid.org/0000-0003-2777-3137

Maksym Maksymov
Doctor of Philosophy (PhD), Senior Researcher
Scientific Research Center of the Armed Forces of Ukraine "State Oceanarium"
Naval Institute of the National University "Odesa Maritime Academy"
ORCID: http://orcid.org/0000-0002-5626-5265

Ruslan Riaboshapka
PhD Student
Department of Software and Computer-Integration Technology
Odesa Polytechnic National University
ORCID: https://orcid.org/0009-0004-2068-0290

ABSTRACT

At the present stage of development of computer simulation of military processes, the problem lies not only in obtaining a visually convincing picture of combat actions, but in reproducing their internal logic in such a way that the modelled process resembles a real one not externally only, but by its sequence, interrelations, dependencies, and consequences. This is especially true in relation to artillery systems. In many modern simulators and computer gaming products, one can observe sufficiently advanced visualization, dynamic effects, and a high degree of graphical realism, while the functioning of artillery means itself is often presented in a simplified form, where separate stages are shown, but not united into one logically complete cycle. Because of this, the issue arises of creating such generalized simulation approaches that would make it possible to reproduce the operation of artillery means not as a set of disconnected effects, but as a full process beginning with the choice of a target and continuing through preparation, aiming, firing, flight, influence of disturbances, target hit, and final action of ammunition.

This book is devoted exactly to such an approach. Its main idea is to consider artillery functioning in a simulation environment as a complete and internally connected cycle, where every stage has its own logic, its own modelling task, and at the same time forms part of the common system. For this reason, the book consistently addresses trajectory formation, sensor and perception issues, accuracy and randomness, the influence of stochastic disturbances, reaction to changing conditions, and the role of all these factors in forming realistic behaviour of artillery means in a simulator. The importance of such an approach lies in the fact that it allows moving away from purely illustrative reproduction of fire action and toward a more physically and logically grounded simulation, where the visible result becomes only the outer manifestation of deeper modelled processes.

A significant feature of the presented material is that the proposed models are generalized and do not include any actual secret tactical or technical characteristics. They were created not for the disclosure of real data, but for the formation of a methodological basis that can be used in educational systems, training environments, computer simulators, and computer gaming. This makes it possible to combine scientific correctness, practical applicability, and safety of use. At the same time, the book is connected not only with simulation itself, but also with automation, computer-integrated technologies, decision support, and operations research, because artillery action is treated here as a complex controlled process influenced by many interrelated factors, including uncertainty, timing, observation, reaction, and probability of result.

Thus, the book offers the reader not a fragmented set of separate models, but a holistic view of artillery simulation as a field where mathematical modelling, stochastic methods, ballistic logic, sensor representation, and decision-making principles are combined into one framework. Precisely because of this, the presented material may be useful both for developers of realistic military simulators and gaming products, and for engineers, researchers, cadets, officers, and all those who are interested in creating more realistic and scientifically grounded models of artillery processes.

Keywords

Artillery systems, simulation modelling, mathematical modelling, automation, computer-integrated technologies, systems analysis, decision support, decision theory, operations research, optimization, stochastic models, probability theory, random processes, ballistic modelling, sensor systems modelling, digital twins, computer simulators, computer gaming, training systems, physics-based modelling, combat process modelling.

CIRCLE OF READERS AND SCOPE OF APPLICATION

We believe that each specialist, whose activities are related to the following areas, can find something useful for him/herself in the book:

– modeling various processes, including battle ones;

– artificial intelligence;

– military training;

– development of new types of armament and equipment, primarily artillery complexes.

First of all, the book should interest the developers of realistic militarized computer games, since the problem of transition from an impressive visual image of the process to its scientific reproduction, especially in relation to artillery, remains very relevant. It is precisely the offered methodology that will allow them to take a step towards such an implementation, presenting to gamers a completely different type of product – a really credible game, where the trajectory, aiming, the influence of random disturbances, counteraction of the object, hitting, exploding a mine, etc., will obey the same logic. And this is exactly what allows the author to consider his/her product having a high level of detail, rather than simply a good-looking product.

At the same time, the book can be useful to developers of simulators of military purpose, because the models proposed in it allow the construction of such an environment that will be able to solve not only demonstration of the process, but also drawing up professional conclusions based on the typical situation, and performing this action several times with changed conditions. And this is exactly the peculiarity of its applied nature: this edition does not propose abstract considerations about realism, but a holistic approach to building a core that provides the required ratio of physicality, randomness and safety of use of the generalized models.

Finally, we would like to say that this book can be of great interest for developers of modern artillery weapons, especially those who deal with issues of control, diagnostics, monitoring of the state of artillery rounds at every stage of functioning – from preparing to firing, launching, flying, falling and finishing hit. For these readers, the value of the book is due to the fact that the author shows how it is possible to describe the complicated process of artillery in the form of interrelated models, which can subsequently be embedded into decision support systems, training complexes, digital twins, future loops of information and control. In other words, it gives not a description of the phenomenon, but a foundation for making the transition from engineering feeling to thinking in models.

And finally, let's formulate the circle of readership, which, first of all, should become interested in the book. It will definitely be of interest to the commanding personnel of artillery units, since it allows one to begin to see artillery not just as a weapon for fire, but as a complex managed system, the effectiveness of which depends on many factors: quality of preparation, quality of initial data, conditions for firing, reaction to perturbations, delays, probabilistic nature of results, etc. Such a view becomes particularly topical nowadays, when commanders should acquire the ability to make management decisions in the spirit of the culture of modeling, rather than relying on personal experience alone. That is why the book can be called an intellectual tool for improving awareness of the logic of artillery action in changing conditions.

Of course, the book will be of interest to cadets, assistants at special military institutions of higher education, as well as students, masters and postgraduates studying at universities majoring in modeling, automation, applied informatics, system analysis, development of new classes of information technologies for complex technical objects, as for them this edition is not only a theme of additional readings on artillery, but an example of how a real multifactored process can be transformed into a set of mathematical, logical and simulation models. It is precisely this feature that makes the book interesting from teaching and scientific point of view, teaching not only about the topic, but also in the culture of building complex interdisciplinary models.

In conclusion, we note that the value of the book is caused by the fact that it unites at once several levels of usefulness: scientific, methodological, engineering, educational, applied, allowing to look at the artillery process as an integrated one, amenable to formalization and digitization, research, learning, subsequent development. Therefore, this edition can turn out to be useful not only for acquaintance, but also for further work – as a source of ideas, a methodological base, a basis for developing new simulators, trainers, control laws, intelligent models of artillery action.

CONTENTS

LIST OF TABLES

LIST OF FIGURES

INTRODUCTION

Scientific and methodological foundations of integrated modelling of artillery operations in simulators and computer gaming

Computer modeling of combat operations became important at the present stage of development of the military-technical sphere, while the logic of reproducing the course of combat processes often loses to graphic realization. As some authors note, there is a significant imbalance between the hyperrealism of visualization quality and the simplification of the logic of the simulation scenarios themselves, in the sphere of military computer games. New weapons appear quickly in them, while the implementation of the current tactics and the full functionality of the combat process is implemented with great difficulty. There is currently a lack of ready-made modules sets that allow reproducing the full life cycle of the use of artillery means with a sufficient degree of realism in the process of computer modeling of combat actions. It causes a need for creating generalized models allowing filling such a niche and ensuring a real simulation of the use of artillery means during combat operations.

This book shows a full simulation cycle of artillery operations in the process of a computer modelling environment. For that purpose, we consider every stage of the process of using artillery means beginning from selecting a target to carrying out a shot and including a missile flight, accounting dynamic disturbances, the moment of hitting a target, an explosion, etc. All those stages are considered as separate sections and form a continuous circle of simulation. Such an approach allows showing the logic of using artillery means at each stage and linking the described stages into one simulation system.

The essence of the considered models' importance lies in the possibility of realizing a clear logic of the functioning of artillery means instead of just visually animating the effect of the release of missiles. Implementation of a full cycle of simulation containing all the components provides a possibility to realize the most physical picture of a battle of artillery means. That is, models take into account ballistic regularities of missiles motion, taking into consideration the unavoidable number of stochastic disturbances at each shot, for example, weather conditions, directionality errors, etc. Accounting of applying stochastic methods into modeling makes it possible to more precisely simulate the behavior of artillery units, considering the randomness of many values – starting from the speed of the released missile and reloading time up

© The Author(s) of individual chapters, 2026 DOI: 10.21303/978-9908-8450-1-2.introduction

to the probability of being detected by the enemy's reconnaissance assets. According to conducted studies, such models have an ability to significantly increase the realism and efficiency of artillery operations in the simulation process, making the simulation close to real conditions and the combat situation itself. That means, on the basis of the considered models, it is possible to implement not only the exterior of the fire effect but also possible decisions logic and shooting results in typical conditions of the battlefield.

It is possible to note that the developed models are generalized ones; they do not contain any actual secret technical and tactical characteristics. Those were created solely as an initial basis for logic that could be used in the process of computer modeling of combat operations. Thus, the given content may become a foundation for improving the simulation realism of using artillery means without revealing any real information. Such an approach allows combining the scientific value of modeling with confidentiality requirements, enabling the use of the obtained results both for educational goals and for creating software complexes of simulation training experiments.

In this book tasks of modeling, diagnostics and information support of processes of functioning of artillery systems in the cycle of preparation and realization of fire and registration of its effect are considered.

In the first part of the book, the analysis of the current state of the automated control of fires of artillery means on the tactical level is carried out; theoretical aspects of functioning of information control systems; approaches to algorithmization of tasks of the artillery units' management and world experience in creation and use of special purpose automatic control systems are considered. The generalization of functional structure of such systems is received in the result of the research, the place of verification of the firing state in the system of artillery fires' management is defined. Obtained results will be interesting to developers of modern information-control systems and tools of automation of combat application of artillery.

In the second part of the book, the task of localizing of the information about the firing state of artillery systems and its verification is considered. Processes of "propellant charge – firing chamber – barrel – projectile – flying path – ground surface hit" are analyzed, methods of definition of parameters of the processes considering analysis of the accompanying phenomena (acoustic, thermodynamic, video metric) during shot were offered. As a result, it is possible to receive a complex of methods allowing to partially verify the separate shooting stages and to use the obtained information for the estimation of the condition of artillery systems.

In the third part of the book, physicochemical processes occurring during shots, namely the process of formation of free carbon in the gas product of combustion of

powder charge was studied. The model of description of gases' temperature distribution in the channel of barrel is proposed, which allows to judge about the conditions of carrying out of thermochemical reaction and formation of muzzle flash. Carried out simulation shows the influence of the parameters of charge and conditions of shots on the character of the muzzle blowout, that can be used for the study of the processes of internal ballistics.

In the fourth part of the book, methods of determining of the condition of artillery systems in the conditions of dynamic perturbations are considered. The model of estimation of the condition of self-propelled artillery systems as multifactor dynamic objects is offered. Using the acoustic, optic, thermodynamic and mechanic parameters allow us to form the system of signs of the suitabilities and estimate the system combat abilities. Obtained results can be used for creation of the blocks of algorithmic decisions of support systems.

In the fifth part of the book, the methods of operational definition of composition and energetic properties of nitro-cellulose powders charges are considered. Library approach of solution of direct and inverse tasks of thermodynamic modeling of process of decomposition of charges is offered. The obtained results allow quickly judging about the conditions of substances taking part in the processes of internal ballistics according to the minimum number of experimental data, also correcting parameters of calculation of the processes of internal ballistics.

In the sixth part of the book, the improvement of the methods and models of management of combat application of artillery systems is devoted. The stochastic models of combat operation of artillery subdivisions on the basis of discrete Markov's processes are offered. Developed approaches allow estimating efficiency of shots and forecast changing of combat ability of artillery system and justify the rational structure of performing of fire tasks.

In the seventh part of the book, the development of the computerized diagnostics system of parameters of shots by analysis of features having various nature is devoted. The approach to synthesis of acoustic signals and video observations of muzzle blowout with the aim of forming of informative diagnostic parameter is offered. Conducted studies have shown the possibility of increase in reliability of determining of the barrel condition and other shooting parameters due to combination of heterogeneous channels of measuring.

In the eighth part of the book, the method of parabolic approximation for determining of the coordinates of the point of fall of an artillery shell is devoted. This method is based on registration of ballistic waves of shots by acoustic spatially distributed sensors and subsequent approximation of the flight path of a projectile by a system of parabolas. Carried out studies show the possibility of determining the

coordinates of the falling points of shells with sufficient accuracy on the basis of the results of one shot.

In the ninth part of the book, the problem of optimal choice of acoustic sensors for registering of ballistic waves of shots is considered. The approach of formation of optimal measurement subsystem on the base of multicriterial analysis with the use of fuzzy logic is offered. Obtained results allow increasing the reliability of acoustic measurements, and are the basis for further implementation of the methods of checking the artillery shoots. Thus, the obtained results presented in the monograph form a unified complex of models, methods and algorithms, aimed at studying the processes of shooting, evaluating the technical condition of artillery systems and improving the effectiveness of their combat application.

In general, the idea of this book is that it considers modeling of the functioning of artillery means as a whole cycle, starting from choosing a target up to exploding ammunition. It is shown how such a holistic approach can give a better understanding of combat simulation and make it more realistic. This volume demonstrates such an approach by considering the existing gap in the theory and practice of computer modeling of combat operations, contributing to more realistic and scientifically accurate simulations of the combat operations of artillery means. Now let's list solved tasks ensuring the simulation realism.

Trajectory of motion. To ensure realism, it is necessary to correctly simulate the physics of the movement of objects. A ballistic trajectory of movement of missiles is calculated according to the laws of mechanics – acceleration due to gravity, air resistance, initial speed, etc., so the shots behave exactly as in real-life. So, modern training systems, for example, imitate ammunition flight accounting the distance, flash, target movement, etc., depending on the type of ammunition. This helps soldiers learn how to correctly aim at a moving target to hit it effectively. In other words, the rocket in the simulator hits where it should hit in real life (given that the shooter takes into account all factors), and not flying directly along a straight line like a laser beam.

Sensors/perception. Another key factor is the modeling of the operation of various sensors/perception devices – tools for detecting and observing objects. In the simulator, it is necessary to requires manual correction in the source file a person's field of view, equipment's scanning radius, radars or cameras work, and much more. It defines if an opponent will react to the player's presence or if equipment can be rotated towards him/her. The task of simulating such sensors becomes quite complicated if you want to model something complex – say, a computer vision system. But without such considerations, realistic behavior cannot be obtained: the game needs to ensure that enemies notice the player only after he steps into their sensors range, and not "see" everything beyond walls or at fantastic distances.

Accuracy and randomness. In real life, nothing works 100% accurately, there are always some mistakes and randomness – the same happens in simulation. For example, artillery fire is scattered: fired missiles hit different points, even if the same conditions are met. In simulation, this can be modeled by introducing some randomness: random change in the missile's speed, slight deviation of the missile from the center of aiming, variability of loading time, or chance of spotting by enemy forces, etc. According to the studies, usage of such stochastic models makes it possible to more accurately reproduce the random nature of many factors – from the speed of missile flights to the probability of its detection by an enemy soldier. That is, the system behavior in the simulation becomes much closer to the real one: not every shot is 100% successful, battles are more unpredictable and similar to the real ones.

Reaction to disturbances. Combat unfolds in a chaotic environment. Another modeling task is teaching the system how to react to external factors – i.e., changes in the situation. After all, a believable simulation implies objects reacting to sudden impacts: does a self-propelled gun remain stable if its base begins to sink into the ground? Does a rocket change direction under a gust of wind? If you want to model a system of automatic correction of artillery batteries, for example, you will consider changes in the position of guns in combat and the impact of outside factors on the firing algorithm. You can also plan ahead for random events: anything from breakdowns and failures of equipment to changes in weather conditions and how characters/equipment reacts to these. Correct processing of such situations in the game leads to greater realism; e.g., decreasing shooting accuracy due to mist, slower movement of equipment in wet soil etc. The player gets the impression of a "living" unpredictable world, just like in reality.

The solution of the listed tasks influences the logic of the simulator. It is exactly the models of trajectories, sensors, accuracy and robustness against disturbances that define the rules of interaction in the virtual world. For example, if your algorithms take into consideration limitations of the field of view, then you get gameplay rules: it becomes possible to sneak past a watchtower without being noticed. If you correctly implement the modeling of ballistic curves, the player must take into account distance and wind when firing a sniper rifle or a mortar. The reactivity of systems to damage or changing weather conditions defines the level of unpredictability of the battle – whether vehicles get stuck in swamps, or tanks survive an explosion at close range. And so on. As a result, a whole set of models obtained by research turns into a certain number of game rules, and the laws of physics become the rules of the game. This allows to create a unified, coherent gameplay, where the events happening on the screen follow the same laws that apply to the real world.

From a toy to education: the didactic potential of simulations.

Of course, a computer simulator can serve not only as an entertaining game. Thanks to realistic models, it can be used as an educational tool. A realistically reproduced environment allows one to simulate various combat situations and rehearse them many times. And the possibility of repetition is incredibly important both in preparation and in practical training. Special systems of simulating different combat situations allow soldiers and officers to repeat the fight as often as necessary to learn good skills. Thus, a person learns something new in small portions with frequent repetition, gradually moving from simple things to complex ones. An illustrative example of this is the Synthetic Training Environment: here you can model almost any battlefield configuration and rehearse difficult stages several times before going into battle – up to 25 hypothetical battles before the first real one! Rehearsal helps to understand the complexity of combat actions: the commander and soldiers see the results of their decisions in different situations, learn to act properly and develop strategies. Moreover, there is no threat to life and health, and you can afford mistakes, repeating the exercise again.

In addition, a realistic simulator creates a safe space for training. By placing a soldier in a virtual battle that resembles a real one, the training system gives him/her the required amount of practice, very similar to the real thing. In serious educational games, players achieve a high level of immersion: they feel like heroes acting out events and experiencing stress akin to real-life stress. At the same time, a virtual environment allows for experimentation, making mistakes and learning from them without real negative consequences. For example, a squad commander in the game can experiment with a risky raid tactic: if it fails, nothing terrible happens – but the lesson about how better to conduct operations stays. So the simulator combines entertainment and training: interactive, interesting gameplay makes it easier to immerse yourself in the game, and the realism of the tasks and ability to draw conclusions improve knowledge of a profession and military affairs.

Realism because it's science.

At the same time, realism is due to the fact that the game simulator uses scientific models. Or, in other words, the backbone of a quality military game is built around the same laws as are used for the relevant calculations in science, or to train engineers. That is, modern game engines rely on the laws of mechanics: using mathematical models, they reproduce the true movement of objects in a virtual world. It means that during the game, equations of movement and interaction are somehow solved: Newton's mechanics determine acceleration and trajectories, the algorithms of collisions handle explosions and collisions, algorithms for working with rigid bodies help determine the behavior of a vehicle when rolling over or colliding with obstacles. Likewise, the modeling of sensor readings relies on real data about the parameters of

sensors: their sensitivity, operating radius, delay and signal noise. That is why a simulator seems to us realistic: its core consists not of invented rules, but of natural laws and proven algorithms.

And in fact, the approach described in this book resembles scientific activity: at first, the problem is formulated (for example, to build a trajectory or sensor model), then mathematical models are created, experiments are carried out (simulations are run), adjustments are made and only after that the obtained solution is integrated into the game. It resembles the creation of a digital copy of the real system: our simulator becomes a model that reproduces the behavior of a tank, plane or soldier as if we were researching a real object. Like in science, simulation allows to check hypotheses: what happens if you increase the weight of the armor piercing shell or reduce the reaction time of the pilot? The answer gives the model. Science and games are therefore related: the scientific approach gives the game mechanics depth and realism, and gaming becomes the embodiment of science.

Implementation of models: from the training system to the game. Everything said above can help the creators to create an effective simulator for training soldiers or for creating exciting video games. The key thing here is the principle: if you want a serious and convincing tool, then use models and do not forget about the "black boxes" and disturbances. Otherwise, there will be no realism, only a showy game.

What does the reader get?

So, after reading this book, a developer or scientist receives a number of significant benefits.

A general understanding of the gunpowder artillerist problems in modern conditions, a comprehensive idea of the essence of shooting as a process, and an idea of possible ways of modeling and optimization.

An arsenal of mathematical tools, methods, and algorithms for solving specific problems.

Knowledge of the principles of building simulation models on the basis of available data and assumptions; examples of using existing databases to build simulation tools.

Recommendations on the choice of methods depending on the tasks solved, the level of available data and knowledge, and the desired level of accuracy.

Information about software solutions used in modeling, and ready-made libraries.

Examples of implementation, analysis, and comparison of results with real ones and with known works.

Information about open problems and further prospects for work in this area.

We think that this list itself makes the book interesting and necessary for those who are faced with the task of solving specific problems associated with modeling processes in artillery.

CHAPTER 1

Current state of automated control systems for field artillery combat employment in condition diagnostics

Maksym Maksymov
Pavlo Gultsov
Oleksandr Toshev
Ruslan Riaboshapka

Abstract

This chapter provides a comprehensive overview of automated artillery command and control systems (ACS) for field artillery at the tactical level, emphasizing their role in condition diagnostics and adaptive fire management.

The theoretical foundations of information and control systems are analyzed, including mathematical modeling, algorithmization of military tasks, and integration of hardware-software components.

International experience in the design and implementation of field artillery ACS, including systems such as TACFIRE (Tactical Fire Direction System) (USA), ADLER (Artillery Data, Location and Evaluation/Reconnaissance system) (Germany), and BATES (Battlefield Artillery Target Engagement System) (United Kingdom), is examined.

Special attention is given to the structure, functionality, and performance metrics of ACS, highlighting the importance of real-time verification of the artillery firing cycle, Multiple Round Simultaneous Impact (MRSI), and "shoot and scoot" tactics.

The chapter also discusses the principles of modern information and communication infrastructure, operational efficiency, and resilience of ACS under complex combat conditions, providing a methodological basis for future development of high-performance automated artillery systems.

Keywords

Automated command and control systems, field artillery, fire control, tactical-level operations, information and communication infrastructure, multiple round simultaneous impact.

© The Author(s) of individual chapters, 2026 DOI: 10.21303/978-9908-8450-1-2.ch1

1.1 Introduction

Modern research in technical and engineering systems increasingly relies on the integration of heterogeneous measurement channels, advanced data analysis methods, and computational modeling approaches. Across various domains, such as energy systems, robotics, materials science, and process engineering, the combination of empirical measurements with analytical and numerical models has proven effective in describing nonlinear dynamic phenomena under conditions of uncertainty and incomplete information [1, 2]. Techniques such as parameter identification, inverse problem solving, approximation models, and library-based process simulations are widely applied to ensure accurate assessment of system states, real-time monitoring, and predictive control [3–5].

Recent studies emphasize the universality of these approaches: methods originally developed for modeling combustion, energy transformations, or reactive material processes have been successfully adapted to contexts ranging from industrial automation to sensor-driven diagnostics [6, 7]. The use of multiple measurement channels – acoustic, optical, thermodynamic, and mechanical – combined with signal processing and data fusion techniques enables the extraction of informative indicators characterizing complex processes [8]. This multidisciplinary framework supports decision-making under dynamic conditions, allowing systems to respond adaptively to disturbances and maintain operational performance [9]. Moreover, practical applications in distributed and modular control systems demonstrate the importance of hierarchical architectures, automated decision algorithms, and optimization of computational resources for both real-time operation and predictive maintenance [10]. The integration of such methods across heterogeneous domains highlights their applicability for monitoring, verification, and evaluation of complex technical processes.

Within this context, the present chapter focuses on tactical-level artillery ACS. The chapter examines methods for planning, support, and control of artillery fire under dynamic combat conditions, emphasizing the verification of system states, optimization of resource allocation, and adaptation to disturbances in real time. By drawing on principles demonstrated in diverse technical fields, the approaches presented aim to enhance both the accuracy and responsiveness of artillery fire control.

1.2 Fundamentals of information and control systems for solving artillery tasks

In the U.S. military doctrine, considerable attention is devoted to the concept of achieving information superiority over a potential adversary in the twenty-first

century [11]. The practical implementation of this concept involves creating conditions under which military formations at various levels gain an advantage in assessing the tactical situation and making decisions regarding the achievement of assigned objectives, the execution of fire missions, and the support of combat operations. This advantage is achieved through the rapid collection, processing, and transmission of intelligence and other operational-tactical information.

An important role in achieving such superiority is assigned to the extensive use of advanced methods and mathematical models of states and processes, technical means of information support, and artificial intelligence systems that ensure the adaptive evolution of successive generations of automated control systems at different levels [12]. Information superiority is achieved through the formation of an information space created by combining centralized and network-centric mechanisms for informing operational units, with a leading role assigned to service-oriented mechanisms for providing requested data. The network-centric and service-based principles of information access embedded in such systems transform each operational element of a military formation into an information-strike or information-fire complex [13], as well as into an information-based reconnaissance-strike element.

Thus, the U.S. Army is developing fundamentally new technologically advanced land forces through the design and deployment of weapons and military equipment that employ information and control technologies. This process, known as digitization, involves the use of digital components in the development of advanced weapons and military equipment associated with the acquisition, exchange, and optimal use of intelligence data across all domains of the battlespace operating within a unified information environment [14].

The current stage in the development of digital technologies in the military domain can therefore be considered a phase of automation of computer-integrated military technologies, whose objective is the creation and application of automatic and automated control systems of varying complexity within a unified information environment.

Research on computer-integrated technologies for conducting combat operations is based on the development of mathematical methods for analyzing combat activities and on defining criteria and rules for the effective control of troops and weapons. In this context, the primary task is the formation of methods and rules for optimizing managerial decisions made by the commander.

The methodological foundation of computer-integrated military technologies is formed by several interrelated theoretical directions.

The theory of information processing for military applications develops optimal methods and models for the acquisition, transmission, collection, storage, and

processing of information in order to ensure its reliability, noise immunity, and confidentiality under existing constraints.

The theory of algorithmization of military tasks and command-and-control processes is intended for the development of methods for forming relationships and interactions in the course of armed conflict, as well as for creating methods for the functioning of military organizational and technical decision-support systems.

The theory of military automated control systems aims to establish principles for the design and analysis of various types of automated systems for troop command and weapon control, as well as for their automation and optimization of operation. Due to the necessity of making decisions in combat conditions with incomplete or partially unreliable information, there emerged a need to develop special methods for generating decisions, which reliability under such conditions must be maximized [14]. Particular attention is therefore devoted to the problem of assessing the quality, timeliness, and completeness of the operational and tactical information used [15].

The information resources of computer-integrated systems are intended to ensure reliable assessment of the situation, the state of the battlefield, weapons, and personnel, as well as to reveal the operational intentions of opposing sides from the perspective of organizational and technical systems.

The application of mathematical models and methods in computer-integrated systems makes it possible to integrate developed functional and information models into automated control systems, thereby enabling command personnel to make decisions within the services of the information environment associated with military-technical, operational-tactical, and military-logistical components [16].

The successful application of mathematical methods and models is closely related to the development of technical means of automation, computational mathematics, and programming for automated weapon control. The tasks of weapon control include the development of fundamental principles of automation, the creation and implementation of specialized devices for the collection, transmission, processing, storage, and visualization of information, as well as the determination of the optimal distribution of functions among operators, automated control systems, and weapons (control objects). The practical achievements of automation and military computer-integrated technologies in the control of tactical-level artillery units have been manifested in the creation of automated fire control complexes [17].

Practical experience in implementing ACS and computer-integrated control systems for military purposes in the armed forces of countries outside NATO has revealed a range of technological, technical, and organizational-economic contradictions [18–20].

First, there are organizational inconsistencies associated with the absence of a unified technical policy for the informatization of the armed forces, as well as with

software and information incompatibility between existing systems and those currently under development. Second, economic inconsistencies arise in the form of duplicated developments and unjustified urgent procurements of imported equipment that require additional specialized studies. Third, technological inconsistencies are related to the limited capabilities of available computing equipment and the relatively low level of the accessible component base.

To understand these contradictions, it is advisable to consider how the informatization and automation of artillery units in non-NATO countries are expected to be implemented. It is necessary to develop a methodology for implementing this complex multi-stage process, which should encompass all levels – from individual samples of weapons and military equipment and personal computing devices to full-scale automated control systems. In the practice of developing large automated control systems, it is generally accepted that the transition to the next, higher level of automated control should occur through the integration of all means of the previous level into a unified system (the "bottom-up" strategy).

The concept of an information and communication infrastructure is proposed as the basis for this approach, although the term is widely used today without a precise definition [21]. The information and communication infrastructure of a military formation can be defined as the set of technical and software means, organizational units, and service facilities that perform all information, telecommunications, and supporting processes required to ensure the functioning of headquarters, services, and operational units.

Particular attention is given to the concept of information technologies, which reflects the contemporary tendency toward the convergence of the notions of automation and informatization in the context of tactical-level artillery. This tendency is explained by the large volume of information that must be collected and processed in order to effectively accomplish the tasks of informatizing the control of artillery combat operations at the tactical level. Using general definitions [22], an information and control technology for special purposes may be defined as a technology organized as a structured set of computing hardware, communication facilities, software tools, and the databases employed. The specific characteristics of such technologies include the need for data and software protection, strict time constraints, and operation by users under conditions of high workload.

At each level of informatization and automation of tactical-level artillery, interaction occurs during the execution of relevant combat tasks under the following conditions:

– reconnaissance activities aimed at collecting information about the enemy, involving the acquisition and synthesis of intelligence data on the state of opposing forces in order to support decisions on their fire engagement;

– decision-making processes that reduce uncertainty and influence the conduct of combat operations;

– control and assessment of the results of fire engagements.

The concept of an information and communication infrastructure for a military formation, intended to support the informatization and automation of tactical-level artillery, is based on the results of research and development in the following areas [14]:

– acquisition of information about friendly forces, atmospheric conditions, and topogeodetic parameters;

– selection of information processing means for each level of command and decision-making;

– selection of high-speed and secure information transmission means;

– organization of reliable information storage and retrieval in relevant databases;

– development of methods for extracting information from reconnaissance results, including the timely detection of the enemy, determination of the coordinates of detected enemy objects, procedures for additional reconnaissance of targets, and control of the results of their engagement;

– development of decision-support methods for optimal planning of the employment of guided artillery projectiles;

– development of automated control systems for various tactical-level artillery units;

– development of methods and means for integration with higher- and lower-level information and control systems.

The concept of an information and communication infrastructure of a military formation, or information environment, has made it possible to reconsider the previously used notions of automation and integrated automation. These concepts may therefore be formulated as follows.

Automation is the process of applying a set of technical, software, and other tools and methods in order to fully or partially relieve the operator from direct participation in the processes of acquisition, transmission, storage, processing, and use of materials, resources, and information in the execution of control tasks. These tools include devices, installations, complexes, and systems [12].

Integrated automation is the process of creating and widely implementing practical automation tools combined into integrated control systems. At the stage of combat operations within organizational and technical systems, integrated automation is understood as the broad and comprehensive introduction of informatization methods and tools into the process of solving command-and-control tasks.

The experience of local wars and armed conflicts has shown that the requirements for achieving information superiority in modern armed forces cannot be fulfilled

without the implementation of advanced information and control technologies. Therefore, attention must be directed toward solving a dual task: the development of intelligent automated control systems for troops and weapons, and the training of specialists capable of effectively operating such systems. The operation of these systems requires personnel who are well versed in operational art, tactics, and the combat employment of different branches of the armed forces, who possess skills in mathematical modeling, and who are familiar with the fundamentals of automatic control theory, systems theory, systems analysis, operations research, and decision-making theory. In addition, such specialists must have deep knowledge in the field of information technologies and be able to apply these competencies in combat operations.

From the presented material on the fundamentals of information and communication infrastructure and information and control infrastructure, it follows that automated control systems designed for solving artillery tasks are based on the concept of an operation, understood as an interrelated and ordered set of methods implemented over time and distributed in space, combined within a unified technological (combat) algorithm. The sequence of actions depends on the available resources and is aimed at engaging detected targets according to their operational significance. Any automated control system, including those for troop and weapon control, implies that the achievement of the operation's objective is ensured through a set of technical means consisting of control objects, control systems, and operating personnel (operators and service specialists) integrated into a unified organizational and technical system. Hereafter, the organization of an operation will be understood as the selection, from the considered set, of such values of parameters and elements of the organizational and technical system that determine the resulting outcome. An organizational and technical system will be defined as a hierarchical human-machine complex that purposefully functions to realize its inherent capabilities in accordance with its intended purpose.

1.3 Special-purpose automated control systems for tactical-level artillery

The main objectives of research on ACS are the analysis and synthesis of automation tools at all hierarchical levels associated with the planning, support, and control of artillery fire. The relevance of addressing these tasks is due to the fact that artillery combat operations are characterized by exceptionally complex conditions under which the control of fire engagement between opposing forces is carried out [23]. A fire control system represents an organized set of functionally interconnected command posts, communication systems, automation facilities, and specialized

systems that ensure the collection, processing, storage, and transmission of information. In a number of existing fire control systems, significant shortcomings have been identified, including excessive centralization of control and low efficiency in generating well-grounded recommendations for operational decisions concerning the execution of fire missions within automated fire control complexes.

It should be noted that automated fire control complexes used in countries outside NATO do not comply with NATO standards. The fire potential of such units is supported by automated fire control complexes at only about 60% of their capabilities, and this level can be achieved only under the condition of reliable functioning of reconnaissance assets, electronic warfare systems, and comprehensive support of combat operations [18].

With the advancement of automation tools for controlling fire engagement, it becomes necessary to expand the capabilities of specialized mathematical and software support of automated fire control complexes, both in solving planning and support tasks and in controlling fire engagement during combat operations. A benchmark in this regard may be the level of automation achieved in the AFATDS system (Advanced Field Artillery Tactical Data System) (USA), which reaches approximately 90–95%. At present, the following directions for further development and improvement of automated control systems can be identified:

– the use of computer technologies at all levels of command to ensure that the majority of tasks are solved in real time;

– the installation on self-propelled artillery systems of individual automated systems for topogeodetic positioning, orientation, restoration of horizontal aiming, and automation of firing processes;

– the expansion of artillery reconnaissance capabilities through the use of unmanned aerial vehicles for fire correction and millimeter-wave radar systems;

– ensuring interaction with real-time reconnaissance assets through communication channels based on different physical principles of signal transmission.

The issue of optimally designing control complexes to ensure their maximum operational effectiveness remains highly relevant and requires continued research at an advanced level in this field. One of the primary objectives in constructing such complexes is to ensure the necessary message exchange speed and the required reliability of data transmission under conditions of enemy interference. Modeling the execution of fire missions imposes a set of requirements on the organizational and technical reconnaissance assets and fire control automated systems, including:

– the ability to perform fire missions across the full range of artillery systems;

– automated fire adjustment from the divisional fire control post based on data received not only from technical reconnaissance assets but also from other sources;

– automated transmission of processed data from reconnaissance systems to end-users via the fire control system;

– automated recording by the ACS of fire results, including the identification of projectile bursts from artillery systems against targets;

– ensuring, during simultaneous firing by multiple artillery systems, that the ratio of registered projectile bursts corresponds to the number of guns.

These requirements can be simultaneously implemented through the following computer-integrated technology chain: reconnaissance assets – fire control ACS – automated artillery system. The foundation of such a system must be specialized mathematical and software support covering all potential data preparation methods and fire control features. This set of operations necessitates the development of new information and control technologies to support the activities of tactical-level artillery units.

By definition, automated control systems comprise personnel and a set of tools to automate their activities, implementing an information and control technology to fulfill the assigned functions [14, 15]. The Fourth Industrial Revolution has expanded the scope of automation across various aspects of human activity, altering the composition, properties, and component base of software-technical automation complexes, as well as the methods for their application in solving practical tasks. ACS developed and implemented in the era of the Fourth Industrial Revolution are hierarchical, geographically distributed computer systems that integrate software-technical complexes, telecommunications equipment, information resources, and a large number of interacting users, all working together to ensure controllability of technological installations and objects.

At the onset of the Fourth Industrial Revolution, special-purpose ACS – systems that provide various types of security affecting the vital functions of the state – have assumed particular importance. Foremost among these are military-purpose systems [14]. This category also includes critical-state management systems, environmentally hazardous facility control systems, emergency response management systems for large-scale disasters, and similar applications. In general, special-purpose systems are employed to manage diverse resources and control equipment, typically under non-standard and critical conditions, where both external and internal disturbances may significantly impact operations.

The specificity of special-purpose ACS lies in the fact that, continuously or at specified intervals, different information and control systems can be generated based on single- or multi-level systems to address diverse tasks aimed at ensuring security.

Typically, special-purpose ACS feature dedicated information and control channels that form loops composed of software-technical resources, automating the

relevant processes and tasks based on models and methods for solving control problems. The information-processing channel is responsible for collecting and initially processing all data necessary for decision-making, including syntactic analysis, aggregation, and computation of performance indicators. The analytical channel, using the obtained data, performs semantic analysis of the current situation, defines control objectives, and generates potential courses of action to achieve them. The control channel coordinates and implements the selected decisions, including the operational management of resources and equipment. In some special-purpose ACS, additional information-analytical channels may also be established.

The primary goal of any special-purpose ACS is the effective control of objects, achievable through the availability of appropriate methods and models for making optimal decisions regarding the management of these objects. These methods and models are developed and adopted to ensure the foundational principles of the ACS, which should also be economically feasible [13].

Maximum objectivity in control is attained through the highest possible formalization of the functions (tasks) performed by personnel, as well as through the completeness and consistency of the information used in decision-making.

Maximum reliability is determined by requirements for reliability indicators, including readiness coefficients for task execution, ensured through "cold" and "hot" redundancy of system elements and equipment, along with systems for the preservation and restoration of information and control resources. It is essential that, when interacting with integrated systems, the ACS readiness coefficients exceed those of the control objects at each task execution cycle.

Real-time interaction between the ACS and the controlled objects, necessary for making and implementing effective decisions, is achieved through the selection of high-performance computing systems, high-speed communication networks, and the organization of information processes using rapid-response software tools.

Maximum survivability of the ACS – defined as the ability to perform assigned functions even when some system elements are deliberately disabled – is ensured by redundancy in resources, allowing operational execution of parts of the information-control technology on functioning system components despite some degradation in accuracy and information consistency.

Maximum operational resilience of the ACS refers to its ability to reliably and coherently transmit data volumes across the information-processing, analytical, and control channels under conditions of external and internal disturbances.

The highest level of information security in the ACS is ensured through a balanced protection of data confidentiality, integrity, and availability, taking into account operational needs and without compromising organizational objectives.

In addition to these principles, the design and operation of special-purpose ACS must adhere to generally accepted principles for the development of complex information systems: openness, modularity, functional independence from hardware-software platforms, and optimization of system development and operational costs.

Analysis of existing foreign ACS for tactical-level artillery demonstrates their compliance with the previously described structure and design principles of special-purpose ACS. Automated systems have been developed and are in the process of implementation to support artillery fire and control operations, addressing tasks such as artillery fire planning, target reconnaissance and analysis, preparation of firing data, and the collection and assessment of information regarding the status, condition, and staffing of one's own units. Notable examples of such systems include the TACFIRE ACS (USA), ADLER (Germany), and BATES (United Kingdom). These systems are based on mobile computing complexes deployed at the command posts of formations and units, as well as in artillery reconnaissance units equipped with specialized hardware. Direct control of weapon systems is carried out by dedicated ACS, such as BCS (Battery Computer System) (USA), IFAB (Integrated Fire Control Artillery Battery system) (Germany), and FACE (Field Artillery Control Equipment) (United Kingdom).

Field artillery ACS, including TACFIRE, ADLER, and BATES, have been adopted and deployed within NATO formations stationed in Europe. The further development of field artillery ACS is closely linked to their integration with artillery reconnaissance systems, as conducted under programs such as AFATDS (USA) and AFFS (Advanced Field Fire Support system) (Germany). Currently, field artillery ACS have achieved widespread adoption within NATO [20]. Their capabilities have been extended to include tasks related to logistics management and equipment maintenance. To evaluate the effectiveness of input-output devices, communications, and computing capabilities of these ACS, a system response time criterion has been introduced. This criterion measures the elapsed time from the entry of target information into the forward observer station or higher-level ACS until the display of the corresponding firing units on gun displays. A classification of field artillery ACS has been established, reflecting both their hierarchical structure and the scope of artillery unit management tasks they address.

The BCS computing system, in service with U.S. field artillery, is designed to control the fire of a battery of 12 guns, and it can operate independently or in conjunction with ACS at all levels. The COMBAT ACS forms the core of the battery-to-battalion level ACS for Israeli field artillery. Its configuration and capabilities are similar to the BCS system, but it manages the fire of 8 guns. Comparable characteristics are found in ACS such as IFAB, ARES (Artillery Reconnaissance and Engagement System), ABACUS (Artillery Battlefield Automated Control and Utility System) (Germany),

ATIBA (Automated Tactical Information for Battlefield Artillery) (France), and SEDAB (Système d'Échange de Données d'Artillerie de Bataille) (Italy).

Battery-to-battalion level ACS enable not only fire control but also the planning of material and logistical support, including ammunition resupply. A representative system of this class is the QUICKFIRE (QuickFire automated artillery fire control system) ACS (United Kingdom), designed to manage the fire of a 24-gun divisional artillery unit as well as other fire assets, including Multiple Launch Rocket System (MLRS). A distinctive feature of this system is its use of a set of predefined commands for automated problem-solving – capabilities that even some higher-level ACS, such as TACFIRE, do not provide. The system simultaneously performs dual computational tasks. Enhanced firing data accuracy is achieved through computational methods that account for four degrees of freedom of the projectile. Corps-level ACS elements support the planning and management of other support assets, including aviation and naval artillery, assess the effects of chemical and nuclear weapons, and handle all aspects of logistical planning.

The TACFIRE ACS, employed in the field artillery of heavy infantry divisions, exemplifies such systems. Its primary structural element is the divisional fire control center, a mobile computing complex incorporating the AN/GYK-12 computer, data input-output equipment, and display devices. The divisional fire control center manages the planning and execution of fire for 100 artillery units, coordinates additional aviation support, stores data on approximately 1,500 targets, and processes up to 60 fire missions per hour based on detected targets.

Within the TACFIRE system, tasks such as target analysis, selection of appropriate equipment for engagement, and computation of firing solutions are carried out. The results are transmitted to the battalion-level ACS fire complexes and supporting attack helicopters. Similarly, the French ATILA (Automated Tactical Information and Logistics Artillery system) ACS, at the unit level, stores in its Iris-35M computer memory the coordinates of up to 36 forward air controllers, 500 targets, 40 no-fire zones, 20 reference points, and data from four artillery support plans.

The LTACFIRE (Light Tactical Fire Direction System) ACS is employed in the field artillery of the U.S. light infantry divisions. At the battery level, the BCS system is utilized, with the divisional fire control center forming its core. The same configuration is applied at higher ACS echelons, as well as in fire support sections within units and formations. The equipment of the LTACFIRE ACS is ten times lighter than that of the TACFIRE ACS. Specifically, it allows for the control of mortar units and gunfire directly from fire control centers without the involvement of BCS systems. Experience with various field artillery ACSs has informed the development of the next generation of systems.

The next-generation systems are designed to include computing units on the guns capable of performing all necessary calculations, including the use of mobile transmission protocols within a secure messaging framework. Increasing the autonomy of fire control assets reduces ACS response times and enhances system survivability. In addition, this allows equipping all system levels with uniform and simpler hardware. Systems of this new generation include the field artillery ACS AFATDS (USA), BATES (UK), ATLAS (France), and ADLER (Germany).

The principles underlying the U.S. Army's prospective ACSs, which also inform the development of baseline ACSs in NATO countries, include: maintaining subordination of different control subsystem levels, ensuring organizational-technical and functional connections between critical system components, employing widely available commercial components, and software standardization. Examples of such special-purpose ACSs are the tactical-level Army Tactical Command and Control System (ATCCS) and the Staff Planning and Decision Support System (SPADSS).

From the presented material, it follows that only next-generation ACSs can significantly increase operational management efficiency, enabling effective conduct of combat operations in modern conditions. In the ATCCS comprehensive system, the primary component is the troop maneuver ACS, with the battery level serving as the initial point for acquiring automated information. German experts' perspective on ACS development differs from that of the U.S. Army. In Germany, the commissioned systems HEROS (Higher Echelon Reconnaissance and Operational System) and ACCS (Artillery Command and Control System) are intended primarily for use at the headquarters level of formations and higher commands. This leads to the main development focus for advanced ACSs: decentralization of combat management. It presupposes that unit commanders, without awaiting orders from higher authorities, should receive information directly from primary sources operating within their area of responsibility – data concerning the enemy, terrain, weather, composition and tactics of friendly forces, and control assets.

It is noted that combat management based on personal observation and issued orders is outdated. To fundamentally improve automation of unit command, the German Army is developing the Integrated Field Information System (IFIS), intended for mechanized infantry, armor, and anti-tank forces. This system allows precise determination of a combat vehicle's location (BMP, tank, ATGM system), movement direction, observation and firing sector, using laser gyroscope-based navigation equipment. The tactical situation, terrain, target coordinates, and textual and graphical messages are displayed on the system interface.

Analysis of open sources identifies two ACS types. The first type, for missile and artillery forces, provides automated collection and processing of information

required to optimize command and control, ensuring the most effective employment of units, subunits, and formations of missile and artillery troops. The second type, for artillery fire, is an automated system integrating sensor complexes and technical means to detect, identify, and recognize targets, prepare artillery pieces for firing, aim, and accomplish target engagement. Some artillery ACSs support MRSI, enabling a target to be struck by multiple projectiles (three to five) so that all reach it simultaneously. This effect is achieved through automatic adjustment of elevation with pre-selected propellant charges, an evolution of the Time on Target firing method.

1.4 Special-purpose command and control systems for tactical-level artillery

At present, reconnaissance assets for topogeodetic, meteorological, and ballistic support employed by tactical-level artillery units and subunits are supplied by various manufacturers. These systems meet modern requirements and provide the necessary conditions for operational use. When determining the architecture of a prospective automated artillery fire control system at the tactical level, primary attention should be focused on communication capabilities that ensure the automation of interaction processes among the forces and assets employed according to the concept of operations defined by the higher commander.

Currently, a wide range of technical equipment with embedded and universal software is available. By applying computer-integrated technology approaches, these components can be combined to create automated artillery fire control systems. The diversity of such components, the need to account for their characteristics, and the significant number and inconsistency of requirements imposed on the systems being developed necessitate the use of specialized mathematical models and methods. In some cases, it becomes necessary to develop new models that enable the determination of optimal characteristics for synthesizing automated control systems from available components.

A distinctive feature of the conducted analysis is the search for system characteristics that allow comparison of different system solutions to the problems under consideration. It should be noted that each system generally has its own connection architecture, which includes several components connected in parallel and in series and therefore possesses specific indicators that characterize its operational properties. At the initial stage, however, it is not advisable to analyze such indicators in detail. In addition, each decision regarding the application of particular equipment is associated with specific features of mathematical, software, information,

organizational, and methodological support required for integrating the field artillery automated control system into higher-level command and control systems.

For the analyzed field artillery automated control systems with different degrees of automation, it is necessary to consider the specific features of their operational use. A common characteristic is that each technical solution includes a base computer and a portable computer located near the gun crew. However, the capabilities of these systems and the tasks assigned to them may differ.

Data were collected on various information and control systems representing the time intervals required to perform a number of typical tasks of artillery units at the battery and battalion levels using different configurations of field artillery automated control systems. **Table 1.1** presents the average time required to perform artillery fire control tasks depending on the level of automation of fire control. The data were sorted and presented for the execution of the same group of tasks under four conditions: a non-automated mode, a mode using an automated forward observer, a fully automated mode, and an automated mode with diagnostic and service capabilities.

Table 1.1 Average time required to perform artillery fire control tasks

No.	Name of the task algorithm	Average time required to perform artillery fire control tasks (s), depending on the level of fire control automation			
		I	II	III	IV
1	Complete preparation for determining firing data	80	25	15	10
2	Target adjustment using a rangefinder and coordinated observation in mountainous terrain with the use of plain-mountain firing tables	115	50	16	11
3	Determination of firing data for a guided artillery projectile	160	75	40	20
4	Determination of firing data and illumination of the area to ensure the required operating range of night vision devices and night sights	220	110	50	25
5	Determination of data for establishing light reference points and alignment lines	260	140	60	30
6	Determination of coordinates by the resection method using measured distances, elevations, and direction angles of reference directions in mountainous terrain	270	150	75	40
7	Determination of coordinates by the resection method using measured angles with a non-oriented instrument, elevations, and direction angles of reference directions in mountainous terrain	280	160	100	50

Note: I – non-automated mode; II – automated mode with the use of an observer (spotter); III – automated mode; IV – automated mode with diagnostics and service support

The tasks were considered only in terms of information and analytical support capabilities, without the possibility of direct control of gun-laying mechanisms.

Analysis of the results of **Table 1.1** shows that calculation errors for firing setups, as well as the determination of corrections during ranging and fire-for-effect, are approximately equal and minor in all modes, except for the non-automated one. The fully automated mode with service support reduces the execution time of individual fire task elements by nearly an order of magnitude.

The conclusions drawn from **Table 1.1** confirmed the validity of the adopted analysis method for applied tasks of an artillery unit at the "battery – battalion" level. For further analysis, it was necessary to obtain data that would reflect the operation of the previously analyzed automation methods of fire control through various information and control systems, integrated with the controlled objects (artillery systems), taking into account the effects on actuator drives. **Table 1.2** [14, 15] presents the average execution time of fire tasks during field firing exercises with artillery units.

Table 1.2 Average execution time of fire tasks

No.	Name of the type of task performed in fire control	Average time required to perform artillery fire control tasks (s), depending on the level of fire control automation			
		I	II	III	IV
1	Reconnaissance and target coordinate determination	750	400	200	150
2	Topogeodetic preparation	1100	500	300	250
3	Meteorological preparation	1200	500	300	250
4	Ballistic preparation	1250	500	300	250
5	Full and abbreviated preparation	1260	500	300	250
6	Fire transfer by visual aiming	1270	500	300	250
7	Target ranging	1400	600	400	380
8	Engagement of targets at night	1480	700	500	400
9	Engagement of targets in mountainous terrain	1500	750	550	450
10	Tasks of the artillery fire observer	1510	800	600	500
11	Engagement of targets with a guided artillery projectile	1520	800	600	500
12	Engagement of targets with a multiple launch rocket system (MLRS)	1750	950	750	700
13	Fire adjustment from a reference point (target) using data from the ranging gun	1760	950	750	700
14	Preparation of barrage and accompanying fires, engagement of moving targets	3200	1600	1200	1100

Note: I – non-automated mode; II – automated mode with the use of an observer (spotter); III – automated mode; IV – automated mode with diagnostics and service support

Processing the data obtained during the artillery exercises showed that the variant of the automated control system with diagnostics and service-analytical calculations reduces the task execution time by almost three times compared to the preparation and fire task execution time in the non-automated mode.

The reduction in execution time compared to the automated mode with a spotter is one and a half times, and compared to the automated mode without diagnostics – only by 20%. It should be noted that in all modes where an automated spotter was integrated, the accuracy of coordinate determination increased. All integrated equipment of the information and control complex in the field artillery ACS for any automated mode ensures the same accuracy in determining the directional angles of reference bearings.

The methods for calculating firing data, embedded in the applied software, allow increasing accuracy by a factor of three.

The accuracy of calculated data at the current level can be improved through the development of additional methods for determining the elevations of artillery formations. The precision of determining the computed deflection from the primary firing direction is approximately the same for all artillery positions.

Regardless of the technical components used, all automated fire adjusters provide roughly the same accuracy in determining corrections during ranging and engagement, where the defining characteristics are atmospheric conditions and the actual initial velocity of the projectile at the moment it exits the gun barrel.

A detailed analysis of **Table 1.2** shows that some fire control tasks are limited by physical time parameters. These include the time for a projectile to travel from the gun barrel to the target and the time required to determine the coordinates of its impact point on the surface. Consequently, the reduction of the total execution time for such tasks is inherently limited. This conclusion is based not on the analysis of absolute time, but on the accumulated duration of completing the fire mission.

One approach to reducing the time required for fire missions is the integration of two types of mathematical models into the fire control system. The first type is a distributed-parameter model of atmospheric conditions and projectile trajectory, which determines all corrections associated with the influence of atmospheric conditions on projectile motion. The second type is a model based on the current state of the gun system and the characteristics of the charge, which determines the initial velocity of the projectile at the moment it leaves the barrel. Thus, two independent directions for modernizing field artillery fire control systems can be distinguished.

The first direction involves integrating additional mathematical models into the field artillery system to reduce the time needed to determine the coordinates of the projectile impact point. At a new level, this allows the calculation of firing data,

significantly shortening preparation and execution times for fire missions. Furthermore, this enables the implementation of different firing modes. The first is MRSI, which allows a target to be struck by several projectiles fired sequentially from a single weapon, all reaching the target simultaneously. The second is "shoot and scoot," a tactic associated with the rapid firing and repositioning of artillery units. The "shoot and scoot" approach is linked to the intensive development of precise automated diagnostic and technical reconnaissance tools in the artillery forces of high-tech militaries. These two modern approaches justify the need to analyze mathematical models of internal and external ballistics to determine the projectile velocity at barrel exit for diagnostic purposes.

The second direction for modernizing field artillery fire control systems results from the rapid pace of combat operations between opposing forces, characterized by a significant increase in the intensity and distributed nature of troop employment, as observed in the modern Russo-Ukrainian war. The use of numerous and diverse fire assets, in terms of equipment and ammunition provisioning, has overcome first- and second-degree information barriers according to Glushko's classification. The only feasible way to maintain control over such a process is the extensive implementation of automation across all stages of artillery unit operations (**Fig. 1.1**).

For this purpose, it is necessary to continuously verify the execution quality of each firing element by every link in order to track possible disturbances in real time and to instantly adjust control.

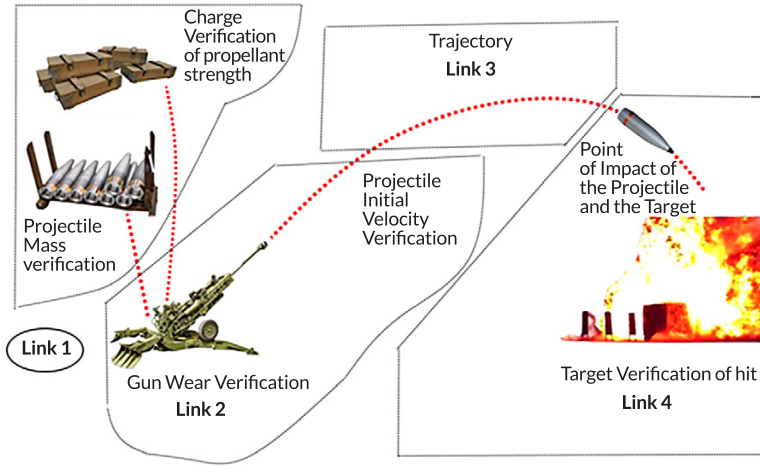

Fig. 1.1 Chain of states of the artillery round life cycle

During the execution of an artillery shot, disturbances are always present. To compensate for them, methods for verifying each link in the artillery firing process are required. Verification is understood as the confirmation of the performance of declared characteristics that directly affect overall effectiveness immediately after each link completes its assigned function for the shot.

An artillery shot consists of sequential links that form the chain of states of the life cycle, which can be represented by the following sequence: "charge – breech – barrel – projectile trajectory – target". To implement such an ACS, it is necessary to synthesize an object-oriented integrated model of the automated system for diagnostics and control of artillery units, which realizes the principles of adaptability, responsiveness, and efficiency through formalized methods of signal analysis and resource management (**Fig. 1.2**).

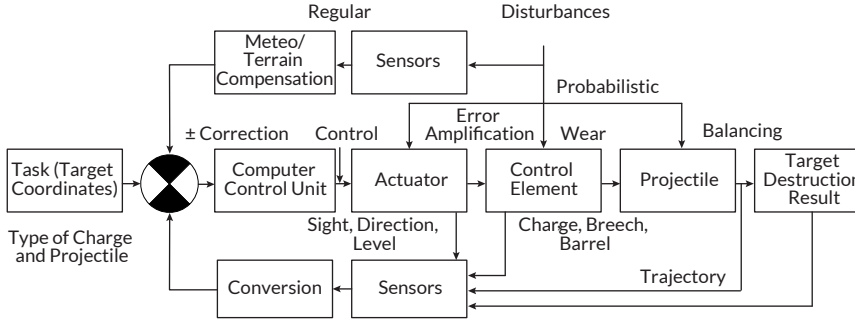

Fig. 1.2 Structural model of the information-analytical system for verification and adaptive artillery fire control

Such an ACS will make it possible to perform verification of the life cycle of each artillery round. This will allow continuous verification of each link in the chain of states to be considered a key condition for effective fire control of an artillery unit within a computer-integrated management system.

1.5 Conclusions

The analysis of ACS for tactical-level artillery allows the following conclusions to be drawn. The main tasks of ACS include planning, support, and control of artillery fire under complex and dynamic combat conditions, ensuring information superiority and timely decision-making. The life cycle of an artillery shot has been identified as

a sequence of linked states: "charge – breech – barrel – projectile trajectory – target". Each state requires continuous verification to maintain operational effectiveness. Methods for verifying the performance of each link in the firing process have been proposed, allows for adaptability and responsiveness of the ACS to disturbances in real time. The integration of object-oriented models of ACS enables optimization of resource management, signal analysis, and automated decision-making, reducing execution times for fire missions while maintaining accuracy. Practical experience with field artillery ACS, including TACFIRE, ADLER, and BATES, demonstrates the importance of hierarchical, distributed, and modular systems for efficient control of artillery units and fire support assets. The implementation of next-generation ACSs enhances fire control efficiency, enables advanced firing modes such as Multiple Rounds Simultaneous Impact and "shoot and scoot", and provides real-time interaction with reconnaissance and sensor systems.

Conflict of interest

The authors declare that they have no conflict of interest in relation to this research, whether financial, personal, authorship or otherwise, that could affect the research and its results presented in this paper.

Use of artificial intelligence statement

Artificial intelligence technology was used in the preparation of this chapter. Specifically, the authors used OpenAI ChatGPT (model GPT-5.2) to assist in editing and structuring introductory text sections and in formulating generalized descriptions of research methodologies for integrating mandatory literature sources into the chapter introduction.

The authors bear full responsibility for the final manuscript. Generative AI tools are not credited and are not responsible for the final results.

Authors' contributions

Maksym Maksymov: Conceptualization, Methodology, Formal analysis, Writing – original draft.

Pavlo Gultsov: Methodology, Investigation, System analysis, Writing – review & editing.

Oleksandr Toshev: Formal analysis, Visualization, Data curation, Interpretation of results, Writing – review & editing.

Ruslan Riaboshapka: Supervision, Validation, Theoretical framework, Writing – review & editing.

References

1. Boltenkov, V., Brunetkin, O., Dobrynin, Y., Maksymova, O., Kuzmenko, V., Gultsov, P. et al. (2021). Devising a method for improving the efficiency of artillery shooting based on the Markov model. Eastern-European Journal of Enterprise Technologies, 6 (3 (114)), 6–17. https://doi.org/10.15587/1729-4061.2021.245854
2. Dobrynin, Y., Volkov, V., Maksymov, M., Boltenkov, V. (2020). Development of physical models for the formation of acoustic waves at artillery shots and study of the possibility of separate registration of waves of various types. Eastern-European Journal of Enterprise Technologies, 4 (5 (106)), 6–15. https://doi.org/10.15587/1729-4061.2020.209847
3. Dobrynin, Y., Brunetkin, O., Maksymov, M., Maksymov, O. (2020). Constructing a method for solving the riccati equations to describe objects parameters in an analytical form. Eastern-European Journal of Enterprise Technologies, 3 (4 (105)), 20–26. https://doi.org/10.15587/1729-4061.2020.205107
4. Brunetkin, O., Beglov, K., Brunetkin, V., Maksymov, O., Maksymova, O., Havaliukh, O. et al. (2020). Construction of a method for representing an approximation model of an object as a set of linear differential models. Eastern-European Journal of Enterprise Technologies, 6 (2 (108)), 66–73. https://doi.org/10.15587/1729-4061.2020.220326
5. Brunetkin, O., Maksymov, M., Brunetkin, V., Maksymov, O., Dobrynin, Y., Kuzmenko, V. et al. (2021). Development of the model and the method for determining the influence of the temperature of gunpowder gases in the gun barrel for explaining visualize of free carbon at shot. Eastern-European Journal of Enterprise Technologies, 4 (1 (112)), 41–53. https://doi.org/10.15587/1729-4061.2021.239150
6. Brunetkin, O., Maksymov, M., Dobrynin, Y., Demydenko, V., Sidelnykov, O. (2024). Development of a process model for determining the composition and energy characteristics of a pyrotechnic mixture using the library method. EUREKA: Physics and Engineering, 5, 99–112. https://doi.org/10.21303/2461-4262.2024.003453
7. Brunetkin, O., Dobrynin, Y., Maksymenko, A., Maksymova, O., Alyokhina, S. (2020). Inverse problem of the composition determination of combustion products for gaseous hydrocarbon fuel. Computational Thermal Sciences:

An International Journal, 12 (6), 477–489. https://doi.org/10.1615/computthermalscien.2020034878
8. Maksymov, M. V., Brunetkin, O. I., Beglov, K. V., Alyokhina, S. V., Butenko, O. V. (2022). Automatic Control for the Slow Pyrolysis of Organic Materials with Variable Composition. Advanced Control Systems, 397–434. https://doi.org/10.1201/9781003337010-16
9. Brunetkin, A., Beglov, K., Maksimov, M. Ulitskaja, E. (2021). Model and method of controlled pyrolysis of organic sub-stances of variable composition. International Scientific Technical Journal "Problems of Control and Informatics", 66 (1), 134–146. https://doi.org/10.34229/1028-0979-2021-1-12
10. Brunetkin, O., Sidelnykov, O., Maksymov, M., Dobrynin, Y. (2025). Improving the model for determining the composition of gunpowder gases during thermal destruction of gunpowder in a limited volume space. Eastern-European Journal of Enterprise Technologies, 3 (6 (135)), 35–45. https://doi.org/10.15587/1729-4061.2025.330654
11. Repilo, Y. I. (2014). Pohliady viiskovykh fakhivtsiv providnykh krain svitu na kontseptsiiu vohnevoho urazhennia protyvnyka v operatsiiakh. Materialy naukovo-praktychnoho seminaru kafedry raketnykh viisk i artylerii. Kyiv: NUOU, 30–40.
12. Vyshnevskyi, Y. V. (2014). Shchodo perspektyv stvorennia avtomatyzovanoi systemy zboru ta obrobky rozviduvalnykh vidomostei. Zbirnyk tez dopovidei naukovo-tekhnichnoi konferentsii "Perspektyvy rozvytku raketnykh viisk i artylerii Sukhoputnykh viisk". Lviv: Akademiia Sukhoputnykh viisk. 40–42. Available at: https://asv.mil.gov.ua/content/nauka/2014/5-6-11-2014_mat_tez_dop.pdf
13. Zahorka, O. M., Kolesnykov, V. O., Koval, V. V., Zahorka, I. O. (2012). Do pytannia zastosuvannia rozviduvalno-udarnykh i rozviduvalno-vohnevykh kompleksiv u merezhetsentrychnii viini. Nauka i tekhnika Povitrianykh Syl Zbroinykh Syl Ukrainy, 3, 8–13. Available at: http://nbuv.gov.ua/UJRN/Nitps_2012_3_5
14. Zahorka, O. M., Koval, V. V., Tiurin, V. V., Maliuha, V. H., Zahorka, I. O. (2016). Osoblyvosti ta pryntsypy pobudovy merezhetsentrychnoi systemy upravlinnia uhrupovannia viisk (syl). Zbirnyk naukovykh prats Kharkivskoho universytetu Povitrianykh Syl. 3, 7–11. Available at: http://nbuv.gov.ua/UJRN/ZKhUPS_2016_3_4
15. Tkachuk, P. P., Budaretskyi, Y. I., Shchavinskyi, Y. V., Prokopenko, V. V. (2015). Vplyv zasobiv avtomatyzatsii upravlinnia pidrozdilamy i vohnem artylerii na efektyvnist yii zastosuvannia. Viiskovo-tekhnichnyi zbirnyk, 12, 75–82. Available at: http://nbuv.gov.ua/UJRN/vtzb_2015_12_16
16. Serhiienko, R. V., Didichenko, O. A. (2014). Dosvid zastosuvannia zasobiv artyleriiskoi rozvidky u kontrbatareinii borotbi. Zbirnyk tez dopovidei naukovo-tekhnichnoi konferentsii "Perspektyvy rozvytku raketnykh viisk

i artylerii Sukhoputnykh viisk". Lviv: Akademiia Sukhoputnykh viisk, 101–103. Available at: https://asv.mil.gov.ua/content/nauka/2014/5-6-11-2014_mat_tez_dop.pdf
17. Bieliaiev, M. I., Tolmachov, O. M. (2015). Monitorynh stanu samokhidnoi artylerii Sukhoputnykh viisk Zbroinykh Syl Ukrainy ta vyznachennia napriamkiv yii rozvytku. Viiskovo-tekhnichnyi zbirnyk, 3, 11–15. Available at: http://nbuv.gov.ua/UJRN/soivt_2015_3_5
18. Techniques for the Fires Brigade (2012). Washington: CreateSpace Independent Publishing Platform, 183. Available at: https://www.amazon.com/Techniques-Publication-3-09-24-3-09-22-November/dp/1481200356
19. Field Manual 2-0 Intelligence (2018). Washington: Department of the Army. Available at: https://irp.fas.org/doddir/army/fm2-0-2018.pdf
20. ADLER II Artillery Computer Network Delivered to Troops. Army Technology. Available at: https://www.army-technology.com/contractors/data/kulr-technology-partners-us-army/pressreleases/press15/
21. Field Manual 3-09 Field Artillery Operations and Fire Support (2014). Washington: Department of the Army, 4–12. Available at: https://www.scribd.com/document/248059115/FM-3-09-Field-Artillery-Operations-and-Fire-Support
22. Fomin, I. M. (2000). Teoretychni osnovy planuvannia artyleriiskoi rozvidky. VAU.
23. Gall, R. (2002). Enlightening the Artillery in the Army of the Future. Soldier and Technology, 13–18.

CHAPTER 2

Information localization and verification of the firing states of an artillery gun

Maksym Maksymov
Pavlo Gultsov
Volodymyr Demydenko
Valentin Davydov

Abstract

This chapter investigates the problem of informational localization and verification of the states that characterize the lifecycle of an individual artillery shot. The study considers the sequential chain of physical processes occurring in the system "propellant charge – chamber – barrel – projectile – flight trajectory – impact with the surface". These processes form the basis for assessing the technical condition and operational efficiency of artillery systems.

A conceptual framework is developed for identifying measurable parameters associated with different stages of the shot process. The approach relies on the analysis of acoustic, thermodynamic, and optoelectronic phenomena accompanying the firing event. Particular attention is given to the diagnostic potential of the acoustic field generated by ballistic and muzzle waves.

A method for verifying the heat of explosion of the propellant charge is proposed. The method is based on determining the gross chemical formula of the propellant gases and performing a thermodynamic evaluation of the energy characteristics of the charge. This approach enables verification of the declared energetic parameters of propellant compositions.

An acoustic method for estimating the initial velocity of the projectile is presented. The method utilizes temporal characteristics of ballistic and muzzle waves recorded at remote measurement points and allows indirect assessment of the wear state of the barrel and chamber.

The chapter also introduces a method for evaluating the energetic efficiency of an artillery gun based on video-metric observation of projectile exit and the expansion of propellant gases. In addition, a technique for verifying the coordinates of

© The Author(s) of individual chapters, 2026 DOI: 10.21303/978-9908-8450-1-2.ch2

projectile impact is proposed using acoustic measurements of the shot-generated wave field along the projectile trajectory.

The presented models and methods provide a basis for partial verification of different stages of the artillery shot process and may serve as elements of integrated automated systems for monitoring the technical condition and operational parameters of artillery weapons.

Keywords

Artillery shot diagnostics, acoustic field of a shot, ballistic and muzzle waves, propellant charge energetics, artillery gun efficiency, projectile trajectory verification.

2.1 Introduction

Modern artillery operations are characterized by increasingly high demands on precision, rapid response, and verification of firing results under dynamic conditions. In contemporary combat and training scenarios, the ability to accurately assess the technical state of artillery systems immediately after a shot is essential for both operational efficiency and safety. The complex interactions between the propellant charge, chamber, barrel, and projectile, along with the influence of environmental factors, require the use of integrated measurement and diagnostic methods to monitor the firing process in real time [1, 2].

Recent studies demonstrate that combining heterogeneous physical measurements – acoustic, thermodynamic, and optoelectronic – can provide a reliable basis for evaluating the performance and condition of artillery systems [3, 4]. Acoustic signals generated during firing, such as ballistic and muzzle waves, carry information about the projectile's initial velocity, barrel wear, and the energetic characteristics of the propellant charge. Meanwhile, high-speed videometric recordings allow observation of projectile exit dynamics and the expansion of propellant gases, which can be used to assess energetic efficiency [5, 6].

Methodological approaches originally developed in related fields – such as the modeling of combustion processes, pyrolysis, and energy transformations in reactive systems – can be adapted for interpreting measurement signals obtained during firing [7, 8]. For instance, analytical solutions of differential equations, parameter identification techniques, and library-based process models provide a flexible framework for describing nonlinear dynamic phenomena in artillery systems. These approaches support the development of partial verification methods for individual stages of a shot, from propellant ignition to projectile impact.

At the same time, operational considerations in artillery units, including rapid repositioning, variation in ammunition properties, and environmental disturbances, necessitate methods that are both accurate and deployable under real conditions [9]. The integration of measurement data with computational methods enables real-time assessment of firing states, minimizing the time between successive shots while maintaining reliability in the determination of energetic and kinematic parameters.

Within this context, the present chapter focuses on the development of diagnostic and verification methods for artillery shots based on the combined analysis of acoustic fields, videometric observations, and thermodynamic measurements. Particular attention is given to the identification of measurable parameters at each stage of the firing process, methods for verifying the heat of explosion of propellant charges, localizing initial projectile velocity, evaluating energetic efficiency, and verifying the coordinates of projectile impact [10]. By presenting a coherent framework for integrating these methods, the chapter lays the foundation for automated monitoring systems capable of supporting both operational decision-making and scientific research in artillery performance assessment.

2.2 General provisions

The firing process of an artillery gun can reasonably be considered as a multifactor dynamic system operating through a sequential transition of states "propellant charge – chamber – barrel – projectile – trajectory – impact with the surface". Such a transition may be formalized in the form of a directed graph of states, in which each link is characterized by a set of thermodynamic, mechanical, and ballistic parameters.

The stochastic nature of variations in propellant properties, barrel wear, projectile mass, and meteorological conditions necessitates the information-based localization of the current system state in real time. In modern automated fire-control systems, verification is performed within a single computational cycle without waiting for the results of the previous shot. This approach makes it possible to minimize time losses and to increase the generalized firing efficiency criterion by nearly five times compared with the classical adjustment-firing scheme.

An analysis of open sources indicates that information localization methods can be systematized according to the physical nature of the measured field.

Photoelectric and videometric methods make it possible to determine projectile velocity and coordinates based on high-speed imaging results [11, 12]. Their advantage lies in high measurement accuracy; however, their effectiveness depends on atmospheric observation conditions.

Radar-based methods, particularly Doppler systems, provide measurements of motion parameters along the initial and intermediate segments of the trajectory [13, 14]. These methods are less sensitive to visibility conditions but require more complex hardware implementation.

Acoustic methods are based on the registration of muzzle and ballistic waves and make it possible both to localize firing positions and to determine projectile velocity [2, 3, 15–17]. Their advantage lies in the relative simplicity of deployment, while the informational content is ensured through the analysis of the temporal and spectral characteristics of the signal.

A separate area is represented by tomographic and thermodynamic methods for monitoring ammunition quality throughout its life cycle [18]. Changes in the physicochemical properties of propellants during long-term storage affect the heat of explosion and, consequently, the initial projectile velocity and the energetic efficiency of the shot. The concept of an electronic ammunition passport appears promising under peacetime conditions; however, under conditions of intensive combat use, methods of operational verification that are independent of production history are more appropriate.

Thus, the information localization of firing states should be based on the direct measurement of physical parameters that determine the energetic and kinematic outcome. The following subsections examine the method for verifying the heat of explosion of the propellant charge and the method for localizing the initial projectile velocity based on acoustic fields as key components of an integrated monitoring system.

At the same time, it should be emphasized that the approaches to information localization based on acoustic, radar, and optoelectronic measurements considered above represent a generalization of known methods described in the literature. The subsequent subsections present the authors' original contributions, including the verification method for the heat of explosion of the propellant charge, the acoustic method for localizing the initial projectile velocity, the videometric method for determining energetic efficiency, and the method for verifying the projectile impact coordinates. These methods are proposed as a unified framework for integrated diagnostics of artillery firing states.

2.3 Method for determining the heat of explosion of the propellant charge as a tool for verifying its state

To confirm the compliance of the energetic characteristics of the propellant charge with the established requirements, an automated system for determining

the heat of explosion is employed together with a corresponding computational-experimental verification method, the schematic diagram of which is shown in **Fig. 2.1**.

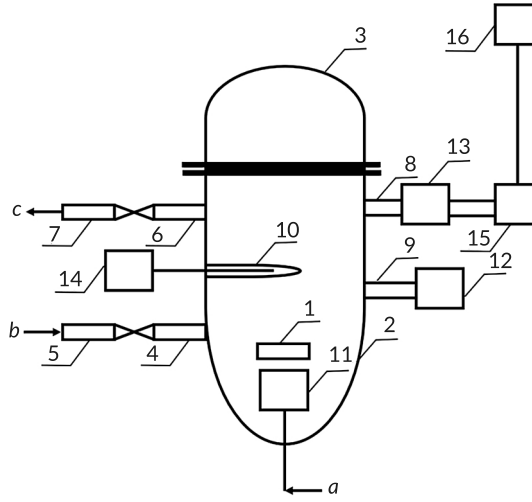

Fig. 2.1 Automated system for determining the heat of explosion of an artillery propellant charge for verification of its quality: *a* – the voltage supply line; *b* – the line supplying inert gas to the tank; *c* – the line for inert gas removal; 1 – the propellant charge sample; 2 – the cylindrical tank; 3 – the flanged cover; 4 – the inlet fitting; 5 – the shut-off equipment; 6 – the outlet fitting; 7 – the shut-off equipment; 8 – the fitting; 9 – the fitting; 10 – the sleeve; 11 – the electric igniter; 12 – the pressure gauge; 13 – the gas pressure regulator; 14 – the thermocouple via the indication device; 15 – the composition of the combustible gas; 16 – personal computer with appropriate software

The automated system for determining the heat of explosion of an artillery propellant charge for quality verification includes a cylindrical tank (2) with an internally heat-insulated surface designed for burning a sample of the propellant charge and collecting the generated propellant gases. The outlet of the gas pressure regulator (13) is connected to the inlet of the installation for determining the composition of the combustible gas during combustion (15), the output of which is connected to a personal computer with appropriate software (16).

In the upper part of the tank, a hermetically sealed flanged cover (3) with thermal insulation is installed; in the lower part, an electric igniter (11) is mounted, while a sleeve (10) for a thermocouple with a temperature indication device (14) is located on the side wall.

An inlet fitting (4) with shut-off equipment for purging with inert gas (5) and an outlet fitting (6) with corresponding shut-off equipment (7) are mounted on the side wall of the tank. In addition, a fitting (9) is provided for connecting a pressure gauge (12), as well as a fitting (8) connected to the gas pressure regulator (13).

Fig. 2.1 additionally designates the propellant charge sample (1), the voltage supply line ("*a*"), the lines supplying inert gas to the tank ("*b*"), and the line for its removal ("*c*").

The installation for determining the composition of combustible gas during its combustion (15) is known from the literature [19]. It includes an energy device with a burner, a system for supplying combustible gas and air with regulating equipment, pipelines for gas and air sampling, flowmeters and flow sensors, a control unit, and a testing device. The burner is connected to the pipelines supplying combustible gas and air. Corresponding flow sensors and regulating equipment are installed on the pipelines supplying combustible gas and air. The supply pipelines are connected to the sampling pipelines, which are routed to the testing device. The control unit interacts with the regulating equipment, flow sensors, flowmeters, and a thermocouple installed in the combustion chamber of the testing device, ensuring control of the combustion regimes.

The testing device contains a cylindrical combustion chamber with coaxially arranged cylinders between which gaps are formed for the passage of air. The chamber is equipped with pipes for supplying combustible gas and air, fitted with temperature measurement devices. Inside the chamber, a thermocouple is installed to monitor the combustion temperature regime.

The proposed method is implemented in the following sequence.

At the first stage, a batch of identical propellant charges of artillery rounds is delivered for verification, for which confirmation of the heat of explosion obtained at the loading plant and documented by the packing arsenal is available. A sample of the propellant charge (1) is taken from a randomly selected round and placed in the cylindrical tank (2) of the system, after which the tank is hermetically sealed with the flanged cover (3).

At the second stage, a specified constant pressure is set in the throttling regulator of the gas pressure regulator (13) for the subsequent throttling of the propellant gas.

The third stage involves removing air from the tank by purging it with inert gas, which is supplied through the inlet fitting (4) with shut-off equipment (5) and discharged through the outlet fitting (6) with corresponding equipment (7).

At the fourth stage, the pressure of the inert gas is monitored by the pressure gauge (12) connected through the fitting (9). After atmospheric pressure has been established, the shut-off equipment (5) and (7) are closed and voltage is supplied to the electric igniter (11), igniting the propellant charge sample (1).

At the fifth stage, the generated propellant gases are directed from the tank (2) through the fitting (8) and the gas pressure regulator (13) to the installation for determining the composition of the combustible gas (15).

At the sixth stage, the propellant gas is burned in an air atmosphere in the installation (15), and the gross formula of the gas formed during the combustion of the propellant charge sample (1) is determined.

At the seventh stage, the obtained gross formula is transmitted to a personal computer with appropriate software. Additionally, the temperature value obtained from the thermocouple via the indication device (14) installed in the sleeve (10) on the wall of the tank (2), the pressure value set by the gas pressure regulator (13), and the declared heat of explosion of the propellant charge are entered.

At the eighth stage, using the computer software, a thermodynamic calculation of the heat of explosion of the propellant charge sample is performed based on the determined gross formula of the propellant gas and the measured process parameters. The obtained value is compared with the declared one, taking into account measurement and calculation errors. If the values coincide within the permissible error, a conclusion is made regarding the positive verification of the heat-of-explosion property of the artillery propellant charge; otherwise, the verification result is considered negative.

The initial data for determining the heat of explosion of the propellant charge are presented in **Table 2.1**. In Example 1, calculated and experimental data are presented concerning the application of the system and the method at site *B*, where assembled rounds of the same type in the amount of *N* units were delivered from arsenal *WW*. For the study, one of the delivered rounds was randomly selected. A sample (1) of the propellant charge was taken from the selected round for the measurement experiment. The sample (1) was placed in the cylindrical tank (2) of the heat-of-explosion determination system.

Similarly, in Example 2, calculated and experimental data are presented concerning the application of the system and the method at site *C*, where assembled rounds of the same type in the amount of *M* units were delivered from arsenal *WV*. An analogous procedure of round selection and sample preparation was performed for Example 2. In both cases, the experiment was carried out and a result was obtained.

From the presented data, the following conclusions can be drawn. The declared heat of explosion of the artillery propellant charge in Example 1 is 950 kJ/kg, and in Example 2 it is 945 kJ/kg (see item 7 of **Table 2.1**). The total relative error of measurements and calculations is 1.5% (see item 6 of **Table 2.1**) and is adopted as the criterion for comparing the declared and calculated values of the heat of explosion. The gross formula of the propellant gas obtained experimentally was determined as $C_1H_{1.44}N_{0.37}O_{1.57}$ for Example 1 and $C_1H_{1.43}N_{0.32}O_{1.56}$ for Example 2 (item 2 of **Table 2.1**).

Table 2.1 Indicators of the properties of quantities obtained during the verification of the heat of explosion of the propellant charge of an artillery round

No.	Name of indicator, unit of measurement	Values of indicators in the experiments	
		Example No. 1	Example No. 2
1	Pressure of the propellant gas during throttling set on the gas pressure regulator, Pa	$1.1 \cdot 10^5$	$1.1 \cdot 10^5$
2	Gross formula of the propellant gas	$C_1H_{1.44}N_{0.37}O_{1.57}$	$C_1H_{1.43}N_{0.32}O_{1.56}$
3	Temperature value recorded by the thermocouple, K	2800	2300
4	Pressure value in the cylindrical tank after the formation of the propellant gas, Pa	$5.1\ 10^5$	$4.8\ 10^5$
5	Total relative measurement and calculation error, %	1.5	1.5
6	Declared heat of explosion of the propellant charge of the artillery round, kJ/kg	950	945
7	Calculated heat of explosion of the propellant charge of the artillery round, kJ/kg	958	890
8	Value of the relative experimental error, %	0.84	5.82
9	Comparison of the errors of the declared and calculated heat of explosion values	$0.84 < 1.5$	$5.82 > 1.5$
10	Conclusion on the comparison of declared and calculated heat of explosion	Equality within the limits of experimental error	No equality within the limits of experimental error
11	Verification result	Positive	Negative

Based on the determined gross formula of the propellant gas and the measured process parameters, the heat of explosion of the propellant charge was calculated, amounting to 958 kJ/kg for Example 1 and 890 kJ/kg for Example 2 (item 7 of **Table 2.1**). The relative experimental errors were determined as 0.84% for Example 1 and 5.82% for Example 2 (item 9 of **Table 2.1**).

An analysis of the obtained results shows that the calculated value of the heat of explosion is primarily influenced by the determined gross formula of the propellant gas and the measured temperature, which define the thermodynamic state of the combustion products. Pressure plays a secondary role under the adopted calculation scheme, while the total measurement and calculation error establishes the admissible range for comparing the calculated and declared values. Therefore, deviations exceeding the specified error threshold may indicate changes in the physicochemical properties of the propellant charge rather than measurement uncertainty.

An analysis of the results presented in **Table 2.1** shows that for Example 1 the verification result is positive, whereas for Example 2 it is negative.

The data obtained from Examples 1 and 2 demonstrate the practical feasibility of verifying the propellant charge of an artillery round using the proposed system and method.

2.4 Method for localizing the initial projectile velocity during the generation of acoustic fields of the shot

There are studies in the field of information technologies that have demonstrated the possibility of performing automated diagnostics of the "barrel-chamber" system state based on the velocity of the projectile exiting the barrel [2, 3, 15–17, 20].

The method is illustrated by the equipment arrangement shown in **Fig. 2.2**. In **Fig. 2.2**, the following are indicated: 1 – gun, 2 – microphone or microphones, 3 – air temperature sensor at the gun, 4 – air pressure sensor at the gun, 5 – air humidity sensor near the gun, 6 – wind direction and speed sensor, 7 – air temperature sensor near the microphone or microphones (2), 8 – air pressure sensor near the microphone or microphones (2), 9 – air humidity sensor near the microphone or microphones (2), 10 – wind direction and speed sensor near the microphone or microphones (2), 11 – ballistic wave, 12 – muzzle wave, S_1 – distance from the gun to the microphone or microphones (2) along the firing direction, S_2 – distance from the microphone or microphones (2) to the location of the ballistic wave (11) along the firing direction at the moment the microphone or microphones (2) registered the muzzle wave (12), S_3 – distance from the gun to the location of the muzzle wave (12) at time t_{bal} (14), when the ballistic wave (11) was registered by the microphone or microphones (2) at distance S_1.

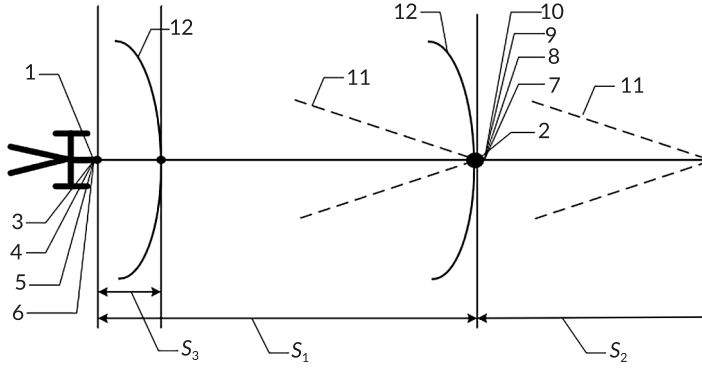

Fig. 2.2 Diagram of the gun and measurement equipment arrangement

In **Fig. 2.3**, the following are shown: 13 – moment of muzzle wave registration t_{muz}, 14 – moment of ballistic wave registration t_{bal}, 15 – time interval recorded by the microphone or microphones (2) between the passage of the ballistic wave t_{bal} and the muzzle wave t_{muz}.

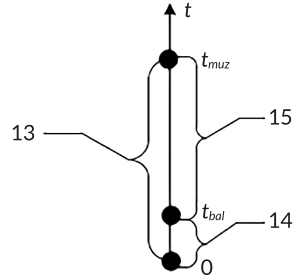

Fig. 2.3 Time diagram of wave registration t_{muz}, t_{bal} at the microphone location

The method is implemented in the following sequence:

Step 1. A gun (1) with a barrel and chamber is placed at the firing position and subjected to inspection. The degree of gun wear is preliminarily assessed by the total number of rounds fired from the gun. The gun is then loaded with a specific projectile and a corresponding propellant charge.

Step 2. A microphone or microphones (2) are placed along the line of fire at a distance of 50–500 meters from the gun (1). The microphone or microphones (2) are positioned along the firing direction for the registration of the ballistic (11) and muzzle (12) waves. Measurements of atmospheric parameters near the gun are carried out using temperature (3), pressure (4), humidity (5), and wind speed and direction (6) sensors. Similar measurements are performed at the location of the microphone using sensors (7–10). Based on the obtained values, a correction to the propagation velocity of the muzzle wave under the existing atmospheric conditions is determined.

Step 3. A shot is fired from the gun (1) in the firing direction.

Step 4. Using the microphones (2), the ballistic wave (11) is first registered. At this moment in time t_{bal} (14), the muzzle wave (12) is located at a distance S_3 from the gun (1). After a time t_{muz} (13), the microphones (2) register the muzzle wave (12) from the shot; at this moment the ballistic wave (11) is located at the total distance $S_1 + S_2$ from the gun (1).

Step 5. From the obtained temporal signal patterns, the amplitude and duration of the ballistic wave signal (11) are determined, as well as the amplitude and the

duration of the first half-period of the muzzle wave (12) at the microphone location (2) at a distance S_1 from the gun (1).

Step 6. The signals from the microphone or microphones (2) are transmitted to an analog-to-digital converter and then to a computer, where the signals are transformed into the spectral domain by computing the Fourier transform. In the spectral domain, the power spectral density (or simply the spectrum) is obtained, characterizing the distribution of signal energy over different frequencies.

Step 7. For the obtained spectra, the width at the level of 0.707 is determined for the ballistic wave signal (11), and the central frequency (frequency of the maximum) is determined for the muzzle wave (12).

Step 8. The travel time of the muzzle wave t_{muz} (13) from the gun (1) to the microphones (2) is determined from the measured distance from the gun (1) to the microphones (2), S_1, and the calculated propagation velocity of the muzzle wave (12).

Step 9. The travel time of the ballistic wave t_{bal} (14) from the gun (1) to the microphones (2) is determined as the difference between the travel time of the muzzle wave t_{muz} (13) to the microphones (2) and the time interval (15) recorded during the passage of the ballistic wave (11).

Step 10. The velocity of the ballistic wave (11) (which corresponds to the instantaneous projectile velocity) is determined using the time t_{bal} (14) at which it is registered by the microphones (2) at a distance S_1 from the gun (1).

Step 11. The calculated actual initial projectile velocity – 558.2 m/s (item 17 in **Table 2.2**) – is compared with the calculated nominal initial projectile velocity – 560 m/s (see item 16 in **Table 2.2**), and a conclusion is drawn regarding the degree of wear of the barrel and chamber based on the change in projectile velocity.

After that, a second shot is fired from the same gun (1) at the firing position, and all the operations described above are repeated.

Table 2.2 shows that the first gun (item 2 in **Table 2.2**) does not exhibit a significant difference between the calculated actual projectile velocities – 558.2 m/s and 556.9 m/s – and the calculated nominal initial velocity of 560 m/s.

The difference between the calculated nominal initial projectile velocity and the calculated actual initial projectile velocity is 0.32% and 0.55%, respectively.

The wear of the first gun is insignificant (**Table 2.2**), since the difference does not exceed the permissible threshold of 8–10%.

This conclusion is based on the proposed method, in which the criterion for assessing barrel and chamber wear is primarily determined by the relative deviation of the calculated actual initial projectile velocity from the nominal (tabulated) value. At the same time, the recorded acoustic parameters (signal amplitudes, durations, and spectral characteristics) are used as auxiliary informative features

that ensure the reliability of velocity determination. Thus, the final conclusion about the degree of wear is formed according to a combined criterion, where the key quantitative indicator is the velocity deviation, supported by the stability of the acoustic signal parameters.

Table 2.2 Indicators of barrel and chamber wear of the artillery gun

No.	Name of indicator, unit of measurement	Value of the indicator for the gun			
		First		Second	
1	Experiment number	1	2	3	4
2	Total number of shots fired from the gun	91		1968	
3	Shot number from the gun	1	2	1	2
4	Distance from the gun to the measuring microphone, m	300			
5	Tabulated firing range according to the sight setting, m	9000			
6	Total correction for meteorological conditions, m	–137	–157	–215	–215
7	Ballistic corrections, m	+12			
8	Calculated firing range, m	8875	8855	8797	8797
9	Actual firing range determined by the rangefinder, m	9165	9082	8665	8671
10	Amplitude of the ballistic wave, Pa	380		240	
11	Duration of the ballistic wave signal, ms	4.8		4.1	
12	Amplitude of the muzzle wave, Pa	140		90	
13	Duration of the first half-period of the muzzle wave, ms	22		14	
14	Spectrum width at the 0.707 level of the ballistic wave signal, Hz	180		250	
15	Central frequency (frequency of the maximum) of the muzzle wave signal spectrum, Hz	12		16	
16	Calculated initial projectile velocity, m/s	560			
17	Calculated actual initial projectile velocity, m/s	558.2	556.9	504.2	504.5

Subsequently, a second gun is placed at the firing position and all the operations listed above are performed. The obtained data are entered into the table. For the second gun (**Table 2.2**), the calculated actual projectile velocities are 504.2 m/s and 504.5 m/s, while the calculated nominal initial projectile velocity is 560 m/s, which corresponds to deviations of 9.96% and 9.91%, respectively.

Thus, as a result of performing the specified sequence of operations for two guns (item 2 of **Table 2.2**), each of which fired two shots (item 3 of **Table 2.2**), a set

of parameters was obtained that characterizes disturbances of the atmospheric environment caused by the shot and calculated from the registration times of the muzzle wave t_{muz} (13) and the ballistic wave t_{bal} (14). On this basis, a conclusion was drawn regarding the level of wear of the barrel bore and the chamber of each gun (items 10–17 of **Table 2.2**). The wear of the second gun is significant, since the calculated actual projectile velocities in the two shots are 9.96% and 9.91% lower than the calculated nominal initial velocity, which is confirmed by the data presented in items 5, 8, and 9 of **Table 2.2**.

The obtained results confirm the possibility of practical application of the method for assessing the wear of the barrel bore and the chamber. Previously, it was considered that rifled barrels of an artillery gun are unsuitable for further use if the total loss of the projectile's initial velocity due to barrel wear reaches 10% or more of the tabulated value.

2.5 Method for determining the energy efficiency of an artillery gun

Studies in the field of automated control systems have demonstrated the possibility of automated diagnostics of the state of the "propellant charge – chamber – barrel – shot" system based on the projectile velocity at the moment it exits the barrel bore and on the parameters of the muzzle emission [1, 5, 21, 22].

The method is aimed at determining the energy efficiency of an artillery gun, which makes it possible to increase the reliability of assessing its current condition. The method is explained by a specific arrangement of equipment shown in **Fig. 2.4–2.6**.

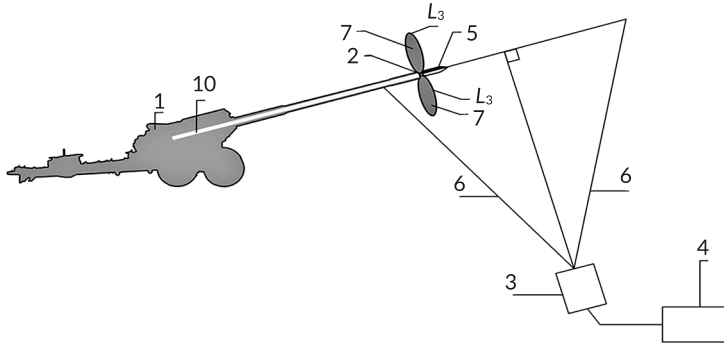

Fig. 2.4 Equipment layout diagram

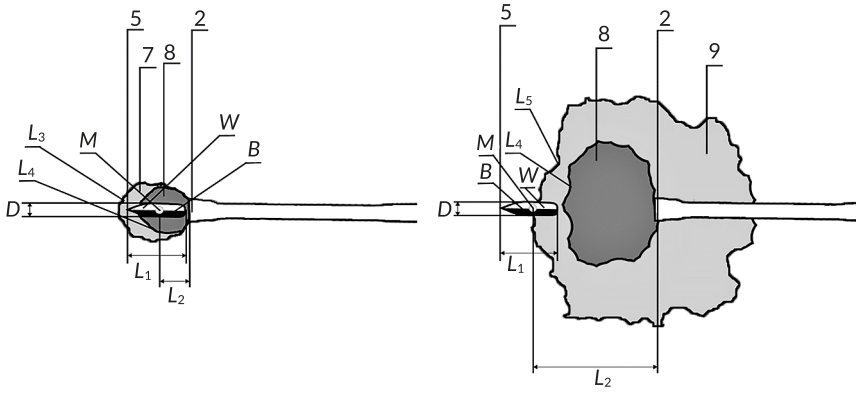

Fig. 2.5 Diagram of two frames displaying fields that register temperature and pressure after the projectile exits the barrel bore (left – the current *i*-th frame of the video stream showing the moment the projectile leaves the muzzle of the gun barrel; right – the current *k*-th frame of the video stream showing the moment of the maximum volume of the flame of burned propellant gases during their expansion to atmospheric pressure)

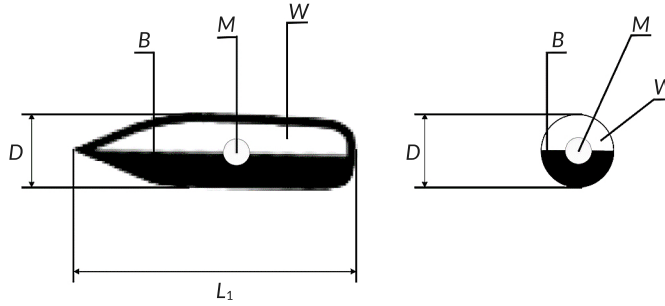

Fig. 2.6 Diagram of binary coloring of the projectile

Artillery gun – 1; muzzle of the gun barrel bore – 2; digital high-frequency wide-angle video camera operating in the visible and infrared spectrum – 3; personal computer with processing software package – 4; projectile used for firing – 5; boundary of the camera field of view – 6; projection of the surface of unburned propellant gases of increased pressure – 7; projection of the surface of the flame of burned propellant gases – 8; projection of the surface of propellant gases expanded to atmospheric pressure and forming the acoustic muzzle wave – 9; internal volume of the barrel tube – 10; projectile caliber diameter – *D*; center of mass of the projectile – *M*; white field of

the binary-colored projectile – W; black field of the binary-colored projectile – B; projectile length – L_1; distance between the center of mass of the projectile (5) and the muzzle of the gun barrel bore – L_2; curved line representing the boundary between the projection of the surface of unburned propellant gases with pressure higher than atmospheric, forming the shock muzzle wave, and the atmosphere – L_3; curved line representing the boundary between the projection of the surface of the flame of burned propellant gases with pressure higher than atmospheric and the unburned propellant gases with pressure higher than atmospheric – L_4; curved line representing the boundary between the projection of the surface of the flame of burned propellant gases with pressure higher than atmospheric and the atmosphere – L_5; volume occupied by high-pressure propellant gases at the moment when the projectile (5) has passed the muzzle of the gun barrel bore (2) (internal volume of the barrel tube (10)) – V.

The method for determining the energy efficiency of an artillery gun is implemented in the following sequence:

Step 1. At the firing position, the artillery gun (1) is positioned so that the muzzle of the gun barrel bore (2) is perpendicular to the line along which the digital high-frequency wide-angle video camera (3) is placed, the latter being connected to a personal computer with a processing software package (4).

The position of the camera relative to the gun is not of fundamental importance.

Step 2. The projectile (5) prepared for firing is painted in two colors, white and black; the boundary line between the colors passes through the projectile nose along the generatrix of its contour (**Fig. 2.6**).

Step 3. The video camera (3) is activated, a shot is fired with the binary-colored projectile (5), recording is performed in the visible and infrared spectra, and the digital video stream is transmitted in real time to the personal computer with the processing software package (4).

Step 4. After the projectile (5) passes through the camera recording boundary (6), recording is stopped and the video camera (3) is switched off.

Step 5. Using the software package (4), the digital video stream is processed and converted into a sequence of frames.

Step 6. The frames are analyzed to detect the projectile, and an array of frames is formed from the moment it exits the muzzle of the barrel bore (2) to the moment it leaves the recording boundary (6).

Step 7. In the personal computer with the processing software package (4), for each time frame:

– the center of mass of the projectile M is determined;

– at point M, the geometric scaling coefficient is determined using the a priori known projectile characteristics (diameter and length) in each time frame;

– the linear distance between the center of mass of the projectile (5) and the muzzle of the gun barrel bore is determined from the image of the barrel muzzle point (2) to point *M* of the projectile image (5), taking into account the geometric scaling coefficient;

– the instantaneous linear velocity of the projectile (5), *v*, is determined;

– the statistically reliable initial linear velocity of the projectile (5), v_{start}, is determined from the first time frames;

– the current color of the binary coloring of the projectile (5) (*W* or *B*) with the corresponding time is determined, and a temporal binary sequence is formed;

– from the temporal binary sequence, the number of rotations of the projectile (5) per unit time or the angular velocity w_{start} of the projectile (5) is determined;

– the length of the curved line L_3, representing the boundary between the projection of the surface of unburned propellant gases and the atmosphere, is determined;

– the length of the curved line L_4, representing the boundary between the projection of the surface of the flame of burned propellant gases and the unburned propellant gases, is determined;

– from the constructed temporal series of lengths and areas, the gradients of pressure variation are determined; the absence of a pressure gradient indicates the formation of the curved line representing the boundary between the projection of the surface of the flame of burned propellant gases and the atmosphere (line L_5).

Step 8. Using the personal computer with the processing software suite (4), for each *i*-th time frame, the volume of propellant gases V_{PG_i}, the temperature of propellant gases T_{PG_i} measured by the video camera (3), and the pressure of propellant gases P_{PG_i} at the front of the muzzle blast wave are determined. Based on these values, the functional dependence $P(V) = f(V)$ is established.

Step 9. The volume of burnt propellant gases V^* at atmospheric pressure is determined along curve L_5 – the boundary between the projection of the surface of burnt propellant gases at pressure above atmospheric and the atmosphere – corresponding to the pressure gradient generated by the shot.

Step 10. The following energies are determined for the projectile (5):

Kinetic energy along the trajectory: the projectile of mass *m* has

$$E_{kin} = \frac{1}{2} m v_{start}^2,$$

measured from the muzzle of the gun barrel (2).

Rotational energy

$$E_{rot} = \frac{1}{2}\left(\frac{D}{2}\right)^2 m w_{start}^2.$$

Work of expanding gases

$$E_g = \int P(V)\mathrm{d}V,$$

where V – the volume of high-pressure propellant gases at the moment the projectile passes through the muzzle (internal barrel volume – 10), and V^* – the volume of burnt propellant gases at atmospheric pressure.

The energetic efficiency of the artillery gun is then calculated as

$$eff = \frac{E_{kin} + E_{rot} + E_g}{E_{charge}},$$

where $E_{charge} = m_c Q_{expl}$ – the energy of the propellant charge used for firing, with m_c the charge mass and Q_{expl} the specific energy of the charge.

Table 2.3 presents the determination of the geometric dimensions of curve L_3 and the projections of the propellant gas surfaces, as well as the volume of gas V_{PG_i} that burns out, from the moment the projectile separates from the muzzle of the gun barrel until 100 ms, obtained through digital processing of the video stream captured by a high-speed wide-angle digital camera (2000 fps) in the visible and infrared spectra.

Table 2.3 Determination of geometric dimensions of curve L_3

Number of the i-th video frame	Recording time, s	Length of the curve line L_3, m	Area of the surface projection 9, m^2	Volume of propellant gases, V_{PG_i}, m^3
002	0.001	2.79	0.39	1.2
010	0.005	13.74	9.65	144.4
020	0.010	15.47	12.23	206.1
049	0.020	16.88	14.56	267.8
060	0.030	17.61	15.84	303.9
080	0.040	18.09	16.72	329.5
100	0.050	18.45	17.38	349.4
120	0.060	18.73	17.92	365.6
140	0.070	18.96	18.36	379.3
160	0.080	19.16	18.74	391.2
180	0.090	19.33	19.08	401.7
200	0.100	19.48	19.37	411.1

Table 2.4 presents the determination of the temperature and the overpressure of the burnt propellant gases above atmospheric pressure from the moment the projectile separates from the muzzle of the gun barrel until 100 ms. These values are obtained by processing the video stream recorded by a high-speed wide-angle digital video camera (2000 fps) with data acquisition in the visible and infrared spectral ranges.

Table 2.4 Determination of the temperature and overpressure of propellant gases above atmospheric pressure

Number of the *i*-th video frame	Recording time, s	Gas temperature T_{PG_i}, K	Calculated overpressure of propellant gases, P_{PG_i}, Pa
002	0.001	303	66273
010	0.005	486	1010
020	0.010	669	973
049	0.020	829	928
060	0.030	832	821
080	0.040	765	696
100	0.050	673	578
120	0.060	580	476
140	0.070	497	393
160	0.080	428	328
180	0.090	372	277
200	0.100	328	239

Based on the presented data, the energetic efficiency of the artillery gun is *eff* = 0.31 (see item 17 in **Table 2.5**). This value corresponds to the typical range for artillery systems of this class, where a significant part of the energy of the propellant charge is dissipated through thermal losses, gas expansion, and acoustic emission. At the same time, a decrease in this value relative to expected levels may indicate increased energy losses associated with barrel wear, incomplete combustion of the propellant charge, or deviations in the internal ballistic process. Therefore, the energetic efficiency parameter can be considered as an integral diagnostic indicator of the technical state of the gun.

If any term in the numerator (items 10, 11, 13 in **Table 2.5**) or in the denominator (item 16 in **Table 2.5**) changes, the value of *eff* also changes. This indicates that

the current shot differs from the previous ones and should not be taken into account, which makes it possible to reduce the time required for gun sighting.

Table 2.5 Determination of the energetic efficiency of the artillery gun

No.	Name of the parameter, unit of measurement	Calculated value
1	Projectile mass, m, kg	46
2	Projectile diameter, D, m	0.152
3	Analyzed video frames	2, 3, 4, 5, 6, 7, 8, 9, 10
4	Time interval, τ, ms	4
5	Distance traveled by the projectile, L_2, m	3.7
6	Average initial linear velocity of the projectile, v_{start}, m/s	925
7	Number of revolutions during the time interval τ	2.6
8	Angular velocity of the projectile, w_{start}, s^{-1}.	650
9	The obtained dependence $P(V) = f(V)$, from **Tables 2.3**, **2.4**	$P(V) = 85042 \cdot V^{-0.882}$
10	Kinetic energy of the projectile, $E_{kin} = 1/2 m v_{start}^2$, J	$1.96 \cdot 10^7$
11	Rotational energy of the projectile $E_{rot} = 1/2 (D/2)^2 m w_{start}^2$, J	$5.6 \cdot 10^4$
12	Integration limits: V – internal volume of the barrel, V^* – volume of the propellant gases at atmospheric pressure, m^3	0.148; 411
13	Work of gas expansion $E_g = \int 85042 V^{-0.882} dV$, J	$8.9 \cdot 10^5$
14	Charge mass, m_c, kg	18.4
15	Specific explosion energy of the charge, Q_{expl}, J/kg	$3.6 \cdot 10^6$
16	Energy of the charge used to fire the projectile, $E_{charge} = m_c Q_{expl}$, J	$6.62 \cdot 10^7$
17	Energetic efficiency of the artillery gun, $eff = (E_{kin} + E_{rot} + E_g) / E_{charge}$	0.31

2.6 Method for verifying the impact coordinate of an artillery projectile on a surface

Studies in the field of automated control systems have demonstrated the possibility of performing automated diagnostics of the system "effective shot – projectile – flight trajectory – impact with the surface" based on the velocity of a projectile moving along a free trajectory [23–28].

This verification method can be considered as the final stage in the operation of modern automated artillery fire control systems, which rely on continuous monitoring of the states of the artillery system: "charge – breech – barrel – projectile – flight trajectory – impact with the surface".

The method is based on the task of determining the impact coordinate of an artillery projectile on a surface through acoustic registration of the sound field generated by the projectile moving along a free trajectory after being fired from an artillery gun (**Fig. 2.7**).

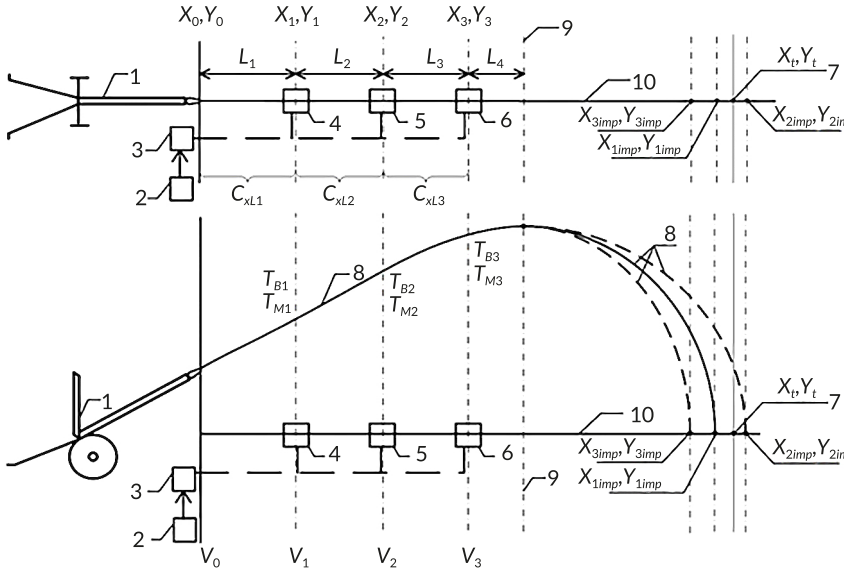

Fig. 2.7 Layout of equipment (top and side views)

Implementation of the proposed method is carried out in the following sequence:

Step 1. Place the artillery gun (1), the meteorological measurement station (2), and the computing device (3). Obtain the coordinates of the gun (1) (X_0, Y_0) and the target (7) (X_t, Y_t), and enter them into the computing device (3).

Step 2. Along the firing line from the gun (1) to the expected table range (9), position the measuring microphones (4), (5), (6), which are connected to the computing device (3). The placement is determined by ensuring equal distances: from the gun to

the first group L_1, between the groups L_2 and L_3, and from the last group to the point where the projectile loses supersonic speed L_4.

Step 3. Record the coordinates of the measuring microphones (4), (5), (6) along the firing line as (X_1, Y_1), (X_2, Y_2), (X_3, Y_3).

Step 4. Connect the measuring microphones (4), (5), (6) to the computing device (3) through switching equipment, synchronize them in time, and input the meteorological data (2).

Step 5. Fire the gun (1), causing the projectile to move along the trajectory (8) toward the target (7) at coordinates (X_t, Y_t). As the projectile travels over the firing line (10), an acoustic field is formed, consisting of ballistic and muzzle waves. Both waves are recorded by the measuring microphones (4), (5), (6). The ballistic wave propagates at supersonic speed, gradually decreasing, while the muzzle wave propagates at the constant speed of sound.

Step 6. Each measuring microphone (4), (5), (6) first records the ballistic wave – (T_{B1}, T_{B2}, T_{B3}), and then the muzzle wave (T_{M1}, T_{M2}, T_{M3}).

Step 7. Calculate the time interval between the events of recording the ballistic and muzzle waves by the microphones (4), (5), (6) that are closest and farthest from the gun.

Step 8. Using the moments of registration of the muzzle (T_{M1}, T_{M2}, T_{M3}) and ballistic (T_{B1}, T_{B2}, T_{B3}) waves by the microphones (4), (5), (6), determine the ballistic wave velocities (V_1, V_2, V_3). These values correspond to the current speed of the projectile at the moments the ballistic wave passes over the respective microphones.

Step 9. Determine the initial projectile velocity V_0 from the firing tables for the given type of charge.

Step 10. Calculate the drag coefficient of the projectile (C_x) between the two nearest groups of microphones.

The integral drag coefficient of the projectile over the monitored section is determined by the expression

$$C_x = 2F_{ff} / (M \cdot S \cdot p \cdot V^2),$$

where F_{ff} – friction force acting on the projectile of mass mmm with air over the monitored section; S – cross-sectional area at the projectile's midsection; ρ – air density; V – average projectile velocity over the section between the two measurement points; M – Mach number.

The impulse of the force is determined for two different measurement points, for example, the first (indices i) and the second (indices j). For the first point: $F_i t_i = mV_i$, hence $F_i = mV_i/t_i$, and for the second point: $F_j t_j = mV_j$, hence $F_j = mV_j / t_j$ and V_j are

the current velocities of the projectile over the measurement points. t_i and t_j are the times of projectile travel from the gun (1) to the measurement points. Then the friction force is $F_{ff} = F_i - F_j$.

Step 11. Determine the trajectory approximation coefficients for the position coordinates (based on velocity, time, and trajectory length): artillery gun (1) – a_1, first measuring microphone or first group of microphones with switching equipment (4) – a_2, second measuring microphone or second group of microphones with switching equipment (5) – a_3, third measuring microphone or third group of microphones with switching equipment (6) – a_4.

Step 12. Construct three approximating parabolic dependencies based on the measured parameters.

The first-type parabola is formed using the coordinates of the gun (1) X_0 and the coordinates of the first X_1 and second X_2 microphone groups, using the trajectory coefficients a_1, a_2, a_3. From this dependency, the projectile-surface impact coordinate X_{1imp} is determined.

The second-type parabola is formed using the coordinates of the gun X_0 and the first X_1 and third X_3 microphone groups, using coefficients a_1, a_2, a_4. From this dependency, the coordinate X_{2imp} is determined.

The third-type parabola is formed using the coordinates of the gun X_0 and the second X_2 and third X_3 microphone groups, using coefficients a_1, a_3, a_4. The coordinate X_{3imp} is determined from this dependency.

Step 13. The lateral deviation coordinates (Y_{1imp}, Y_{2imp}, Y_{3imp}) caused by the rotational motion of the projectile (derivation) are determined for the three parabolic dependencies.

Step 14. Calculate the arithmetic mean of the three projectile-surface impact coordinates (X_{1imp}, Y_{1imp}), (X_{2imp}, Y_{2imp}), and (X_{3imp}, Y_{3imp}), which represents the projectile impact location according to the proposed method.

The use of parabolic approximation in the proposed method is justified for trajectory segments where the projectile motion can be considered smooth and weakly perturbed. Under conditions of significant meteorological disturbances, complex terrain, or non-standard variations in projectile velocity along the observation segment, the approximation accuracy may decrease. In such cases, refinement of the approximation model or the use of additional measurement points may be required.

Tables 2.6, **2.7** present the calculation results illustrating the application of the method for determining the projectile-surface impact coordinate based on the acoustic registration of the sound field generated by the ballistic and muzzle waves.

Table 2.6 Determination of the approximation parabola coefficients

Name of the parameter being determined		Parameter values for the microphone number along the firing line		
		1	2	3
Distance to the target, km			15	
Distance from the gun to the microphone (L), m		5436	7789	9896
Projectile velocity at the measurement point, m/s		674.2	583.3	519.4
Length of the projectile trajectory to the measurement point, m		7111	10188	12944
Ballistic wave registration time, s		10	15	20
Muzzle blast wave registration time, s		16.4	23.5	29.8
Time interval between ballistic and muzzle blast wave registrations, s		6.4	8.5	9.8
Integral drag coefficient over the section		0.025940	0.016011	0.010749
Approximation parabola coefficients $y = A \cdot L^2 + B \cdot L$	A	–0.000096	–0.000088	–0.00008
	B	1.3182	1.2772	1.1937

Table 2.7 Determination of the projectile-surface impact coordinate

Name of the parameter being determined	Parameters corresponding to the coefficients of the approximating parabola		
	–0.000096	**–0.000088**	**–0.00008**
	1.3182	**1.2772**	**1.1937**
Calculated coordinates of the projectile impact with the surface, m	13794	14511	15001
Lateral deviation coordinates	29	33	36
Average impact coordinates of the projectile, m		(14435; 33)	

2.7 Conclusions

The results of the study allow the following conclusions to be drawn.

The main links in the chain of states "charge – chamber – barrel – projectile – flight trajectory – impact with the surface" have been identified, which characterize the life cycle of an artillery shot.

The possibility of informational localization of individual shot states has been demonstrated based on parameters of acoustic, thermodynamic, and videometric processes accompanying the shot.

A method for verifying the explosive energy of the propellant charge has been developed, based on determining the gross formula of the propellant gas and performing a subsequent thermodynamic calculation of its energetic characteristics.

An acoustic method for localizing the initial velocity of the artillery projectile based on the parameters of ballistic and muzzle waves has been proposed.

A method for determining the energetic efficiency of an artillery gun has been developed, relying on videometric registration of the projectile's exit from the barrel and the expansion of propellant gases.

A method for verifying the coordinates of the projectile's impact with the surface has been proposed, based on the analysis of the shot's acoustic fields.

Conflict of interest

The authors declare that they have no conflict of interest in relation to this research, whether financial, personal, authorship or otherwise, that could affect the research and its results presented in this paper.

Use of artificial intelligence statement

Artificial intelligence technology was used in the preparation of this chapter. Specifically, the authors used OpenAI ChatGPT (model GPT-5.2) to assist in editing and structuring introductory text sections and in formulating generalized descriptions of research methodologies for integrating mandatory literature sources into the chapter introduction.

The authors bear full responsibility for the final manuscript. Generative AI tools are not credited and are not responsible for the final results.

Authors' contributions

Maksym Maksymov: Conceptualization, Methodology, Development of models and methods, Formal analysis, Writing – original draft.

Pavlo Gultsov: Methodology, Investigation, Data analysis, Writing – review & editing.

Volodymyr Demydenko: Investigation, Validation, Interpretation of results, Writing – review & editing.

Valentin Davydov: Formal analysis, Visualization, Data curation, Writing – review & editing.

References

1. Boltenkov, V., Brunetkin, O., Dobrynin, Y., Maksymova, O., Kuzmenko, V., Gultsov, P. et al. (2021). Devising a method for improving the efficiency of artillery shooting based on the Markov model. Eastern-European Journal of Enterprise Technologies, 6 (3 (114)), 6–17. https://doi.org/10.15587/1729-4061.2021.245854
2. Dobrynin, Y., Volkov, V., Maksymov, M., Boltenkov, V. (2020). Development of physical models for the formation of acoustic waves at artillery shots and study of the possibility of separate registration of waves of various types. Eastern-European Journal of Enterprise Technologies, 4 (5 (106)), 6–15. https://doi.org/10.15587/1729-4061.2020.209847
3. Dobrynin, Y., Brunetkin, O., Maksymov, M., Maksymov, O. (2020). Constructing a method for solving the riccati equations to describe objects parameters in an analytical form. Eastern-European Journal of Enterprise Technologies, 3 (4 (105)), 20–26. https://doi.org/10.15587/1729-4061.2020.205107
4. Brunetkin, O., Beglov, K., Brunetkin, V., Maksymov, O., Maksymova, O., Havaliukh, O. et al. (2020). Construction of a method for representing an approximation model of an object as a set of linear differential models. Eastern-European Journal of Enterprise Technologies, 6 (2 (108)), 66–73. https://doi.org/10.15587/1729-4061.2020.220326
5. Brunetkin, O., Maksymov, M., Brunetkin, V., Maksymov, O., Dobrynin, Y., Kuzmenko, V. et al. (2021). Development of the model and the method for determining the influence of the temperature of gunpowder gases in the gun barrel for explaining visualize of free carbon at shot. Eastern-European Journal of Enterprise Technologies, 4 (1 (112)), 41–53. https://doi.org/10.15587/1729-4061.2021.239150
6. Brunetkin, O., Maksymov, M., Dobrynin, Y., Demydenko, V., Sidelnykov, O. (2024). Development of a process model for determining the composition and energy characteristics of a pyrotechnic mixture using the library method. EUREKA: Physics and Engineering, 5, 99–112. https://doi.org/10.21303/2461-4262.2024.003453
7. Brunetkin, O., Dobrynin, Y., Maksymenko, A., Maksymova, O., Alyokhina, S. (2020). Inverse problem of the composition determination of combustion products for gaseous hydrocarbon fuel. Computational Thermal Sciences:

An International Journal, 12 (6), 477–489. https://doi.org/10.1615/computthermalscien.2020034878
8. Maksymov, M. V., Brunetkin, O. I., Beglov, K. V., Alyokhina, S. V., Butenko, O. V. (2022). Automatic Control for the Slow Pyrolysis of Organic Materials with Variable Composition. Advanced Control Systems. River Publishers, 397–434. https://doi.org/10.1201/9781003337010-16
9. Brunetkin, A., Beglov, K., Maksimov, M. Ulitskaja, E. (2021). Model and method of controlled pyrolysis of organic sub-stances of variable composition. International Scientific Technical Journal "Problems of Control and Informatics", 66 (1), 134–146. https://doi.org/10.34229/1028-0979-2021-1-12
10. Brunetkin, O., Sidelnykov, O., Maksymov, M., Dobrynin, Y. (2025). Improving the model for determining the composition of gunpowder gases during thermal destruction of gunpowder in a limited volume space. Eastern-European Journal of Enterprise Technologies, 3 (6 (135)), 35–45. https://doi.org/10.15587/1729-4061.2025.330654
11. Katsev, I. (2018). Evaluation method of the artillery's effectiveness against unitary target. International Scientific Journal "Security & Future", 2 (4), 196–198. Available at: https://stumejournals.com/journals/confsec/2018/4/196.full.pdf
12. Field Manual 3-09 Field Artillery Operations and Fire Support (2014). Washington: Department of the Army, 4–12. Available at: https://www.scribd.com/document/248059115/FM-3-09-Field-Artillery-Operations-and-Fire-Support
13. ADLER II Artillery Computer Network Delivered to Troops. Army Technology. Available at: https://www.army-technology.com/contractors/data/kulr-technology-partners-us-army/pressreleases/press15/
14. Field Manual 3-09.22 Tactics, Techniques, and Procedures for Corps Artillery, Division Artillery, and Field Artillery Brigade Operations (2001). Washington: Department of the Army. Available at: https://www.globalsecurity.org/military/library/policy/army/fm/3-09-22/index.html
15. Dobrynin, Y., Maksymov, M., Boltenkov, V. (2020). Development of a method for determining the wear of artillery barrels by acoustic fields of shots. Eastern-European Journal of Enterprise Technologies, 3 (5 (105)), 6–18. https://doi.org/10.15587/1729-4061.2020.206114
16. Dobrynin, Ye., Davydov, V. (2020). Simulation model of the information technology for the technical diagnosis of the impulse heat machine. Odes'kyi Politechnichnyi Universytet Pratsi, 2 (61), 95–103. https://doi.org/10.15276/opu.2.61.2020.11
17. Dobrynin, Y. V., Boltenkov, V. O., Maksymov, M. V. (2020). Information technology for automated assessment of the artillery barrels wear based on SVM

classifier. Applied Aspects of Information Technology, 3 (3), 117–132. https://doi.org/10.15276/aait.03.2020.1
18. Tkachyk, P. P., Budaretskiy, Y. I., Shchavinskiy, Y. V., Prokopenko, V. V. (2015). Influence of automation control units and artillery fire on the effectiveness of its application. Military Technical Collection, 12, 75–82. https://doi.org/10.33577/2312-4458.12.2015.75-82
19. Maksymov, M. V., Brunetkin, O. I., Lysiuk, O. V., Tarakhtii, O. S. (2019). Pat. No. 120216 UA. Ustanovka dlia vyznachennia skladu horiuchoho hazu pry yoho spaliuvanni. No. a201712785; declared: 22.12.2017; published: 25.10.2019, Bul. No. 20.
20. Brunetkin, O., Dobrynin, Y., Maksymenko, A., Maksymova, O., Alyokhina, S. (2020). Model and method of conditional formula determination of oxygen-containing hydrocarbon fuel in combustion. Energetika, 66 (1). https://doi.org/10.6001/energetika.v66i1.4298
21. Dobrynin, Y. V., Boltenkov, V. O., Kuzmenko, V. V., Maksymov, O. M. (2022). Development of a universal binary classifier of the state of artillery barrels by the physical fields of shots. Applied Aspects of Information Technology, 5 (4), 289–302. https://doi.org/10.15276/aait.05.2022.19
22. Brunetkin, O., Kuzmenko, V., Soloviova, O. (2022). Mathematical model of energy transformation processes in barrel system for determining shooting performance. Energy Engineering and Control Systems, 8 (1), 28–39. https://doi.org/10.23939/jeecs2022.01.028
23. Maksymov, M. V., Boltenkov, V. O., Gultsov, P. S., Maksymov, O. M. (2023). Verification of artillery fire under the influence of random disturbances for the computer game ARMA 3. Applied Aspects of Information Technology, 6 (4), 362–375. https://doi.org/10.15276/aait.06.2023.24
24. Maksymova, O. B., Boltenkov, V. O., Maksymov, M. V., Gultsov, P. S., Maksymov, O. M. (2023). Development and optimization of simulation models and methods for controlling virtual artillery units in game scenarios. Herald of Advanced Information Technology, 6 (4), 320–337. https://doi.org/10.15276/hait.06.2023.21
25. Maksymova, O., Boltyonkov, V., Gultsov, P., Maksymov, O. (2023). Improvement of the model and method of artillery installation target damage control with minimal combat capability loss. Odes'kyi Politechnichnyi Universytet Pratsi, 2 (68), 98–115. https://doi.org/10.15276/opu.2.68.2023.11
26. Maksymov, M. V., Hultsov, P. S., Boltyonkov, V. O., Maksymov, O. M. (2024). Method for verification of artillery firing under the influence of random disturbances. Maritime Security and Defense, 1, 36–49. https://doi.org/10.32782/msd/2024.1/05

27. Tarakhtiy, O. S., Gultsov, P. S., Maksymov, O. M. (2024). Udoskonalennia metodu i modeli keruvannia boiovoiu zdatnistiu artyleriiskoi harmaty. Proceedings of the 5th International Scientific and Practical Conference. Tokyo: CPN Publishing Group, 256–261. Available at: https://sci-conf.com.ua/v-mizhnarodna-naukovo-praktichna-konferentsiya-topical-aspects-of-modern-scientific-research-25-27-01-2024-tokio-yaponiya-arhiv
28. Tarakhtiy, O. S., Hultsov, P. S., Maksymov, O. M. (2024). Udoskonalennia metodu i modeli keruvannia boiovoiu zdatnisttiu artyleriiskoi harmaty. European Congress of Scientific Achievements. Proceedings of the 1st International Scientific and Practical Conference. Barcelona: Barca Academy Publishing, 120–125. Available at: https://sci-conf.com.ua/wp-content/uploads/2024/01/EUROPEAN-CONGRESS-OF-SCIENTIFIC-ACHIEVEMENTS-29-31.01.24.pdf

CHAPTER 3

Model of free carbon formation when firing an artillery piece

Oleksandr Brunetkin
Pavlo Gultsov
Oleksandr Sidelnykov

Abstract

A phenomenon present in almost every shot, yet rarely addressed or explained in the literature, has been identified. It manifests itself in the muzzle discharge in the form of a certain volume of soot. The Boudouard thermochemical reaction (also referred to in some sources as the Boudouard-Bell reaction carbon monoxide disproportionation), which accounts for soot formation in propellant gases during firing, has been identified. The conditions under which this reaction can occur are discussed. A distinctive feature of this reaction is the formation of a condensed carbon phase during the firing process after gasification of the propellant charge.

Based on the physicochemical processes governing the expansion of propellant gases in the gun barrel, a mathematical model is proposed that makes it possible to estimate the temperature distribution during firing. The initial model is constructed using generally accepted assumptions. The modeling results obtained on its basis can therefore only be regarded as approximate. For this reason, the method relies on simple calculations, making it unnecessary to employ high-performance computing equipment.

A simulation of the temperature distribution of propellant gases along the barrel, between the chamber and the moving projectile, was carried out using a model system similar to the 2A38 artillery system. The possibility of varying the extent of the Boudouard-Bell reaction zone (the soot formation zone) depending on the initial parameters is demonstrated. The use of both fresh and degraded propellant charges was modeled. Full and reduced charges were considered. The simulation results reveal the cause of possible initiation of a secondary muzzle flash, both from the frontal side and from the side of the muzzle brake.

Keywords

Gun, propellant gases, temperature distribution, disproportionation reaction, soot, muzzle flash.

© The Author(s) of individual chapters, 2026 DOI: 10.21303/978-9908-8450-1-2.ch3

3.1 The role of muzzle discharge in assessing the parameters of internal ballistics processes

In many cases, when solving internal ballistics problems, the thermodestruction (thermal (thermochemical) decomposition) process of a propellant charge is considered under the following assumptions:

– a lumped-parameter model of the thermochemical transformation of the propellant charge is used;

– once formed, the composition of the propellant gases (PG) is assumed to remain unchanged ("frozen") throughout the entire firing cycle;

– the temperature and pressure of the propellant gases are treated as time-dependent variables but are assumed to be spatially uniform over the entire length of the bore behind the projectile at any given moment.

These assumptions are restrictive, yet well balanced for the model employed. Such a model makes it possible to identify general trends and the order of magnitude of the parameters governing internal ballistics processes. Subsequently, the obtained values are refined using empirical correction coefficients.

This approach is effective when the composition of the nitrocellulose (NC) propellant is known and specified. However, during storage, propellants undergo changes in composition and energetic characteristics (degradation). In peacetime conditions, this issue is addressed through laboratory monitoring of propellant condition and their disposal when necessary. Under conditions of intensive use (combat conditions), propellants may be supplied from various storage depots or even from different countries with uncontrolled storage conditions. As a result, batches of charges may be encountered, which characteristics would require disposal in peacetime. At the same time, instrumental inspection of such large volumes of propellants, especially under field conditions, is impracticable.

Changes in propellant composition, often uncontrolled, lead to variations in the parameters of internal ballistics processes. This, in turn, results in reduced firing accuracy, the need to expend a greater number of projectiles to engage a target, increased wear of materiel, and decreased combat survivability of a unit due to longer exposure time at firing positions [1].

Muzzle discharge and the subsequent muzzle flash are among the effects accompanying a shot. These phenomena are usually attributed to external ballistics, more precisely to muzzle (transitional) phenomena. In classical ballistics, muzzle discharge is often identified as a transitional region between internal and external ballistics. It can therefore be assumed that its features and characteristics are shaped by internal ballistics processes, representing a manifestation

of the thermodestruction of the propellant and reflecting the specific nature of these processes.

Muzzle discharge and muzzle flash can be recorded by video with minimal expenditure of time and resources under virtually any conditions, including combat. Analysis of their features and characteristics may serve as a basis for analyzing and assessing the parameters of internal ballistics processes and, ultimately, for evaluating the condition of propellant charges.

3.2 Characteristics of the muzzle discharge

Nitrocellulose propellants are generally classified as smokeless powders. Laboratory experiments record only small amounts of condensed-phase products during and after the thermal decomposition of nitrocellulose propellants. In the available literature, the presence of such products is mainly attributed to various additives contained in the propellant formulations. However, frame-by-frame imaging of the firing process (**Fig. 3.1–3.3**) reveals a different picture. In the muzzle discharge, prior to the onset of the muzzle flash, a substantial amount of soot is observed. The presence of soot in the discharge is the result of reactions occurring inside the barrel during the firing process. Nevertheless, a well-substantiated and generally accepted explanation of these reactions is absent from the available literature.

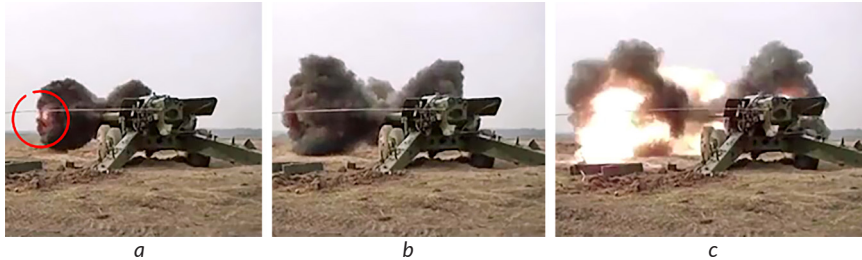

a *b* *c*

Fig. 3.1 Stages in the development of the muzzle discharge of a 152-mm 2A36 gun shot, recorded from ground level: *a* – initial stage characterized by the ejection of soot lobes from the muzzle with the onset of ignition inside one of the lobes; *b* – intermediate stage showing significant expansion of the soot lobes with weak internal combustion traces; *c* – final stage with further enlargement of the discharge cloud and extensive visible flaming within the soot formation

The composition of a propellant and its energetic characteristics can be inferred from the composition of its thermal decomposition products-namely, the propellant

gases (PG). However, even the qualitative composition of PG is reported inconsistently across different sources. Most nitrocellulose (NC) propellants are characterized by a negative oxygen balance. Under these conditions, it remains unclear which compounds are formed in the PG and in what proportions the oxygen contained in the NC propellant participates in their formation.

a *b* *c*

Fig. 3.2 Stages in the development of the muzzle discharge of a 152-mm 2A36 gun shot, recorded from an elevated vantage point: *a* – initial stage showing a three-lobed soot discharge (left, right, and forward lobes) with the onset of ignition inside the lobes; *b* – intermediate stage characterized by full involvement of the discharge cloud in visible flaming; *c* – final stage where the soot clouds are observed at a considerable distance from the muzzle during burnout, while a lighter-colored gaseous jet emerges from the barrel

a *b*

Fig. 3.3 Examples illustrating the presence of soot in the muzzle discharge: *a*, *b* – intermediate combustion phases of soot clouds recorded between the onset of ignition and full involvement of the discharge in flame

Thus, a number of sources, for example [2], assert that PG consists predominantly of gaseous reaction products in the form of vapors of H_2O, CO, CO_2, H_2, and N_2. This description corresponds to the Kistiakowsky-Wilson rule. A negative oxygen balance indeed favors the formation of free hydrogen. However, such an assumption is not supported by the composition of the products of combustion and detonation of nitrated high-energy materials. In particular, studies [3, 4] report the

presence of soot in explosion products. In [5], not only is the presence of soot in the muzzle exhaust documented, but an attempt is also made to quantify it in the course of investigating the muzzle flash. At the same time, the mechanisms responsible for its formation are not discussed.

In [6], a modified Kistiakowsky-Wilson rule is proposed. According to this rule, oxygen from nitro compounds first completely binds hydrogen atoms to form H_2O vapor. It then binds carbon atoms to form CO, and only thereafter does the remaining oxygen further oxidize CO to CO_2. On this basis, the appearance of free carbon in PG in the form of soot can be explained. However, under such a scheme and with a negative oxygen balance, there is insufficient oxygen even to bind all carbon atoms to CO; the formation of H_2 and appreciable amounts of CO_2 is not accounted for.

Thus, the composition of PG corresponds neither to the original nor to the modified Kistiakowsky-Wilson rule, nor to the composition of PG obtained under laboratory conditions. In addition to CO and H_2O vapor, PG contains CO_2, H_2, and as shown in **Fig. 3.1–3.3** – free carbon in the form of soot.

An analysis of **Fig. 3.1–3.3** also makes it possible to identify other features of the muzzle exhaust and muzzle flash and, consequently, potential characteristics of the internal ballistic processes of propellant thermal decomposition:

– in [7], the muzzle flash is attributed to the ignition in air of combustible PG components, namely CO and H_2. The initiating factor is assumed to be the muzzle blast, which causes additional heating of the PG. Given the finite spatial extent of the blast, ignition would be expected to occur over an extended surface. However, the images in **Fig. 3.1**, ***a*** and **Fig. 3.2**, ***a*** demonstrate point-like ignition at the leading front of the exhaust plume, in its central region (outlined in red). At the same time, the photograph in **Fig. 3.3**, ***b*** indicates the possibility of PG ignition on the opposite side of the muzzle exhaust – near the muzzle brake – which cannot be explained by the action of the muzzle blast;

– within the framework of the PG composition discussed above, the intense luminosity of the muzzle flash can be explained by soot combustion. Combustion of gaseous H_2 and CO in air is practically colorless. In **Fig. 3.2**, ***b***, against the bright background of burning soot, a low-contrast gaseous jet can be distinguished (outlined in red). It is located in the leading part of the exhaust plume. A similar jet can also be identified in the trailing part of the muzzle exhaust (**Fig. 3.2**, ***c***, outlined in yellow). The inhomogeneous structure of the muzzle exhaust may be caused by longitudinal nonuniformity in the composition of PG. This, in turn, may indicate a similar nonuniformity in the PG composition along the barrel length at the moment the projectile exits the muzzle.

3.3 Possible causes of the specific features of the muzzle exhaust as a consequence of internal ballistics processes

In the previous section, the following characteristic features of the muzzle exhaust were identified:

– the presence of a significant amount of condensed carbon (soot);

– the possibility of muzzle flash initiation in various regions of the muzzle exhaust;

– heterogeneity of the muzzle exhaust structure with respect to the composition of the PG.

When the muzzle exhaust is considered as a transitional region, its distinctive features should be interpreted as a consequence of internal ballistics processes associated with the thermal decomposition of NC propellant. However, a lumped-parameter model of these processes does not allow the aforementioned features to be adequately explained.

At present, computational resources make it possible to solve internal ballistics problems using distributed-parameter formulations. Increasing model complexity may potentially improve the accuracy and reliability of the results. At the same time, model modification should not be limited solely to increasing computational complexity, but should also incorporate more subtle physical and chemical effects. The following studies may be cited as illustrative examples. Thus, in [8] the solution is obtained within a one-dimensional formulation, whereas in [9] a three-dimensional formulation is employed. In both studies, only the motion of propellant gases inside the barrel is considered. Their composition is assumed to remain constant during the motion. Despite the significantly higher computational complexity of the approach used in [9], the results obtained in both studies are comparable. In another case, the article [10] investigates the muzzle flash process. A model is employed that describes gas-dynamic processes in a two-dimensional formulation, as well as ignition and combustion of propellant gases in atmospheric oxygen. The reversibility of chemical reactions is taken into account, and reaction rates are calculated. It is correctly noted that the characteristics of the muzzle exhaust and muzzle flash depend on the parameters of internal ballistics processes. However, despite the detailed modeling of the exhaust and flash, the internal ballistics processes themselves are treated by neglecting multicomponent effects and chemical reactions. As a result, the possibility of free carbon formation during firing is not considered, nor is its influence on the muzzle flash process taken into account.

In many cases, chemical reactions of NC propellant thermal decomposition during firing are considered from the standpoint of chemical equilibrium. This approach is justified by the high temperatures and pressures at which these processes

occur. However, significant variations of these parameters during the firing process – both in time and along the barrel length at any given moment – may give rise to reversible chemical reactions between the formed components of the propellant gases. For example, the computational results presented in [1] demonstrate that, at certain moments in time, temperature differences along the propellant gas column may reach 500 K or more.

The equilibrium composition calculation method makes it possible to determine the relative proportions of the components constituting the propellant gases and their temperature, but not the actual list of species itself. The set of possible reaction products is specified prior to the calculation. Thus, in [11], results of propellant gas composition calculations based on three different models are presented. Each model assumes a different composition of propellant gases. Some components are common to all models; however, their calculated quantities for the same propellant may differ by several times depending on the model used. Among the considered approaches, the Kamlet-Jacobs model included free carbon and carbon dioxide (CO_2) in the propellant gas composition, but did not account for the presence of carbon monoxide (CO). As a result, calculations based on this model for various propellant formulations yielded free carbon contents of 20–30%, which clearly contradicts practical ballistic applications of propellant mixtures. Moreover, the calculated combustion products do not contain hydrogen or other combustible species, which also contradicts the flame observed when combustion products exit the barrel. These results indicate the necessity of an adequate selection of the propellant gas composition to enable correct calculation of their quantities.

The article [12] presents results of equilibrium composition calculations for the reaction products of methane (CH_4) with oxygen (O_2) under oxygen-deficient conditions (oxidizer excess coefficient $\alpha = 0.6$, corresponding to a negative oxygen balance). The list of possible reaction products included H_2O, H_2, CO_2, CO, and free carbon (C_{crb}). The equilibrium composition of reaction products corresponding to temperatures ranging from the combustion temperature (~1780 K) down to 500 K was analyzed. A characteristic feature is noted in [12]. At the combustion temperature, free carbon is not detected. However, as the temperature decreases, starting from approximately 1300–1200 K, the possibility of free carbon formation is shown. Simultaneously, the amount of CO decreases while the amount of CO_2 increases. Beginning at temperatures of approximately 700 K, the calculated results no longer indicate the presence of CO. Under normal ambient conditions, such behavior is not observed. A mixture of methane (CH_4) and oxygen (O_2) under normal conditions remains stable in the absence of external influences, and free

carbon is not formed. This is explained by the extremely low reaction rate, despite the thermodynamic possibility of the reaction.

A chemical reaction exhibiting similar characteristics is well known. This is the Boudouard-Bell reaction, representing the disproportionation of carbon monoxide (CO) into free carbon

$$2 \cdot CO \leftrightarrow C\downarrow + CO_2 + Q. \tag{3.1}$$

This reaction is characterized by reversibility. At elevated temperatures up to approximately 1300 K, the equilibrium is almost completely shifted toward CO formation. Nevertheless, the reverse reaction remains exothermic. At the same time, equilibrium calculations indicate the formation of a certain amount of free carbon, which is associated with the endergonic nature of CO disproportionation. At temperatures of about 400 K, the thermodynamic equilibrium of the Boudouard-Bell reaction is shifted toward the formation of CO_2 and C. However, under normal or near-normal conditions, CO remains stable due to the low rate of the disproportionation reaction.

During firing, by the moment the projectile exits the barrel, the temperature of the propellant gases decreases to values of approximately 1000 K, corresponding to a shift of the thermodynamic equilibrium of the disproportionation reaction toward the formation of condensed carbon. At the same time, a high pressure of the propellant gases is maintained, which may reach approximately 50 MPa. In accordance with Le Chatelier's principle, high pressure favors a shift of the equilibrium toward the formation of a condensed phase. The disproportionation reaction of CO is of second order. In this case, at identical propellant-gas temperatures, the rate of formation of condensed carbon in the barrel system, compared with laboratory conditions (0.1 MPa), increases by a factor of about $(50/0.1)^2$, i.e., approximately 250,000. This estimate should be regarded as an order-of-magnitude illustration rather than a detailed kinetic description.

It is necessary to consider the possible influence of the process described by reaction (3.1) on changes in the pressure of the propellant gases in the barrel channel as the projectile moves. After completion of the thermodestruction of the propellant charge, the barrel volume behind the projectile continues to increase as it travels, while the amount of propellant gas does not increase. This stage is characterized by an accelerated decrease in propellant-gas pressure. However, under these conditions, prerequisites arise for reaction (3.1) to proceed. Its result is a twofold reduction in the volume of the reacting fraction of the propellant gases, which may locally affect pressure evolution.

3.4 Simplified one-dimensional model of internal ballistics processes

3.4.1 Composition of propellant gases

The structure of the muzzle blast and muzzle flash makes it possible to assess the nature of the distribution of PG parameters along the barrel length at the moment the projectile exits the muzzle. Accordingly, the current composition and energy characteristics of the propellant charge can be estimated from the PG parameters. Such an assessment may be carried out using the library-based method described in [12, 13]. A distinctive feature of this method is the high speed of evaluating the state of the propellant charge. However, this requires the prior creation of a database that reflects the possible values of PG parameters as functions of varying propellant charge compositions and energy characteristics. This, in turn, necessitates solving the internal ballistics problem a very large number of times (hundreds of millions or more). In doing so, the PG parameters along the barrel length must be obtained in a distributed form. Modern computational resources make it possible to perform such calculations within a reasonable time frame. Nevertheless, to adequately represent the PG parameter values, the employed model should be as simple as possible.

The development of such a model is a multistage process involving an assessment of the assumptions adopted at each stage, with a gradual increase in model complexity up to the required level. At the initial stage, it is necessary to evaluate the feasibility of adequately reproducing the character of variation of PG parameters for the chosen overall model structure and computational strategy under the most permissive assumptions.

To assess the possible equilibrium composition of propellant gases at different temperatures, calculations were performed for a propellant charge, which composition is given in [14] and presented in **Table 3.1**.

Table 3.1 Initial composition of the NC propellant charge

Component	Substance	%	Molecular formula
Energetic base	Nitrocellulose	96.0	$C_6H_{7.7}N_{2.3}O_{9.6}$
Plasticizer	Ethanol	0.5	C_2H_6O
	Diethyl ether	0.5	$C_4H_{10}O$
Chemical stability stabilizer	Diphenylamine	1.0	$C_{12}H_{11}N$
Impurity substances	Water (moisture)	2.0	H_2O

Based on these data, the gross formula (molecular formula) of the propellant charge was calculated. The formula is expressed relative to a single carbon atom

$$C_1H_{1.44}N_{0.37}O_{1.57}. \tag{3.2}$$

The determination of the propellant gases' composition is based on solving a system of equations that includes the law of mass action, the law of conservation of matter, and Dalton's law. The enthalpy of formation is also used for both the propellant charge and the components of the propellant gases. The calculation is based on equating the enthalpy of the propellant to the sum of the enthalpies of formation of the propellant gas components, taking their temperature into account.

A distinctive feature of this approach is the specific form of the mass-action equations. The equations are formulated based on the formation reactions of possible propellant gas components from elementary chemical substances [15]. For example:

$$\begin{aligned} &H_2O \rightleftarrows 2\cdot H + O, \\ &CO_2 \rightleftarrows C + 2\cdot O. \end{aligned} \tag{3.3}$$

This form of representation is universal. It allows for the construction of a closed system of equations based on a list of substances that may be present in the mixture. In the established models describing the firing process, the composition of the propellant gases for the propellant charge is determined based on the following list of constituent components

$$H_2O, CO_2, CO, H_2, CH_4, N_2. \tag{3.4}$$

To account for the potential formation of soot, this list is supplemented with an additional component, denoted as C_{crb} (finely dispersed condensed carbon phase). The consideration of carbon in the propellant gases is a specific feature of the model used in the calculations. The method for calculating the thermodynamic parameters of the gaseous mixture in the presence of a condensed phase is given in [15].

The equilibrium composition of the propellant gases at various temperatures is shown in **Fig. 3.4**.

From the calculation results presented in the graphs (**Fig. 3.4**), it follows that the molar concentrations of the propellant gas components remain almost constant over a wide range of temperatures during their expansion in the firing process. However, as noted in [12], at temperatures of 1200–1300 K and below, the quantitative composition of the propellant gas components changes. Condensed

carbon appears. The amounts of not only carbon-containing elements but also all other elements (except for nitrogen, N_2) are altered.

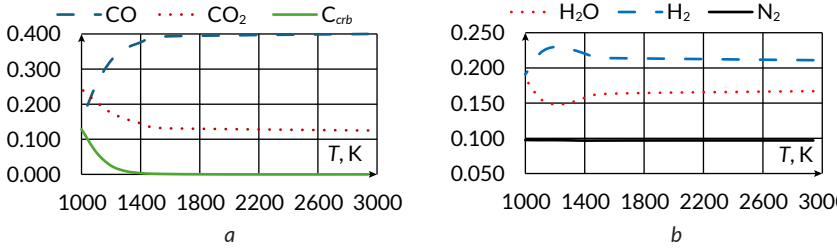

Fig. 3.4 Molar concentrations of propellant gas components as a function of temperature *T*: *a* – carbon-containing components; *b* – carbon-free components

3.4.2 Method for determining propellant gas temperature along the barrel during firing for a distributed-parameter model

At the first stage of developing a model for internal ballistics processes, the values of parameters governing the gas-dynamic processes (pressure and temperature) occurring in the PG along the barrel length at each moment of the shot are averaged. This procedure simplifies the solution. The justification for its use lies in the minor influence of deviations of pressure and temperature from their mean values on the processes under consideration.

For instance, in [16], calculations were performed for a 100 mm, caliber gun with a chamber length of $l_c = 1\,\text{m}$ and a barrel length of $l_d = 5\,\text{m}$. The charge mass varied in the range of 2.5–45 kg. Pressure values were determined at the breech face and at the base of the projectile as it passed the muzzle. For all calculations, the deviation of pressure at the base of the projectile from that at the breech face ranged from 6% to 53%. Deviations of pressure values in different parts of the space behind the moving projectile can affect the accuracy of determining the projectile velocity, but have practically no effect on the composition of the propellant gases. High pressures, regardless of their magnitude, under high PG temperatures imply an equilibrium composition.

Many sources do not use data on the distribution of PG temperature along the barrel during projectile motion. When using models that do not account for the formation of a condensed phase, such information is unnecessary. It is assumed that, during the shot, within the temperature range of the PG, their composition

remains practically unchanged. This is confirmed by the calculation results shown in **Fig. 3.4**. In the range from the combustion temperature (2940 K) to the temperature at which a significant amount of soot begins to form (~1400 K), the PG composition remains nearly constant.

The temporal behavior of the muzzle blast (**Fig. 3.1**–**3.3**) indicates not only the potential for condensed phase formation but also the non-uniformity of this process along the barrel. To identify the principal possibility of conditions supporting the disproportionation reaction of carbon monoxide, modeling of the PG temperature distribution along the barrel during the shot is necessary. Let's consider the model and the projectile firing process. Let's introduce a set of assumptions corresponding to the first stage of model development:

– the burn rate of the propellant charge depends solely on pressure;

– the propellant volume is neglected;

– PG pressure is uniform (averaged) at all points between the breech face and the base of the projectile;

– during projectile motion, PG movement along the barrel is one-dimensional, with no mixing of newly formed gases with previously generated PG;

– the PG expansion process is adiabatic, with a known adiabatic index;

– backpressure in front of the projectile is neglected;

– energy expenditures for processes other than projectile acceleration are accounted for using a coefficient that increases the projectile mass in calculations (a fictitious projectile mass);

– PG is considered an ideal gas mixture, and covolume effects are neglected.

To account for the PG temperature distribution along the barrel, the mathematical model (MM) must be expressed in partial differential form, which usually requires numerical solution methods. For preliminary assessment of temperature distribution under the adopted assumptions, this approach is impractical. The following approach has been proposed to describe the firing process:

– projectile motion along the barrel is roughly divided into two stages: during propellant combustion and after its completion;

– the propellant burns in discrete portions of equal mass;

– the pressure at which the next portion of the charge burns is assumed constant and equal to the pressure after the previous step of PG expansion. This pressure determines the burning time t_i of the current portion, which also defines the time step for the calculation. The time interval for burning each portion (and thus for the calculation step) is variable depending on the current pressure;

– formation of each new portion of PG mass m_i occurs without affecting the existing PG (e.g., outside the barrel). This step corresponds to the assumption of

neglecting the propellant volume, and thus the change in pre-chamber volume as the propellant burns;

– the newly formed PG portion enters the chamber instantly through its end surface (**Fig. 3.5**). The pressure rises instantaneously, forming a new value p_i, determined by the added PG, as well as the volume ($w_0, w_1, ..., w_{i-1}$) and pressure of the pre-existing PG;

– during the time interval t_i (duration of the current calculation step), PG expansion and projectile acceleration occur (without additional PG input). At the end of this interval, the PG pressure is determined, which is used to calculate the burning time of the next portion of the propellant in the following time step;

– after the propellant is fully burned, the expansion of PG and projectile acceleration are calculated until the projectile exits the barrel.

Fig. 3.5 Diagram of the formation of the incoming gas fraction at the current calculation step

At this stage, the PG temperature distribution along the barrel during the shot is estimated. Average values of certain quantities, corresponding to modern barrel systems, are used in the calculation relationships.

In describing propellant properties, their energetic characteristic is conventionally expressed as their strength *f*. At the same time, the calculation is based on the enthalpy of the NC thermal decomposition reaction. Let's estimate the relationship between these quantities. Assume: the combustion process is isoenthalpic (constant-enthalpy process); the gas-phase process is adiabatic. According to the adopted assumptions

$$I_{sp}^{G} = I_{sp}^{PG} = \frac{\gamma}{\gamma - 1} \cdot f, \tag{3.5}$$

where I_{sp}^{G} – the specific enthalpy of gunpowder; I_{sp}^{PG} – the specific enthalpy of gunpowder gases; γ – the adiabatic index; f – the propellant force.

Let's assume $\gamma = 1.2$, $f = 950$ kJ/kg. In this case $I_{sp}^{G} = 5700$ kJ/kg. Further calculations were performed taking these values into account:

Step 1. From equation (3.5), the temperature of the propellant gas (PG) is determined, and from the equation of state, the amount of propellant charge required to

generate the forcing pressure in the breech chamber is calculated. The magnitude of the forcing pressure, the volume of the breech chamber (excluding the charge volume), and the adiabatic index are specified. Based on the fraction of the charge burned, the enthalpy of the considered PG volume is determined. The remaining mass of the propellant charge is calculated, and the number of calculation steps is selected. The mass of the portion of the charge m_i, which combustion is considered in a single calculation step, is determined. All portions have equal masses. The forcing pressure serves as the initial pressure for the next calculation step and determines the burning rate of the corresponding portion of the propellant charge. This PG volume is hereinafter denoted as w_0 (**Fig. 3.5**).

Step 2. Using the final pressure obtained in Step 1, the burning time t_i of the portion m_i of the propellant charge is determined. A linear burning law $u_1 = u_0 \cdot p$ and a constant burning surface area F are assumed. Accordingly

$$m_i = (u_0 \cdot p) \cdot F \cdot t_i \Rightarrow t_i = \frac{m_i}{(u_0 \cdot F) \cdot p}. \tag{3.6}$$

The method for determining the expression in parentheses is described below.

Step 3. The generated portion of PG is introduced (instantaneously) into the breech chamber without changing its volume. According to the current calculation step number i, this portion of PG is hereinafter denoted as w_i. The enthalpy (I_i^n) of the PG is calculated as the sum of the enthalpy from the end of the previous calculation step and that contributed by the current portion. According to

$$I_i^n = \frac{\gamma}{\gamma - 1} \cdot P_i^n \cdot W_i^n \Rightarrow P_i^n = \frac{\gamma - 1}{\gamma} \cdot \frac{I_i^n}{W_i^n} \tag{3.7}$$

the mixture pressure (P_i^n) at the beginning of the calculation step is determined. Considering the assumption that the PG volumes from the respective calculation steps do not mix, their updated values are calculated.

Step 4. Expansion of the PG and acceleration of the projectile during the current calculation step occur over the time t_i determined in Step 2 and are described by the relation

$$\varphi M \frac{d^2x}{dt^2} = P \cdot S, \tag{3.8}$$

here M – the projectile mass; φ – the coefficient accounting for the effective mass of the projectile; x – the length of the breech chamber; P – the PG pressure; and S – the cross-sectional area of the barrel.

The value of P is determined from the relation describing the adiabatic expansion of the gas

$$(P_i^n)\cdot(W_i^n)^\gamma=(P_i)\cdot(W_i)^\gamma \Rightarrow P_i=(P_i^n)\cdot\left(\frac{W_i^n}{W_i}\right)^\gamma, \tag{3.9}$$

where P_i^n, W_i^n – the pressure and volume of the breech chamber at the initial moment of the calculation step (corresponding to the values at the end of the previous step); and P_i, W_i – the pressure and volume at the current moment of the calculation.

Taking into account $W_i = S \cdot x_i$ and equation (3.9), expression (3.8) can be rewritten as

$$\frac{d^2x}{dt^2}-\frac{r}{(x)^\gamma}=0, \text{ where } r=\frac{P_i^n\cdot S\cdot(x_i^n)^\gamma}{\varphi\cdot M}, \tag{3.10}$$

here x_i^n – denotes the length of the projectile space at the initial moment of the calculation step.

Let's linearize the second term of equation (3.10) at the point x_i^n. As initial conditions, it is possible to use the values of x_i^n and the projectile velocity v_i^n at the initial moment of the current calculation step (the final velocity from the previous calculation step). Assuming, as before, $\gamma = 1.2$, the solution of (3.10) can be expressed as

$$x(t)=\frac{v^n}{\sqrt{d_1}}\sin(\sqrt{d_1}\cdot t)-\frac{5}{6}x_i^n\cos(\sqrt{d_1}\cdot t)+\frac{11}{6}x_i^n, \text{ where } d_1=\frac{6r}{5x_i^n}. \tag{3.11}$$

By substituting the value of t_i into this expression, the magnitude of the charge-free space x_i^k at the end of the current calculation step is determined, and from the derivative of (3.11)

$$v=x'(t)=v^n\cos(\sqrt{d_1}\cdot t)+\frac{5}{6}x_i^n\sqrt{d_1}\sin(\sqrt{d_1}\cdot t) \tag{3.12}$$

the velocity of the v_i^k projectile at this instant.

Step 5. Under the assumptions adopted, based on the first law of thermodynamics

$$\Delta U = A. \tag{3.13}$$

Taking into account the adiabatic expansion of the propellant gases and, accordingly, $I = \gamma \cdot U$, it follows from equation (3.13) that by the end of the current computational step

$$I_{res} = I_{com} - \gamma \cdot \varphi M \frac{(v_i^k)^2}{2}, \tag{3.14}$$

here ΔU – the change in the internal energy of the propellant gases expended to perform the work A required to accelerate the projectile with the fictitious mass φM; I_{com} – the total enthalpy introduced with the propellant gases into the behind-the-projectile space; and I_{res} – the residual enthalpy at the end of the current computational step after the work of projectile acceleration has been performed. Equation (3.14) may be regarded as a simplified enthalpy-based analogue of the Résal equation. From the relation

$$I_{res} = \frac{\gamma}{\gamma - 1} \cdot P_i^k \cdot W_i^k \Rightarrow P_i^k = \frac{\gamma - 1}{\gamma} \cdot \frac{I_{res}}{W_i^k} \tag{3.15}$$

the pressure of the propellant gases at the end of the calculation step is determined.

Step 6. If, by the beginning of the next calculation step, the entire propellant charge has not been consumed, proceed to Step 2.

Step 7. The calculation is performed in accordance with the method described in Steps 2–5, but without accounting for the inflow of propellant gases into the behind-the-projectile space. The termination time of the calculation is defined as the instant when the projectile reaches the muzzle.

In the course of the calculation, for each propellant-gas element w_i (**Fig. 3.5**), the current temperature can be determined from the equation of state.

3.4.3 Results of modeling the temperature distribution in the barrel region between the chamber and the moving projectile

For the model system (**Table 3.2**) corresponding to the 2A36 gun, the temperature distribution of the propellant gases along the barrel length during the firing process at various time instants was calculated using the method described in the previous section.

The averaged firing characteristics were selected so that the characteristic terminal parameters of the shot were close to the corresponding terminal parameters of the real system (**Table 3.3**).

As a result of the calculations, it was established that when 0.5 kg of propellant charge is burned with the projectile fixed in the chamber, a pressure of approximately $3.06 \cdot 10^7$ Pa is reached, which is close to the adopted value of the forcing pressure. The subsequent combustion process of the remaining portion of the

charge with a mass of 10.5 kg was approximated using a discrete scheme and divided into 35 computational steps with a mass increment of $\Delta m = m_i = 0.3\,\text{kg}$ at each step.

Table 3.2 Firing parameters of the model artillery system

Name	Symbol	Value
Caliber	d, m	0.152
Barrel cross-sectional area	S, m^2	0.0181
Free volume of the propellant chamber (excluding propellant volume)	W_{KC}, m^3	0.0155
Length of the free volume of the propellant chamber	x_{KC}, m	0.85
Projectile mass	M, kg	46
Propellant mass (reduced charge)	m, kg	11
Specific enthalpy of the propellant	I, J/kg	$5.7 \cdot 10^6$
Adiabatic index	γ	1.2

Table 3.3 Characteristic values

Name	Symbol	Value
Forcing pressure	P_p, Pa	$3 \cdot 10^7$
Projectile velocity (for the reduced charge)	V, m/s	775
Projectile velocity at the end of propellant combustion ($\tilde{V} = 0.8 \cdot V$)	$\tilde{V}$, m/s	620

By adjusting the value of the expression in parentheses in formula (3.6), the calculated velocity values $\tilde{V}$ = 633.5 m/s and V = 774.5 m/s were obtained, which are in satisfactory agreement with the reference data presented in **Table 3.3**. In these calculations, the parameter value $u_0 \cdot F = 8.65 \cdot 10^{-8}$ m^3/s was adopted.

Since, during the calculations, the main reference quantities were reproduced with a high degree of proximity to the specified values, it can be reasonably assumed that the resulting calculated temperature distribution of the propellant gases in the space behind the projectile adequately reflects the actual behavior of the process under consideration.

The graphs presented below show the results of the calculations performed on the basis of the data from **Tables 3.2**, **3.3**. **Fig. 3.6** illustrates the variation of propellant gas pressure, while **Fig. 3.7** presents the temperature distribution in the space behind the projectile for different projectile positions corresponding to the scheme shown in **Fig. 3.5**.

It should be noted that the pressure values in **Fig. 3.6** are referred to a point rigidly attached to the base of the projectile, which explains why the initial section

of the curve does not originate at zero. In this case, the abscissa coordinate is determined by the length of the charge chamber, while the ordinate represents the forcing pressure.

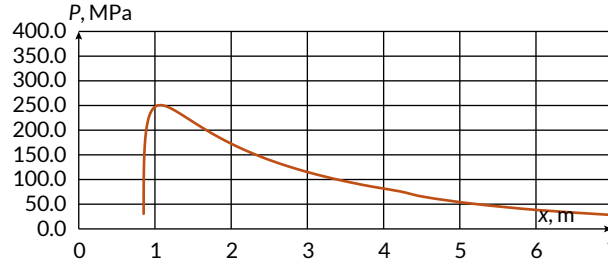

Fig. 3.6 Results of the calculation of the change in the chamber pressure for a reduced charge of fresh propellant in the space behind the projectile
*Source: data from the **Tables 3.2**, **3.3***

In **Fig. 3.7**, the temperature fields are shown for points corresponding to different portions of the propellant gases. All the portions considered have the same mass (0.3 kg in the present calculation); however, due to differences in the instantaneous pressure, their spatial extent in the space behind the projectile is not the same. For this reason, the initial abscissa coordinates of curves 1, 2, and 3 in **Fig. 3.7** do not coincide, which reflects the physical features of the propellant gas distribution during the firing process.

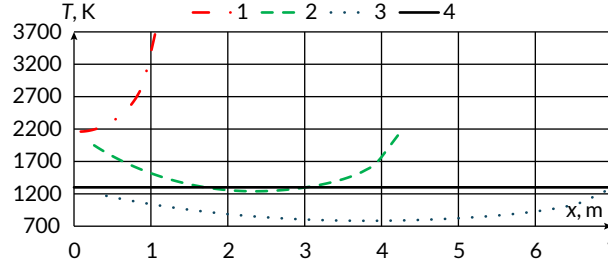

Fig. 3.7 Results of the calculation of changes in the propellant gas temperature for a reduced charge of fresh propellant. Distribution of the propellant gas temperature at various projectile positions: 1 – at the moment of maximum pressure in the space behind the projectile; 2 – at the end of propellant charge combustion; 3 – when the projectile is at the muzzle; 4 – temperature boundary of the Boudouard-Bell reaction
*Source: data from the **Tables 3.2**, **3.3***

Analysis of the results of the performed calculations shows that up to the point of complete combustion of the propellant charge, the conditions for the Boudouard-Bell reaction in the cartridge space are practically absent. This is clearly illustrated by the temperature distributions shown in **Fig. 3.7** (curves 1 and 2): at this stage, the temperature of the propellant gases along the entire length of the cartridge volume predominantly exceeds the lower threshold for the onset of the aforementioned reaction (see also the boundary curve 4 in **Fig. 3.7**). Thus, during the active combustion period of the charge, the formation of a condensed phase in the form of soot is thermodynamically not realized.

A different situation is observed during the subsequent expansion stage of the propellant gases after the completion of charge combustion, which corresponds to the temperature distribution shown in **Fig. 3.7** (curve 3). At this stage, regions are formed in the cartridge space where the temperature drops below the threshold for the carbon monoxide disproportionation reaction, creating conditions for the Boudouard-Bell reaction and, consequently, for the formation of a condensed carbon phase. At the moment the projectile passes the muzzle, the highest temperatures are maintained near the base of the projectile and the base of the chamber.

In the central part of the propellant gas volume, the temperature remains below the threshold value corresponding to the onset of the CO disproportionation reaction for the longest period. It is precisely in this zone that the most intensive formation of the condensed phase is expected, which may have a noticeable effect on the composition of the firing products and the characteristics of the exiting gases.

In order to assess the influence of the degree of degradation of the propellant charge on the magnitude of the main firing parameters, an additional calculation was performed for the propellant with the same gross formula (3.2) but with an 8% reduction in its energy capacity (propellant degradation). Using the adopted specific enthalpy value of I = 5240J/kg and other initial data corresponding to **Tables 3.2**, **3.3**, the calculated dependencies presented in **Fig. 3.8**, **3.9** were obtained. For convenience of comparison, the notations and graphical representations analogous to those shown in **Fig. 3.6**, **3.7** were used.

As a result of the performed calculations, the characteristic velocities of the combustion products were determined, amounting to $\tilde{V} = 618.5$ m/s and V = 750 m/s. A comparison of the obtained values with the previously calculated corresponding values for fresh propellant showed that the difference between them does not exceed 2.5–3.5%, which indicates the preservation of the overall gas-dynamic characteristics of the process and confirms the correctness of the adopted computational model.

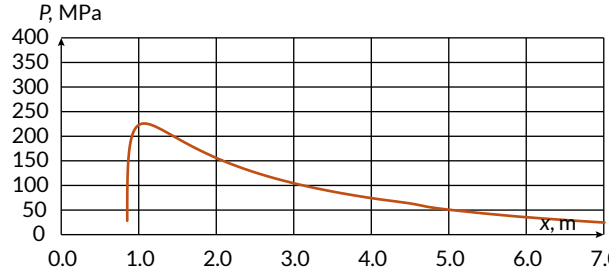

Fig. 3.8 Results of the calculation of the change in the propellant gas pressure for a reduced charge when its energy capacity is decreased by 8% in the space behind the projectile
*Source: data from the **Tables 3.2**, **3.3***

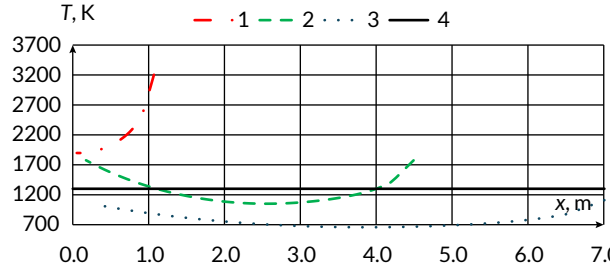

Fig. 3.9 Results of the calculation of changes in the propellant gas temperature for a reduced propellant charge when its energy capacity is decreased by 8%. Distribution of the propellant gas temperature at various projectile positions: 1 – at the moment of maximum pressure in the space behind the projectile; 2 – at the end of propellant charge combustion; 3 – when the projectile is located at the muzzle; 4 – temperature boundary of the Boudouard-Bell reaction
*Source: data from the **Tables 3.2**, **3.3***

The pattern of changes in the pressure and temperature profiles of the combustion products generally remained similar to those shown in **Fig. 3.6**, **3.7**. At the same time, the absolute values of these parameters underwent significant changes. In particular, in the considered case, the expected decrease in maximum pressure is observed. Simultaneously, the temperature levels in most of the combustion products' volume, as well as during the majority of the process duration, remain below the threshold value that determines the possibility of the Boudouard-Bell reaction occurring. This circumstance indicates a reduction in the intensity of this reaction and, consequently, an increased likelihood of the formation of a condensed phase, primarily carbon.

To assess the range of variation in the temperature of the combustion products when varying the charge amount, an additional calculation was performed for a mass of fresh propellant m = 18.4 kg, corresponding to the full charge. The results of this calculation are presented in **Fig. 3.10**, **3.11**. In their presentation, the notations and range of displayed quantities are consistent with those used in **Fig. 3.6**, **3.7**. This ensures a clear comparison and continuity in the analysis of the obtained data.

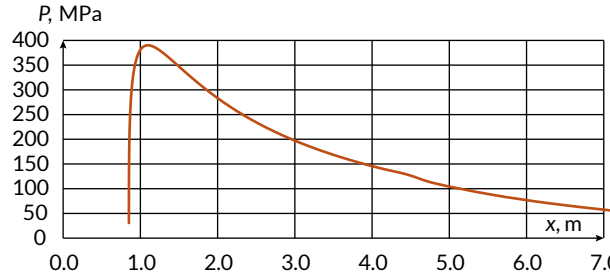

Fig. 3.10 Results of the calculation of the change in the propellant gas pressure for a full charge of fresh propellant in the space behind the projectile
*Source: data from the **Tables 3.2**, **3.3***

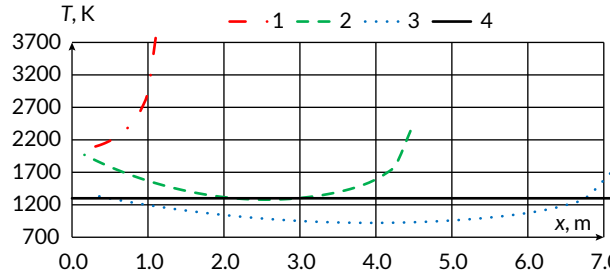

Fig. 3.11 Results of the calculation of the change in the propellant gas temperature for a full charge of fresh propellant. Distribution of the propellant gas temperature at various projectile positions: 1 – at the moment of maximum pressure in the space behind the projectile; 2 – at the end of propellant charge combustion; 3 – when the projectile is at the muzzle; 4 – the temperature boundary of the Boudouard-Bell reaction
*Source: data from the **Tables 3.2**, **3.3***

For the case under consideration, the reference values of the characteristic velocities were taken as V = 945 m/s and $\tilde{V}$ = 756 m/s. The conducted calculations yielded refined values of these parameters, amounting to V = 944 m/s and

$\tilde{V} = 780$ m/s, respectively. The practical coincidence of one of the velocities with the reference value and the moderate deviation of the other indicate satisfactory agreement of the calculated data with the initial assumptions and confirm the robustness of the chosen model for describing the process.

A characteristic feature of the obtained results is that the temperature of the combustion products near the bottom of the charge chamber, as well as in the muzzle region, exceeds the threshold value that determines the possibility of the Boudouard-Bell reaction. This circumstance is of fundamental importance for interpreting the physicochemical processes accompanying the muzzle blast. Under conditions where the temperature exceeds this threshold, the formation of a condensed carbon phase becomes thermodynamically unfavorable, and consequently, the sooty component in the combustion products does not form.

In other words, during the initial and final phases of the muzzle blast, the presence of soot in the ejected combustion products is not expected, which may have a noticeable effect both on the optical characteristics of the muzzle flame and on the overall structure of the gas outflow from the barrel.

3.4.4 What the calculation results show: determination of the ignition point and the shape of the muzzle flash

The considered model of internal ballistics processes is based on a number of fundamental assumptions that allow a significant simplification of the mathematical description of the phenomena taking place, thereby making the model suitable for performing preliminary calculations. In particular, the model employs averaged parameters of the propellant gases, simplified relations for their expansion, and idealized boundary conditions, which undoubtedly limits the strict applicability of the model. Nevertheless, a comparison of the simulation results with known experimental and computational data shows that the obtained dependencies of propellant gas pressure variations along the barrel during a shot do not contradict, either qualitatively or quantitatively, the generally accepted concepts of internal ballistics.

At the same time, an analysis of the thermal regime of the propellant gases revealed a number of features worthy of separate consideration. The nature of the temperature variation of propellant gases along the barrel during a shot proved to be considerably more complex and cannot be described by a monotonic or quasi-linear distribution. The performed calculations showed that, for a significant portion of the shot duration, the propellant gas temperature values in the initial and muzzle regions of the barrel exceed the corresponding values in its central part. Thus, the

temperature field in the barrel exhibits a pronouncedly non-uniform character, with temperature maxima localized in regions different from the geometric center of the space behind the projectile.

It should be noted that in most available sources, such a feature of the temperature distribution is either not considered or not explicitly recorded, which is likely due both to the limited capabilities of experimentally measuring the propellant gas temperature along the barrel and to the use of simpler computational models. At the same time, a similar pattern of temperature variation along the barrel can be observed, for example, in [8], which presents numerical simulation results demonstrating elevated temperature values near the beginning and end of the barrel (**Fig. 3.12**). In this figure, the horizontal axis represents coordinates along the barrel length from the breech (0) to the muzzle (7), and the vertical axis represents time during the shot. Points at the boundary between parts of the image in the upper-left and lower-right corners (light blue) indicate the position of the projectile base (horizontal axis) at the corresponding moments in time (vertical axis). The distance from any point on this boundary to the vertical axis represents, at the corresponding moment (vertical axis), the length of the barrel portion behind the projectile occupied by the propellant gases. Changes in the color scale along this segment reflect the spatial distribution of propellant gas temperatures behind the projectile at the given moment.

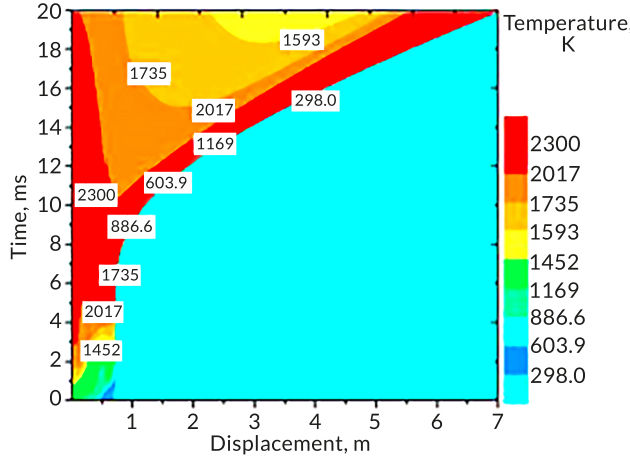

Fig. 3.12 Temperature distribution along the barrel of a large-caliber gun during a shot
Source: [8]

The results obtained in the present work, despite their approximate nature, can be considered as a theoretical basis for further analysis of the relationship between the parameters of the propellant gas expansion process in the barrel and the features of muzzle flash formation. In particular, the identified non-uniformity of the temperature field may have a significant impact on the intensity of chemical and gas-dynamic processes in the muzzle region, which opens up prospects for a more detailed study of the mechanisms of muzzle flash initiation and development based on refined internal ballistics models.

Analysis of images of the muzzle blast and the accompanying flash shows that their structure and characteristics vary significantly depending on the firing conditions. The observed diversity of spatio-temporal forms of the muzzle blast indicates the complex nature of the physicochemical processes occurring in the projectile chamber.

As a characteristic example, consider the results of muzzle blast visualization for the 2A36 gun. The images presented in **Fig. 3.1**, **3.3** clearly show that soot clouds are present along the entire length of the muzzle blast. The soot is evenly distributed along the jet, giving the blast a uniform dark appearance accompanied by intense glow during subsequent combustion.

A different picture is observed in **Fig. 3.2**. In this case, the soot-containing region occupies only part of the muzzle blast, and its volume is noticeably smaller compared to the corresponding regions in **Fig. 3.1**, **3.3**. Moreover, at least two zones with almost no soot can be distinguished in the structure of the muzzle blast in **Fig. 3.2**. The first is located at the front of the blast, ahead of the soot cloud (**Fig. 3.2**, ***b***) and is highlighted with a red contour. The second zone is behind the soot cloud, closer to the muzzle face of the barrel (**Fig. 3.2**, ***c***), and is marked with a yellow contour. It should be noted that against the bright glow of burning soot, these zones are weakly visible and become discernible only upon detailed image analysis.

One of the characteristic features of the muzzle blast is the spatial location of the muzzle flash initiation point. Analysis of the experimental data presented in **Fig. 3.1**, ***a*** and **Fig. 3.2**, ***a*** shows that in some cases, ignition of the muzzle blast is initiated at the front of the soot cloud, highlighted in red in the corresponding images. At the same time, the results shown in **Fig. 3.3**, ***b*** indicate a qualitatively different scenario: the initiation of the muzzle flash occurs in a region immediately adjacent to the muzzle face. Thus, experimental observations reveal variability in the location of the ignition zone.

These features of the muzzle blast and flash are explained by the results of approximate thermochemical calculations based on the proposed model. The data presented in **Fig. 3.7**, **3.9** indicate that by the time the projectile reaches the muzzle, temperature conditions favorable for the Boudouard-Bell reaction, accompanied by solid carbon (soot) formation, are established along almost the entire barrel length.

However, the realization of these conditions strongly depends on the state of the propellant charge.

In the case of a degraded propellant charge (**Fig. 3.9**), the temperature of the PG drops below the threshold value corresponding to the onset of carbon monoxide disproportionation even before the projectile exits the barrel. This leads to a high likelihood of soot formation throughout the projectile chamber. As a result, soot particles are present along the entire length of the muzzle blast, which is consistent with the experimental observations shown in **Fig. 3.1**, **3.3**, ***b***.

A different situation occurs when using a fresh propellant charge (**Fig. 3.7**). In this case, the PG temperature drops below the characteristic level of approximately 1300 K only in localized regions – near the chamber and at the base of the projectile – and only during the final stage of its travel through the barrel, immediately before exiting the bore. Under these conditions, the likelihood of soot formation in the initial and final phases of the muzzle blast is significantly lower than in its middle part. Such a distribution of the soot phase may correspond to the experimental picture shown in **Fig. 3.2**.

Definitive confirmation of this scenario is provided by the calculations for a full fresh propellant charge (**Fig. 3.11**). According to these data, by the time the projectile is near the muzzle, the high PG temperature in the chamber and at the base of the projectile prevents soot formation along the entire projectile chamber. Therefore, soot inclusions in the muzzle blast occupy only a limited section of its length, which also agrees with experimental observations (**Fig. 3.2**).

The spatial location of the muzzle flash initiation point can be further explained by considering the PG temperature profile along the barrel. Calculations show the presence of temperature maxima in the chamber region and near the muzzle face. The ignition temperatures of the main combustible components of the muzzle blast – hydrogen (around 800 K) and carbon monoxide (around 900 K) – play a significant role. As follows from the calculation data (**Fig. 3.6**–**3.8**), during PG expansion and outflow, their temperature can fall below these limits, and this decrease continues even after the gases exit the barrel.

As a result, under certain combinations of firing parameters, propellant charge state, and thermodynamic outflow conditions, ignition of the combustible components of the muzzle blast may not occur. In such cases, a muzzle flash does not form, as observed in **Fig. 3.13**.

Thus, the presence, spatial localization, and intensity of the muzzle flash are determined by the combined influence of the temperature field of the propellant gases, the kinetics of soot formation, and the ignition conditions of the gas phase outside the bore.

a *b*

Fig. 3.13 Stages of muzzle blast development of a 155 mm M109 (Paladin) self-propelled howitzer round. No muzzle flash occurred. Yuma Test Range: *a* – developed muzzle blast cloud with pronounced lateral lobes observed in the absence of visible ignition; *b* – further expansion and rarefaction of the discharge cloud without flame formation
Source: [17]

The examples presented above clearly demonstrate the complex, multivalued, and nonlinear relationship between the parameters of the internal ballistic processes of a shot and its external manifestations, in particular the characteristics of the muzzle outflow and the muzzle flash. The formation of these external effects is governed by the combined action of thermo-gas-dynamic processes within the bore, the evolution of propellant-gas pressure, the burning rate of the charge, as well as the conditions of combustion-product discharge beyond the muzzle. Even minor variations in internal parameters may lead to qualitatively different external manifestations, which substantially complicates the direct interpretation of observed effects.

At the same time, the parameters of internal ballistics are not invariant and depend to a large extent on the current condition of the elements of the artillery system. Among the determining factors, first and foremost, are the condition of the propellant charge and the technical state of the barrel. The degree of propellant-charge degradation caused by aging, moisture exposure, thermal cycling, and mechanical damage leads to changes in its energetic and kinetic characteristics, including the burning rate, heat of explosion, and gas generation. Similarly, wear of the bore – manifested as an increase in diameter, distortion of rifling geometry, and changes in surface roughness – has a noticeable effect on projectile motion conditions, propellant-gas leakage, and the pressure distribution along the barrel.

The combined influence of these factors results in internal ballistic parameters effectively carrying information about the current technical condition of the artillery system. Consequently, given an adequate physico-mathematical model

describing the relationship between internal processes and the external manifestations of a shot, it becomes fundamentally possible to develop a method for diagnosing the system state directly during firing and in real time.

The proposed model makes it possible to treat this problem as an inverse problem of internal ballistics, in which the internal parameters of the system – including the degree of barrel wear and the degree of propellant-charge degradation – must be reconstructed from measured or recorded external indicators of the shot (parameters of the muzzle outflow, the intensity and shape of the muzzle flash, and the temporal characteristics of gas discharge).

It should be noted that solving inverse problems of internal ballistics is associated with significant computational difficulties. These arise from the nonlinearity of the governing equations, their stiffness, and the non-uniqueness of the correspondence between internal parameters and observable external effects. Direct numerical solution of such a problem in real time is generally difficult or practically impossible when using standard computational approaches.

To overcome these limitations and to enable the operational use of results during firing, it is expedient to apply the so-called "library" method [13]. The essence of this method lies in the preliminary formation of an extensive array (library) of solutions to the direct internal ballistics problem for various combinations of system state parameters. Each element of the library corresponds to a set of characteristics of the external manifestations of a shot, calculated or obtained experimentally for a fixed state of the artillery system.

Within the framework of the problem under consideration, the library can be formed by recording the parameters of the muzzle outflow and muzzle flash for known and fixed values of barrel wear and propellant-charge degradation. During actual firing, the measured external parameters are compared with the library entries, which makes it possible to estimate the current state of the system with acceptable accuracy and minimal computational cost. This approach provides a compromise between the physical fidelity of the model and the requirements for computational efficiency, making it promising for practical implementation in technical monitoring systems and automated control of artillery complexes.

Conflict of interest

The authors declare that they have no conflict of interest in relation to this research, whether financial, personal, authorship or otherwise, that could affect the research and its results presented in this paper.

Use of artificial intelligence statement

The authors declare that they did not use artificial intelligence tools in preparing this manuscript.

Authors' contributions

Oleksandr Brunetkin: Conceptualization, Methodology, Theoretical framework, Numerical simulation, Data analysis, Thermochemical analysis, Mathematical modeling, Writing – original draft.

Pavlo Gultsov: Literature review, Data curation, Comparative analysis, Model validation, Visualization, Writing – review & editing.

Oleksandr Sidelnykov: Experimental data interpretation, Image analysis of muzzle phenomena, Formal analysis, Interpretation of results, Validation, Writing – review & editing.

References

1. Brunetkin, O., Maksymov, M., Brunetkin, V., Maksymov, O., Dobrynin, Y., Kuzmenko, V., Gultsov, P. (2021). Development of the model and the method for determining the influence of the temperature of gunpowder gases in the gun barrel for explaining visualize of free carbon at shot. Eastern-European Journal of Enterprise Technologies, 4 (1 (112)), 41–53. https://doi.org/10.15587/1729-4061.2021.239150
2. Jensen, T. L., Moxnes, J. F., Unneberg, E., Dullum, O. (2014). Calculation of Decomposition Products from Components of Gunpowder by using ReaxFF Reactive Force Field Molecular Dynamics and Thermodynamic Calculations of Equilibrium Composition. Propellants, Explosives, Pyrotechnics, 39 (6), 830–837. https://doi.org/10.1002/prep.201300198
3. Pantea, D., Brochu, S., Thiboutot, S., Ampleman, G., Scholz, G. (2006). A morphological investigation of soot produced by the detonation of munitions. Chemosphere, 65 (5), 821–831. https://doi.org/10.1016/j.chemosphere.2006.03.027
4. Podlesak, D. W., Huber, R. C., Amato, R. S., Dattelbaum, D. M., Firestone, M. A., Gustavsen, R. L. et al. (2017). Characterization of detonation soot produced during steady and overdriven conditions for three high explosive formulations. AIP Conference Proceedings, 1793, 030006. https://doi.org/10.1063/1.4971464

5. Yan, C., Zhu, C. (2023). Quantitative assessment method of muzzle flash and smoke at high noise level on field environment. Scientific Reports, 13 (1). https://doi.org/10.1038/s41598-023-27722-0
6. Muthurajan, H., Ghee, H. (2008). Software Development for the Detonation Product Analysis of High Energetic Materials – Part I. Central European Journal of Energetic Materials, 5 (3–4), 19–35. Available at: https://www.researchgate.net/publication/228786423_Software_Development_for_the_Detonation_Product_Analysis_of_High_Energetic_Materials-Part_I
7. Li, P., Zhang, X. (2021). Numerical research on adverse effect of muzzle flow formed by muzzle brake considering secondary combustion. Defence Technology, 17 (4), 1178–1189. https://doi.org/10.1016/j.dt.2020.06.019
8. Rashad, M., Zhang, X., El Sadek, H. (2014). Interior Ballistic Two-Phase Flow Model of Guided-Projectile Gun System Utilizing Stick Propellant Charge. Propellants, Explosives, Pyrotechnics, 39. https://doi.org/10.1002/prep.201400034
9. Otón-Martínez, R. A., Velasco, F. J. S., Nicolás-Pérez, F., García-Cascales, J. R., Mur-Sanz de Galdeano, R. (2021). Three-Dimensional Numerical Modeling of Internal Ballistics for Solid Propellant Combinations. Mathematics, 9 (21), 2714. https://doi.org/10.3390/math9212714
10. Kozlov, O., Maksymov, O., Maksymov, M., Riaboshapka, R. (2025). Fuzzy Control Model with Automated Rule Base Generation for Artillery Systems in Game Simulators. Energy Engineering and Control Systems, 11 (2), 157–168. https://doi.org/10.23939/jeecs2025.02.157
11. Paraschiv, T., Tiganescu, T. V., Iorga, G. O., Ginghina, R. E., Grigoroiu, O. C. (2020). Experimental and Theoretical Study on Three Combustion Models for the Determination of the Performance Parameters of Nitrocellulose – Based Propellants. Revista de Chimie, 71 (9), 87–97. https://doi.org/10.37358/rc.20.9.8320
12. Brunetkin, O., Maksymov, M., Dobrynin, Y., Demydenko, V., Sidelnykov, O. (2024). Development of a process model for determining the composition and energy characteristics of a pyrotechnic mixture using the library method. EUREKA: Physics and Engineering, 5, 99–112. https://doi.org/10.21303/2461-4262.2024.003453
13. Brunetkin, O., Davydov, V., Butenko, O., Lysiuk, G., Bondarenko, A. (2019). Determining the composition of burned gas using the method of constraints as a problem of model interpretation. Eastern-European Journal of Enterprise Technologies, 3 (6 (99)), 22–30. https://doi.org/10.15587/1729-4061.2019.169219
14. Anipko, O. B., Khaykov, V. L. (2012). Methods analysis for assessment of propellant charges as a part of the artillery ammunition monitoring system.

Integrirovannye tekhnologii i energosberezhenie, 3, 60–71. Available at: http://repository.kpi.kharkov.ua/handle/KhPI-Press/2199

15. Brunetkin, O., Maksymov, M. V., Maksymenko, A., Maksymov, M. M. (2019). Development of the unified model for identification of composition of products from incineration, gasification, and slow pyrolysis. Eastern-European Journal of Enterprise Technologies, 4 (6 (100)), 25–31. https://doi.org/10.15587/1729-4061.2019.176422
16. Rusyak, I. G., Tenenev, V. A. (2020). Modeling of ballistics of an artillery shot taking into account the spatial distribution of parameters and backpressure. Computer Research and Modeling, 12 (5), 1123–1147. https://doi.org/10.20537/2076-7633-2020-12-5-1123-1147
17. Official U. S. Army Twitter. Available at: https://x.com/USArmy

CHAPTER 4

Methods for determining the states of an artillery gun under dynamic disturbances

Oksana Maksymova
Pavlo Gultsov
Volodymyr Demydenko
Yevhenii Dobrynin

Abstract

This chapter develops a comprehensive model for assessing the technical condition and combat capabilities of a self-propelled artillery system (SPAS) considered as a complex dynamic object operating under conditions of cumulative wear and exposure to external combat factors. An approach to formalizing the system state is proposed, based on the integration of acoustic, visual, thermodynamic, and mechanical parameters with the construction of a generalized system of serviceability criteria.

Mathematical models are developed to describe the acoustic field of a shot, the processes of formation and evolution of the muzzle discharge, as well as methods for evaluating barrel stability with account taken of thermal and mechanical wear factors. An information model of artillery barrel operation is formulated, incorporating multivector serviceability conditions and enabling automation of residual life calculations.

A state tree of the system is constructed for rank-based assessment of the current technical condition, and combat capability criteria are integrated into a unified decision-making model using the ideal point method. An analytical relationship is derived to determine the required number of rounds to engage a target with a specified probability, together with a time-based model for evaluating mission execution that considers a window of particular vulnerability and maneuverability constraints. Computational examples demonstrate the practical implementation of the proposed approach and its applicability to assessing the risk of system loss and substantiating the advisability of opening fire.

The results establish a methodological foundation for further automation of condition monitoring of artillery systems and may be employed as an algorithmic module within decision-support systems for combat employment.

© The Author(s) of individual chapters, 2026 DOI: 10.21303/978-9908-8450-1-2.ch4

Keywords
Self-propelled artillery system, dynamic assessment, combat capability, barrel service life, state tree, decision-making model, time budget.

4.1 Introduction

Modern artillery systems operate in highly dynamic conditions characterized by rapid fire exchange, intensive mechanical and thermal loading, and the necessity for continuous assessment of technical state and combat readiness. Under such conditions, traditional static evaluation approaches are insufficient, and operational monitoring based on physical signals generated during firing becomes essential.

Acoustic emissions, thermal radiation of muzzle gases, mechanical vibrations, and optical manifestations of the muzzle blast contain informative data about internal ballistic processes and system condition. Processing such heterogeneous information requires mathematical models combining physical description with statistical estimation and parameter identification techniques [1–3].

Existing studies have addressed individual aspects of artillery system assessment, including acoustic monitoring of firing processes, thermal diagnostics of barrel condition, and statistical models for projectile trajectory estimation. In many of these works, attention is primarily focused on the analysis of specific physical signals or on isolated parameters characterizing firing efficiency and barrel wear. While such approaches provide valuable diagnostic information, they are typically limited to separate subsystems or measurement modalities and do not explicitly integrate operational factors such as ammunition availability, mobility constraints, and survivability considerations. In contrast, the approach proposed in this chapter aims to combine heterogeneous physical indicators with operational parameters within a unified dynamic framework for evaluating the current combat capability of a self-propelled artillery system.

Repeated thermal and mechanical loading leads to barrel wear, erosion, and structural degradation, which affect projectile velocity and firing accuracy. Therefore, predictive models for resource estimation based on operational data are required to evaluate residual service life and system performance [4–6].

Modern combat doctrine emphasizes high-mobility tactics such as "shoot-and-scoot", where fire missions are followed by immediate relocation to reduce vulnerability. Decision-making must account for technical parameters, ammunition availability, mobility constraints, and survivability. Formalized state models and transition-based representations provide a unified framework for integrating these factors [7–9].

This chapter develops a system of dynamic criteria for evaluating the current combat capability of a SPAS. The criteria include firing efficiency, accuracy degradation, ammunition stock, mobility level, and ability to operate under partial system damage. Their aggregation into an integrated metric enables quantitative comparison of operational states and supports tactical decision-making.

Special attention is given to engagement scenarios involving high-value time-critical targets. In such situations, feasibility analysis must consider probabilistic hit models, time constraints, and survivability risks. The proposed framework integrates resource assessment, mobility analysis, and probabilistic engagement modeling into a coherent structure suitable for practical implementation in automated support systems [10].

The methodological approach is illustrated using parameters typical for modern 155-mm self-propelled artillery systems, with the Archer SPAS (BAE Systems, Sweden) used as a representative prototype for numerical modeling.

4.2 Analysis of models and methods for determining the states of an artillery gun

Mobility of artillery is a determining factor in preserving combat capability, since counter-battery warfare systems enable the adversary to rapidly detect firing positions and deliver a retaliatory strike. This has led to the widespread adoption of the "shoot-and-scoot" tactic, which involves executing a fire mission followed by an immediate change of position. Modern artillery systems, due to their high rate of fire and mobility, implement multiple cycles of "shot – displacement – shot" within a short time interval [11].

Scientific sources consider models that account for rate of fire, targeting procedures, firing errors, and the probability of target engagement, as well as approaches to selecting positions and routes with regard to terrain topology and feedback control [12]. The Markov model of artillery combat describes the organization of fire but does not account for the reduction in effectiveness caused by combat damage during maneuvering. Studies [13, 14] emphasize temporal parameters of combat and the minimization of target engagement time while considering the risk of detection after the first shot.

For the analysis of the artillery system state, informational features of a shot are considered (**Fig. 4.1**). The main features include the acoustic fields of the ballistic and muzzle waves (MW), as well as visual manifestations of the muzzle discharge in the visible and infrared spectra. Assessment of system operability additionally accounts for barrel wear, deterioration of the running gear, and possible combat damage.

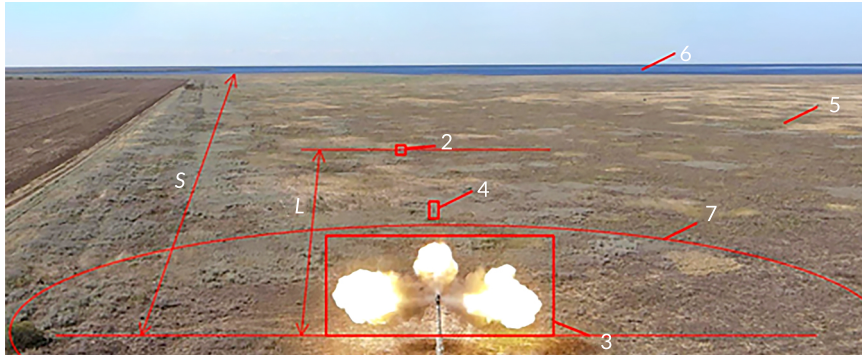

Fig. 4.1 Situational layout of the artillery system: 1 – gun; 2 – measuring system; 3 – propellant gases forming a shock-acoustic wave; 4 – projectile on a ballistic trajectory; 5 – mainland surface of the training ground; 6 – sea surface of the training ground; 7 – boundary of transition from the shock MW to the acoustic MW; *S* – distance from the firing position to the target; *L* – distance from the firing position to the location of the measuring system

4.3 Acoustic waves for the identification of artillery guns

Acoustic field of a shot is formed by ballistic and muzzle waves and can be used to determine the location of an artillery system [15]. Physical models and experimental data make it possible to establish the main parameters of these waves and assess their informational value.

When a projectile flies at a velocity $V > c$, a ballistic wave (BW) is formed with a front in the form of a Mach cone. The opening angle is determined by

$$Q_M = \arcsin(1/M), M > 1, \tag{4.1}$$

where M – the Mach number.

The BW signal is a short-duration broadband pulse lasting 3–8 ms with a characteristic frequency band of 1–10 kHz. Its amplitude and temporal parameters can be estimated using the empirical acoustic model of a shock wave generated by a supersonic projectile (Whitman model), which is applied in studies devoted to estimating flight parameters based on acoustic signals:

$$A = \frac{0.53P_0(M^2-1)^{1/8}\varphi}{d_{sM}^{3/4}l^{3/4}}, \tag{4.2}$$

$$T_N \approx \frac{1.82\varphi}{c}\left(\frac{M\varphi}{l}\right)^{1/4}, \tag{4.3}$$

while the rise (and decay) time of the pulse front is

$$t_r = t_d \approx \frac{\lambda}{c}\frac{P_0}{A},$$

where A – the amplitude of the BW, Pa; T_N – the duration of the main part of the pulse; $t_r \approx t_d$ – the duration of the rise and decay fronts of the BW pulse, respectively; P_0 – the atmospheric pressure; φ – the projectile caliber; l – the projectile length; d_{sM} – the shortest distance from the recording point to the Mach cone; c – the speed of sound in air; $\lambda \approx 6.8 \times 10^{-8}$ m – the mean free path of an air molecule.

The BW is recorded by a microphone only if the observation point lies inside the Mach cone. At a certain point along the trajectory, the projectile velocity becomes lower than the speed of sound, and the wave disappears; therefore, it must be recorded at relatively short distances from the firing point. Due to the short rise time of the BW, it must be recorded with a high sampling rate.

The MW is formed as a result of the expansion of propellant gases after the projectile exits the barrel. It propagates at the speed of sound and has an impulsive character with a sound pressure level of up to 150 dB. The signal duration is 30–50 ms, and the main spectral range extends up to 100 Hz.

The shape of the overpressure pulse can be described by the generalized Friedlander model

$$P_{mw} = A_{mw}\left(1 - \frac{t}{T_0}\right)e^{-\beta t/T_0}, \tag{4.4}$$

where A_{mw} – the pulse amplitude; T_0 and β – parameters defining the pulse shape.

Alternatively, the Berlage model is applied to describe the oscillatory structure of the pulse tail

$$P_{mw}^{B} = A_{mw}t^{nr}e^{-\alpha t}\sin(2\pi f_0 t), \tag{4.5}$$

where nr – the exponent characterizing the power-law rise rate of the leading front of the MW; α – the attenuation coefficient of the oscillatory process of the MW; f_0 – the dominant frequency.

The MW front has a spherical character; however, at distances exceeding 50 m it may be considered planar. For ranges up to 2–3 km, the amplitude of the muzzle wave typically exceeds that of the ballistic wave by a factor of 2–3 [15].

Within the structure of the acoustic signal, the ballistic wave is recorded earlier than the MW, since $V > c$. After the short ballistic wave impulse, a pause is observed, followed – after a temporal delay – by the arrival of the muzzle wave. The total duration of recording the signal of a single shot is approximately 0.6 s.

When recording signals in the near-ground atmospheric layer, the dominant interference is wind noise, which spectral density decreases proportionally to $1/f$, corresponding to the "pink noise" model. Experimental data confirm the adequacy of such a description.

A typical representation of the recorded acoustic field at SNR = 10 dB is shown in **Fig. 4.2**. The segments corresponding to the ballistic wave and the muzzle wave are clearly identified in the recording against the noise background. Analysis of experimental data confirms the adequacy of the pink noise model for describing real interference.

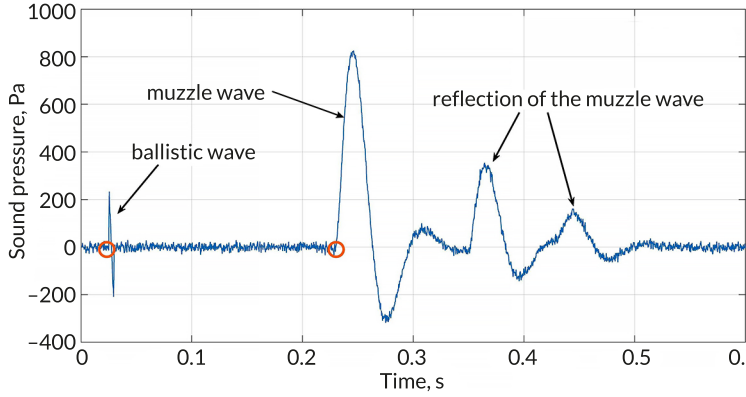

Fig. 4.2 Typical view of the recorded acoustic field

4.4 Visual field of propellant gases in the muzzle discharge

The muzzle discharge of propellant gases after the projectile exits the barrel exhibits a complex spatial structure formed by the axial flow and lateral jets through the openings of the muzzle brake. The dynamics of its development contain informative features for the identification of the artillery system. Their registration is possible by means of high-speed video recording. Experimental data from field firing tests were used for the analysis [16].

Studies [17, 18] substantiate the feasibility of using video data of the muzzle discharge for diagnosing the state of an artillery system. Temporal changes in the geometric parameters and temperature of the gases during the transition from a shock wave to an acoustic wave have been recorded.

Fig. 4.3 presents a generalized frame-by-frame sequence of the development of the muzzle discharge for different variants of propellant charges at characteristic time moments of 0.04 s and 0.12 s after the projectile exits the barrel. The selected intervals correspond to the initial stage of gas volume formation and the stage of its intensive expansion. A comparison of the frames indicates significant differences in the spatial configuration and luminosity intensity for charges with different energy characteristics.

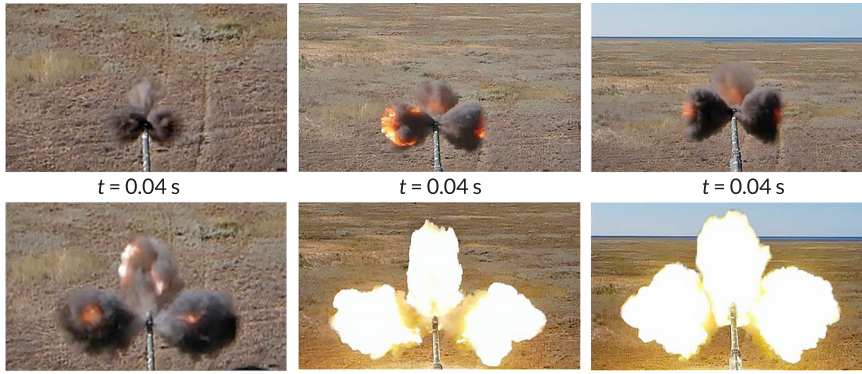

Fig. 4.3 Development of the muzzle discharge for different variants of propellant charges at characteristic time moments: *a* – shot with minimum propellant charge; *b* – shot with full propellant charge; *c* – shot with the first propellant charge

The complete temporal evolution of the process within the interval of 0.04–0.16 s is presented in **Table 4.1**. Joint data processing revealed differences in the projected pressure and temperature distributions for different charges. The transition time from the shock wave to the acoustic wave depends on the charge energy and lies within 0.04–0.12 s after projectile exit.

Geometric and temperature parameters of the muzzle discharge can be used as identification features of a shot.

The time interval from 0 to 0.20 s is characterized by intensive formation and expansion of the muzzle discharge volume, which is analyzed in detail for

different charge variants (**Fig. 4.3**, **Table 4.1**). Further development of the process is mainly determined by the interaction between the gas volume and the atmospheric environment.

Table 4.1 Perimeter of the generatrix, projected area, and gas temperature in the muzzle discharge within the time interval of 0.16 s after projectile exit

Time, s	Minimum charge			Full charge			First charge		
	Perimeter, m	Area, m^2	Temperature, K	Perimeter, m	Area, m^2	Temperature, K	Perimeter, m	Area, m^2	Temperature, K
0.04	10.17	3.76	1020	16.14	9.21	1420	19.12	11.45	1390
0.08	17.77	10.52	910	25.97	16.97	1330	25.88	21.6	1290
0.12	22.72	16.46	950	33.64	26.85	1250	34.77	33.94	1200
0.16	64.72	23.99	1180	39.35	25.4	1100	40.84	41.74	1050

The analysis results make it possible to distinguish two independent identification channels. The first is the variation of the projected area of the muzzle discharge volume, which increases monotonically until pressure equalizes with the atmosphere, after which its evolution is governed by diffusion and wind-driven processes [18, 19]. The dynamics of this process are observed within the time interval of 0–0.2 s and are characterized by a stable tendency toward an increase in the projected area.

The second is the temperature characteristic of the gas volume, which decreases during expansion but may exhibit a local maximum at the moment of oxidation of combustion products in the atmosphere. The mixing of propellant gases with atmospheric oxygen is accompanied by oxidation of soot particles and additional energy release, which explains the possible temperature surge and the appearance of a flame.

Within the time interval up to 0.20 s, a characteristic spatiotemporal structure of the muzzle discharge is formed, after which the process transitions to a stage of gradual reconfiguration and interaction with the atmospheric environment.

Fig. 4.4 illustrates the development of the three-lobed shape of the muzzle discharge within the interval of 0.24–0.54 s after the shot. The frame sequence is presented with a time step of $\Delta t = 0.08$ s. Visual features of the shot persist for up to 1 s after the projectile exits the barrel.

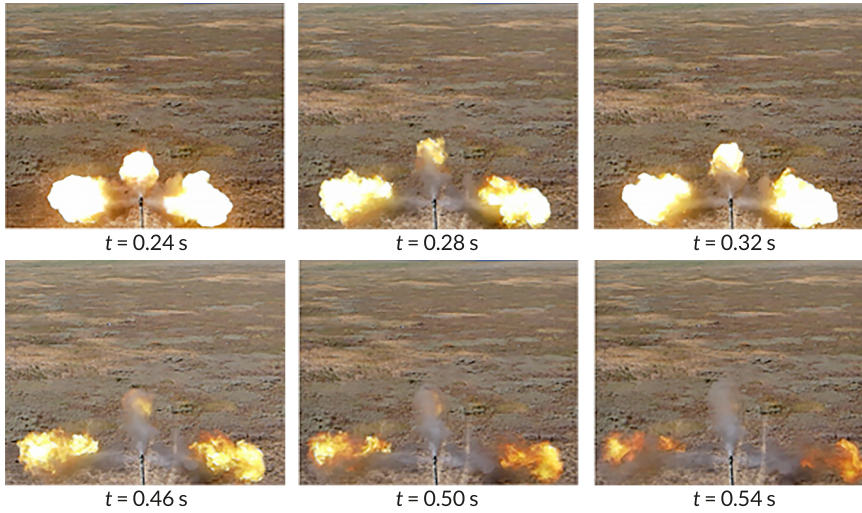

Fig. 4.4 Demonstration of the three-lobed muzzle discharge of the artillery system as a function of time after the shot

4.5 Methods for calculating the stability of artillery system barrels

4.5.1 Methods and models for calculating the stability of an artillery barrel

Barrel stability (service life) is determined by the wear rate of the bore and depends on two groups of factors – thermal and mechanical.

Thermal factors include:

– heating of the bore by propellant gases with temperatures of 2000–3500 K;

– heating of the bore surface due to frictional heat in the contact zone of the projectile driving bands;

– heat generation within the barrel metal caused by deformation under the pressure of propellant gases and the impact interaction of the projectile's centering band with the rifling.

Mechanical factors are associated with wear of the heated barrel resulting from erosive removal of metal by the flow of propellant gases, as well as wear in the clearances between the projectile driving band and the bore surface and its guiding elements.

The wear intensity is determined by the gas temperature, the projectile muzzle velocity, the barrel caliber, and the material properties. The permissible number of shots N is estimated using the empirical relationship

$$N = \frac{K_T}{C_q^3 v_0^{4.5} d^{2.5}}, \tag{4.6}$$

where K_T – the temperature coefficient accounting for the energy capacity of the propellant and the characteristics of the barrel steel; C_q – the weapon power; v_0 – the projectile muzzle velocity; d – the bore diameter.

For guns with similar ballistics and a constant propellant grade, K_T is assumed to be constant.

If the value of the coefficient K_T is unknown, expression (4.6) is conveniently used for a comparative assessment of stability when varying the muzzle velocity, caliber, and projectile mass. As a first approximation, K_T may be taken for medium-caliber guns as $K_T \approx 7 \times 10^{24}$. It is important to correctly determine stability for high-power systems characterized by $Cq = mv_0^2 / 2d^3 \approx 400$ tf · m/dm^3.

The firing mode significantly affects barrel heating and, consequently, its service life. At high rates of fire, critical deformations and a reduction in accuracy are possible; therefore, stability control is ensured by limiting burst length and intervals between shots.

For calculating the stability of such systems, Yustrov's expression may be applied

$$N = \frac{xy}{d^2} \frac{C_q v_0^2 \sigma \varepsilon}{\lambda \mu k_1}, \tag{4.7}$$

where $x = f_1(p_{max}, R, k, Q_h)$; p_{max} – the maximum pressure in the barrel bore; R – the gas constant of the propellant gases; k – the adiabatic exponent of the propellant gases; $y = f_2(d, n)$; n – the rate of fire; $\lambda = L_c / d$, where L_c – the barrel length; σ – the ultimate tensile strength of the barrel material; ε – the relative tangential strain of the barrel walls; μ – the friction coefficient of the driving band against the barrel walls; k_1 – the compressive strength of the driving band material; C_q – has the dimension of gf/cm^3; d – has the dimension of cm. Barrel stability N is determined by a 10% reduction in the muzzle velocity v_0.

Various empirical relationships (Yustrov, Linthe, Gabo, Slukhotsky) are used to estimate service life, taking into account geometric, ballistic, and technological parameters. However, their applicability is limited to specific experimental conditions; therefore, modern systems require adaptation of the models based on actual operational data.

4.5.2 Methods and models for calculating the stability of the "barrel – charge – projectile" system

Methods and models of wear and stability are considered as a consequence of the transition from lumped to distributed system properties. This approach is necessary for predicting barrel stability without conducting experimental testing and for evaluating the effectiveness of technological measures aimed at reducing wear. Mathematical models must take into account the characteristics of the "barrel – charge – projectile" system and the effectiveness of the applied technologies.

The complexity of modeling is determined by the large number of factors influencing wear and stability. A simulation model should include the calculation of the barrel temperature field, bore wear characteristics, internal ballistic parameters of the shot, projectile dispersion for a worn barrel, and the functional limit of the projectile driving elements.

In calculation methods, reliance on "analogs" creates the problem of the absence of reference values. Therefore, modern computational approaches employ fundamental mathematical models with a high level of generalization rather than empirical formulas based on lumped properties. Thermal field modeling is performed under firing regimes typical for the barrel and involves the selection of "analogues" based on heat transfer and wear results.

The specific diametral wear Δd_{spec} is calculated per shot, taking into account the geometry of the bore, the firing regime, instantaneous heat transfer and cooling coefficients, as well as the thermophysical properties of the material. The maximum surface temperature of the bore T_l^m is determined for a series of cross-sections. Based on this value, the material damage characteristic of the bore δ_d and the corresponding energy expenditures for damage formation A_d are determined.

The empirical dependence of the specific diametral wear can be expressed as a power function

$$\Delta d = A(T_l^m)^{\alpha}(\delta_d)^{\beta}(A_d)^{\gamma}, \tag{4.11}$$

where A – the experimental coefficient; α, β, γ – experimentally determined exponents.

The values of the arguments and the coefficient A are determined on the basis of design – ballistic and operational data, taking into account the adopted calculation method. The application of the dependence to new weapon systems is valid within the limits of parametric similarity to the reference "analogue" for which its identification was performed.

Based on Δd, the following barrel bore parameters are calculated: the elongation of the chamber $\Delta\lambda_1$, the increase in projectile travel distance until complete engagement of the driving band $\Delta\lambda_2$, and the area of propellant gas breakthrough δS. Neglecting the longitudinal wear δl and approximating the wear curve by a straight line, let's obtain:

$$\Delta\lambda_1 = 0.5d\,\mathrm{ctg}\beta\left(1-\frac{D_0-d}{\Delta d}\right),$$
$$\Delta\lambda_2 = 0.5d\,\mathrm{ctg}\beta,$$
$$\delta S = 0.5\pi d\Delta d\left(1-\frac{D_0-d}{\Delta d}\right). \qquad (4.12)$$

These dependencies are valid under the condition that $(D_0-d)/\Delta d<1$.

Otherwise, $\Delta\lambda_1 = 0$, $\delta S = 0$, and only the geometry of the forcing cone changes.

The value of cot β is corrected based on experimental data. The calculation is performed for the extreme values of the expected number of shots (N_1, N_2) or for a single number of shots N.

To assess the internal ballistic characteristics of the shot and the reduction in muzzle velocity, the internal ballistic problem for a worn barrel is solved, taking into account the engagement of the driving band and gas leakage. The failure criterion of the driving elements is determined simultaneously. Methods of plasticity theory account for the dynamic deformation of the driving band (DB) and make it possible to determine whether the protrusions of the DB will be sheared and whether the barrel will reach its stability limit at a given level of wear.

Barrel stability is assessed by comparing the reduction in muzzle velocity Δv_0 and the shear of the driving band. This can be performed for a given N or for an admissible velocity reduction Δv_0^{perm} at which the corresponding $\Delta\lambda_1$, $\Delta\lambda_2$, and δS are determined.

To evaluate stability according to the criterion of projectile dispersion or ovality of impact holes, the external ballistic problem is solved, taking into account the initial deviations of translational, rotational, and nutation velocities caused by bore wear.

4.6 Information modeling of artillery barrel operation

The task of modeling the operation of an artillery barrel is associated with incomplete or redundant and potentially contradictory input data. This specificity necessitates a stepwise consideration of the process, taking into account the intensity of combat operations.

4.6.1 Automation of modeling of artillery barrel operation

Automation must ensure the input of any initial data obtained during operation, as well as monitoring of the limiting properties of the barrel required for mission execution.

The result of modeling artillery barrel operation is the acquisition of reliable data on the service life and the characteristics of its variation depending on the initial firing conditions. The system must provide the possibility, at the operator's discretion, to use non-limit values of the input data to extend the period of resource utilization without violating the logic of combat operations.

The formation of different scenarios for the use of residual service life is envisaged.

The informational nature of the process makes it possible not only to automate modeling but also to optimize it in real time on the basis of modern computing systems. The information model is considered as a set of mathematical models of distributed properties, models of serviceability states, and interface tools for displaying results. The basis for constructing the information model is the need to assess the barrel state, ensured by a set of model-based calculations of its current properties. The sources for model formation include technical documentation of the weapon system, results of range and ballistics tests, as well as statistical data from serial production.

The model input data include constants of mechanical, thermophysical, and chemical-kinetic quantities, as well as data arrays of properties required for calculations.

The analysis of the processes occurring in the barrel during operation has made it possible to identify groups of parameters for evaluating the residual service life.

The first group characterizes the general, longitudinal, and local strength of the barrel. The serviceability condition for this group has the form $\sigma \le [\sigma]$ and $P_1 \le [P]$, where $\sigma = \{\sigma_{eq}, \sigma_{ej}, \sigma_{mb}\}$ – the vector of calculated strength parameters; $P_1 = \{p_1^{el}, p_1^{scr}, p_2^{sh}, p_{\text{lim}}, p_{fail}\}$ – the vector of calculated allowable elastic and resistance parameters; $[\sigma]$ – the vector of allowable stress values; $[P]$ – the vector of required resistance values; the corresponding safety factors are determined experimentally; σ_{eq} – the equivalent stress in the barrel rifling; σ_{ej} – the maximum stress in the region of injection holes; σ_{mb} – the maximum stress before the muzzle thickening; p_1^{el} – the elastic limit of the monoblock; p_1^{scr} – the limit of possible resistance of the reinforced (banded) barrel; p_2^{sh} – the elastic resistance of the barrel sleeve; p_{lim} – the conditional elastic limit; p_{fail} – the destructive pressure.

The second group characterizes changes in the shape, dimensions, and surface condition of the bore and is defined by the condition $\delta \le [\delta]$. The components of the vector describe the state of the bore with respect to wear and may be determined either analytically or experimentally: $\{\Delta d_{wps}, \Delta\lambda_{ch}, \delta_m, \delta_{st}, \delta_{pl}, \delta_T, l_{cr}\}$ where Δd_{wps} – the

diametral wear per shot; $\Delta\lambda_{ch}$ – the chamber elongation; δ_m – the depth of the melting zone; δ_{st} – the depth of the structural transformation zone; δ_{pl} – the depth of the plastic deformation zone; δ_T – the thermal expansion of the bore; l_{cr} – the average crack length.

The third group describes the barrel as a mechanical vibrational system and is defined by the condition $\gamma \le [\gamma]$, where the vector components are $\gamma = \{\gamma_m, f_{st}, EI, \nu_i\}$, γ_m – the muzzle angle; f_{st} – the static deflection of the barrel under its own weight; EI – the bending stiffness of the barrel; ν_i – the natural frequencies corresponding to radial, transverse, and longitudinal vibration modes.

The fourth group characterizes the barrel as a structural element of the system and is defined by the condition $\varepsilon \le [\varepsilon]$, where the vector components are $\varepsilon = \{Q_b, J_i, x_{cm}, \delta r_j, T_{ch}, P_b\}$ where Q_b – the barrel mass; J_i (i = 1, 2) – the mass moments of inertia; x_{cm} – the coordinate of the center of mass; δr_j – the radial expansion of the barrel at the junction with the cradle; T_{ch} – the chamber surface temperature; P_b – the force acting on the breech.

The thermal factor affects all groups of parameters and determines changes in the permissible stress values and material properties. This influence extends both to the magnitude of the parameter on the left-hand side of the inequality and to the magnitude within the allowable limit.

Non-uniform heating of the barrel wall leads to the development of thermal stresses and to a reduction in the allowable stress due to the degradation of the strength properties of structural steel at elevated temperatures.

The maximum surface temperature of the barrel is a determining factor in wear and must be taken into account within the second group.

For different groups of barrel parameters associated with possible failure during operation, different characteristics of the thermal field are significant.

For the parameters of the first group, the temperature gradient and the overall heating level are important; for the second group, the maximum temperatures are significant; for the third group, the longitudinal temperature gradient is decisive; and for the fourth group, the integral thermal characteristic δr_j is relevant.

Therefore, the thermal aspect of the serviceability conditions is expressed by the inequality $T \le [T]$, where the vector of characteristic thermal parameters is $T = \{T_{b0}, T_{\max}, T_{ch0}, \Delta T_L, T_{p(x)}, T_{cool}, T_{avg(r)}\}$ where T_{b0} – the bore surface temperature at the beginning of rifling before the current shot, characterizing the overall heating level; $T_{\max}$ – the maximum bore surface temperature; T_{ch0} – the chamber surface temperature before cartridge insertion; ΔT_L – the longitudinal temperature difference of the average wall temperature along the barrel; $T_{p(x)}$ – the temperature profile at the cross-section corresponding to the maximum pressure; T_{cool} – the coolant

temperature at the outlet of the continuous cooling system; $T_{avg(r)}$ – the average temperature across the wall thickness.

Each of the listed property vectors should be understood as open, since the development of concepts regarding barrel serviceability expands the set of parameters. The system of inequalities forms a generalized model of the serviceability conditions. Its practical implementation requires the accumulation and systematization of experimental data, followed by iterative verification for new weapon systems.

4.6.2 Automation of calculations using internal ballistic models for assessing barrel condition and service life

Modern computational tools make it possible to automate the solution of internal ballistics problems and the assessment of barrel stability parameters, including the modeling of gas-dynamic processes, optimization problems, and inverse calculations.

Classical approaches include empirical, analytical, and hybrid methods for solving the main internal ballistic problem, in particular models based on the generalized thermodynamic scheme of STANAG 4367.

4.7 Method for dynamic assessment of the current combat capability of an individual self-propelled artillery system

4.7.1 System of criteria for dynamic assessment of combat capability

Let's consider a new combat unit – a next-generation SPAS. As a prototype, the Archer SPAS manufactured by BAE Systems (Sweden) [20] is selected, and its tactical and technical characteristics are adopted as the baseline for subsequent modeling.

Let's assume that the general scheme of combat employment of an individual SPAS has the following structure. During targeting, i.e., determining the priority of targets and the sequence of their engagement [21], the system is assigned N targets T_i by the higher-level command, and their coordinates $(x_i^T, y_i^T), i = 1,...,N$, are communicated for sequential engagement.

Target engagement is carried out from prepared firing positions $FP_i, i = 1,...,N$, each of which lies within the firing range corresponding to the respective target. After firing at target T_i from position i, and in accordance with the "shoot-and-scoot" concept, the SPAS moves to position $I + 1$ to engage target (**Fig. 4.5**).

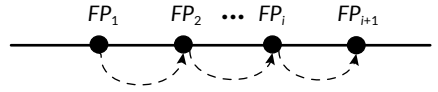

Fig. 4.5 Scheme of movement of the SPAS according to the "shoot-and-scoot" concept

Since combat capability can be assessed using different indicators, the following criteria were selected:

1. Current shot effectiveness. Shot effectiveness is determined by relation (4.13) according to [1]. This implies that the projectile muzzle velocity, reduced due to barrel wear, $(v_0^{table} - \Delta v_0^t)/v_0^{table}$, at the moment of assessment t is at least 0.95 of the tabulated value v_0^{table}. In the proposed methodology, the level of correct assessment of current shot effectiveness is determined using a rank-based control criterion:

$$Crit_1 = (v_0^{table} - \Delta v_0^t)/v_0^{table}, \tag{4.13}$$

$$Crit_1 = \begin{cases} 1, n_{shot}^t \le 25; \\ 1/2, 25 < n_{shot}^t \le 40; \\ 1/3, n_{shot}^t > 40, \end{cases} \tag{4.14}$$

where Δv_0^t – the deviation of the muzzle velocity from the tabulated value; n_{shot}^t – the number of shots fired from the barrel from the time of the last instrumental assessment of the muzzle velocity v_0 up to the moment of firing t.

The acceptance criterion is defined by the condition $Crit_1 \ge 0.95$.

2. Shooting accuracy reduction factor. This criterion accounts for combat damage (indirect hits) inflicted on the SPAS by the adversary, $n_{attacks}$. Such damage reduces the probability of a shot hitting the target p_{fact} compared with the probability of hitting without damage p:

$$Crit_2 = p_{fact}/p, \tag{4.15}$$

$$Crit_2 = \begin{cases} 1, n_{attacs} = 0, \\ 1/2, n_{attacs} = 1, \\ 1/3, n_{attacs} = 2. \end{cases} \tag{4.16}$$

3. Residual ammunition stock (ammunition stock). The assessment of the residual ammunition stock at time t, AS_t, is performed according to the criterion

$$Crit_3 = AS_t = (AS_{full} - n_{shots}^t)/AS_{full}, \tag{4.17}$$

where AS_{full} – the full ammunition load of the SPAS. The critically low value of the criterion $Crit_3$ is considered to be $AS_t^* = 3$ (for $AS_{full} = 21$).

4. Capability of firing in MRSI mode. The ability to fire in MRSI (Multiple Rounds Simultaneous Impact) mode may become unavailable due to indirect enemy hits causing failure of the vertical barrel elevation mechanism or its control system. Accordingly, the capability of firing in MRSI mode is evaluated according to the criterion:

$$Crit_5 = \begin{cases} 1, n_{attacs} < 2, \\ 0, n_{attacs} \geq 2. \end{cases} \tag{4.18}$$

The value 1 indicates the possibility of operating in MRSI mode, while 0 denotes its loss as a result of damage to the vertical elevation mechanism or its control system when $n_{attacs} \geq 2$.

5. Rate of fire. The rate of fire of the SPAS may decrease due to indirect enemy projectile hits. The current rate of fire RF_t is proposed to be evaluated according to the following criterion:

$$Crit_4 = \begin{cases} 1, level = 1, \\ 1/2, level = 2, \\ 1/3, level = 3. \end{cases} \tag{4.19}$$

The first level of rate of fire corresponds to the situation $RF_t = RF_{max}$ shots per minute, where RF_{max} is the maximum rate of fire; the second level of rate of fire corresponds to the condition $RF_t = RF_{max} - 2$; the third level of rate of fire corresponds to the condition $RF_t = RF_{max} - 3$.

6. Residual mobility. The SPAS movement from one firing position to another may be carried out either via roads or across rough terrain. Despite the adaptability of next-generation systems to movement along complex off-road routes, the tires of wheeled chassis may be damaged during such movement, resulting in a temporary reduction in speed and a decrease in mobility. The residual mobility at time t is proposed to be evaluated according to the criterion:

$$Crit_6 = \begin{cases} 1, level = 1, \\ 1/2, level = 2, \\ 1/3, level = 3. \end{cases} \tag{4.20}$$

Let v_t denote the average speed of movement of the SPAS over the time interval t. In this case, mobility corresponds to the first level if $v_t = v_{max}$, where v_{max} – the

maximum movement speed; to the second level if $v_t = v_{max} / 2$; and to the third level if $v_t = v_{max} / 3$.

The six proposed criteria can be integrated into a unified assessment of the current combat capability of the SPAS using an aggregation based on the ideal point method with the L_2 norm

$$Crit_t^{ideal\_point} = \sqrt{\sum_{k=1}^{6} w_k (Crit_k - Crit_k^{ideal\_point})^2}, \quad \sum_{k=1}^{6} w_k = 1, \tag{4.21}$$

where $Crit_t^{ideal\_point}$ – the maximum possible value of the corresponding criterion; w_k – the weight of the respective criterion determined in accordance with the combat situation.

The proposed approach provides an integrated assessment of the current system state based on criteria (4.13)–(4.20).

4.7.2 Selection of the movement route between firing positions

It should be emphasized that the movement of the SPAS between firing positions may be carried out either along roads or across rough terrain, as shown in **Fig. 4.6**.

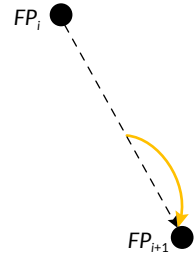

Fig. 4.6 Movement of the SPAS from position FP_i to position FP_{i+1} (yellow – road, black – rough terrain)

When moving along roads, the high travel speed significantly reduces the relocation time. However, roadways are typically subject to intensive enemy fire. Therefore, there is a risk of the SPAS being hit during movement.

When moving across rough terrain, the system's speed is lower; at the same time, wear of the running gear increases, but the probability of being targeted by enemy fire decreases and the movement trajectory becomes shorter.

If several possible routes exist for movement from position FP_i to position FP_{i+1}, the optimal one can be selected by solving a two-criteria transportation problem with minimization of the objective functions – ravel time t and losses Q:

$$\begin{cases} F_{tr}^1 = \min t(FP_i \Rightarrow FP_{i+1}), i = 1,...,n; \\ F_{tr}^2 = \min Q(FP_i \Rightarrow FP_{i+1}). \end{cases} \quad (4.22)$$

In this case, losses are evaluated as the product of the probability of a hit and the cost of the SPAS. It is proposed to assume that the probability of a hit is proportional to the time spent moving along a road under enemy fire. The two-criteria transportation problem is reduced to a linear programming problem. Its solution time on a computer of average performance does not exceed 5 seconds.

4.7.3 Model of combat operations in an exceptional tactical situation

Let's consider the combat employment of the SPAS in an exceptional tactical situation. The main task is counter-battery warfare, within which the system, using the "shoot-and-scoot" tactic, sequentially engages N targets T_i, moving between firing positions FP_i, $i = 1, ..., N$.

Consider a situation in which, after engaging target T_i from position FP_i, information is received about the appearance of a high-value target (EDT – especial danger target) requiring immediate engagement. The EDT is not an artillery battery but has significantly higher combat value. It must be engaged within a "window of especial danger" (WED) Δt_{WED}. The EDT is considered destroyed provided that at least two hits occur with probability p^*.

After receiving targeting information, the SPAS makes a short stop and opens fire from a temporary firing position (TFP). The spatial and temporal schemes are shown in **Fig. 4.7**, **4.8**.

It is assumed that after completing firing at position FP_i, a dynamic assessment of the current combat capability of the SPAS is performed using the method formulated above.

Based on the conducted dynamic assessment, a state tree of the SPAS is formed (**Fig. 4.9**), reflecting the most probable variants of event development.

Before constructing the decision tree, it is assumed that the SPAS moves on prepared road surfaces and that its mobility is not restricted by external conditions. Under such assumptions, criterion $Crit_6$ is set equal to one and does not affect the structure of the state tree.

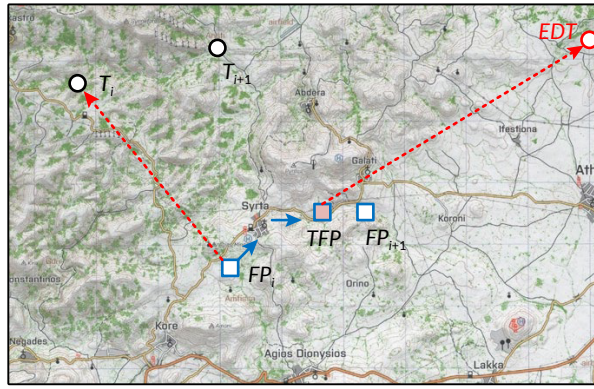

Fig. 4.7 Spatial scheme of firing at the EDT

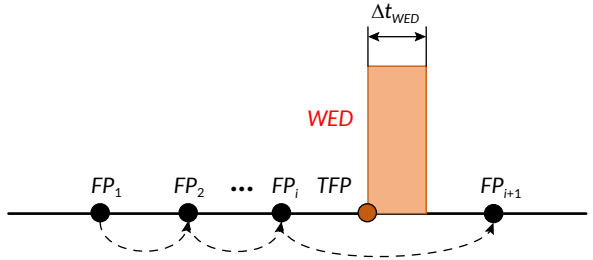

Fig. 4.8 Temporal scheme of firing at the EDT

The first branching level corresponds to criteria $Crit_1$ – $Crit_5$, while subsequent levels reflect the capability to perform combat operations and the rank-based assessment of parameters. The current state is represented by the tuple $State^t < 1,n1;\ 2,n2;\ 3,n3;\ 4,n4;\ 5,n5 >$, where $n1 \in \{1.1, 1.2, 1.3\}$, $n2 \in \{2.1, 2.2, 2.3\}$, $n3 \in \{3.1, 3.2\}$, $n4 \in \{4.1, 4.2\}$, $n5 \in \{5.1, 5.2, 5.3\}$ is the numbers of the terminal branches.

Further, the sequence for assessing the possibility of engaging the EDT is as follows.

Let the probability of a hit with a single shot in the ideal state be equal to p. Taking into account the current state, the adjusted value of p is determined in accordance with the state tree. Assuming independence of shots, the required number of shots n^* to ensure K hits with probability p^* is determined from the inequality

$$1-(1-p)^{n^*-K} \geq 1-p^* \geq (1-p)^{n^*-K}. \qquad (4.23)$$

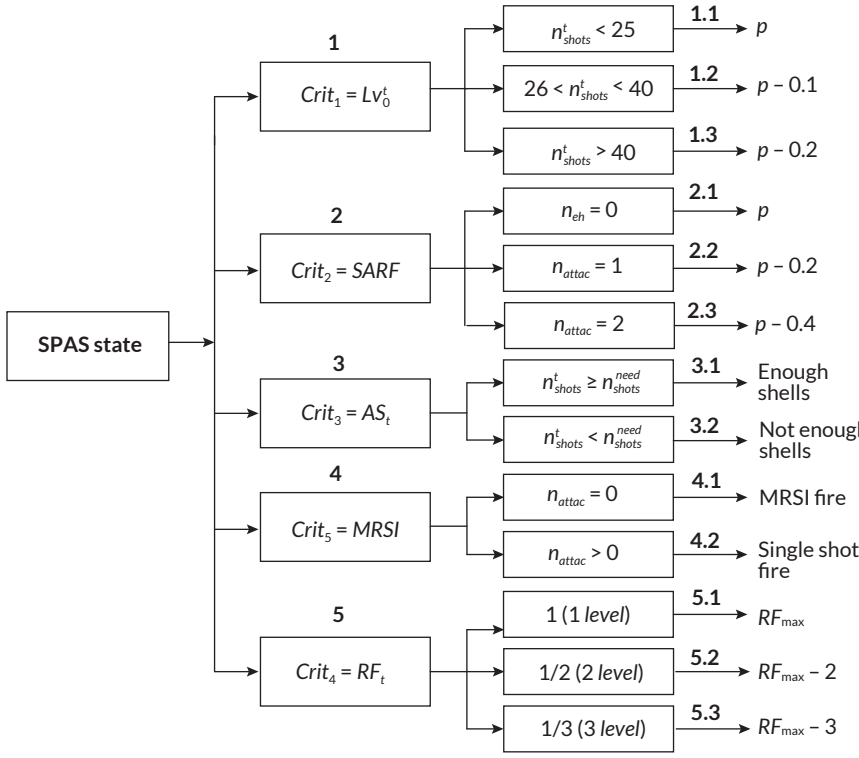

Fig. 4.9 State tree of the combat capability of the SPAS prior to the initial moment of engagement of the EDT

From this, the following relationship is obtained

$$n^* = \log(1-p^*)/\log(1-p)+K. \tag{4.24}$$

The formula is applicable for $0 < p < 1$.
After rounding

$$n^{**} = \lceil n^* \rceil \tag{4.25}$$

the number of shots required to destroy the target with probability p^* can be obtained. A visualization of relationship (4.24) is presented in **Fig. 4.10**.

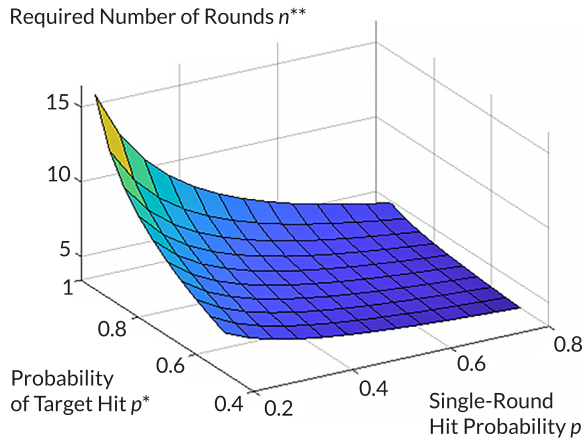

Fig. 4.10 Graphical representation of relationship (4.24)

Considering the discrete nature of the variable n^{**} (**Fig. 4.10**), only nodal values are used.

The obtained value n^* is correlated with the available ammunition load according to Criterion 3. If $n^{**} > (AS_{full} - n^t_{shot})$, the assigned task is infeasible. It is provided that the ammunition load is sufficient, the input data of Criterion 4 are verified. If firing in the MRSI mode is not possible, the operation can only be carried out by single shots with a rate of fire determined according to Criterion 5.

Subsequently, the time budget required to engage a high-priority target is assessed. The time allocated for accomplishing the fire mission against the EDT, denoted as t^*, includes the time required to prepare the artillery system for firing during a short halt t_{prep_fire}, the firing time $t_{fire} = n^{**} / RF_t$, and the projectile time of flight to the EDT t_{flight}

$$t^* = t_{prep\_fire} + t_{fire} + t_{flight}. \tag{4.26}$$

This time shall not exceed the duration of the window of enhanced danger Δt_{WED}

$$t^* < \Delta t_{WED}. \tag{4.27}$$

If condition (4.27) is not satisfied, the execution of the mission is considered impractical.

The safety of the artillery system is associated with the possibility of its detection by enemy artillery covering the EDT. It is assumed that detection occurs after four

shots [22]. In this case, the time of possible engagement of the artillery system is determined by the following expression

$$t_{fire}^{enemy} = 4 / RF_t + t_{prep}^{enemy} + t_{flight}, \tag{4.28}$$

where t_{fire}^{enemy} – the time required by the enemy to determine the coordinates of the TFP and prepare for firing. It is assumed here that the enemy covering artillery is deployed close to the EDT; therefore, the projectile time of flight is approximately the same as that from the TFP to the EDT.

If $t_{fire} + t_{flight} < t_{fire}^{enemy}$, the mission can be accomplished even under the risk of losing the artillery system, which is justified by the higher value of the EDT. If $t_{fire} + t_{flight} > t_{fire}^{enemy}$, the maneuverability criterion becomes decisive, and the artillery system must immediately leave the TFP.

4.7.4 Example of calculation and analysis of results

The effectiveness of the SPAS in engaging the EDT is evaluated under the condition of achieving the specified probability of destruction $p^* = 0.95$. The duration of the window of enhanced danger is $\Delta t_{WED} = 300$ s. The projectile time of flight is $t_{flight} = 60$ s; an analogous value is assumed for the projectiles of the enemy's covering artillery.

According to the results of the dynamic assessment, the SPAS is in the state $State^t <1,1.1;\ 2,2.1;\ 3,3.1;\ 4,4.1;\ 5,5.1>$, which corresponds to the "ideal point". The probability of a hit with a single shot is $p = 0.9$. According to (4.25), to ensure $p^* = 0.95$, $n^{**} = 4$ shots are required. Firing is conducted in the MRSI mode; the firing time is $t_{fire} = 30$ s, and the preparation time before opening fire is $t_{prep\_fire} = 20$ s.

The total time required to accomplish the mission is

$$t^* = t_{prep\_fire} + t_{fire} + t_{flight} = 20 + 30 + 60 = 110 \text{ s},$$

$110 \text{ s} < \Delta t_{WED} = 300$ s – therefore, the mission can be accomplished.

If detection occurs after the fourth shot during the 60 s projectile flight time, the system, moving at a speed of 60 km/h, relocates approximately 1 km from the TFP, thereby avoiding engagement.

The calculation results for different technical states of the system are summarized in **Table 4.2**, which makes it possible to compare the impact of system degradation on the required number of shots, mission duration, and final outcome.

Table 4.2 Comparative results of evaluating the SPAS effectiveness for different technical states

Example No.	State of the SPAS	p	n^{**}	t_{fire}, s	t^{*}, s	Result
1	Ideal	0.9	4	30	110	Mission without losses
2	Partial degradation	0.7	7	70	150	Mission with risk
3	Significant degradation	0.5	10	120	200	Mission with SPAS loss

Analysis of the tabulated data confirms a regular increase in mission execution time and in the required number of shots as the technical condition of the SPAS deteriorates, which increases the risk of its destruction.

The presented examples demonstrate the implementation of the four-component model of combat operations of the SPAS (**Fig. 4.11**).

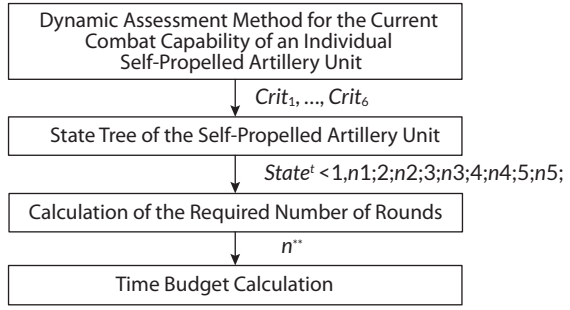

Fig. 4.11 Four-component model of combat operations of an individual SPAS

The obtained results are consistent with previously reported studies on acoustic identification of artillery shots and barrel wear modeling [15–19]. In contrast to earlier approaches focused on individual subsystems, the proposed method integrates acoustic, visual, thermodynamic, and mechanical parameters into a unified decision-support framework.

4.8 Conclusions

This chapter develops a comprehensive model for assessing the state of an artillery system as a multifactor dynamic object operating under conditions of accumulated wear and external combat impact. The integration of acoustic, visual, thermodynamic,

and mechanical parameters into a unified system for quantitative evaluation of technical condition and residual service life is substantiated. A state tree of the system is constructed, formalizing possible technical configurations of the SPAS and enabling a rank-based assessment of its combat capabilities. An analytical expression is derived for determining the required number of shots to engage a target with a specified probability, establishing a link between the system state and mission parameters.

A model for temporal evaluation of combat mission execution is proposed, taking into account the balance between firing time, maneuvering time, and the target engagement time window. An integrated system of combat capability criteria is developed with aggregation of indicators using the ideal point method, ensuring justified decision-making regarding the feasibility of opening fire.

The obtained results form a methodological basis for further automation of artillery system condition monitoring and may be implemented as an algorithmic module in decision support systems for combat employment.

Conflict of interest

The authors declare that they have no conflict of interest in relation to this research, whether financial, personal, authorship or otherwise, that could affect the research and its results presented in this paper.

Use of artificial intelligence statement

Artificial intelligence technology was used in the preparation of this chapter. Specifically, the authors used OpenAI ChatGPT (model GPT-5.2) to assist in editing and structuring introductory text sections and in formulating generalized descriptions of research methodologies for integrating mandatory literature sources into the chapter introduction.

The authors bear full responsibility for the final manuscript. Generative AI tools are not credited and are not responsible for the final results.

Authors' contributions

Oksana Maksymova: Conceptualization, Methodology, Development of integrated system model, Supervision, Writing – original draft.

Pavlo Gultsov: Literature review, Data curation, Comparative analysis, Writing – review & editing.

Volodymyr Demydenko: Mathematical modeling, Numerical analysis, Model validation, Visualization.

Yevhenii Dobrynin: Formal analysis, Development of evaluation criteria, Interpretation of results, Writing – review & editing.

References

1. Boltenkov, V., Brunetkin, O., Dobrynin, Y., Maksymova, O., Kuzmenko, V., Gultsov, P. et al. (2021). Devising a method for improving the efficiency of artillery shooting based on the Markov model. Eastern-European Journal of Enterprise Technologies, 6 (3 (114)), 6–17. https://doi.org/10.15587/1729-4061.2021.245854
2. Dobrynin, Y., Volkov, V., Maksymov, M., Boltenkov, V. (2020). Development of physical models for the formation of acoustic waves at artillery shots and study of the possibility of separate registration of waves of various types. Eastern-European Journal of Enterprise Technologies, 4 (5 (106)), 6–15. https://doi.org/10.15587/1729-4061.2020.209847
3. Dobrynin, Y., Brunetkin, O., Maksymov, M., Maksymov, O. (2020). Constructing a method for solving the riccati equations to describe objects parameters in an analytical form. Eastern-European Journal of Enterprise Technologies, 3 (4 (105)), 20–26. https://doi.org/10.15587/1729-4061.2020.205107
4. Brunetkin, O., Beglov, K., Brunetkin, V., Maksymov, O., Maksymova, O., Havaliukh, O. et al. (2020). Construction of a method for representing an approximation model of an object as a set of linear differential models. Eastern-European Journal of Enterprise Technologies, 6 (2 (108)), 66–73. https://doi.org/10.15587/1729-4061.2020.220326
5. Brunetkin, O., Maksymov, M., Brunetkin, V., Maksymov, O., Dobrynin, Y., Kuzmenko, V. et al. (2021). Development of the model and the method for determining the influence of the temperature of gunpowder gases in the gun barrel for explaining visualize of free carbon at shot. Eastern-European Journal of Enterprise Technologies, 4 (1 (112)), 41–53. https://doi.org/10.15587/1729-4061.2021.239150
6. Brunetkin, O., Maksymov, M., Dobrynin, Y., Demydenko, V., Sidelnykov, O. (2024). Development of a process model for determining the composition and energy characteristics of a pyrotechnic mixture using the library method.

EUREKA: Physics and Engineering, 5, 99–112. https://doi.org/10.21303/2461-4262.2024.003453
7. Brunetkin, O., Dobrynin, Y., Maksymenko, A., Maksymova, O., Alyokhina, S. (2020). Inverse problem of the composition determination of combustion products for gaseous hydrocarbon fuel. Computational Thermal Sciences: An International Journal, 12 (6), 477–489. https://doi.org/10.1615/computthermalscien.2020034878
8. Maksymov, M. V., Brunetkin, O. I., Beglov, K. V., Alyokhina, S. V., Butenko, O. V. (2022). Automatic Control for the Slow Pyrolysis of Organic Materials with Variable Composition. Advanced Control Systems. River Publishers, 397–434. https://doi.org/10.1201/9781003337010-16
9. Brunetkin, O. I., Beglov, K. V., Maksymov, M. M., Ulytska, O. O. (2021). Model and method of controlled pyrolysis of organic substances ofvariable composition. International Scientific Technical Journal "Problems of Control and Informatics", 66 (1), 134–146. https://doi.org/10.34229/1028-0979-2021-1-12
10. Brunetkin, O., Sidelnykov, O., Maksymov, M., Dobrynin, Y. (2025). Improving the model for determining the composition of gunpowder gases during thermal destruction of gunpowder in a limited volume space. Eastern-European Journal of Enterprise Technologies, 3 (6 (135)), 35–45. https://doi.org/10.15587/1729-4061.2025.330654
11. Miller, S. W. (2017). Shoot and scoot. Armada International. Available at: https://www.armadainternational.com/2017/08/shoot-scoot-artillery/
12. Nadler, J., Eilbott, J. (1971). Optimal Sequential Aim Corrections for Attacking a Stationary Point Target. Operations Research, 19 (3), 685–697. https://doi.org/10.1287/opre.19.3.685
13. Shim, Y., Atkinson, M. P. (2018). Analysis of artillery shoot-and-scoot tactics. Naval Research Logistics (NRL), 65 (3), 242–274. https://doi.org/10.1002/nav.21803
14. Guzik D. M. (1988). Markov model for measuring artillery fire support effectiveness [Master's thesis; Naval Postgraduate School].
15. Akman, Ç. (2017). Multishooter localization with acoustic sensors [Master's thesis; Middle East Technical University].
16. Brunetkin, O., Kuzmenko, V., Soloviova, O. (2022). Mathematical model of energy transformation processes in barrel system for determining shooting performance. Energy Engineering and Control Systems, 8 (1), 28–39. https://doi.org/10.23939/jeecs2022.01.028
17. Dobrynin, Y. V., Boltenkov, V. O., Kuzmenko, V. V., Maksymov, O. M. (2022). Development of a universal binary classifier of the state of artillery barrels by

the physical fields of shots. Applied Aspects of Information Technology, 5 (4), 289–302. https://doi.org/10.15276/aait.05.2022.19
18. Maksymov, M. V., Kuzmenko, V. V., Soloviova, O. V. (2021). Method for determining the temperature of powder gases along the barrel length during the firing process. Results of Modern Scientific Research and Development. Proceedings of the 7th International Scientific and Practical Conference. Madrid: Barca Academy Publishing, 95–99. Available at: https://sci-conf.com.ua/vii-mezhdunarodnaya-nauchno-prakticheskaya-konferentsiya-results-of-modern-scientific-research-and-development-19-21-sentyabrya-2021-goda-madrid-ispaniya-arhiv/
19. Tarakhtii, O. S., Kuzmenko, V. V. (2022). Avtomatyzovane diahnostuvannia postriliv artyleriiskoi harmaty na osnovi parametriv, yaki maiut riznu fizychnu pryrodu vynyknennia. Eurasian Scientific Discussions. Proceedings of the 10th International Scientific and Practical Conference. Barcelona: Barca Academy Publishing, 149–156. Available at: https://sci-conf.com.ua/wp-content/uploads/2022/10/EURASIAN-SCIENTIFIC-DISCUSSIONS-23-25.10.22.pdf
20. ARCHER Mobile Howitzer. BAE Systems. Available at: https://www.baesystems.com/en/product/archer
21. Horbenko, V., Kuchynska, A., Hudym, V. (2023). Features of targeting in current combined and future multi-domain operations. Air Power of Ukraine, 2 (5), 10–16. https://doi.org/10.33099/2786-7714-2023-2-5-10-16
22. Kopp, C. (2005). Artillery for the army: Precision fire with mobility. Defence Today, 4 (3), 12–16. Available at: https://www.ausairpower.net/SP/DT-SPH-0705.p

CHAPTER 5

Methods for rapid determination of the composition and condition of nitrocellulose propellants based on thermodynamic modeling

Oleksandr Brunetkin
Oksana Maksymova
Yevhenii Dobrynin
Oleksandr Sidelnykov

Abstract

A method for rapid verification of the composition and energetic characteristics of nitrocellulose propellants is presented. It is based on a library approach to solving direct and inverse problems of thermal decomposition modeling. The library method forms a multidimensional array of solutions by varying elemental composition, enthalpy, and combustion conditions. This approach allows efficient determination of propellant composition from measurable parameters, primarily the temperature and combustion conditions of the reaction products, even in ill-conditioned inverse problems. An algorithm for encoding initial parameters and a procedure for successive data reduction ensure unambiguous reconstruction of the composition. Special attention is given to modeling combustion in closed volumes, selecting real-gas equations of state, accounting for pressure effects, chemical equilibrium, and possible formation of condensed phases. The results provide a theoretical and methodological basis for practical tools to rapidly assess propellant condition and refine internal ballistics parameters under limited information.

Keywords

Nitrocellulose propellants, library method, rapid composition verification, inverse identification problems, Amagat's law, Peng-Robinson equation of state.

5.1 Introduction

Reliable determination of the composition and energetic characteristics of nitrocellulose propellants remains a critical task for both research applications and practical firing conditions. In real operation, propellant properties evolve due to storage

© The Author(s) of individual chapters, 2026 DOI: 10.21303/978-9908-8450-1-2.ch5

aging, manufacturing variability, and differences between laboratory and firing environments. As a result, the actual state of a propellant charge may differ substantially from nominal data, which complicates internal ballistics calculations and reduces the reliability of predicted firing parameters. Traditional laboratory methods provide accurate information but are often too slow or technically demanding to support rapid decision-making when only limited experimental data are available.

A key difficulty arises from the inverse nature of the problem: the composition of a propellant must be inferred from indirectly measurable quantities such as combustion temperature, pressure, or gas parameters. These inverse identification problems are typically ill-conditioned, meaning that small measurement uncertainties can lead to significant ambiguities in the reconstructed composition. Direct analytical reconstruction is therefore impractical in many cases, which necessitates alternative computational approaches capable of operating under uncertainty while maintaining sufficient speed for practical use.

This chapter presents a methodology for rapid determination of nitrocellulose propellant composition and condition based on thermodynamic modeling and a library-based computational strategy. The proposed approach separates the process into a preparatory stage, during which a large set of direct thermodynamic problems is solved and structured into a searchable data array, and an operational stage, where experimentally measured parameters are matched with pre-calculated solutions. Such separation allows the main computational burden to be transferred to an offline phase, enabling fast identification procedures under field or laboratory conditions with limited resources.

Particular attention is given to modeling the thermal decomposition of propellants under conditions that differ from conventional laboratory assumptions. These include combustion in closed volumes, the use of real-gas equations of state at elevated pressures, and the possible formation of condensed phases. By combining equilibrium modeling with an efficient encoding and data-reduction procedure, the chapter aims to provide a consistent framework for rapid verification of propellant composition and for improving the accuracy of internal ballistics calculations when only partial experimental information is available.

5.2 Condition of the propellant charge

5.2.1 Reasons for the need for rapid determination of propellant condition

The replenishment rate of propellant stocks depends on production capacity and resources, while storage conditions influence their long-term stability. A distinctive

feature of nitrocellulose (NC) propellants is the gradual change in their chemical composition and performance during storage. Even under controlled conditions, degradation processes cannot be completely prevented. As a result, the characteristics of propelling charges may vary significantly, especially after the expiration of guaranteed storage periods.

Selective batch testing and limited data for individual charges complicate firing planning, since variations in propellant properties affect ballistic performance. During intensive operations, these challenges increase due to the use of charges from different production batches and storage conditions.

These factors highlight the necessity of developing methods for rapid assessment of propellant condition directly at the point of use.

5.2.2 Features of the thermal decomposition process of nitrocellulose propellant

The thermal decomposition of NC propellants strongly depends on environmental conditions. Laboratory studies typically report predominantly gaseous reaction products [1], whereas firing experiments indicate the formation of condensed free carbon, visually observed as soot ejection with propellant gases [2]. The discrepancy is mainly attributed to differences in pressure and temperature during decomposition. According to [2], free carbon formation may occur via carbon monoxide disproportionation (Boudouard-Bell reaction). This effect should be considered when applying laboratory data to internal ballistics modeling.

5.3 Determination of the composition of a nitrocellulose propellant charge

5.3.1 Selection of a method for the rapid determination of the composition of nitrocellulose propellant and shot parameters

Models of internal ballistics processes, as well as of the thermal decomposition of NC propellant under laboratory conditions, are in many cases based on the consideration of equilibrium reactions of propellant gas formation. In such models, the gross formula of the propellant is sufficient for calculations. However, direct experimental determination of gas composition requires complex laboratory techniques.

Gas chromatography is widely used [3], but it has limitations such as long analysis times and sequential determination of components.

New methods, such as Raman spectroscopy, are being studied, but they are still mainly at the laboratory stage and difficult to use in the field [4].

A method was proposed to determine the composition of organic fuel gas from measured combustion data [5]. A similar approach can be used for nitrocellulose propellant.

The following features of the method proposed in [5] should be noted. The model links the composition of the fuel with its combustion products using chemical equilibrium and mass conservation for the main elements (C, H, O, N) [5]. This allows solving the inverse problem of determining the fuel composition from measured data

$$C_{m_C}H_{m_H}O_{m_O}N_{m_N}. \tag{5.1}$$

A list of possible gaseous reaction products is specified, for example

$$CO, CO_2, H_2O, H_2, N_2. \tag{5.2}$$

A balance is constructed between the chemical elements in the initial substances (5.1) and the reaction products (5.2). The element balance is formed on the basis of the law of mass action for the equations of formation of the corresponding reaction product components. For example, for CO_2

$$CO_2 \leftrightarrow C + 2 \cdot O. \tag{5.3}$$

In addition, mass conservation equations are written for each chemical element from (5.1). Chemical equilibrium constants for gaseous components are most often specified in terms of partial pressures. In this case, it is more rational for the concentrations in the mass action equations to be numerically equal to the partial pressures of the corresponding components. To relate concentrations to partial pressures, the total amount of substance M_T is introduced. Dalton's law is applied to close the system of equations

$$K_{CO_2}(T) = \frac{P_C \cdot P_O^2}{P_{CO_2}}, \tag{5.4}$$

where T – the temperature of the mixture of reaction products, determined as a result of the calculations; P_C, P_O, P_{CO_2} – the partial pressures of the terms in equation (5.3), numerically equal to their concentrations.

On the basis of such a model, the inverse problem can also be solved. The mathematical model determines the interrelation between its parameters. Their assignment as input data or calculation results is subjective in nature. In the example considered above, the following are chosen as input data: the gross formula of the fuel gas in the form

$$C_{b_C} H_{b_H} O_{b_O} N_{b_N}, \tag{5.5}$$

the gross formula of the oxidizer, for example oxygen O_2 or air, the ratio of their volumetric flow rates (V_V), and the chemical equilibrium constants for all combustion products $K_P^i(T)$. The calculation results are the partial pressures (P_i) of the combustion product components (5.2) and their temperature T.

The unknown coefficients b_C, b_H, b_O, b_N are treated as additional unknowns, while the measured temperature is input data. Changing V_V then affects the fuel formula and combustion temperature. Experiments vary input parameters, measure the combustion products, and then use the model to determine the fuel composition. Direct solution can be difficult due to poor conditioning, so the library method is applied [6].

5.3.2 Library method for determining the composition of a gaseous fuel

The library method solves direct and inverse problems efficiently through two stages: preparation and solution selection. During preparation, multiple calculations are performed with varied input data to create a library of solutions.

The library is populated by repeatedly solving the direct problem while varying key parameters, including the elemental composition, the volumetric ratio of fuel and oxidizer (V_V), and the enthalpy of the combustible gas. Normalization of the elemental composition reduces the number of required solutions without losing information.

During the solution selection stage, input data are matched with stored library entries, and the corresponding solution is selected. This allows rapid determination of firing parameters for specified propellant compositions.

For the inverse problem, the same gas temperature may correspond to different propellant compositions. Measurement errors make this more pronounced, necessitating a specialized algorithm to determine NC propellant composition from technological parameters.

5.3.2.1 Procedure for filling the library

When generating the library, a specific feature should be noted. The results of solving the direct problem are transformed into a form suitable for practical use in searching for a solution.

The main portion of the calculated data array obtained from solving the direct problem consists of the partial pressures of gaseous components in the combustion products (CP) mixture. When determining the composition of the initial fuel, these quantities are not directly involved and, therefore, are not included in the generated library.

The fuel composition is formed by varying the parameters d_H, d_O, d_N, thus defining a specific elemental composition of the fuel for each realization of the direct problem.

For each such case, the ratio of volumetric flow rates of the fuel and oxidizer, V_V, is determined.

For all possible combinations of the input parameters V_V, d_H, d_O, d_N, I_t that arise during their variation within specified ranges, an attempt is made to solve the direct problem of determining the combustion products temperature. In some cases, the considered combinations of fuel composition and its enthalpy turn out to be physically incompatible, which makes obtaining a solution impossible. Such calculation variants are excluded from further consideration.

For the remaining successfully implemented variants of the direct problem solution, the set of initial parameters d_H, d_O, d_N, I_t are encoded as a single numerical identifier based on the positional principle of decimal number representation. Each parameter is normalized within predefined bounds (5.6)

$$\tilde{d}_H = \frac{d_H - d_H^l}{d_H^r - d_H^l} \cdot 100, \tag{5.6}$$

after which the normalized values are encoded into a single positional identifier "*E*" (**Fig. 5.1**).

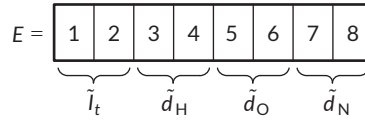

Fig. 5.1 Diagram of positional representation in the form of a single number of normalized values of the original data

As a result, information complexes are formed in which each pair of output parameters of the direct problem solution – the combustion products temperature T and the volumetric flow rate ratio V_V – corresponds to a unique number "E" that contains, in a packed form, the values of the input parameters that led to this solution.

At the next stage, the results of calculating the combustion products temperature T and the volumetric flow rate ratio V_V are structured into a discretized $T - V_V$ plane with predefined resolution. The discretization step is selected according to the required computational accuracy and experimental resolution, while cell boundaries are defined by relations (5.7)–(5.9):

$$\Delta T = \frac{T^r - T^l}{N},\ \Delta V = \frac{V_V^r - V_V^l}{M}, \tag{5.7}$$

where N and M – the numbers of discretization elements (intervals) along the temperature T axis and the volumetric flow rate ratio V_V axis, respectively. Cell boundaries on the $T - V_V$ plane are given by:

$$T_i^l = T^l + \Delta T \cdot (i-1),\ T_i^r = T^r + \Delta T \cdot i,\ i \in [0, N]. \tag{5.8}$$

$$\begin{aligned}(V_V)_j^l &= (V_V)^l + \Delta V \cdot (j-1),\\ (V_V)_j^r &= (V_V)^r + \Delta V \cdot j,\ j \in [0, M],\end{aligned} \tag{5.9}$$

where i and j – the cell indices along the corresponding T and V_V axes.

Each cell on the $T - V_V$ plane is associated with a vector of dimension L (**Fig. 5.2**), whose elements are the values of numbers E_k corresponding to direct problem solutions that fall within this cell. Each cell contains a vector of encoded identifiers E_k sorted along the enthalpy axis I_t. The leading digits of E_k correspond to enthalpy intervals.

Only those E_k values that fall within the specified enthalpy variation limits are placed into the elements of each vector.

Thus, as a result of preliminary solving a set of direct problems and subsequent processing of the calculated data, a working three-dimensional array is formed. The values contained in this array can be used to determine the composition of various types of fuels, provided that their gross formulas include the chemical elements used in forming the array. The presence of all elements is not mandatory. In particular, the formed array can be used to determine the composition of both oxygen-containing and oxygen-free hydrocarbon fuels when they are combusted either in air or in oxygen without nitrogen admixture.

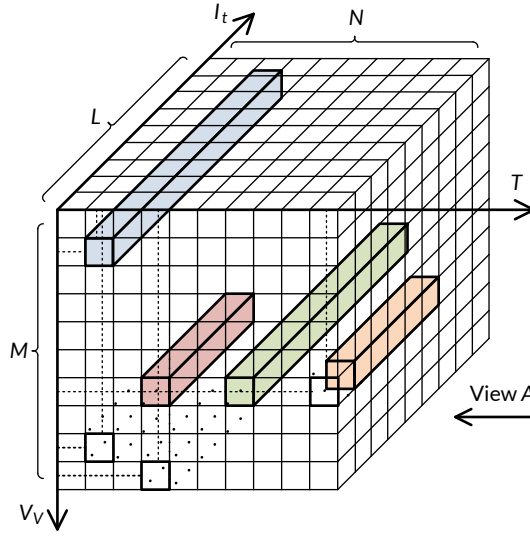

Fig. 5.2 Scheme of forming a structured working three-dimensional array based on the input data and the results of solving the direct problem

5.3.2.2 Determination of fuel composition using library data (inverse problem)

The method for determining the fuel composition using the constructed working three-dimensional array is implemented as a sequential procedure of data selection and reduction, based on matching experimentally measured parameters with the results of a previously solved set of direct problems.

At the first stage, the ratio of volumetric flow rates of oxidizer and fuel $(V_V)_j$ is varied and fixed. For each prescribed value, the temperature of the combustion products T_j is measured. The number of variations and corresponding measurements is determined by the number of unknown fuel composition parameters. The unknown parameters of the fuel composition, including elemental amounts and enthalpy, are then narrowed down by selecting library entries consistent with the measurements.

In accordance with the experimentally obtained values T_j and $(V_V)_j$, the corresponding cells are selected on the $T - V_V$ plane of the working three-dimensional array; these cells are shown in **Fig. 5.2** by dashed lines, along with the associated vectors highlighted in color. The data contained in the remaining vectors of the array are

not used at this stage of the analysis. The elements of each selected vector are the numbers E_k, which encode all possible combinations of the parameters d_H, d_O, d_N, I_t, that ensure attainment of the measured temperature T_j at the given volumetric flow ratio corresponding to the selected cell.

At the next step, the selected vectors are projected onto the $V_V - I_t$ plane (view *A* in **Fig. 5.2**), or, in effect, onto the enthalpy axis I_t. Possible variants of the mutual arrangement of the vector projections are schematically shown in **Fig. 5.3** and highlighted in color. Since, for all variations of the volumetric flow ratio, the composition and enthalpy of the fuel being determined remain unknown but invariant, the corresponding values of the numbers E_k must be present in all considered vectors. On this basis, a subset of elements common to all projected vectors is identified; in **Fig. 5.3** this subset is denoted as region *D*. Under real conditions, this region may cover more than two discretization intervals along the enthalpy axis. All other vector elements are excluded from further consideration.

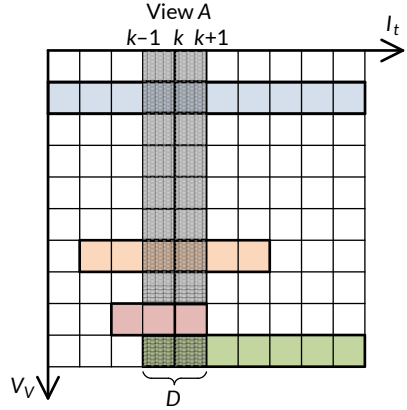

Fig. 5.3 Example of projection of the selected vectors

The most significant digits of E_k encode the fuel enthalpy. During filtering, encoded numbers are iteratively reordered so that each parameter becomes the leading digit at the corresponding stage (**Fig. 5.4**), enabling successive reduction of admissible solutions.

The described procedure is successively repeated until all quantities from the list of parameters to be determined – d_H, d_O, d_N, I_t – have been used. At each subsequent stage, the selection of numbers is performed not by coincidence of enthalpy I_t, but by the value of the parameter encoded in the most significant digits of the

number E_k at the current step. Thus, during the second pass this parameter is d_H, during the third pass it is d_O, and so on. With each new pass, the number of considered E_k values decreases.

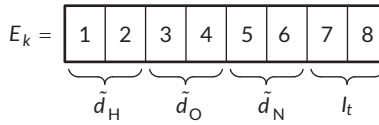

Fig. 5.4 Positional representation scheme in the form of a single number composed of normalized values of the original data after their rearrangement

As a result, a single number E_k remains, which contains the values of the original parameters in a packed form. These values are consistent with all experimentally measured temperatures T_j at the specified volumetric flow ratios $(V_v)_j$. This number uniquely defines the sought fuel composition and enthalpy.

5.3.3 Library method for determining the composition of nitrocellulose propellant

5.3.3.1 Specific features of solving the direct problem when populating the library and determining propellant gas parameters during a shot

The library method is used to solve the inverse problem – determination of the composition of NC propellant. The library is populated based on repeated solutions of the direct problem, i.e., determination of the physical characteristics of propellant gases (PG) under controlled variation of the propellant composition. In the case considered, the physical characteristics of propellant gases during a shot are also determined by solving the direct problem for a previously identified NC propellant composition. In both cases, equilibrium models of propellant gas formation are employed. Under these conditions, the use of identical modeling approaches is considered justified.

Calculation of the propellant gas composition using an equilibrium model that allows for the formation of free carbon predicts its presence. However, laboratory experiments do not confirm this. This does not indicate an error in the equilibrium model but reflects the absence of conditions required for the Boudouard-Bell reaction. To use a single model for solving both the direct and inverse problems, it is sufficient to account for the presence or absence of the possibility of condensed-phase (free carbon) formation.

In the example discussed above, when determining the composition of the combustion products of an organic fuel, only the gaseous phase was considered. In this case, the use of partial pressures is justified. This approach is applied in most calculations of the composition and temperature of propellant gases. However, when the possibility of condensed carbon formation is taken into account, computational difficulties arise in determining its amount via partial pressure. It appears more rational to construct a model using mole fractions of the propellant gas components. This approach allows representation of the composition in both gaseous and condensed phases.

Equilibrium models employ an equation of state (EOS) that defines the relationship between p, V, T under thermodynamic equilibrium. The specific form of the EOS depends on the parameter ranges involved. The thermal decomposition of NC propellant is accompanied by high temperatures of 2500–3500 K. At such temperatures and at moderate pressures typical of most laboratory experiments, the ideal gas equation of state is often used, especially at the initial stage of calculations.

At high pressures characteristic of firing conditions, it becomes necessary to account for the finite molecular volume and intermolecular attraction. In this case, a real-gas equation of state is used. Depending on pressure and temperature, ideal-gas, Noble-Abel, virial, and cubic equations of state may be applied. For high-pressure firing conditions, the Peng-Robinson EOS provides the most stable numerical behavior [2].

When increased accuracy is required, more advanced real-gas EOS may be applied; however, for high-pressure firing conditions the Peng-Robinson EOS provides the most stable numerical behavior and is therefore adopted in this work [2]. This property is more important than high accuracy at low pressures.

All numerical calculations were performed using custom-developed software written in C++. The computational experiments included large-scale equilibrium simulations for generating the initial dataset and constructing the solution library. Calculations were carried out on personal computers equipped with Intel Core i5 and i7 processors and 8 GB RAM under Windows 10 OS. Graphical dependencies and diagrams presented in this chapter were prepared using Microsoft Excel.

5.3.3.2 Model of the propellant gas formation process using mole fractions

The possibility of the presence of a condensed phase in the composition of propellant gases is not the only reason necessitating the modernization of the model and algorithm described in Section 5.2.2.1 for determining the composition of propellant gases.

In the original model, the pressures of the gaseous reaction products are expressed in pascals (Pa). The chemical equilibrium constants K_P given in reference literature are defined for such quantities. In the modified model, the quantities of the gaseous components of the propellant gases are expressed in bars (bar). In this case, the partial pressures of the gaseous combustion products are equal to their mole fractions. The amounts of condensed substances can also be expressed in the same units. To write the equations in accordance with the law of mass action, chemical equilibrium constants K_X defined in terms of mole fractions must be introduced. For a reversible reaction of the form

$$aA + bB \Leftrightarrow cC + dD, \tag{5.10}$$

the constants K_P and K_X are related by

$$K_P = K_X \cdot P^{(c+d-a-b)} \Rightarrow K_X = \frac{K_P}{P^{(c+d-a-b)}}, \tag{5.11}$$

where A, B, C, D are the chemical species participating in the reaction; a, b, c, d are the stoichiometric coefficients; P is the pressure of the mixture of gaseous reaction products expressed in Pa; K_P is the chemical equilibrium constant defined in terms of partial pressures (a reference value).

For example, for a reaction of the form

$$H_2O \Leftrightarrow 2 \cdot H + O \Rightarrow K_X = \frac{K_P}{P^{(c+d-a-b)}} = \frac{K_P}{P^{(2+1-1)}} = \frac{K_P}{P^2}. \tag{5.12}$$

A distinctive feature of the model is the introduction of the equation describing soot formation

$$C_{crb} \Leftrightarrow C \Rightarrow \frac{P_C}{P_{C_{crb}}} = K_{X(C_{crb})}(T), \tag{5.13}$$

where P_C [bar] is the partial pressure and simultaneously the mole fraction of carbon vapor; $P_{C_{crb}}$ is the mole fraction of the formed soot; $K_{X(C_{crb})}(T)$ is the chemical equilibrium constant for the corresponding temperature.

When writing the law of conservation of matter for carbon, the amount of formed soot is taken into account in the balance of propellant combustion products, as in the original version.

The resulting system of equations is nonlinear. The solution is obtained iteratively on the basis of a linearized system of equations. During linearization, it is also necessary to account for the specific features of the mass-action-law equations arising

from the different aggregate states of the propellant gases and soot. In the original model, it was assumed that, at a given temperature, the partial pressure of carbon is independent of the amount of its condensed phase. In this case, when linearizing equation (5.13), the derivative of P_C was set equal to zero. In the present model, the calculation is performed using mole fractions. In this case, the components P_C and $P_{C_{crb}}$ in equation (5.13) have the same status. When linearizing this equation, derivatives are taken with respect to both quantities.

5.3.3.3 Influence of experimental conditions on the model of the thermal decomposition process of nitrocellulose propellant

In the original version of the library method [6], the library was populated by modeling the combustion process in an open vessel at constant pressure. The effect of changing the ratio of gaseous fuel and oxidizer on the temperature of the combustion products was used. Due to the constancy of the pressure of the combustion products, as well as the use of the partial pressures of the reaction product components as a measure of their concentration, Dalton's law was used as the closing relation – the pressure in the chamber is equal to the sum of the partial pressures of the reaction products.

When applying the library method to determine the composition of NC propellant, this approach does not correspond to the experimental conditions. Combustion of propellant samples occurs in a closed volume. The pressure of the propellant gases is variable, while their volume is constant. In a closed vessel, varying propellant mass changes afterburning conditions and gas temperature due to oxygen balance effects. When air is used instead of oxygen, nitrogen contained in the air will also act as a inert ballast gas.

At constant vessel volume, instead of the partial pressures of the propellant gas components, their partial volumes are used

$$V_i = V_{im} \cdot n_i, \tag{5.14}$$

where V_{im} is the volume of one mole of the corresponding gaseous component of the propellant gases at the temperature and pressure of the gas mixture; n_i is the number of moles of the corresponding gaseous component of the propellant gas mixture.

The value V_{im} is determined from the equation of state.

Consider an example of an equilibrium model of thermal decomposition of NC propellant with an overall (gross) formula of the form (5.5), although other chemical

elements may be added if necessary. For the selected reaction products (5.2), with the addition of condensed carbon C_{crb}, the equations of their formation are written as:

$$\begin{aligned}&H_2O \rightleftarrows 2\cdot H+O, CO_2 \rightleftarrows C+2\cdot O, CO \rightleftarrows C+O,\\ &H_2 \rightleftarrows 2\cdot H, O_2 \rightleftarrows 2\cdot O, N_2 \rightleftarrows 2\cdot N, C_{crb} \rightleftarrows C,\end{aligned} \tag{5.15}$$

and the chemical equilibrium equations for them are:

$$\begin{aligned}&\frac{n_H^2\cdot n_O}{n_{H_2O}}=K_{nH_2O}(T,P), \frac{n_C\cdot n_O^2}{n_{CO_2}}=K_{nCO_2}(T,P),\\ &\frac{n_C\cdot n_O}{n_{CO}}=K_{nCO}(T,P), \frac{n_H^2}{n_{H_2}}=K_{nH_2}(T,P),\\ &\frac{n_O^2}{n_{O_2}}=K_{nO_2}(T,P), \frac{n_N^2}{n_{N_2}}=K_{nN_2}(T,P), \frac{n_C}{n_{C_{crb}}}=K_{nC_{crb}}(T,P).\end{aligned} \tag{5.16}$$

Material balance equations:

– for [C]: $m\cdot\frac{b_C}{\mu_\Sigma}=n_{CO_2}+n_{CO}+n_C+n_{C_{crb}}$;

– for [H]: $m\cdot\frac{b_H}{\mu_\Sigma}=2\cdot n_{H_2O}+2\cdot n_{H_2}+n_H$;

– for [O]: $2\cdot n_{air}\cdot\varepsilon_{O_2}+m\cdot\frac{b_O}{\mu_\Sigma}=n_{H_2O}+2\cdot n_{CO_2}+n_{CO}+2\cdot n_{O_2}+n_O$;

– for [N]: $2\cdot n_{air}\cdot\varepsilon_{N_2}+m\cdot\frac{b_N}{\mu_\Sigma}=2\cdot n_{N_2}+n_N$, (5.17)

where n_{air} is the number of moles of air in the vessel before the start of propellant combustion; $\varepsilon_{O_2}, \varepsilon_{N_2}$ is the fraction of the corresponding gas in air; m is the mass of propellant subjected to thermal decomposition; b_C, b_H, b_O, b_N are the numbers of atoms of the corresponding chemical elements in the overall formula of the propellant; μ_Σ is the molecular mass corresponding to the overall formula of the propellant used.

When partial volumes (5.14) are employed in the model under consideration, the closing relation is the equation expressing Amagat's law (fr. *Émile Amagat*). For the adopted list (5.2) of gaseous products of NC propellant thermal decomposition, it has the following form

$$V=n_{H_2O}V_{(m)H_2O}+n_{CO_2}V_{(m)CO_2}+n_{CO}V_{(m)CO}+n_{H_2}V_{(m)H_2}+n_{O_2}V_{(m)O_2}+n_{N_2}V_{(m)N_2}. \tag{5.18}$$

In this equation, the terms on the right-hand side correspond to equation (5.14). In the carbon material balance equation (5.17), the term $n_{C_{crb}}$ is included to account for the presence of condensed carbon. In equation (5.18), the corresponding term is absent. This is due to the small volume of the condensed phase compared to the gaseous phase.

When the numbers of moles n_i are used as the unknowns, it is necessary to determine the molar chemical equilibrium constants $K_{ni}(T,P)$ used in (5.16).

For equations of the form (5.10), the state of chemical equilibrium expressed in terms of molar constants is written as

$$\frac{n_C^c \cdot n_D^d}{n_A^a \cdot n_B^b} = K_n, \tag{5.19}$$

where n_C, n_D, n_A, n_B are the numbers of moles of the corresponding substances A, B, C, D; K_n is the chemical equilibrium constant based on the number of moles.

The partial pressures p_i can be expressed in terms of mole fractions as

$$p_i = X_i \cdot P_\Sigma = \frac{n_i}{\sum n_i} \cdot P_\Sigma, \tag{5.20}$$

where X_i are the mole fractions; P_Σ is the total pressure of the gas mixture; n_i is the number of moles of the corresponding substance; Σn_i is the total number of moles of the gaseous reaction products.

The chemical equilibrium constants expressed in terms of partial pressures for equations (5.10) have the form

$$K_P = \frac{p_C^c \cdot p_D^d}{p_A^a \cdot p_B^b}, \tag{5.21}$$

where the quantities p_i are expressed in (bar). For this reason, P_Σ in (5.20) and in the subsequent transformations is also expressed in bar.

As a result, from (5.20) and (5.21) it follows that

$$K_P = \frac{\left(\frac{n_C}{\sum n_i} \cdot P_\Sigma\right)^c \cdot \left(\frac{n_D}{\sum n_i} \cdot P_\Sigma\right)^d}{\left(\frac{n_A}{\sum n_i} \cdot P_\Sigma\right)^a \cdot \left(\frac{n_B}{\sum n_i} \cdot P_\Sigma\right)^b} = \frac{n_C^c \cdot n_D^d}{n_A^a \cdot n_B^b} \cdot \frac{\left(\frac{P_\Sigma}{\sum n_i}\right)^c \cdot \left(\frac{P_\Sigma}{\sum n_i}\right)^d}{\left(\frac{P_\Sigma}{\sum n_i}\right)^a \cdot \left(\frac{P_\Sigma}{\sum n_i}\right)^b} = K_n \cdot \left(\frac{P_\Sigma}{\sum n_i}\right)^{c+d-a-b}. \tag{5.22}$$

From this it follows that

$$K_n(T,P)=K_P(T)\cdot\left(\frac{\sum n_i}{P_\Sigma}\right)^{c+d-a-b}, \tag{5.23}$$

which confirms the dependence of the quantity K_n, adopted in (5.16), not only on temperature but also on the pressure of the gas mixture. From (5.23), taking into account the equilibrium equation for the condensed phase (5.16), it follows that

$$K_{nU}(T,P)=K_P(T)\cdot\left(\frac{\sum n_i}{P_\Sigma}\right)^{1-1}=K_P(T)\cdot 1=K_P(T). \tag{5.24}$$

Pressure affects the position of equilibrium for reactions accompanied by a change in the number of moles of gas according to Le Chatelier's principle (fr. *Le Chatelier*). The quantities V for the corresponding gas and the total pressure P_Σ are related by the real gas equation of state.

5.3.3.4 Effect of pressure magnitude on the composition of propellant gases

In experimental studies, when different amounts of propellant are burned in a closed vessel, the pressure may reach tens of bar. Under firing conditions, this value can reach several thousand bar. A change in pressure leads to a change in the compressibility factor

$$Z=\frac{PV_m}{RT}, \tag{5.25}$$

and, consequently, to a change in the molar concentrations of the gases even when their mass remains constant. Here, V_m is the molar volume.

Calculated compressibility factors obtained using different equations of state (van der Waals, Noble-Abel, and Peng-Robinson) demonstrate substantial discrepancies over a wide pressure range (**Fig. 5.5–5.7**). These differences confirm that the choice of equation of state significantly affects the predicted composition of propellant gases and justify the use of the Peng-Robinson EOS for high-pressure conditions.

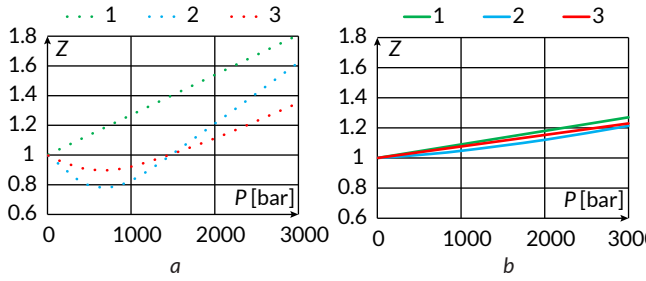

Fig. 5.5 Compressibility factor *Z* as a function of pressure *P* for water vapor (H_2O): *a* – at a temperature of 1000 K; *b* – at a temperature of 3000 K; 1 – using the Noble-Abel equation (covolume); 2 – using the van der Waals equation; 3 – using the Peng-Robinson equation

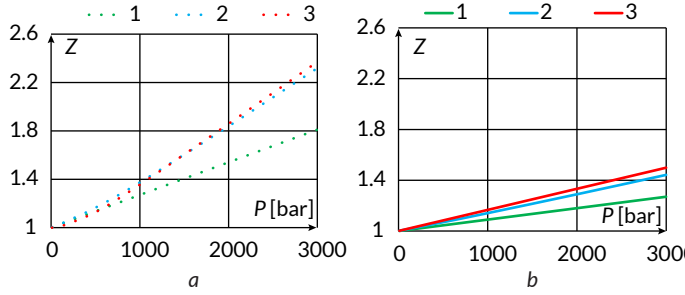

Fig. 5.6 Compressibility factor *Z* as a function of pressure *P* for carbon monoxide (CO): *a* – at a temperature of 1000 K; *b* – at a temperature of 3000 K; 1 – using the Noble-Abel equation (covolume); 2 – using the van der Waals equation; 3 – using the Peng-Robinson equation

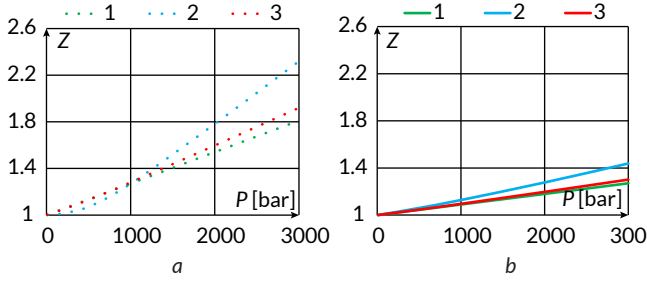

Fig. 5.7 Compressibility factor *Z* as a function of pressure *P* for carbon dioxide (CO_2): *a* – at a temperature of 1000 K; *b* – at a temperature of 3000 K; 1 – using the Noble-Abel equation (covolume); 2 – using the van der Waals equation; 3 – using the Peng-Robinson equation

5.3.3.5 Effect of pressure on the molar equilibrium constant

In addition to affecting molar concentrations, pressure variations according to relation (5.26) can significantly influence molar equilibrium constants even at nearly constant gas temperature. Within the framework of the mathematical model (5.19)–(5.21), computational studies were carried out on the thermal decomposition process of SB1 propellant [11], characterized by the normalized gross formula $C_1H_{1.19}N_{0.384}O_{1.45}$ and an enthalpy of formation $H_f = -96.38$ kJ/mol (normalized per one carbon atom).

Modeling was performed for an evacuated chamber of 0.01 m^3 (10 liters) at propellant masses of 20 and 2400 g, without accounting for condensed carbon formation. The computational case with a mass of 20 g reproduces conditions close to laboratory experiments, while the second corresponds to conditions typical of a firing scenario. The results of the calculations are presented in **Table 5.1**.

Table 5.1 lists: m – burned propellant mass; K_n – molar equilibrium constant; n_i/n_Σ – mole fraction of each component. The last column shows the ratio of the molar equilibrium constants for the experimental and firing conditions. For both propellant masses, the same combustion gas temperature is reached, T [K] = 2070. When burning $m = 20$ g of propellant, the pressure in the vessel is $P = 14.7$ bar. When burning $m = 2400$ g, $P = 2530$ bar.

Table 5.1 Molar equilibrium constants and molar fractions of thermal decomposition products of NC propellant

Component	m [g] = 20		m [g] = 2400		$K_{n\,20} / K_{n\,2400}$
	K_n	n_i/n_Σ	K_n	n_i/n_Σ	
CO_2	4.57E-29	1.19E-01	2.23E-29	9.24E-02	2.05
CO	3.42E-22	4.40E-01	2.38E-22	4.67E-01	1.43
H_2O	1.04E-14	1.35E-01	5.09E-15	1.59E-01	2.05
NO	6.69E-12	3.92E-10	4.67E-12	5.98E-08	1.43
H_2	3.63E-07	1.99E-01	2.53E-07	1.73E-01	1.43
O_2	6.71E-08	1.47E-13	4.69E-08	7.10E-11	1.43
N_2	3.13E-19	1.08E-01	2.18E-19	1.07E-01	1.43

5.3.3.6 Consideration of condensed carbon formation during the thermal decomposition of nitrocellulose propellant

To ensure comparability, database generation and firing simulations must use a unified model. However, a paradoxical situation arises. Equilibrium calculations

that include condensed carbon predict its formation in significant amounts. At the same time, experimental studies of the thermal decomposition of nitrocellulose propellant at low pressure under laboratory conditions do not reveal the formation of free carbon.

On the other hand, in solving internal ballistics problems, the possibility of carbon formation is not taken into account, whereas photographic evidence of firing (**Fig. 5.8**) demonstrates its limitations. A substantial amount of carbon is formed, and it burns out only during the development of the muzzle flash.

Fig. 5.8 Example of condensed carbon (soot) ejection during firing

In [2], a possible mechanism for the formation of condensed carbon during firing was proposed, and in [9, 10] it was examined with respect to various conditions. Based on model (5.14)–(5.17), calculations were performed to simulate the thermal decomposition process of SB1 propellant [11] in an evacuated vessel with a volume of 0.01 m^3 (10 liters). Mass fractions of propellant gas components relative to propellant mass are presented in **Table 5.2**. The Peng-Robinson equation of state was used to describe real gas behavior.

Columns 2–3 show mass fractions with and without condensed carbon. These conditions were modeled by the presence or absence of component (5.13) in the model. The comparison confirms the validity of including condensed carbon formation even when it is not observed. The presence of free carbon (C_{crb}) is not detected. The data presented in columns 2 and 3 correspond to the pyrolytic phase of the shot (the propellant combustion phase).

Columns 4 and 5 (**Table 5.2**) present data corresponding to the expansion process of propellant gases during the thermodynamic stage of the shot at temperatures T = 1000 K and 900 K, respectively. The calculations were performed using the

same model as for the results in column 2. In this case, the formation of free carbon is observed.

Table 5.2 Mass fractions of propellant gases

Component	Percentage of gunpowder mass (2400 g)			
	T [K] = 2070	T [K] = 2070	T [K] = 1000	T [K] = 900
	P [bar] = 2530	P [bar] = 2530	P [bar] = 890	P [bar] = 670
CO_2	17.4	17.4	42.3	49.6
CO	56.0	56.0	25.7	11.7
H_2O	12.3	12.3	11.3	14.4
NO	0.0	0.0	0.0	0.0
H_2	1.5	1.5	1.6	1.3
O_2	0.0	0.0	0.0	0.0
N_2	12.9	12.9	12.9	12.9
C_{crb}	0.0	0.0	6.2	10.2

Calculations of the thermal decomposition of SB1 propellant [11] were performed in a sealed vessel with a volume of 0.01 m^3 (10 L) filled with air. The mass of the propellant charge in the calculations varied from 1 to 20 g, which corresponds to the conditions of experimental studies aimed at determining propellant composition using the library method [6]. The modeling results are presented in **Fig. 5.9** as dependencies of the number of moles of individual propellant gas components on the mass of the burned propellant. The propellant under consideration is characterized by a negative oxygen balance; as a result, the propellant gases formed during thermal decomposition are incompletely oxidized. Additional oxidation of these products occurs due to the oxygen contained in the air inside the vessel.

For propellant masses up to 6 g, the oxygen in the vessel exceeds the stoichiometric requirement for complete afterburning. In the computational model, the corresponding portion of oxygen is treated as an oxidizer participating in the reactions of complete afterburning, whereas the remaining oxygen, together with the nitrogen of the air, is considered as inert ballast gas. These components are taken into account when determining the thermodynamic parameters of the entire gas mixture, in particular its temperature.

When the propellant mass exceeds 6 g, the oxygen content in the vessel becomes insufficient to ensure complete afterburning of the propellant gases.

The boundary shown in **Fig. 5.9** clearly separates the regions corresponding to excess oxygen ($m < 6$ g) and oxygen deficiency ($m > 6$ g), which is of fundamental importance for the interpretation of the modeling results and for the subsequent application of the library method.

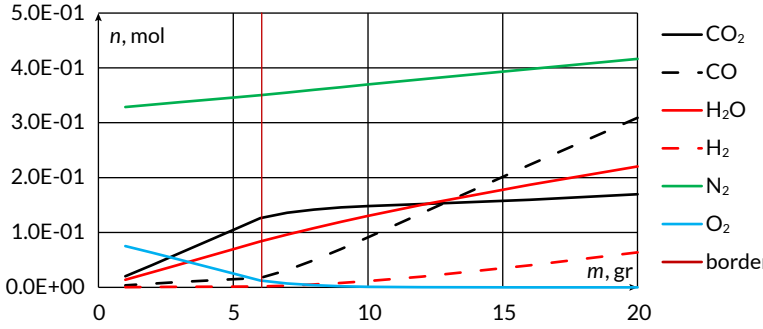

Fig. 5.9 Number of moles of propellant gas components as a function of the mass of propellant burned in a vessel of volume $V = 0.01$ m^3 filled with air

The limiting value of the propellant mass burned in a vessel of a given volume filled with air is also identified by the nature of the variation of thermodynamic parameters, in particular the temperature, of the propellant gases. The corresponding trends are shown in **Fig. 5.10**, **5.11**.

The obtained data correspond to the conditions of the numerical experiment, the results of which are presented in **Fig. 5.9**. In these plots, as in **Fig. 5.9**, the boundary separating the regions of excess oxygen ($m < 6$ g) and oxygen deficiency ($m > 6$ g) is clearly discernible.

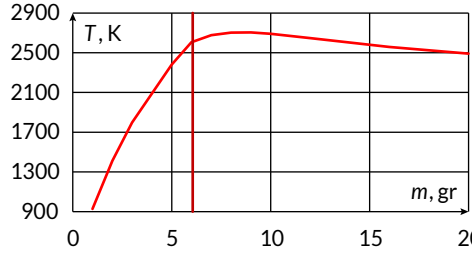

Fig. 5.10 Variation of the temperature of the propellant gas mixture as a function of the propellant mass burned in a vessel of volume $V = 0.01$ m^3 filled with air

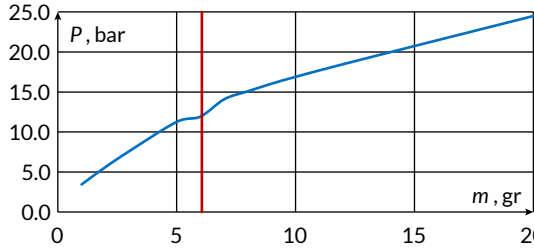

Fig. 5.11 Variation of the pressure of the propellant gas mixture as a function of the propellant mass burned in a vessel of volume $V = 0.01\ m^3$ filled with air

5.4 Conclusions

The presented material demonstrates that the problem of verifying the composition and energetic characteristics of nitrocellulose propellants under real operating conditions is substantially more complex than assumed within conventional laboratory approaches. The primary reason is the combined effect of storage degradation and differences between laboratory and firing conditions.

The analysis confirms that the use of averaged batch data does not provide the required accuracy for internal ballistics calculations, especially after expiration of the guaranteed storage period or when charges of mixed origin are used. This circumstance substantiates the need to move from selective laboratory control to methods of rapid, in-situ assessment of the current propellant state directly at the point of use.

The differences between laboratory conditions and firing conditions are not only quantitative but also qualitative. In particular, the possible formation of condensed carbon at high pressures and temperatures fundamentally alters the composition of reaction products and the energy balance of the system. Neglecting this effect in internal ballistics models may lead to systematic errors in the estimation of pressure, temperature, and energetic characteristics of propellant gases.

The proposed library method demonstrates its effectiveness as a tool for solving ill-conditioned inverse problems in which a theoretically possible direct analytical reconstruction of propellant composition from measured parameters is practically infeasible. A key advantage of the method is the separation of the computational process into two stages: a resource-intensive preparatory stage for generating the solution library and a fast search stage suitable for operational use. This approach

shifts the main computational burden to the "laboratory" phase and minimizes computational requirements under field conditions.

A distinctive feature of the method is the encoding of composition and enthalpy parameters as numerical identifiers, enabling rapid filtering of admissible solutions even under measurement uncertainty. Adapting the method to closed-volume combustion conditions and employing mole fractions with Amagat's law ensures consistency between laboratory modeling and firing simulations. The Peng-Robinson EOS provides a unified description across the entire pressure range considered.

The obtained results demonstrate that the influence of pressure on the composition of propellant gases at a fixed temperature manifests not only through changes in the compressibility factor and, consequently, molar concentrations, but also through variations in molar equilibrium constants (**Table 5.1**). These constants can vary over a wide range – from approximately 40% to nearly a twofold change – leading to noticeable changes in mixture composition. For example, the mole fraction of CO_2 may differ by ~22%, H_2O by ~18%, and H_2 by ~13%. Accounting for this effect explains discrepancies among propellant gas compositions proposed in various empirical models, for which pressure and temperature conditions are often not explicitly specified. The transition from calculations based on partial pressures to those based on molar concentrations made it possible to identify this factor and to justify the use of experimental data obtained at low pressures for firing conditions.

The issue of condensed carbon (soot) formation during the thermal decomposition of nitrocellulose propellants remains debatable only at the level of theoretical models. Experimental observations, including photographic evidence and published studies, unequivocally confirm the practical occurrence of this process. Most internal ballistics calculations focus on the pyrodynamic stage of firing, characterized by high temperatures. Calculations show that, at this stage, conditions for condensed carbon formation are absent, and accounting for or neglecting its formation does not affect the calculated composition of propellant gases.

A different situation arises during the thermodynamic stage of propellant gas expansion, when additional chemical reactions may occur at still high temperatures and pressures. One such reaction is the disproportionation of carbon monoxide (the Boudouard reaction). According to Le Chatelier's principle, increasing pressure shifts the equilibrium of this reaction toward the formation of free carbon. Temperatures on the order of 1000 K and pressures of 30–90 MPa create conditions under which the reaction rate increases by several orders of magnitude compared with normal laboratory conditions. This explains discrepancies between

equilibrium calculations and experimental data and confirms the role of pressure as a key factor in soot formation.

Hydrogen and water vapor in propellant gases further shift the equilibrium, supporting this mechanism. Within the refined model, not only qualitative but also quantitative estimates of condensed carbon formation become possible. Calculations show that during the thermodynamic ex pansion stage its amount may reach 10–16% of the propellant mass, in good agreement with literature data.

The proposed model enables calculation of the composition and parameters of nitrocellulose propellant thermal decomposition products at moderate pressures, thereby allowing the formation of a library of calculated data. Using this library to determine propellant composition requires variation of propellant gas afterburning conditions, including preliminary filling of the experimental vessel with air or other oxygen-containing mixtures.

Conflict of interest

The authors declare that they have no conflict of interest in relation to this research, whether financial, personal, authorship or otherwise, that could affect the research and its results presented in this paper.

Use of artificial intelligence statement

The authors confirm that they did not use artificial intelligence technologies when creating the current work.

Authors' contributions

Oleksandr Brunetkin: Conceptualization, Methodology, Development of library-based verification method, Supervision, Writing – original draft.

Oksana Maksymova: Thermochemical modeling, Data analysis, Numerical simulations, Visualization.

Yevhenii Dobrynin: Formal analysis, Validation of computational models, Interpretation of results, Writing – review & editing.

Oleksandr Sidelnykov: Literature review, Data curation, Comparative analysis, Writing – review & editing.

References

1. Boltenkov, V., Brunetkin, O., Dobrynin, Y., Maksymova, O., Kuzmenko, V., Gultsov, P. et al. (2021). Devising a method for improving the efficiency of artillery shooting based on the Markov model. Eastern-European Journal of Enterprise Technologies, 6 (3 (114)), 6–17. https://doi.org/10.15587/1729-4061.2021.245854
2. Dobrynin, Y., Volkov, V., Maksymov, M., Boltenkov, V. (2020). Development of physical models for the formation of acoustic waves at artillery shots and study of the possibility of separate registration of waves of various types. Eastern-European Journal of Enterprise Technologies, 4 (5 (106)), 6–15. https://doi.org/10.15587/1729-4061.2020.209847
3. Dobrynin, Y., Brunetkin, O., Maksymov, M., Maksymov, O . (2020). Constructing a method for solving the riccati equations to describe objects parameters in an analytical form. Eastern-European Journal of Enterprise Technologies, 3 (4 (105)), 20–26. https://doi.org/10.15587/1729-4061.2020.205107
4. Brunetkin, O., Beglov, K., Brunetkin, V., Maksymov, O., Maksymova, O., Havaliukh, O., Demydenko, V. (2020). Construction of a method for representing an approximation model of an object as a set of linear differential models. Eastern-European Journal of Enterprise Technologies, 6 (2 (108)), 66–73. https://doi.org/10.15587/1729-4061.2020.220326
5. Brunetkin, O., Maksymov, M., Brunetkin, V., Maksymov, O., Dobrynin, Y., Kuzmenko, V., Gultsov, P. (2021). Development of the model and the method for determining the influence of the temperature of gunpowder gases in the gun barrel for explaining visualize of free carbon at shot. Eastern-European Journal of Enterprise Technologies, 4 (1 (112)), 41–53. https://doi.org/10.15587/1729-4061.2021.239150
6. Brunetkin, O., Maksymov, M., Dobrynin, Y., Demydenko, V., Sidelnykov, O. (2024). Development of a process model for determining the composition and energy characteristics of a pyrotechnic mixture using the library method. EUREKA: Physics and Engineering, 5, 99–112. https://doi.org/10.21303/2461-4262.2024.003453
7. Brunetkin, O., Dobrynin, Y., Maksymenko, A., Maksymova, O., Alyokhina, S. (2020). Inverse problem of the composition determination of combustion products for gaseous hydrocarbon fuel. Computational Thermal Sciences: An International Journal, 12 (6), 477–489. https://doi.org/10.1615/computthermalscien.2020034878
8. Maksymov, M. V., Brunetkin, O. I., Beglov, K. V., Alyokhina, S. V., Butenko, O. V. (2022). Automatic Control for the Slow Pyrolysis of Organic Materials with

Variable Composition. Advanced Control Systems. River Publishers, 397–434. https://doi.org/10.1201/9781003337010-16
9. Brunetkin, O., Beglov, K., Maksimov, M., Ulitskaja, E. (2023). Model and method of controlled pyrolysis of organic sub-stances of variable composition. International Scientific Technical Journal "Problems of Control and Informatics", 66 (1), 134–146. https://doi.org/10.34229/1028-0979-2021-1-12
10. Brunetkin, O., Sidelnykov, O., Maksymov, M., Dobrynin, Y. (2025). Improving the model for determining the composition of gunpowder gases during thermal destruction of gunpowder in a limited volume space. Eastern-European Journal of Enterprise Technologies, 3 (6 (135)), 35–45. https://doi.org/10.15587/1729-4061.2025.330654
11. Dobrynin, Y., Maksymov, M., Boltenkov, V. (2020). Development of a method for determining the wear of artillery barrels by acoustic fields of shots. Eastern-European Journal of Enterprise Technologies, 3 (5 (105)), 6–18. https://doi.org/10.15587/1729-4061.2020.206114
12. Dobrynin, Y. V., Boltenkov, V. O., Maksymov, M. V. (2020). Information technology for automated assessment of the artillery barrels wear based on SVM classifier. Applied Aspects of Information Technology, 3 (3), 117–132. https://doi.org/10.15276/aait.03.2020.1
13. Suykens, J. A. K., Van Gestel, T., De Brabanter, J., De Moor, B., Vandewalle, J. (2002). Least Squares Support Vector Machines. Singapore: World Scientific, 295.
14. Xia, X.-L., Jiao, W., Li, K., Irwin, G. (2013). A Novel Sparse Least Squares Support Vector Machines. Mathematical Problems in Engineering, 2013, 1–10. https://doi.org/10.1155/2013/602341
15. LS-SVMlab toolbox. Available at: https://www.esat.kuleuven.be/sista/lssvmlab/
16. James, G., Witten, D., Hastie, T., Tibshirani, R. (2013). Support Vector Machines. An Introduction to Statistical Learning. Springer Texts in Statistics, Vol. 103. New York: Springer, 337–372. https://doi.org/10.1007/978-1-4614-7138-7_9

CHAPTER 6

Improving methods and models for artillery combat control

Pavlo Gultsov
Oksana Maksymova
Yevhenii Dobrynin

Abstract

This chapter deals with methodological approaches to estimating the effectiveness of the combat employment of artillery units considering minimization of the loss of combat capability. The definition of combat capability is proposed, which is seen as the ability of a unit to perform assigned tasks under specified operating and external conditions. The influence of external factors and loads on the state of the unit and on the intensity of failure of its elements is analyzed. A stochastic model of the combat operation of an artillery battery is presented. The model is based on a discrete Markov chain structure which allows to estimate time and dynamic characteristics, including the recovery rate, the probability of destructing a target and the average firing time. Criteria for an effective shot are defined. The use of a combined criterion to estimate combat effectiveness is justified. The proposed approaches provide a scientific basis to predict combat capability, optimize control processes and decision-making in automated systems for estimating artillery fire effectiveness.

Simulation results demonstrate that the proposed approach allows maintaining the combat capability at a level of 0.78–0.81 for a 10-shot mission, while the ratio between optimal and worst mission structures reaches values from 4 to 10.

Keywords

Combat capability, artillery unit, stochastic modeling, firing effectiveness, Markov model, combat employment control.

6.1 Introduction

This section describes the problem of improving the control efficiency of the combat employment of an artillery unit in conditions of counter-battery engagements

© The Author(s) of individual chapters, 2026 DOI: 10.21303/978-9908-8450-1-2.ch6

with existing disturbances connected with changes of firing positions and with the influence of the opposing side. Earlier results aiming at minimizing the loss of combat capability of an artillery unit and reducing the time needed to complete a fire mission are summarized and extended [1, 2].

It was used an approach to form a generalized criterion for estimating the combat employment of an artillery unit which accounts for firing accuracy, time indicators and ammunition expenditure [2, 3]. Stochastic simulation based on Markov models is used to analyze the combat process. The model for computing the current probabilistic state of combat capability of an artillery unit was also improved taking into account sudden failures and failures caused by the loss of combat capability, as well as the method for forming states when the opposing side fires to destroy the current firing position and when this position is changed.

6.2 General provisions on an effective shot

In this section, it is possible to assume that the combat capability of an artillery unit is determined by quantitative parameters. They are the muzzle velocity of the projectile, the speed of transporting the unit between firing positions and the energy characteristic of the artillery charge which is evaluated by the strength of the powder.

An artillery unit is considered combat-capable when the muzzle velocity matches the tabulated value, the transportation speed meets the regulatory norms and the powder strength corresponds to its grade during verification [1, 4].

Forming the generalized criterion for estimating the combat employment of an artillery unit, several simplifications are adopted.

Regular firing errors are connected with topological features of the current firing position and the routes of transporting a unit between positions. They are not detailed further.

The location of the target and meteorological conditions are accounted for during firing preparation. The model considers only changes in properties that directly influence combat capability: muzzle velocity, transportation speed, and powder strength in the charge [1, 4].

Some provisions of the modern decision-making theory are used to analyze the gun firing process [2].

To estimate the effectiveness of the combat employment of an artillery unit, the concept of a generalized criterion is used. It is formed by aggregating partial indicators. The partial indicators are normalized to their maximum values.

Accuracy indicator

$$Crit_{accuracy} = \frac{CEP_{fire}}{CEP_D}, \tag{6.1}$$

task execution time indicator

$$Crit_{time} = \frac{time_{fire}}{time_{fire}^{limit}}, \tag{6.2}$$

ammunition expenditure indicator

$$Crit_{ammo} = \frac{n_{shoot}^{non\_eff}}{n_{shoot}^{total}}, \tag{6.3}$$

where CEP_{fire} – the circular error probable (CEP) of firing; CEP_D – the CEP for range D; $time_{fire}$ – the firing time of the artillery unit to hit the target; $time_{fire}^{limit}$ – the time limit of firing at the current position; $n_{shoot}^{non\_eff}$ – the number of ineffective shots; n_{shoot}^{total} – the total number of shots.

For guns of caliber above 122 mm CEP_D can be assumed to be about 1% D (that is, $R = 0.01D$). Field data show that the time indicator usually does not exceed 0.75. In real conditions, it is 0.6–0.7 of the full firing time [1].

Accounting for these indicators, the generalized criterion is formed as the distance to the ideal point using the L_2 norm

$$Crit_0^{ideal\_point} = \sqrt{\sum_{i=1}^{n} (Crit_i - Crit_i^{ideal\_point})^2}, i = 1,...,n, CEP_D, \tag{6.4}$$

where $Crit_i^{ideal\_point}$ – the value of partial indicators at the ideal point in an n-dimensional space, where all indicators take their minimum values; $Crit_i \in \{Crit_{accuracy}, Crit_{time}, Crit_{ammo}\}$ – the partial indicators of the generalized criterion.

A shot is considered ineffective when the muzzle velocity satisfies $v_0 < 0.95 v_{table\_fire}$. A shot is effective when the artillery projectile hits a circle of radius $R = 1\% D$ with probability at least 0.5 [1].

6.3 Modeling the combat operation of artillery unit

In this section, the main criterion for estimating the combat operation of an artillery unit is combat capability. This indicator describes the ability of the unit to perform a combat task with effectiveness not lower than a specified level.

It decreases under the influence of external factors, including the actions of opposing units [5–7].

Combat capability is regarded as the degree of resistance of an artillery unit to external impacts. It is a relative indicator in the range from 0 to 1. It reflects the current state of the unit during a combat task [5].

Combat capability includes resistance to mechanical, thermal and electrical loads, vibration, shocks and environmental impacts. It also includes the ability to counteract the opposing side that aim to reduce the effectiveness of combat employment.

In practice, the combat capability state is estimated by analyzing the operability of the elements of the artillery unit under specified loads. This makes it possible to determine the failure intensity for the corresponding operating modes [8, 9].

Changing the load conditions and repeated estimate of operability will allow to determine how failure intensity depends on the magnitude of impacts. In this context, failure intensity can serve as a general quantitative measure of the combat capability of an artillery unit [10].

This interpretation makes it possible to quantitatively evaluate the impact of operational and enemy-induced factors on combat capability and to directly compare different combat scenarios using a unified numerical indicator.

To describe combat capability in military practice, probabilistic models are widely used. In such models, the state of an artillery unit is determined by two components. They are sudden failures and failures due to wear of unit elements [11, 12]. Sudden failures are usually modeled by an exponential law. In this case, combat capability is interpreted as the probability of failure-free operation and is defined as

$$P(t)=e^{-\lambda t}, \tag{6.5}$$

where λ – the intensity of sudden failures. It affects the muzzle velocity of the projectile, the transportation speed between firing positions and the energy characteristic of the artillery charge (powder strength).

In the general case

$$\lambda=-\frac{1}{P(t)}\frac{dP(t)}{dt}. \tag{6.6}$$

The following relation is important for any distribution law

$$\lambda=\frac{f(t)}{P(t)}, \text{where } f(t)=-\frac{dP(t)}{dt}, \tag{6.7}$$

where $f(t)$ – the probability frequency of failures.

In normal combat operation, the failure intensity is constant for the exponential law. When combat capability is lost, the failure intensity begins to grow. Failures due to the loss of combat capability are added to sudden failures. In engineering practice, they are modeled by a normal distribution

$$P_w(t)=\frac{1}{\sigma\sqrt{2\pi}}\int_t^{\infty} e^{-(t-M)^2/2\sigma^2}\,dt, \tag{6.8}$$

where M – the mean value of the combat capability of the artillery unit.

The standard deviation from the mean combat capability is defined as

$$\sigma=\sqrt{\frac{\sum(t-M)^2}{N}}, \tag{6.9}$$

where N – the number of failures during time t.

The joint probability of the combat capability of an artillery unit, taking into account all types of failures over the period from $t_0=0$ to t is defined as

$$P(t)=e^{-\lambda t}P_w(t). \tag{6.10}$$

In the case of a partial loss of combat capability, the joint probability is

$$P(t)=e^{-\lambda t}\frac{P_w(t_0+t)}{P_w(t_0)}. \tag{6.11}$$

Expression (6.11) allows one to estimate the combat capability of an artillery unit at any time. However, it has drawbacks for this study. Unregulated operation of a technical artillery unit leads to increased wear. According to field observations, failure intensity strongly depends on the quality of operation of the artillery unit according to its technical requirements [13, 14].

When the load exceeds the nominal level, a noticeable increase in the number of failures is observed. At the same time, the proposed expression does not account for a sudden decrease in combat capability when the artillery unit is hit by the opposing side. In contrast, failure intensity decreases when the load becomes lower than the nominal level [2, 3].

As these factors primarily affect failure intensity, the following expression is used for reliability modeling

$$P(t)=e^{-\int_T^{T+t}\lambda dt}=e^{-\lambda_s t+\int_T^{T+t}\lambda_w dt}, \tag{6.12}$$

where λ_s – the intensity of sudden failures, and λ_w – the intensity of failures caused by the loss of combat capability.

To determine the failure intensity due to the loss of combat capability, the following approach is used. From (6.7), in the general case, failure intensity is defined as $\lambda = f(t)/P(t)$.

In the simulation, the combat capability of the artillery unit changes by Δt at each iteration of the current operating time. Then, let's use expression (6.12) to compute the current value of the failure intensity due to the loss of combat capability.

If, at the current simulation iteration, the unit is under a forced impact that speeds up the loss of combat capability, an additional value Δt_w is added to the operating time. This value corresponds to the degree of combat capability reduction. The expression $P(t) = e^{-\lambda t}$ describes the change of combat capability over time when only sudden failures are present. The expression $P(t) = P_w(T+t)/P_w(t)$ describes the change of combat capability during combat operation without considering destruction by the opposing side [1, 2].

6.4 Stochastic model of firing of an artillery unit

The artillery battery model [1] makes it possible to study combat-operation conditions for different types of artillery weapons – from mortars to heavy self-propelled systems. This is achieved by changing the tuning parameters. The model is given as a non-reduced positive recurrent Markov chain. Within it, the artillery battery is represented as a single whole. This enables comparison of weapon systems and combat-operation algorithms.

The state-space equations are solved as limiting distributions, which ID determined by the properties of the Markov chain. The simulation result is the time interval during which the battery remains in a state that provides fire support [1, 15].

The logical structure of the model of artillery battery combat-operation is based on practical experience of its use. While occupying a new firing position, the battery usually remains unnoticed by the opposing side. A main detection tool is a passive acoustic counter-battery radar.

Detection of the first shot by the radar makes it possible to locate the battery with a certain error and a given probability [13, 16].

The detection probabilities for a single shot and for a salvo are assumed to be the same. The overall detection probability depends on the number of shots fired before detection.

The flow of targets of different types over time is modeled as a homogeneous Poisson process. For each target type, the artillery battery performs a predefined number of shots.

The battery changes its firing position after completing a specified number of shots, taking into account the available information about possible detection. If such information is received, the battery leaves the firing position with high probability before the opposing side begins an attack.

While moving between firing positions, the artillery battery does not provide fire support. If the opposing side attacks the current firing position, the battery suffers combat losses and damage. This can cause a temporary or irreversible loss of the ability to perform combat tasks.

With this combat logic described above, the recurrent Markov chain for the artillery battery includes the following states. Each state can reduce the current combat capability to a different extent when the corresponding events occur [1]:

– is at a firing position and provides fire support; the battery is not detected by the opposing side;

– is at a firing position and provides fire support; the battery is detected by the opposing side but has no information about the detection;

– is at a firing position, does not provide fire support, is detected by the opposing side, has information about the detection, and prepares to change the firing position;

– is moving to a new firing position and does not provide fire support;

– cannot provide fire support due to ammunition depletion or a complete loss of combat capability.

For simulating mission execution, a set of input data is formed. It includes parameters that describe detection and engagement conditions, such as the number of targets, target detection rate, the number of shots needed to hit one target and the probability of battery detection during firing. Another group includes time and dynamic characteristics of combat operation. They are the average firing time before an opposing attack after detection, the battery recovery rate after an attack, the speed of movement between firing positions, the probability of an attack during movement, and the decision-making and exit time from a firing position [1, 9].

The process of changing the combat employment of the artillery battery is represented as a graph, shown in **Fig. 6.1**. The vertices of the graph correspond to current battery states, and the edges describe transitions between these states.

The initial state S_0 defines the readiness of the battery for combat employment on condition of n guns availability for simultaneous firing. The following states S_i ($i=1,...,n$) describe a shot fired simultaneously by i guns. The edge

weight l_{ij} is the probability of a Markov process transition from state S_i to state S_j. It is denoted as $p_{ij}, i, j = 0,...,n$.

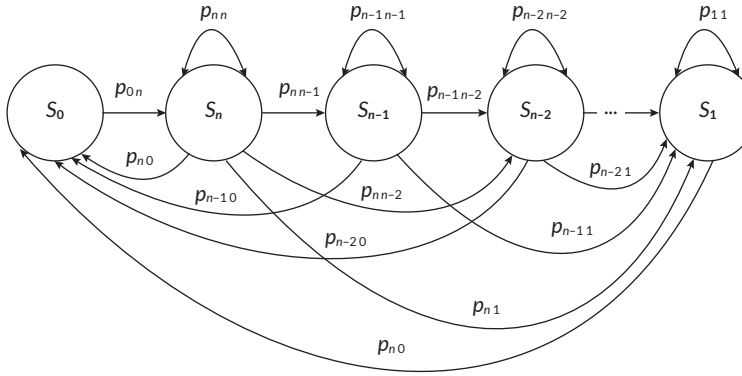

Fig. 6.1 Markov graph of states and transition probabilities

As the states are random, the process can be considered Markov. The stochastic model of automated control also accounts for disturbances. A characteristic disturbance is the difference between the current and the initial muzzle velocities of the projectile, Δv_0. It is caused by chamber wear $\Delta v_0^{\lambda\_chamb}$, barrel wear Δv_0^{barrel} and uncertainty in the charge energy, Δv_0^{charge}. If all three types of disturbances occur simultaneously, the shot effectiveness can be considered an infinitesimal value.

As the disturbances are random, let's consider the probability that the corresponding factor does not affect the shot result:

$$p_1 = p(\Delta v_0^{\lambda\_chamb}),$$
$$p_2 = p(\Delta v_0^{barrel}),$$
$$p_3 = p(\Delta v_0^{charge}). \qquad (6.13)$$

Then the probability of the presence of the corresponding disturbance factor is:

$$p_1 = 1 - p(\Delta v_0^{\lambda\_chamb}),$$
$$p_2 = 1 - p(\Delta v_0^{barrel}),$$
$$p_3 = 1 - p(\Delta v_0^{charge}). \qquad (6.14)$$

Thus, the transition matrix between states in the Markov modeling has the form:

$$P=\begin{Vmatrix} 0 & p_{0n} & 0 & 0 & \cdots & 0 \\ p_{n0} & p_{nn} & p_{nn-1} & p_{nn-2} & \cdots & p_{n1} \\ p_{n-10} & 0 & p_{n-1n-1} & p_{n-1n-2} & \cdots & p_{n-11} \\ p_{n-20} & 0 & 0 & p_{n-2n-2} & \cdots & p_{n-21} \\ \cdots & \cdots & \cdots & \cdots & \cdots & \cdots \\ p_{10} & 0 & 0 & 0 & \cdots & p_{11} \end{Vmatrix}. \quad (6.15)$$

The goal of the Markov model is to determine the number of shots for which the probability of hitting the target is not less than a specified value.

The transition matrix is filled as follows. The first row contains a single non-zero element $p_{0n}=1$. This means that a transition from the initial state to state S_n is possible only when all n guns are ready for combat employment.

The other elements are computed using row i as an example:

$$i=1,...,n;$$

$$p_{i0}=1-\sum_{j=1}^{n}p_{ij};\ p_{ij}=\begin{cases} C_i^j p^j q^{i-j},\ j\le i; \\ 0,\ j>i, \end{cases} \quad (6.16)$$

where p is the probability of an effective shot.

The sum of elements in each row equals 1. Therefore, the matrix satisfies the stochasticity condition.

Thus, the control process can be interpreted as a sequence of states. Each state corresponds to the ability to perform an effective shot by a certain number of artillery units.

If an ineffective shot occurs at the current simulation step, the corresponding unit is excluded from the subsequent mission execution process. Firing continues using a smaller number of units.

A limiting state is possible where all units perform ineffective shots. In this case, according to the adopted conditions, the combat task becomes impossible.

Using model (6.16), it is possible to compute the probability of effective shots after M cycles of combat employment of the artillery battery

$$P_M=(P_0)^M, \quad (6.17)$$

where P_0 – the transition probability matrix after the first firing cycle.

Let's take the number of effective shots as the expected value of a random variable that describes the number of guns that perform an effective shot. For this purpose, it is possible to introduce the state vector sv_i. Its components indicate which guns participate in an effective shot

$$sv_i = \left[sv_j = 1,\ j = i;\ sv_j = 0,\ j \neq i;\ j = 1,...,n \right]^{\mathrm{T}}. \tag{6.18}$$

An example of using the Markov model to evaluate the combat employment results for a battery of 6 guns is given below. The probability of an effective shot when the corresponding disturbances are absent is: $p_1 = 0.95$ (no chamber wear), $p_2 = 0.95$ (no barrel wear), and $p_3 = 0.9$ (no uncertainty of charge energy). Then the probability of an effective shot in the absence of all three types of disturbances is $p = p_1 p_2 p_3 = 0.81225$. This value illustrates that even moderate degradations of individual subsystems lead to a significant cumulative reduction in firing effectiveness, which is explicitly captured by the proposed Markov-based model.

Table 6.1 shows the results of computing the transition matrix between states according to the Markov model (6.16).

Table 6.1 Transition probability matrix

State	S_0	S_6	S_5	S_4	S_3	S_2	S_1
S_0	0	1	0	0	0	0	0
S_6	4E-05	0.2872	0.3983	0.2302	0.0709	0.0123	0.0011
S_5	0.0002	0	0.3536	0.4086	0.1889	0.0437	0.0051
S_4	0.0012	0	0	0.4353	0.4025	0.1395	0.0215
S_3	0.4365	0	0	0	0.4025	0.1395	0.0215
S_2	0.0353	0	0	0	0	0.6598	0.305
S_1	0.188	0	0	0	0	0	0.812

The obtained transition probabilities allow estimating not only the expected number of effective shots, but also the rate of degradation of the artillery battery as guns are sequentially excluded from mission execution.

6.5 Model of combat employment of an artillery unit

Let's consider a model of the control problem for the combat operation of an artillery unit in the following setting. Artillery unit AU1 must perform a combat task.

The task is to destroy a stationary target with n shots on condition of full firing preparation with the probability of firing position change.

To solve the problem, let's introduce assumptions required for modeling. A finite number of firing positions and a given number of shots n required to engage the target is assumed. The minimum number of shots from one firing position equals one. Thus, at least one shot must be fired from each current position.

A change of firing position does not allow returning to previous positions. Movement from one position to a neighboring one is carried out sequentially along one of s roads. The roads differ in surface quality and in the probability that the artillery unit is hit by the opposing side.

When AU1 performs the combat task, it is assumed that artillery unit AU2 does not move and can be hit [1].

The initial combat capability of artillery unit AU1 is denoted as K_{init}. The mathematical model is built to determine the current combat capability of AU1. It accounts for a decrease due to enemy fire and due to movement between firing positions while continuing the target engagement task [1, 18, 19].

To account for system dynamics, artillery units AU1 and AU2 are considered within three generalized action processes, denoted as A, B, and C.

For the artillery unit AU1, process A corresponds to being at a firing position and includes the following stages:

A1 – transition from march mode to combat mode;

A2 – combat operation against the target;

A3 – transition from combat mode at the firing position to march mode.

Process B corresponds to changing the firing position by AU1.

For AU2, process C corresponds to being at a firing position and includes:

C1 – combat operation against stationary target AU1 from the moment of its first shot until the end of the transition from combat mode to march mode;

C2 – combat operation against moving target AU1 during its firing position change.

The events that occur during mission execution are characterized by the following time intervals:

A1 – time interval of AU1 transition from march mode to combat mode at a firing position: t_{mb};

A2 – time interval of AU1 operation against the target at a firing position for one shot: t_{AU1}, for several shots, the total time increases in proportion to their number;

A3 – time interval of AU1 transition from combat mode at a firing position to march mode: t_{bm};

B – march time when changing the firing position along road j ($i=1,...,s$): t_m^j;

C1 – time interval of AU2 operation against AU1 for one shot: t_{AU2}, and the projectile flight time to a stationary target: t_{st};

C2 – the total interval t_m^j along road j and the interval of AU1 transition from march mode to combat mode at a firing position: t_{bm}.

The current combat capability state of AU1 is influenced by all events that reduce it.

The impact of event A2 (combat operation of AU1 at a firing position) is characterized by:

– a decrease in combat capability due to barrel wear per one shot: k_i^{bar};

– a decrease in combat capability due to chassis wear per one shot: $k_i^{chassis}$.

The impact of event B on the change of AU1 combat capability during transportation along road j is characterized by a decrease due to barrel wear k_{bar}^j and chassis wear $k_{chassis}^j$.

The impact of event C1 on the change of AU1 combat capability is characterized by the decrease value k_{hit}. It is determined by the number of shells d fired from AU2 at AU1 to stop its firing

$$k_{hit} = \sum_{j=1}^{d} \frac{1}{j(j+1)}. \tag{6.19}$$

The number of shells d is computed under the condition that AU1 fires a_i shots at firing position i ($i = 1,...,n$)

$$d = \mathrm{INT}\left(\frac{a_i \cdot t_{AU1} + t_{bm} - (t_{AU1} + t_{st})}{t_{AU2} + t_{st}} \right), \tag{6.20}$$

where INT( ) denotes taking the integer part of the resulting value.

The impact of event C2 is characterized by the decrease value k_{move}^j. This decrease is due to unit wear under enemy fire during transportation along road j.

The combat capability of AU1 after combat operation at firing position i is computed as

$$PA_i = PB_{i-1} - (k_{hit} + k_{bar} \cdot a_i + k_{chassis} \cdot t_{AU1} \cdot a_i), \tag{6.21}$$

where PB_{i-1} – the combat capability of AU1 after changing position $i-1 \to i$. By definition, $PB_0 = K_{init}$.

The decrease in combat capability when changing position $i \to i+1$ ($i = 1,...,n-1$) is computed as

$$PB_i = PA_i - (k_{bar}^j + k_{chassis}^j + k_{move}^j). \tag{6.22}$$

The combat capability of AU1 after completing the combat task with n shots, if the last shot is performed at position k ($k \le n$), equals PA_i.

6.6 Method for finding a solution to the combat employment problem for an artillery unit of the attacking side

For developing a computational method for solving the combat employment problem for the attacking artillery unit under enemy fire, a set of input data is defined for further simulation. Enemy fire affects the current firing position and also affects the unit during position change.

Let's introduce an array $a[1...n]$. Element $a(i)$ defines the number of shots fired at firing position i.

Let's also use an array $b[1...n-1]$. Element $b(i)$ corresponds to the number of the road chosen for movement from firing position i to the next one.

The current mission structure is an ordered sequence of the numbers of shots at each firing position and the road numbers used for changing positions

$$a(1)b(1)\cdot a(2)b(2)...a(n).$$

Let's set the initial combat capability of AU1 to $K_{init} = 0.965$.

Table 6.2 shows the time intervals of the corresponding actions of AU1 at a firing position, taking into account opposition by the opposing side.

Table 6.3 presents the parameters that characterize how movement between firing positions affects the combat capability of the unit, depending on the chosen road.

Table 6.2 Time intervals of actions during AU1 mission execution at a firing position under opposing fire

Time for	Value
AU1 transition from march mode to combat mode at a firing position, t_{mb}	5 min
AU1 operation against the target at a firing position per one shot, t_{AU1}	15 s
AU2 operation at its firing position against AU1 per one shot, t_{AU2}	20 s
AU1 transition from combat mode at a firing position to march mode, t_{bm}	2 min
Projectile flight time to the target. It defines the start of opposing fire for a stationary target, t_{st}	35 s
Range to the target	12 000 m

Table 6.3 Parameters that affect combat capability when changing positions

Parameters affecting the unit combat capability and the operating time depending on the chosen road	Road No. 1	Road No. 2	Road No. 3
March time when changing the firing position, t_m^j, s	180	720	1440
Decrease in AU1 combat capability due to barrel wear during transportation, k_{bar}^j	0.000025	0.000055	0.000075
Decrease in AU1 combat capability due to chassis wear during transportation, $k_{chassis}^j$	0.00074	0.00094	0.0024
Decrease in AU1 combat capability due to enemy fire impact during transportation, k_{move}^j	0.000055	0.00003	0.000015

The proposed method for computing the combat employment model includes a general algorithm and specialized algorithms:

– the "Positions" algorithm determines the current number of shells used at each position;

– the "Position change" algorithm determines the sequence of road numbers used for movement between positions;

– the "Combat readiness" algorithm determines the final combat capability of AU1 for the current structure;

– the "Time" algorithm determines the total mission time for the current structure.

Using the input data from **Tables 6.2**, **6.3**, the general algorithm forms the current mission structure $a(1)b(1)\cdot a(2)b(2)...a(n)$. It then computes the final combat capability of the artillery unit accounting for losses due to enemy fire, as well as the movement between firing positions to continue the target engagement task.

Before presenting a formal algorithm description, it is useful to explain the logic of forming the mission structure using a simplified example.

Assume that artillery unit AU1 performs a task from two firing positions. Movement between the first and the second position is possible along several alternative routes. They differ in march duration and in their impact on combat capability. At each position, AU1 can fire one or several shots and then change position.

In this case, the mission structure is an ordered sequence of decisions which includes the number of shots fired at each firing position and the choice of the movement route between neighboring positions.

For two firing positions, such a structure can be written as

$a(1)b(1)a(2)$.

Here $a(1)$ and $a(2)$ define the number of shots at the first and second positions, respectively. Value $b(1)$ is the road number chosen for movement between them.

For example, the structure $a(1)=2$, $b(1)=3$, $a(2)=1$ means two shots at the first position, movement to the second position along Road No. 3, and one shot at the second position.

For a given structure, the total mission time is the sum of deployment time at each position, firing time, packing time, and the march time between positions. For each firing position, let's use the time intervals in **Table 6.2**. For movement, let's use the march time t_m^j, from **Table 6.3**. Thus, the chosen road $b(1)$ directly affects the total mission time.

Similarly, the final combat capability is computed by accounting for its decrease during firing and during movement between positions. During position change, it is possible to account for barrel wear, chassis wear, and enemy impact during movement. These decreases depend on the chosen route and are given by k_{bar}^j, $k_{chassis}^j$ and k_{move}^j (**Table 6.3**).

It is evident that another admissible structure, for example, $a(1)=1$, $b(1)=1$, $a(2)=2$, leads to different values of total time and to a different level of combat capability decrease. Fewer shots at the first position reduce the time under enemy fire. A shorter route reduces march time and changes the losses during transportation.

For an arbitrary number of firing positions, the mission structure is a sequence of decisions

$$a(1)b(1)a(2)b(2)...a(n).$$

This sequence uniquely defines a combat scenario for the artillery unit. A comparative analysis of all admissible structures makes it possible to find those that provide extreme values of mission time and of preservation combat capability. This is implemented by the algorithm below.

For clarity, let's recall the meaning of the indices used below:

– i – the firing position number where combat operation is performed;

– j – the road number chosen for movement between firing positions;

– n – the total number of firing positions in the mission;

– k – the number of the last firing position in the current mission structure.

All indices below are used in accordance with the given explanations.

The general algorithm is implemented as the following sequence of steps:

Step 1. Set the initial mission scenario by taking $a(1)=\cdots a(n)=1$. Thus, one shot is planned at each firing position. Here $k=n$ is the number of positions in the scenario.

Step 2. Initialize variables for extreme values of combat capability and mission time: $P_{max}=0$ (maximum combat capability), $P_{min}=1$ (minimum combat capability), $T_{max}=0$ (maximum total time), and $T_{min}=10^{10}$ (minimum total time).

Step 3. Set the initial movement scenario by taking $b(1)=\cdots b(k-1)=1$. Thus, Road No. 1 is chosen at each movement stage.

Step 4. For the current scenario, compute the final combat capability of AU1 using the "Combat capability" algorithm.

Step 5. For the current scenario, compute the total mission time using the "Time" algorithm. The time includes firing-position time and movement time.

Step 6. Compare the obtained final combat capability $PA(k)$ and the total time T with the current extreme values P_{max}, P_{min}, T_{max}, and T_{min}.

If, for the current scenario, combat capability or total time values exceed or, respectively, decrease registered before extreme values, update them. Store the mission structure arrays $a[1...n]$ and $b[1...n-1]$ that correspond to the new extreme values of combat capability or time.

Step 7. For a fixed number of shots across firing positions, enumerate all admissible scenarios of movement between positions. For this, use the "Position change" algorithm to form the next variant of array $b[1...k-1]$ corresponding to another choice of routes between positions.

After forming a new movement scenario, repeat Steps 4–6 to compute the final combat capability and the total time of the mission. Continue until all route combinations for the current shot structure are considered.

Step 8. After enumerating all admissible movement scenarios for the current shot structure, form the next scenario of distributing shots across firing positions. Use the "Positions" algorithm to change elements of array $a[1...n]$.

For a new shot structure, re-initialize enumeration of movement scenarios by setting $b(1)=\cdots b(k-1)=1$, and return to Step 3. Continue until all admissible shot distributions are considered.

Step 9. After enumerating all admissible mission structures, determine the final extreme values of combat capability and mission time, as well as corresponding scenarios.

Computation results include final values P_{max}, P_{min}, T_{max}, and T_{min}, and mission structures – arrays $a[1...n]$ and $b[1...n-1]$ which provide these extreme values.

Step 10. Form the algorithm outputs. They include the numerical values of combat capability and mission time, and a description of the corresponding mission scenarios.

Step 11. Output the results in a form convenient for further analysis. The algorithm is complete.

The "Positions" algorithm takes the input array $a[1...k]$, which defines the current mission structure within the general algorithm:

Step 1. Determine m, the index of the last non-zero element of array a of the current mission structure.

Step 2. Increase the number of shots at the previous firing position

$$a(m-1)=a(m-1)+1.$$

Step 3. Adjust element $a(m)$ with the constraint on the total number of shots:

– if $a(m)=1$, set $a(m)=0$;

– if $a(m)=n-m$, then sequentially for $a(m+1),...,a(m+i)$ set the value 1 while the constraint $\sum_{j=1}^{m+i} a(j)\le n$ is satisfied;

– otherwise, decrease $a(m)$ by 1: $a(m)=a(m)-1$.

Step 4. Return the updated array $a[1...k]$ which defines the next admissible mission structure.

The "Position change" algorithm takes the input array $b[1...k-1]$, which defines the chosen roads for movement between consecutive firing positions within the current mission structure:

Step 1. Determine m, the index of the last element of array b, which value equals 1 or 2.

Step 2. Form the next structure of position change:

– if $m=k-1$, the value of the last element increases: $b(k-1)=b(k-1)+1$;

– otherwise, increase $b(m)$ by 1 and set all following elements to 1:

$$b(m)=b(m)+1,$$

$$b(i)=1,(i=m+1...k-1).$$

Step 3. Return the updated array $b[1...k-1]$. It defines the next admissible variant of choosing a route between firing positions.

The "Combat capability" algorithm takes the input arrays $a[1...k]$ and $b[1...k-1]$ from the general algorithm. They define the current mission structure for artillery unit AU1:

Step 1. Set the initial combat capability of AU1 at the first firing position as $PB(1)=K_{init}$.

Step 2. For each firing position $i=1...k$, perform Steps 3–7.

Step 3. Compute the number of shells d according to equation (6.20).

Step 4. Compute the combat capability decrease coefficient of AU1 due to hits from AU2 according to equation (6.19).

Step 5. Compute the combat capability decrease of AU1 during firing against the target

$$k_{wear} = (k_{bar} + k_{chassis}) \cdot t_{AU1} \cdot a(i). \tag{6.23}$$

Step 6. Compute the combat capability of AU1 after work at position i

$$PA_i = PB_i - (k_{hit} + k_{wear}). \tag{6.24}$$

Step 7. For movement between neighboring firing positions i and $i+1$ $(i = =1...k-1)$, compute the decrease of AU1 combat capability due to movement along the selected route

$$PB_{i+1} = PA_i - (k_{bar}^{b(i)} + k_{chassis}^{b(i)} + k_{move}^{b(i)}). \tag{6.25}$$

Step 8. The algorithm output is $PA(k)$, the combat capability of AU1 corresponding to the current mission structure.

The "Time" algorithm takes the input $a[1...k]$ and $b[1...k-1]$ from the general algorithm. They define the current mission structure for artillery unit AU1:

Step 1. Set the initial total mission time as $T = 0$.

Step 2. For each firing position $i = 1...k$, perform Steps 3–4.

Step 3. Add the duration of AU1 operation at the i-th firing position, including deployment, firing, and packing time

$$T = T + t_{mb} + a(i) \cdot t_{AU1} + t_{bm}. \tag{6.26}$$

Step 4. If $i \neq k$, add the march time to the next firing position. It is determined by road choice $b(i)$

$$T = T + t_{bm}^{b(i)}. \tag{6.27}$$

Step 5. The algorithm output is the total time T for AU1 mission execution for the current mission structure.

6.7 Conclusions

The study of the decrease in combat capability of an artillery unit, in the problem setting of Section 6.3, corresponds to selecting a mission structure from a large but finite set of possible options. Formally, such a problem can be treated as Pareto-oriented or as a dynamic programming problem.

However, the limited number of input parameters and variable arguments made it possible to obtain all possible solutions by a full direct enumerating. The simulation results for the selected modeling options are given in **Tables 6.6**, **6.7**.

The characteristics of variable arguments used in the simulation experiment are presented in **Table 6.4**. They define admissible values for the number of shots at firing positions and parameters that influence the mission structure.

Table 6.4 Characteristics of variable arguments of the combat employment model

Characteristic	Value 1	Value 2	Value 3	Value 4
1. Start of opposing fire after the first shot of the attacker t_{st}, s	35	43	51	59
2. Number of shells to destroy a stationary target n, pcs	4	6	8	10

Parameters that characterize the change in combat capability during movement between firing positions, depending on the selected route, are given in **Table 6.5**. These parameters account for wear of the main system components and the influence of the opposing side during the march.

Table 6.5 Parameters that affect combat capability when changing a firing position

Combat capability reduction parameter for AU1	Modeling option X			Modeling option Y		
	Road					
	1	2	3	1	2	3
1. Due to barrel wear during transportation, k^j_{bar}	$2.5 \cdot 10^{-5}$	$5.5 \cdot 10^{-5}$	$7.5 \cdot 10^{-5}$	$2.5 \cdot 10^{-4}$	$5.5 \cdot 10^{-4}$	$7.5 \cdot 10^{-4}$
2. Due to chassis wear during transportation, $k^j_{chassis}$	$7.4 \cdot 10^{-4}$	$9.4 \cdot 10^{-4}$	$2.4 \cdot 10^{-3}$	$7.4 \cdot 10^{-3}$	$9.4 \cdot 10^{-3}$	$2.4 \cdot 10^{-2}$
3. Due to wear under enemy fire during transportation, k^j_{move}	$5.5 \cdot 10^{-5}$	$3.0 \cdot 10^{-5}$	$1.5 \cdot 10^{-5}$	$5.5 \cdot 10^{-4}$	$3.0 \cdot 10^{-4}$	$1.5 \cdot 10^{-4}$

Table 6.6 Distribution of all possible combat capability values for 10 shots for two modeling options

Distribution interval	Modeling option *X*				Modeling option *Y*			
	Fire start, t_{st}, s				Fire start, t_{st}, s			
	35	43	51	59	35	43	51	59
1	2	3	4	5	6	7	8	9
(0.075; 0.100]	0	0	0	0	37	0	0	0
(0.100; 0.125]	0	0	0	0	120	2	0	0
(0.125; 0.150]	202	7	1	0	53	5	1	0
(0.150; 0.175]	0	0	0	0	833	0	0	0
(0.175; 0.200]	0	0	0	0	6144	6	0	0
(0.200; 0.225]	0	0	0	0	23026	325	5	0
(0.225; 0.250]	0	0	0	0	35117	1350	176	4
(0.250; 0.275]	0	0	0	0	16902	2217	471	81
(0.275; 0.300]	120	0	0	0	1373	941	355	110
(0.300; 0.325]	83283	4851	1023	208	0	12	16	13
(0.575; 0.600]	0	0	0	0	1	1	1	1
(0.600; 0.625]	0	0	0	0	171	171	171	171
(0.625; 0.650]	0	0	0	0	1978	1986	1986	1986
(0.650; 0.675]	0	0	0	0	13363	14196	14196	14196
(0.675; 0.700]	0	0	0	0	44613	50766	50772	50772
(0.700; 0.725]	0	0	0	0	65746	89247	89567	89572
(0.725; 0.750]	0	0	0	0	37652	74350	75524	75696
(0.750; 0.775]	0	0	0	0	5670	24651	26397	26787
(0.775; 0.800]	8086	8206	8206	8206	15	1915	504	2749
(0.800; 0.825]	161123	249077	252914	253730	0	0	2	6
Structures and corresponding extreme values of combat capability								
For max combat capability value	**Shot number sequence**							
	2, 2, 2, 2, 2	2, 4, 4	5, 5	4, 6	2, 2, 2, 2, 2	2, 4, 4	5, 5	4, 6
	Road number sequence while changing positions							
	1, 1, 1, 1	1, 1	1	1	1, 1, 1, 1	1, 1	1	1
	Combat capability value							
	0.8117	0.8134	0.8142	0.8142	0.7822	0.7986	0.8068	0.8068
	Time							
	2680	1590	1050	1050	2680	1590	1050	1050

Continuation of Table 6.6

1	2	3	4	5	6	7	8	9
For min combat capability value	**Shot number sequence**							
	1, 1, 1, 7	1, 9	10	1, 1, 1, 7	1, 1, 1, 7	1, 9	10	1, 1, 1, 7
	Road number sequence while changing positions							
	3, 3, 3	3		3, 3, 3	3, 3, 3	3		3, 3, 3
	Combat capability value							
	0.1409	0.1458	0.1483	0.3075	0.0736	0.1234	0.1483	0.2403
	Time							
	5910	2310	510	5910	5910	2310	510	5910

Table 6.7 Distribution of all possible combat capability values for 4 shots for two modeling options

Distribution interval	Modeling option *X*				Modeling option *Y*			
	Fire start, t_{st}, s				Fire start, t_{st}, s			
	35	**43**	**51**	**59**	**35**	**43**	**51**	**59**
(0.375; 0.400]	0	0	0	0	6	0	0	0
(0.400; 0.425]	7	0	0	0	1	0	0	0
(0.825; 0.850]	0	0	0	0	7	7	7	7
(0.850; 0.875]	0	0	0	0	28	28	28	28
(0.875; 0.900]	7	7	7	7	22	28	28	28
(0.900; 0.925]	50	57	57	57	0	1	1	1
Structures and corresponding extreme values of combat capability								
For max combat capability value	**Shot number sequence**							
	2,2	4	4	4	2,2	4	4	4
	Road number sequence while changing positions							
	1	–	–	–	1	–	–	–
	Combat capability value							
	0.9042	0.905	0.905	0.905	0.8968	0.905	0.905	0.905
	Time							
	960	420	420	420	960	960	960	960
For min combat capability value	**Shot number sequence**							
	1, 3	1, 1, 1, 1	1, 1, 1, 1	1, 1, 1, 1	1, 3	1, 1, 1, 1	1, 1, 1, 1	1, 1, 1, 1
	Road number sequence while changing positions							
	3	3, 3, 3	3, 3, 3	3, 3, 3	3	3, 3, 3	3, 3, 3	3, 3, 3
	Combat capability value							
	0.4025	0.8975	0.8975	0.8975	0.3801	0.8303	0.8303	0.8303
	Time							
	2220	5820	5820	5820	2220	5820	5820	5820

During the simulation experiment, it was assumed that all shots are effective [1, 17]. The hit probability for the artillery unit was assumed to be at least 0.5. The decrease in combat capability of the attacking artillery unit due to hits by the opposing side between consecutive shots is described by the relation used in Step 4 of the "Combat capability" algorithm.

The results in **Tables 6.6**, **6.7** characterize mission execution for a large series of shots (10 shots) and for a small series of shots (4 shots), respectively. For each series, the best and the worst options are shown in terms of combat capability loss and mission time.

It is noteworthy that the computed combat capability value can be negative in some cases. From a physical point of view, this corresponds to the loss of the artillery unit. The larger the absolute value of this negative number, the earlier the loss occurs at previous stages of the mission for the considered structure.

The analysis in **Tables 6.6**, **6.7** shows that for each considered shot series there exists a mission structure that provides the minimum decrease in combat capability at an admissible mission time.

At the same time, optimizing the structure only for maximum combat capability preservation does not always lead to the minimum mission time. Conversely, the structures that provide the minimum time can, in some cases, cause a significant decrease in combat capability, up to the physical loss of the artillery unit due to opposing fire.

For the considered case, 262,144 combat capability values are computed for each modeling option, taking into account changes in all computational arguments.

This makes it possible to quantitatively assess the dispersion of admissible combat scenarios and to identify mission structures that ensure a 4–10 times higher preservation of combat capability compared to the worst-case solutions.

For a 10-shot mission in modeling option *X*, the initial combat capability of 0.965 changed within a wide range. The highest concentration of results (169,209 values) corresponds to the start of opposing fire at 35 s. In this case, combat capability varies from 0.775 to 0.825. Similar bands were observed for other moments of time: 43 s gave 257,283 values, 51 s gave 261,120 values, and 59 s gave 261,936 values.

In modeling option *Y*, combat capability also decreased from 0.965. However, the band for 35 s is wider, from 0.575 to 0.825, with 169,209 results. For other moments of time, the value bands are similar: 43 s gives 257,283 values, 51 s gives 261,120 values, and 59 s gives 261,936 values.

In both models (*X* and *Y*), 9.330 negative combat capability values were observed at 35 s. This indicates the actual loss of the artillery unit. For other moments of time, negative values did not occur.

The analysis of shot allocation showed that optimal solutions range from a uniform distribution, with two shots at each of the first five firing positions, to a concentrated fire pattern with five shots from each of the first two positions.

When choosing movement routes between positions, the best results correspond to the faster but more dangerous road option (Road No. 1).

The ratio of combat capability values for the best and the worst solutions in the considered cases ranges from 4 to 10. From a practical point of view, this means that an informed choice of shot distribution and movement routes allows either to preserve combat capability above 0.8 or, alternatively, to significantly reduce mission time at the cost of controlled combat capability degradation.

Qualitatively similar patterns are observed analyzing the results of **Tables 6.6**, **6.7**.

When the number of shots decreases, the total number of admissible mission structures reduces. The range of final combat capability values becomes narrower. The ratio between the best and the worst options becomes less than 2.

At the same time, for a smaller number of shots, the number of possible firing positions increases. This raises the variability of the mission structure.

The analysis of mission time based on **Tables 6.6**, **6.7** shows that for most computed structures, the best option in terms of combat capability preservation also corresponds to the minimum mission time.

However, for scenarios with a large number of shots, solutions exist where mission time decreases significantly. This is achieved by a sharp reduction of combat capability to critical values. Combat capability values in the range 0.1–0.2 correspond, in practical terms, to the actual loss of the artillery unit due to opposing fire.

The analysis of **Table 6.7** shows that the artillery unit can be employed with no more than two shots at each firing position without a significant decrease in combat capability. Under these conditions, an acceptable level of combat survivability is maintained throughout the mission.

If a mission with up to ten shots is oriented mainly to defensive conditions, then engaging a target with no more than four shots from one firing position is more typical for offensive operations. In this case, reducing the time spent under opposing fire plays a key role [1, 8].

This is confirmed by the worst scenarios considered. In these scenarios, movement between firing positions is performed without accounting for route characteristics and the related combat capability losses. Such scenarios correspond to intensive offensive operations. In them, priority is given to reducing mission time, even at the cost of a large decrease in combat capability.

In this context, the classical "shoot and scoot" tactic [20, 21], which is typical for offensive operations, can be interpreted, based on the modeling results, as a "hide

and shoot" tactic. This interpretation prioritizes concealment and minimization of the time under opposing fire.

The simulation experiment shows that the developed simulation model and the state-control method for the artillery unit were further developed by including random dynamic external and internal disturbances that accompany mission execution.

As a result, the proposed method provides both quantitative advantages, expressed in numerical estimates of combat capability, mission time and their ratios, and qualitative advantages, such as the ability to formally compare offensive and defensive employment strategies within a unified modeling framework.

Conflict of interest

The authors declare that they have no conflict of interest in relation to this research, whether financial, personal, authorship or otherwise, that could affect the research and its results presented in this paper.

Use of artificial intelligence statement

The authors declare that they did not use artificial intelligence tools in preparing this manuscript.

Authors' contributions

Pavlo Gultsov: Conceptualization, Methodology, Development of stochastic and simulation models, Writing – original draft.

Oksana Maksymova: Data analysis, Numerical simulations, Validation of models, Visualization of results.

Yevhenii Dobrynin: Formal analysis, Interpretation of simulation outcomes, Writing – review & editing.

References

1. Boltenkov, V., Brunetkin, O., Dobrynin, Y., Maksymova, O., Kuzmenko, V., Gultsov, P. et al. (2021). Devising a method for improving the efficiency of

artillery shooting based on the Markov model. Eastern-European Journal of Enterprise Technologies, 6 (3 (114)), 6–17. https://doi.org/10.15587/1729-4061.2021.245854
2. Dobrynin, Y., Brunetkin, O., Maksymov, M., Maksymov, O. (2020). Constructing a method for solving the riccati equations to describe objects parameters in an analytical form. Eastern-European Journal of Enterprise Technologies, 3 (4 (105)), 20–26. https://doi.org/10.15587/1729-4061.2020.205107
3. Brunetkin, O., Beglov, K., Brunetkin, V., Maksymov, O., Maksymova, O., Havaliukh, O., Demydenko, V. (2020). Construction of a method for representing an approximation model of an object as a set of linear differential models. Eastern-European Journal of Enterprise Technologies, 6 (2 (108)), 66–73. https://doi.org/10.15587/1729-4061.2020.220326
4. Brunetkin, O., Maksymov, M., Brunetkin, V., Maksymov, O., Dobrynin, Y., Kuzmenko, V., Gultsov, P. (2021). Development of the model and the method for determining the influence of the temperature of gunpowder gases in the gun barrel for explaining visualize of free carbon at shot. Eastern-European Journal of Enterprise Technologies, 4 (1 (112)), 41–53. https://doi.org/10.15587/1729-4061.2021.239150
5. Maksymova, O., Boltyonkov, V., Gultsov, P., Maksymov, O. (2023). Improvement of the model and method of artillery installation target damage control with minimal combat capability loss. Proceedings of Odesa Polytechnic University, 2 (68), 98–115. https://doi.org/10.15276/opu.2.68.2023.11
6. Tarakhtii, O. S., Gultsov, P. S., Maksymov, O. M. (2023). Pat. No. 127193. Sposib vyznachennia koordynaty zustrichi artyleriiskoho snariada z poverkhneiu. Declareted: 28.04.2021; published: 31.05.2023, Bul. No. 22.
7. Tarakhtii, O. S., Gultsov, P. S., Maksymov, O. M. (2024). Udoskonalennia modeli keruvannia boiovoiu zdatnistiu artyleriiskoi harmaty. Topical Aspects of Modern Scientific Research. Proceedings of the 5th International Scientific and Practical Conference. Tokyo: CPN Publishing Group, 256–261. Available at: https://sci-conf.com.ua/v-mizhnarodna-naukovo-praktichna-konferentsiya-topical-aspects-of-modern-scientific-research-25-27-01-2024-tokio-yaponiya-arhiv/
8. Tarakhtii, O. S., Gultsov, P. S., Maksymov, O. M. (2024). Metod parabolichnoi aproksymatsii vyznachennia koordynaty zitknennia artyleriiskoho snariada z poverkhneiu. Modern Problems of Science, Education and Society. Proceedings of the 12th International Scientific and Practical Conference. Kyiv, 324–330. Available at: https://sci-conf.com.ua/xii-mizhnarodna-naukovo-praktichna-konferentsiya-modern-problems-of-science-education-and-society-5-7-02-2024-kiyiv-ukrayina-arhiv/

9. Maksymov, M. V., Boltenkov, V. O., Gultsov, P. S., Maksymov, O. M. (2023). Verification of artillery fire under the influence of random disturbances for the computer game ARMA 3. Applied Aspects of Information Technology, 6 (4), 362–375. https://doi.org/10.15276/aait.06.2023.24
10. Dobrynin, Y. V., Boltenkov, V. O., Maksymov, M. V. (2020). Information technology for automated assessment of the artillery barrels wear based on SVM classifier. Applied Aspects of Information Technology, 3 (3), 117–132. https://doi.org/10.15276/aait.03.2020.1
11. Dobrynin, Y., Maksymov, M., Boltenkov, V. (2020). Development of a method for determining the wear of artillery barrels by acoustic fields of shots. Eastern-European Journal of Enterprise Technologies, 3 (5 (105)), 6–18. https://doi.org/10.15587/1729-4061.2020.206114
12. Maksimova, O. B., Davydov, V. O., Babych, S. V. (2016). Optimization of Control of Heat Supply Systems of Urban Districts. Journal of Automation and Information Sciences, 48 (4), 69–89. https://doi.org/10.1615/jautomatinfscien.v48.i4.70
13. Dobrynin, Y., Volkov, V., Maksymov, M., Boltenkov, V. (2020). Development of physical models for the formation of acoustic waves at artillery shots and study of the possibility of separate registration of waves of various types. Eastern-European Journal of Enterprise Technologies, 4 (5 (106)), 6–15. https://doi.org/10.15587/1729-4061.2020.209847
14. Maksymov, M. V., Brunetkin, O. I., Beglov, K. V., Alyokhina, S. V., Butenko, O. V. (2022). Automatic Control for the Slow Pyrolysis of Organic Materials with Variable Composition. Advanced Control Systemss: Theory and Applications. Series in Automation, Control and Robotics. River Publishers, 397–434. https://doi.org/10.1201/9781003337010-16
15. Brunetkin, O., Maksymov, M., Dobrynin, Y., Demydenko, V., Sidelnykov, O. (2024). Development of a process model for determining the composition and energy characteristics of a pyrotechnic mixture using the library method. EUREKA: Physics and Engineering, 5, 99–112. https://doi.org/10.21303/2461-4262.2024.003453
16. Brunetkin, O., Dobrynin, Y., Maksymenko, A., Maksymova, O., Alyokhina, S. (2020). Inverse problem of the composition determination of combustion products for gaseous hydrocarbon fuel. Computational Thermal Sciences: An International Journal, 12 (6), 477–489. https://doi.org/10.1615/computthermalscien.2020034878
17. Brunetkin, O. I., Beglov, K. V., Maksymov, M. M., Ulytska, O. O. (2021). Model and method of controlled pyrolysis of organic sub-stances of variable

composition. Problems of Control and Informatics, 66 (1), 134–146. https://doi.org/10.34229/1028-0979-2021-1-12
18. Brunetkin, O., Dobrynin, Y., Maksymenko, A., Maksymova, O., Alyokhina, S. (2020). Model and method of conditional formula determination of oxygen-containing hydrocarbon fuel in combustion. Energetika, 66 (1). https://doi.org/10.6001/energetika.v66i1.4298
19. Brunetkin, O., Sidelnykov, O., Maksymov, M., Dobrynin, Y. (2025). Improving the model for determining the composition of gunpowder gases during thermal destruction of gunpowder in a limited volume space. Eastern-European Journal of Enterprise Technologies, 3 (6 (135)), 35–45. https://doi.org/10.15587/1729-4061.2025.330654
20. Shim, Y., Atkinson, M. P. (2018). Analysis of artillery shoot-and-scoot tactics. Naval Research Logistics, 65 (3), 242–274. https://doi.org/10.1002/nav.21803
21. Koba, M. (1996). Artillery Strike Force. Fort Leavenworth: School of Advanced Military Studies, United States Army Command and General Staff College.

CHAPTER 7

Automated system for diagnostics of shot state parameters based on features of different physical nature

Volodymyr Demydenko
Yevhenii Dobrynin
Oleksii Maksymov
Ruslan Riaboshapka

Abstract

This chapter presents an integrated approach to the verification and diagnostic assessment of an artillery shot based on the joint analysis of acoustic signals and optoelectronic observations.

The proposed method combines physical modeling of ballistic and muzzle wave formation with data processing techniques aimed at extracting informative parameters from heterogeneous measurement channels.

Particular attention is paid to the synchronization of acoustic records with video-based observations of the muzzle blast dynamics, which allows improving the reliability of determining key shot characteristics. A unified framework for representing measured and tabulated parameters is introduced, enabling consistent comparison of experimental data with reference values.

The chapter discusses the principles of feature selection, the formation of diagnostic indicators, and the interpretation of results under conditions of incomplete or uncertain information.

The obtained results demonstrate that the integration of acoustic and visual data provides additional robustness of diagnostic conclusions and can be used to enhance automated monitoring systems for artillery equipment.

The proposed approach may be applied to the development of advanced verification procedures and to the improvement of decision-support tools in complex technical systems where direct measurement of internal processes is limited.

Keywords

Acoustic diagnostics, muzzle blast dynamics, artillery shot verification, optoelectronic monitoring, parameter estimation, signal processing.

© The Author(s) of individual chapters, 2026 DOI: 10.21303/978-9908-8450-1-2.ch7

7.1 Introduction

The development of modern diagnostic and monitoring methods for complex technical systems increasingly relies on the integration of heterogeneous measurement channels and advanced data processing techniques. In the case of artillery systems, the analysis of acoustic fields, optical observations, and indirect physical indicators makes it possible to obtain informative features describing the state of the firing process and the technical condition of the weapon. Such an approach requires the application of unified mathematical models capable of describing nonlinear dynamic phenomena under conditions of uncertainty and incomplete measurement information [1, 2].

A significant number of recent studies demonstrate that the effective analysis of dynamic physical processes is based on approximation models, inverse problem formulations, and analytical representations of system parameters. In particular, approaches involving sets of linear differential models, analytical solutions of Riccati-type equations, and parameter identification techniques provide a flexible framework for describing complex processes of various physical nature, including ballistic, acoustic, and physicochemical phenomena [3–7]. These methods enable the reduction of computational complexity while preserving sufficient accuracy for practical applications.

Another important aspect of modern research is the transferability of modeling principles between different scientific domains. Methods originally developed for describing combustion processes, pyrolysis of materials, or energy transformations in reactive systems can be successfully adapted for analyzing measurement signals obtained during artillery firing. The use of library-based modeling approaches, adaptive process representations, and models of systems with variable composition demonstrates the universality of mathematical tools for interpreting experimental data and constructing diagnostic indicators [8–10].

Within this context, acoustic and optoelectronic data acquired during a shot can be interpreted as manifestations of coupled dynamic processes governed by the physics of gas expansion, wave propagation, and interaction of combustion products with the environment. Physical models of acoustic wave formation and studies of ballistic processes provide the theoretical foundation for extracting informative parameters from measurement records and for constructing classification or estimation procedures [1, 5, 10].

Therefore, the development of integrated diagnostic approaches based on heterogeneous physical fields represents a relevant scientific and applied task. The combination of mathematical modeling, signal processing, and experimental analysis creates prerequisites for improving the reliability of state assessment methods and for extending the functionality of automated diagnostic systems operating under real-world conditions [1–10].

The present chapter focuses on the development of a diagnostic framework for artillery shot verification based on the combined analysis of acoustic measurements and video recordings of muzzle blast dynamics. Particular attention is given to the formation of informative indicators derived from heterogeneous data sources and to the harmonization of measured and reference parameters within a unified analytical scheme. The proposed approach aims to improve the reliability of identifying shot characteristics under real operating conditions, where direct observation of internal ballistic processes is limited. The following sections describe the structure of the experimental data, the principles of parameter representation, and the procedures used for extracting diagnostic features from synchronized acoustic and visual records.

7.2 Methods for detection of diagnostic features of shot state parameters

The system of automated diagnostics of artillery shot state parameters is based on two independent methods that use diagnostic features of different physical nature. In the first diagnostic channel, the features are formed by acoustic waves of two types – muzzle and ballistic waves. In the second diagnostic channel, the features are formed by the presence of free carbon in the propellant gases during the shot. The general scheme of the automated diagnostic system is shown in **Fig. 7.1**.

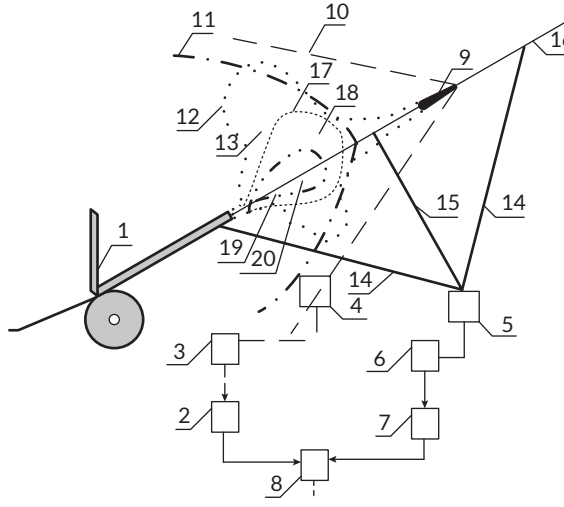

Fig. 7.1 General scheme of the automated system for diagnostics of shot state parameters

The first channel registers acoustic fields that arise during the projectile motion after leaving the barrel bore. The diagnostic characteristic in this case is the projectile velocity. The improved diagnostic method of the first independent channel, which is based on the difference between the velocities of the muzzle and ballistic waves, is implemented according to the sequence given below.

The detection of the diagnostic feature of the shot state based on projectile velocity V_p^{meas} is performed as follows:

Step 1. The artillery gun 1 is loaded with a projectile with a specified propellant charge which, according to the firing tables, should provide the initial projectile velocity V_p^{tab}.

Step 2. A microphone 4 is placed on the firing line at a known distance from gun 1; it is connected to the analog-to-digital converter equipment 3 and to computer 2. The microphone 4 is positioned along the firing direction line 16 to register the ballistic wave 10 and the muzzle wave 11. Subsequently, the velocity of the muzzle wave from gun 1 to microphone 4 is determined taking into account the averaged atmospheric parameters near gun 1 and microphone 4.

Step 3. After the shot from gun 1, along the firing direction 16, the microphone 4 records the signal of the ballistic wave 10 from the projectile 9 moving along the firing direction line 16; at this moment of time t_{bw} the muzzle wave 11 is located at some distance from gun 1, and after a time t_{mw} the microphone 4 registers the spectrum of the muzzle wave 11 generated by the shot of gun 1.

Step 4. From the obtained current signal spectra, the amplitude and duration of the ballistic wave signal 10 are determined, as well as the amplitude and the duration of the first half-period of the muzzle wave 11 at the microphone location at a known distance from gun 1.

Step 5. The signals from microphone 4 are transmitted to the analog-to-digital converter 3 and then to computer 2, where the signals are transformed into the spectral domain. In the spectral domain, the spectral energy density of the signal is determined over frequency.

Step 6. For the obtained spectra, the width at the 0.707 level is fixed for the ballistic wave signal 10, and the central frequency (frequency of maximum) is determined for the muzzle wave 11.

Step 7. The propagation time of the muzzle wave t_{bw} 11 from gun 1 to microphone 4 is determined using the known distance between gun 1 and microphone 4 and the calculated propagation velocity of the muzzle wave 11.

Step 8. The propagation time of the ballistic wave t_{bw} is determined as the difference between the propagation time of the muzzle wave and the time interval between the registration of the ballistic and muzzle waves by the microphone.

Step 9. The velocity of the ballistic wave 10, which corresponds to the actual projectile velocity V_p^{meas}, is determined from the time t_{bw} of its registration by microphone 4 or using the known distance between gun 1 and microphone 4.

Step 10. The measured projectile velocity V_p^{meas} is compared with the tabulated projectile velocity V_p^{tab}, and the diagnostic feature is obtained based on the change in projectile velocity.

The possibility of implementing the second channel is considered in [5]. In this approach, the formation of free carbon is proposed as a diagnostic characteristic. The suggested diagnostic method of the second independent channel is based on the appearance of free carbon in the muzzle blast of powder gases, which expand to atmospheric pressure after the moment when the projectile leaves the gun barrel, and it is implemented in the following way.

Detection of the diagnostic feature by the presence of free carbon is performed according to the following sequence:

Step 1. The artillery gun 1 is positioned so that the muzzle section of the gun barrel is perpendicular to line 15. Along this line a digital high-frequency wide-angle video camera 5 is installed, which is connected to a personal computer 6 where a software package for video stream processing is loaded.

Step 2. The video camera 5 is switched on and recording starts in the visible and infrared ranges. After the shot, the digital video stream is transmitted in real time to the personal computer 6 with the processing software.

Step 3. Video recording is stopped and the video camera 5 is switched off after the projectile 9 passes the boundary of the camera field of view 14.

Step 4. The video stream is converted into a sequence of frames using the personal computer with the software package 6, and this sequence is transferred to the analysis module 7.

Step 5. Each frame is analyzed in the analysis module 7 in order to detect the image of projectile 9 in the frame. The time frames containing the projectile image are selected into a separate array starting from the moment when the projectile image separates from the muzzle edge of gun 1 up to the moment when the projectile image is no longer present.

Step 6. For each time frame further processing is performed if the necessary data for calculation are available.

Step 7. In the frame image the position of the center of mass of projectile 9 is determined, and at this point the coefficient of geometric recalculation of linear dimensions is obtained using the a priori known dimensions of the projectile (diameter and length).

Step 8. The linear distance between the center of mass of projectile 9 and the muzzle section of the gun barrel is determined from the image of the muzzle section

of gun 1 to the point of the projectile center of mass, taking into account the geometric recalculation coefficient, and the averaged instantaneous velocity of projectile 9 on this segment is evaluated V_p^{avg}.

Step 9. A statistically reliable initial linear velocity of projectile 9 V_p^{meas} is calculated after analysis of all time frames.

Step 10. The length of curved line 19 – the boundary between the projection of the free carbon surface and the powder gases 20, when present, which exit the gun barrel into the atmosphere with excessive pressure during the observation time interval – is determined, and time series of lengths 19 and areas 20 are formed; these characteristics constitute a diagnostic feature of the shot state parameters.

Step 11. The length of curved line 17 – the boundary between the projection of surface 18 of powder gases and free carbon at the stage of instantaneous ignition with pressure higher than atmospheric and the surrounding atmosphere – is determined over the observation interval, forming a muzzle shock wave in the atmosphere and generating time series of lengths 17 and areas 18.

Step 12. The length of curved line 12 – the boundary between the projection of the burned powder gas surface 13 with atmospheric pressure and the atmosphere, formed by the volume of the powder exhaust and the surrounding air during the observation interval – is determined, and time series of lengths 12 and areas 13 are formed.

Step 13. Based on the formed time series of lengths and areas, pressure change gradients are evaluated; the absence of a pressure gradient indicates the formation of a curved boundary line between the projection of powder gases and the atmosphere, which characterizes the transition between stages of the muzzle blast: free carbon with hot powder gases without mixture ignition; expansion of the mixture in the air atmosphere with ignition and afterburning; and stabilization of the pressure of powder gases that have burned in the atmospheric air.

Step 14. Using personal computer 6 with the software complex and the calculation-analysis module 7, the current volume of powder gases and their temperature are determined for each time frame; the temperature is measured by the digital high-frequency wide-angle video camera operating in the visible and infrared ranges 5, and the current pressure of powder gases at the front of the muzzle shock wave is calculated.

Step 15. The volume of burned powder gases at atmospheric pressure is determined along curved line 12 – the boundary between the projection of the flame surface of burned powder gases 13 and the atmosphere.

Thus, two methods are proposed that are based on measurements of physical fields of different nature, but describe one process – the artillery shot.

7.3 Muzzle blast video recording

The muzzle blast during firing from modern large-caliber weapons has a complex three-lobed shape (**Fig. 7.2**).

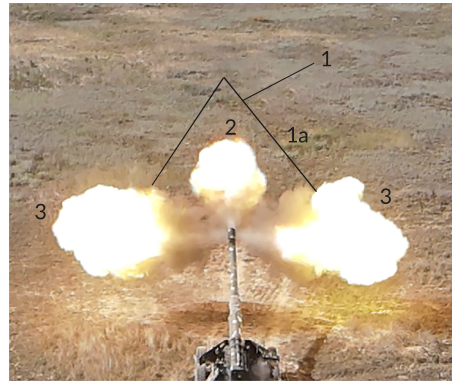

Fig. 7.2 Muzzle blast formed during a shot from a 152-mm gun: 1 – projectile; 1a – mach cone accompanying the projectile; 2 – frontal exhaust of powder gases; 3 – lateral exhausts of powder gases through the compensator (muzzle brake) openings of the gun

The frontal exhaust of powder gases is associated with their eruption from the barrel, while the left and right lateral exhausts are formed when the combustion products exit through the openings of the gun's compensator. For diagnosing the barrel's condition, it is important to obtain the maximum amount of information on the dynamics of muzzle blast development. This is achieved by high-speed video recording of the muzzle blast from different angles.

The field experiment was carried out during training firing of 152-mm towed guns. Shots were performed with two guns: Gun No. 1 – with a barrel of minimal wear (91 shots); Gun No. 2 – with a barrel of significant wear (1968 shots). During subsequent firing, physical fields were recorded from 59 shots: 34 from Gun No. 1 and 25 from Gun No. 2.

The scheme of video recording during firing is shown in **Fig. 7.3**.

In the scheme (**Fig. 7.3**), the origin *O* is aligned with the muzzle of the gun barrel (1). The *Ox* axis coincides with the firing direction. The projectile (2), after leaving the muzzle, moves along its trajectory. Upon the projectile's exit, frontal (3) and lateral (4, 5) muzzle blasts are formed. At a distance of $l_1 = 60–100$ m on a line perpendicular to the firing direction, a ground-based high-speed video system is installed.

The video system consists of a visible-range camera (6) and an infrared (IR) camera (7). This setup (6, 7) is used to record the dynamics of the muzzle blast development from a ground-level side view. A high-speed camera (8) is positioned along an inclined line in the vertical plane at a distance of $l_2 = 60–100$ m. During the experiment, camera (8) was mounted on a hovering unmanned aerial vehicle. Camera (8) records the muzzle blast from a vertical perspective. The video streams from cameras (6–8) are synchronized and transmitted via radio and wired channels to a computing workstation.

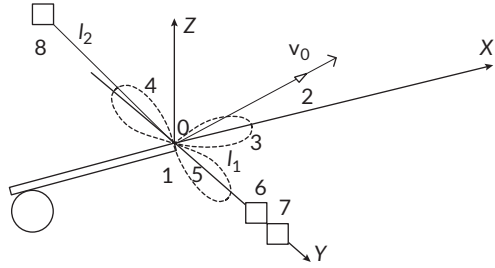

Fig. 7.3 Scheme of muzzle blast video recording during a shot: 1 – gun barrel; 2 – projectile; 3 – frontal exhaust; 4, 5 – left and right lateral exhausts; 6 – ground-based visible-range video camera for recording the horizontal side view; 7 – infrared-range video camera; 8 – visible-range video camera for recording the vertical view

In the experiment, the following equipment was used:

1) infrared camera: high-speed MWIR Science-Grade Camera FLIR X6980; resolution 640 × 512 px; frame rate up to 1004 Hz; standard ND2 filter used: (250...2000)°C; dynamic range 14 bit; real-time connection via Ethernet port;

2) visible spectrum cameras: high-speed FASTCAM MINI WX camera, shockwave-protected; resolution 1920 × 1080 px; frame rate from 240 Hz; linear imaging (without lens or perspective distortions); real-time video signal connection;

3) workstation for processing recorded data: GPU: RTX 3080; CPU: 4.5 GHz, 12 cores; storage: SSD 4 TB M.2 NVME; RAM: 64 GB; OS: Windows 10.

During all shots, acoustic fields – ballistic and muzzle waves – were additionally recorded. Since the methods of their registration are discussed in detail in works [2, 11, 12], they are not covered in this section.

Fig. 7.4 shows consecutive frames of the muzzle blast dynamics in a top vertical view.

Analysis of consecutive frames reveals significant differences between muzzle blasts from worn and serviceable barrels. This allows considering the possibility of creating an automatic barrel condition classifier based on video data.

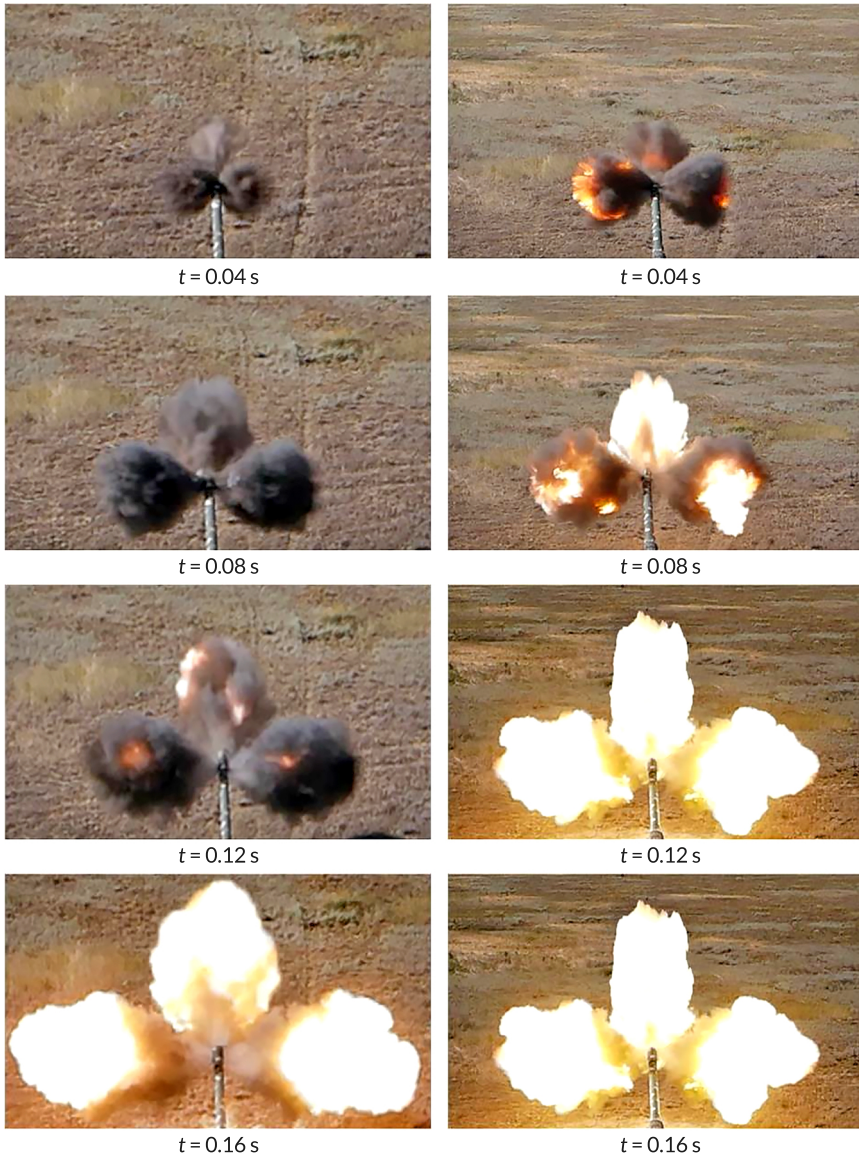

Fig. 7.4 Sequential frames of the muzzle blast development dynamics in the upper vertical view: *a* – shot from a worn barrel; *b* – shot from a non-worn barrel

7.4 Method for forming diagnostic features of the muzzle blast based on video analysis

The procedure for forming diagnostic features of the muzzle blast based on video analysis is implemented as follows:

Step 1. Synchronous video recording is performed with all cameras, and shortly after, the shot is fired. Two visible-spectrum video streams from cameras (6) – file_1 (horizontal view) and (8) – file_2 (vertical view), as well as the IR stream from camera (7) – file_1ir, are transmitted to the computer.

Step 2. The video streams (file_1), (file_2), and (file_1ir) are converted into a synchronized sequence of frames with discrete time stamps.

Step 3. Each frame is analyzed to locate the projectile in the image. An array of frames containing the projectile is then formed – from the moment it separates from the barrel muzzle or leaves the powder-gas cloud until it disappears from the frame.

Step 4. For each frame, if IR stream data (file_1ir) is available, the projection of the temperature field is analyzed. The frames from all three video streams are synchronized and form two geometric projections of the muzzle blast, as well as, if data is available, the distribution of the average temperature field.

Step 5. On the side-view frame, the position of the projectile's center of mass is determined. At this point, a geometric scaling coefficient for linear dimensions is calculated based on the a priori known projectile dimensions (diameter and length).

Step 6. The actual distance between the center of mass of the projectile and the barrel muzzle is determined, taking into account the geometric conversion factor. The average velocity of the projectile along this segment is then calculated.

Step 7. Based on the analysis of all frames, the statistically reliable initial velocity of the projectile is determined immediately after leaving the barrel V_0^{val}.

Step 8. From the IR frames, the length of the boundary between the projections of free carbon, gunpowder gases, and the atmosphere is determined, as well as the area of this region, if present.

Step 9. Using frames from cameras (6) and (8), the areas of the muzzle flash projections are determined, based on which the current volume of the muzzle flash is calculated.

Step 10. For each time frame, the current pressure of the gunpowder gases at the front of the muzzle shock wave is calculated. The current gas pressure of the muzzle flash is determined from the average temperature, the current gas volume, and the characteristics of the gas contained in the muzzle flash. Reaching atmospheric pressure indicates the disappearance of the shock wave as a diagnostic feature.

Step 11. Analysis of the obtained calculation vectors. Two vectors are formed during the analysis: pressure and temperature of the muzzle flash gases. The pressure vector shows a monotonic decrease to the atmospheric value. The temperature vector may show a monotonic decrease, a jump followed by decline, or a stabilization section.

The presence of free carbon is indicated by a temperature jump or stabilization, explained by additional oxidation during mixing with atmospheric oxygen. This temperature property of the muzzle gas volume confirms that during its expansion and mixing with atmospheric oxygen, additional oxidation of free carbon occurs, releasing extra energy, which produces the described temperature characteristic.

Fig. 7.5 shows a diagram of the processing of the video information stream corresponding to the described methodology.

Below are the key operations of the methodology that require illustration. **Fig. 7.6** shows a condensed video sequence of combined frames from the vertical and side views, highlighting the key moments of the projectile exit and the development of the muzzle blast.

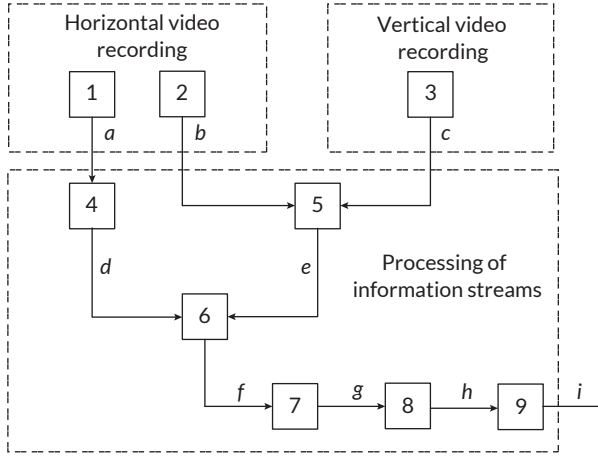

Fig. 7.5. Diagram of the processing of video information streams: 1 – IR spectrum camera; 2 – side-view camera; 3 – vertical-view camera; 4 – preliminary processing of IR video stream; 5 – preliminary processing of visible-spectrum video stream; 6 – frame image alignment; 7 – detection of analysis regions in the frame; 8 – detection of the IR spectrum image of the muzzle gas region in the frame; 9 – calculation of the perimeter and area of the muzzle gas volume; *a* – IR spectrum video stream; *b* – visible-spectrum video stream; *c* – visible-spectrum video stream; *d* – normalized set of IR spectrum frame images; *e* – normalized set of visible-spectrum frame images; *f* – time-based set array (time, frame, position); *g* – array of numerical characteristics; *h* – array of numerical characteristics; *i* – two formed vectors of characteristics

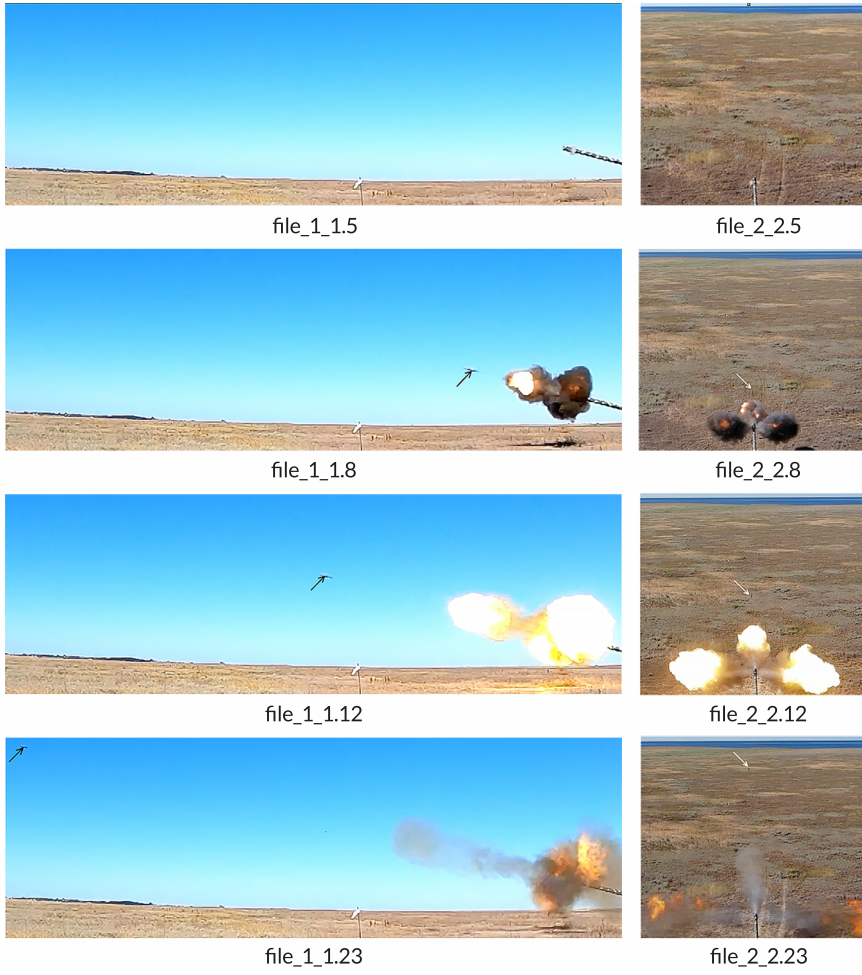

Fig. 7.6 Typical sequence of overlaid frames (file_1, file_2) from vertical and side views. Four key moments are shown: the first frame (5), intermediate frames (8, 12), and the last frame (23), illustrating the projectile flight and the development of the muzzle blast (the projectile is indicated by arrows)

After converting the video streams (file_1) and (file_2) into frame sequences, for each pair of frames file_1_1.i and file_2_2.i, filtering, extraction of closed contours, and determination of their geometric dimensions relative to the baseline size –

the outer diameter of the gun barrel – were performed using the OpenCV library. From the processed frame of camera file_1_1.i, the diameter D_1 and length L_1 of the frontal muzzle blast were determined. Additionally, the diameter D_2 of the left-side muzzle blast through the muzzle brake was measured. It was assumed that the diameters of the right and left side blasts are equal in the current frame. From the processed frame of the vertical camera file_2_2.i, the lengths L_2 of the left-side muzzle blast and L_3 of the right-side muzzle blast from the gun with the muzzle brake were determined (**Fig. 7.7**).

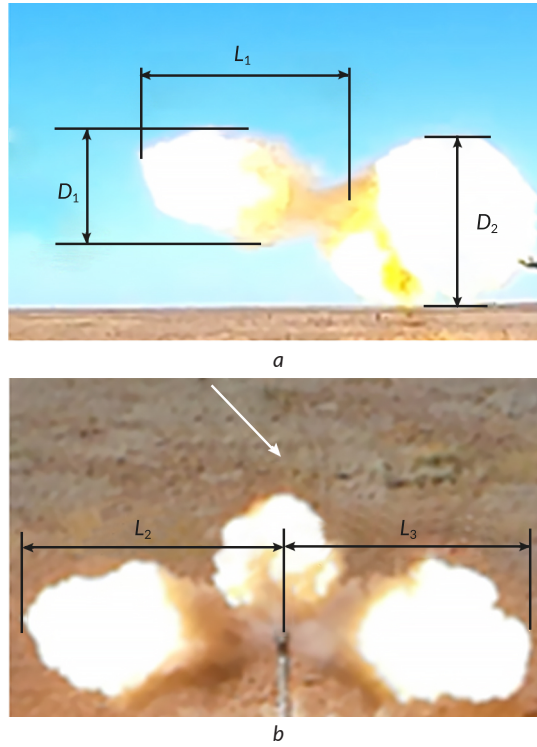

Fig. 7.7 Determination of muzzle gas dimensions:
a – determination of geometric dimensions from the side-view camera;
b – determination of geometric dimensions from the vertical-view camera

It was assumed that the obtained geometric dimensions of the "lobes" of the muzzle blast correspond to bodies in the form of rotational ellipsoids. In this case,

the total current volume of the muzzle blast was determined as the sum of the volumes of three geometric bodies

$$V_i = \frac{4}{3}\pi(L_1 D_1^2 + L_2 D_2^2 + L_3 D_3^2).$$

The current pressure P_i in the gas volume V_i with an average temperature T_i is determined based on the ideal gas law, using the Mendeleev-Clapeyron equation

$$P_i V_i = \frac{m}{M} R T_i.$$

This assumption is acceptable for the considered stage of the muzzle blast expansion, when the powder gases rapidly expand into the atmosphere and the pressure decreases to values close to atmospheric pressure. Under these conditions, the deviation of the gas mixture behavior from the ideal gas model does not significantly affect the calculated pressure estimates.

While the gas expands from the barrel into the air atmosphere after exiting the muzzle, it is assumed that no chemical reactions occur in the muzzle-blast gas; that is, the gas mixture maintains a constant composition. For this reason, the molar mass M of the gas mixture in the system "charging chamber – barrel bore – muzzle blast" is constant. Accordingly, the mass m of the gas mixture contained within the entire muzzle system ("charging chamber – barrel bore – muzzle blast") remains unchanged. The universal gas constant is also constant. The product $(m/M)R$ is therefore treated as a constant value for the calculations, and its detailed evaluation is presented in [5]. It should be noted that for each shot this product has its own value and depends on the propellant charge, the powder type, its granulometric properties, and the wear condition of the barrel system.

The temperature T_i is determined from horizontal recording using an infrared video camera that captures temperature data in file (file_1ir). Based on the correspondence between video frames file_1_1.i and file_1_1ir.i, the property of the measured temperature is extended to the entire portion of the muzzle-blast gases of the given fragment.

Fig. 7.8 presents the results of joint processing of frames from the video sequences (file_1), (file_2), (file_1ir), demonstrating changes in gas pressure and temperature within the muzzle blast. **Fig. 7.8** was obtained by processing the video sequence shown in **Fig. 7.6** (the left column corresponds to a shot from a barrel with high wear, the right column corresponds to a shot from a barrel without wear).

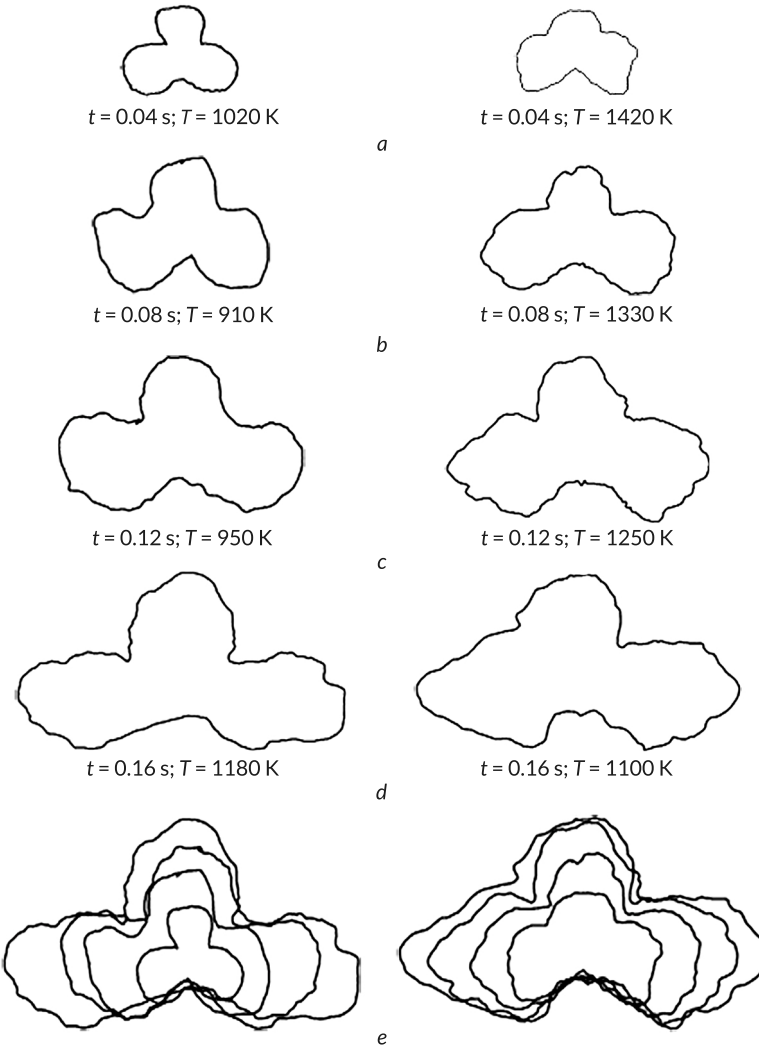

Fig. 7.8 Results of joint processing of frames from the video sequences (file_1), (file_2), (file_1ir), demonstrating changes in gas pressure and temperature in the muzzle blast (rows *a*, *b*, *c*, *d*) for two different barrel conditions; row *e* shows the gas pressure gradient in the muzzle blast. In the first case, the shock wave transformed into an acoustic wave within the time interval from 0.08 s to 0.12 s after projectile exit, whereas in the second case – from the beginning of the exit up to 0.04 s

7.5 Selection of informative parameters for classification of barrel condition based on analysis of video recordings of muzzle blast dynamics

By analogy with classification based on acoustic fields, for classification using video recordings of the muzzle blast the main objective of video analysis is the selection of informative features that distinguish a worn barrel from a defect-free one. Analysis of the obtained video sequences made it possible to form a set of informative parameters (IP) used for binary classification of defect-free and worn barrels.

The following parameters were used as the main classification features:

– $F_{1,i}^{vid}$ – the perimeter of the contour bounding the muzzle-blast region in the frame recorded at time t s after the shot – L_t; the perimeter was calculated for time instants t = 0.04 s, 0.08 s, 0.12 s, 0.16 s, thus forming four informative parameters (IP): $F_{1,0.04}^{vid}$, $F_{1,0.08}^{vid}$, $F_{1,0.12}^{vid}$, $F_{1,0.16}^{vid}$;

– $F_{2,i}^{vid}$ – the projection area of a part of the muzzle blast onto the image plane at time t s after the shot – S_t; it was calculated for the same time instants, forming four additional informative parameters (IP): $F_{2,0.04}^{vid5}, F_{2,0.08}^{vid6}, F_{2,0.12}^{vid7}, F_{2,0.16}^{vid8}$.

These time instants correspond to characteristic stages of muzzle blast development identified during the preliminary analysis of the video sequences. The selected moments provide stable measurements of geometric parameters while keeping the dimensionality of the feature vector limited.

The volume of a part of the muzzle blast at time instants t = 0.04 s, 0.08 s, 0.12 s, 0.16 s was used as informative parameters from the 9th to the 12th:

$$F_{3,0.04}^{vid9}, F_{3,0.08}^{vid10}, F_{3,0.12}^{vid11}, F_{3,0.16}^{vid12}.$$

Since previous experiments revealed differences in the dynamics of changes in the volume of a part of the muzzle blast, the following derived features were formed:

– $F_{4,40-120}^{vid13}$ – estimation of the growth rate of the volume of a part of the muzzle blast in the time interval from 40 ms to 120 ms;

– $F_{4,120-160}^{vid14}$ – estimation of the growth rate of the volume of a part of the muzzle blast in the time interval from 120 ms to 160 ms.

These features were calculated as follows:

$$V_{40-120}^{meas} = \frac{V_{120} - V_{40}}{80},$$

$$V_{120-160}^{meas} = \frac{V_{160} - V_{120}}{40}.$$

For all recorded shots, 14 informative parameters were calculated.

Since the SVM (support vector machine) classifier [12] proved effective for classifying barrel condition based on ballistic and muzzle acoustic waves, this classifier was also tested for assessing barrel condition from muzzle flash video recordings. Unlike [12], in this case a more efficient variant of SVM was chosen – the least squares support vector machines (LSSVM) method [13]. LSSVM is a modified SVM approach that reduces the problem to solving linear systems of equations, effectively transforming it into a linear programming task, whereas the classical SVM method requires solving a quadratic programming problem. The LSSVM method significantly reduces computation time while maintaining classification quality. Its use also allows for a substantial reduction (by 2–4 times) in the required training dataset [14]. The LSSVM method is implemented as a MATLAB Toolbox [15].

For the binary classification of barrel condition from muzzle flash video recordings, feature vectors were calculated for 59 recordings obtained during the experiment. The standard procedure of training, tuning, and testing the LSSVM classifier [13, 14] was then performed. All the above-mentioned informative features were normalized to the interval [0, 1]. The training dataset for tuning and training the classifier consisted of feature vectors from 30 randomly selected recordings. After training, the classifier's performance was evaluated using a test dataset consisting of feature vectors from 25 recordings, 13 of which were from shots with a defect-free barrel, and 12 from a worn barrel. The remaining four recordings were not included in the training or test subsets and were reserved as additional data for verifying the stability of the obtained results.

Until now, classification quality was quantified using a single metric – accuracy, defined as the ratio of correctly classified objects to the total number of objects [16]. This measure alone is not sufficient. The classification logic and results are presented in **Table 7.1**. Columns 2 and 3 of **Table 7.1** indicate the true classes corresponding to the barrel condition. The rows of **Table 7.1** show the classifier's decisions, indicating to which of the two classes the classifier assigned each shot. Each cell at the intersection of a row and a column contains the number of true or false classification outcomes.

Since the primary goal of classification is to detect barrel condition, the state "Barrel truly worn" is considered the true positive condition, whereas the opposite state, "Barrel truly operational", is considered the true negative condition. Classifier outputs may therefore be: "Barrel worn", which is a true positive decision, and "Barrel operational", which is a true negative decision. The meaning of false positive and false negative decisions is evident from **Table 7.1**. The corresponding

cells in **Table 7.1** show the quantitative classification results for the examined dataset.

Table 7.1 Logic of barrel condition classification results

Barrel condition	True positive condition	True negative condition
Classifier decision	"Barrel actually worn"	"Barrel actually serviceable"
Classified as: "barrel worn"	True positives (*TP*)	False negatives (*FN*)
Classified as: "barrel serviceable"	False positives (*FP*)	True negatives (*TN*)

The classification quality was evaluated using three metrics.

The first metric is the Type I classification error, defined as the proportion of classifier decisions that identify a worn barrel as serviceable

$$F_1 = \frac{FN}{N_{def}},$$

where N_{def} – the actual number of worn barrels.

The second metric, Type II classification error, is defined as the proportion of classifier decisions that identify a serviceable barrel as worn

$$F_2 = \frac{FP}{N_{ok}},$$

where N_{ok} – the actual number of serviceable barrels.

Undoubtedly, a Type I error is more critical in terms of consequences, but in combat conditions, a Type II error also has operational impact, as it leads to removing a serviceable gun from the field and transporting it to a technical unit for diagnostics.

Therefore, a third metric is introduced, which serves as a generalized measure of classification quality and indicates the probability of error-free barrel condition classification

$$P_0 = 1 - (F_1 + F_2).$$

The summarized results of barrel condition classification based on different physical fields and their combinations are presented in **Table 7.2**.

Table 7.2 Comparative results of barrel condition classification based on different physical fields of the shot

Indicators	Classification results based on analysis				
	BW	MW	BW + MW	MDV	BW + MW + MDV
P_0 – probability of correct classification	0.29	0.44	0.60	0.52	0.77
F_1 – Type I error	0.33	0.25	0.17	0.33	0.08
F_2 – Type II error	0.38	0.31	0.23	0.15	0.15

Note: MDV – video recording of muzzle blast dynamics

7.6 Investigation of classifier generality

The practical interest lies in exploring the possibility of classifying barrel condition based on different physical fields and their combination. Below, the classification results for the acoustic fields of ballistic and muzzle waves and their combination, summarized in **Table 7.2**, are analyzed. For this purpose, the informative features used for training and testing the classifier are those detailed in [2, 11, 12]. The training and test samples coincide with those used for classification from the video recording of muzzle blast dynamics.

To assess the generality of the approach, classification was performed using the acoustic field of the ballistic wave, the muzzle wave, their combination, as well as in combination with the MDV.

The results presented in **Table 7.2** show a significant increase in classification accuracy when all physical fields of the shot are used in combination.

This effect can be explained by the fact that the acoustic and video channels are based on physical fields of different nature and are affected by different sources of measurement uncertainty. Therefore, their classification errors are only partially correlated, and the joint use of these channels increases the robustness of the diagnostic system.

The highest performance is achieved when combining the informative features of the acoustic fields with the MDV.

The automated system for diagnosing shot parameters (**Fig. 7.9**) consists of hardware and software components. The hardware component includes three elements: I – a set of technical means for measuring the acoustic field generated by muzzle and ballistic waves; II – a set of technical means for horizontal and vertical video recording of muzzle gases; IV – a mobile device for displaying the obtained shot parameter results within the automated diagnostic system (**Fig. 7.9**).

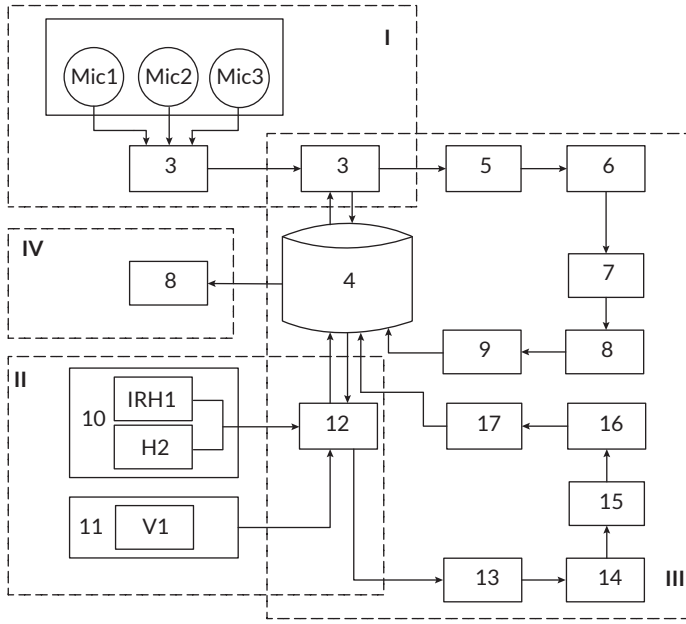

Fig. 7.9 Diagram of the automated system for diagnosing shot parameter states

The subsequent processing of the collected information is performed by the software component III, presented as the overall structure for processing information obtained from various physical fields during the shot (**Fig. 7.9**). The software component includes: an integrated database; programs for processing recordings, signals, images, and video sequences, as well as for extracting and accumulating informative features; SVM and LSSVM classifiers:

– I – a set of technical means providing measurement of the acoustic field generated by muzzle and ballistic waves;

– II – a set of technical means providing horizontal and vertical video recording of the muzzle gas plume;

– III – general structure of the software component for digital processing of information obtained from various physical fields during the shot;

– IV – mobile device for displaying results obtained in the automated system for diagnosing shot parameter states;

– 1 – group of measurement microphones for acoustic wave characteristics.

– 2 – multichannel 16-bit ADC;

– 3 – field computer for calculating acoustic wave parameters;
– 4 – integrated database;
– 5 – recording processing (extraction of ballistic and muzzle wave signals);
– 6 – recording processing (extraction of sets of informative features of the acoustic field);
– 7 – formation and training of the SVM acoustic field classifier;
– 8 – shot classification using acoustic diagnostic features;
– 9 – classification result of the shot based on the acoustic field;
– 10 – group of horizontal video cameras (IRH1 – infrared horizontal, H2 – horizontal);
– 11 – vertical video camera V1;
– 12 – field computer for processing muzzle gas video images;
– 13 – video recording processing;
– 14 – processing of individual image frames;
– 15 – formation and training of the LSSVM classifier for muzzle gas images;
– 16 – shot classification using diagnostic features obtained from the muzzle gas;
– 17 – classification result of the shot based on processing of muzzle gas images;
– 18 – classification result of the shot based on the combination of muzzle gas video and acoustic shot fields.

A field experiment was conducted using a set of technical means for recording muzzle blast and a system for measuring the acoustic field generated during training firings of towed guns. The hardware setup for the gun position included three measurement condenser microphones – Rode NT1-A, Rode NT-USB, and DPA 4062-OC – connected to a MacBook Pro 15 via a 16-bit, multi-channel ADC TASCAM 102i. The specifications of the measurement microphones were as follows: frequency range 20 Hz–20 kHz; signal-to-noise ratio 81 dB; sensitivity 32 dB relative to 1 V/Pa; dynamic range 132 dB.

7.7 Conclusions

A field experiment was conducted to record the muzzle blast of propellant gases accompanying gunfire using high-speed cameras in both visible and infrared ranges from multiple observation angles. The experiment revealed significant differences in the dynamics of muzzle blast development between firings from defect-free and worn barrels. The obtained results served as a basis for developing a barrel condition classifier based on muzzle blast video recordings. A methodology for analyzing synchronized video streams was developed.

The analysis identified informative features that distinguish muzzle blasts from defect-free and worn barrels. This allowed the development of a binary classifier based on least squares support vector machines (LSSVM). To assess classification quality, in addition to first- and second-type classification errors, an integral performance metric – the probability of error-free classification – was proposed. It was established that, for the experimental dataset, the classification errors based on the analysis of muzzle blast video recordings are: the first-type error $F_1 = 0.33$; the second-type error $F_2 = 0.15$; probability of error-free classification $P_0 = 0.52$.

A concept for a universal barrel condition classifier was proposed. The concept involves classification based on both muzzle blast video recordings and the acoustic fields of the shot – ballistic and muzzle waves. It was shown that, in this case, the probability of error-free classification increases to 0.77. The proposed concept made it possible to develop and investigate an automated system for diagnosing shot condition parameters.

Conflict of interest

The authors declare that they have no conflict of interest in relation to this research, whether financial, personal, authorship or otherwise, that could affect the research and its results presented in this paper.

Use of artificial intelligence statement

Artificial intelligence technology was used in the preparation of this chapter. Specifically, the authors used OpenAI ChatGPT (model GPT-5.2) to assist in editing and structuring introductory text sections and in formulating generalized descriptions of research methodologies for integrating mandatory literature sources into the chapter introduction.

The authors bear full responsibility for the final manuscript. Generative AI tools are not credited and are not responsible for the final results.

Authors' contributions

Volodymyr Demydenko: Conceptualization, Methodology, Experimental design, Integration of acoustic and visual data, Writing – original draft.

Yevhenii Dobrynin: Data processing, Feature extraction, Development of classification algorithms, Validation of results.

Oleksii Maksymov: Analysis of synchronized measurement channels, Performance assessment, Interpretation of results.

Ruslan Riaboshapka: Visualization of results, Technical support of experiments, Writing – review & editing.

References

1. Boltenkov, V., Brunetkin, O., Dobrynin, Y., Maksymova, O., Kuzmenko, V., Gultsov, P. et al. (2021). Devising a method for improving the efficiency of artillery shooting based on the Markov model. Eastern-European Journal of Enterprise Technologies, 6 (3 (114)), 6–17. https://doi.org/10.15587/1729-4061.2021.245854
2. Dobrynin, Y., Volkov, V., Maksymov, M., Boltenkov, V. (2020). Development of physical models for the formation of acoustic waves at artillery shots and study of the possibility of separate registration of waves of various types. Eastern-European Journal of Enterprise Technologies, 4 (5 (106)), 6–15. https://doi.org/10.15587/1729-4061.2020.209847
3. Dobrynin, Y., Brunetkin, O., Maksymov, M., Maksymov, O. (2020). Constructing a method for solving the riccati equations to describe objects parameters in an analytical form. Eastern-European Journal of Enterprise Technologies, 3 (4 (105)), 20–26. https://doi.org/10.15587/1729-4061.2020.205107
4. Brunetkin, O., Beglov, K., Brunetkin, V., Maksymov, O., Maksymova, O., Havaliukh, O., Demydenko, V. (2020). Construction of a method for representing an approximation model of an object as a set of linear differential models. Eastern-European Journal of Enterprise Technologies, 6 (2 (108)), 66–73. https://doi.org/10.15587/1729-4061.2020.220326
5. Brunetkin, O., Maksymov, M., Brunetkin, V., Maksymov, O., Dobrynin, Y., Kuzmenko, V., Gultsov, P. (2021). Development of the model and the method for determining the influence of the temperature of gunpowder gases in the gun barrel for explaining visualize of free carbon at shot. Eastern-European Journal of Enterprise Technologies, 4 (1 (112)), 41–53. https://doi.org/10.15587/1729-4061.2021.239150
6. Brunetkin, O., Maksymov, M., Dobrynin, Y., Demydenko, V., Sidelnykov, O. (2024). Development of a process model for determining the composition and energy characteristics of a pyrotechnic mixture using the library method. EUREKA: Physics and Engineering, 5, 99–112. https://doi.org/10.21303/2461-4262.2024.003453

7. Brunetkin, O., Dobrynin, Y., Maksymenko, A., Maksymova, O., Alyokhina, S. (2020). Inverse problem of the composition determination of combustion products for gaseous hydrocarbon fuel. Computational Thermal Sciences: An International Journal, 12 (6), 477–489. https://doi.org/10.1615/computthermalscien.2020034878
8. Maksymov, M. V., Brunetkin, O. I., Beglov, K. V., Alyokhina, S. V., Butenko, O. V. (2022). Automatic Control for the Slow Pyrolysis of Organic Materials with Variable Composition. Advanced Control Systems: Theory and Applications. Series in Automation, Control and Robotics. River Publishers, 397–434. https://doi.org/10.1201/9781003337010-16
9. Brunetkin, O. I., Beglov, K. V., Maksymov, M. M., Ulytska, O. O. (2021). Model and method of controlled pyrolysis of organic substances of variable composition. Problems of Control and Informatics, 66 (1), 134–146. https://doi.org/10.34229/1028-0979-2021-1-12
10. Brunetkin, O., Sidelnykov, O., Maksymov, M., Dobrynin, Y. (2025). Improving the model for determining the composition of gunpowder gases during thermal destruction of gunpowder in a limited volume space. Eastern-European Journal of Enterprise Technologies, 3 (6 (135)), 35–45. https://doi.org/10.15587/1729-4061.2025.330654
11. Dobrynin, Y., Maksymov, M., Boltenkov, V. (2020). Development of a method for determining the wear of artillery barrels by acoustic fields of shots. Eastern-European Journal of Enterprise Technologies, 3 (5 (105)), 6–18. https://doi.org/10.15587/1729-4061.2020.206114
12. Dobrynin, Y. V., Boltenkov, V. O., Maksymov, M. V. (2020). Information technology for automated assessment of the artillery barrels wear based on SVM classifier. Applied Aspects of Information Technology, 3 (3), 117–132. https://doi.org/10.15276/aait.03.2020.1
13. Suykens, J. A. K., Van Gestel, T., De Brabanter, J., De Moor, B., Vandewalle, J. (2002). Least Squares Support Vector Machines. Singapore: World Scientific, 295. https://doi.org/10.1142/5089
14. Xia, X.-L., Jiao, W., Li, K., Irwin, G. (2013). A Novel Sparse Least Squares Support Vector Machines. Mathematical Problems in Engineering, 2013, 1–10. https://doi.org/10.1155/2013/602341
15. LS-SVMlab toolbox. Available at: https://www.esat.kuleuven.be/sista/lssvmlab/
16. James, G., Witten, D., Hastie, T., Tibshirani, R. (2013). Support Vector Machines. An Introduction to Statistical Learning. New York: Springer, 337–372. https://doi.org/10.1007/978-1-4614-7138-7_9

CHAPTER 8

Method of parabolic approximation for determining the impact point coordinates of an artillery projectile

Pavlo Gultsov
Viktor Boltenkov
Yevhenii Dobrynin
Oleksii Maksymov

Abstract

This section considers a method for verifying an artillery shot under conditions of random disturbances, which is based on the registration of acoustic fields formed by ballistic and muzzle waves. The position of the proposed approach among modern technologies for ensuring the accuracy of artillery fire is demonstrated, and the feasibility of using the ballistic wave as a source of useful information for estimating projectile flight parameters is substantiated.

A general description of the method, the layout of the measuring equipment, and the sequence of measurement data processing are presented. The method is based on recording the moments when the projectile passes over spatially separated observation points, followed by approximation of the flight trajectory using a system of parabolas. The proposed algorithm takes into account possible changes in the relative positions of the measurement points with respect to the ascending and descending branches of the trajectory, which makes it possible to partially compensate for random disturbances caused by instability of the initial velocity and other firing-related factors.

The effectiveness of the method is investigated by means of simulation modeling for a large-caliber artillery projectile, taking into account random disturbances of temporal parameters. It is shown that the use of a system of approximating parabolas provides estimation of the projectile impact point coordinates with an error on the order of fractions of a percent of the firing range. A comparative analysis with the traditional method of compensating random disturbances by successive corrective shots is carried out, and the results of a field experiment involving the registration of ballistic wave signals are presented. The obtained results confirm

© The Author(s) of individual chapters, 2026 DOI: 10.21303/978-9908-8450-1-2.ch8

the fundamental possibility of verifying an artillery shot using a single firing with acceptable accuracy.

Keywords

Artillery shot, firing verification, ballistic wave, acoustic reconnaissance, trajectory approximation, random disturbances.

8.1 Introduction

Modern conditions of employment of artillery units are characterized by high dynamics of combat operations, an increasing role of counter-battery warfare, and strict limitations on the duration of fire impact. Under such conditions, the effectiveness of artillery fire is determined not only by the accuracy of ballistic calculations but also by the ability to promptly verify the results of a shot and rapidly adjust fire taking into account real firing conditions. This, in turn, necessitates a transition from classical counter-battery engagement schemes to short-duration fire tactics with immediate relocation of firing positions of the "shoot-and-scoot" type [1, 2].

Achieving the required level of combat effectiveness of artillery units under such conditions is impossible without extensive use of modern information technologies, automated fire control systems, and specialized geoinformation tools. The calculation of artillery projectile flight trajectories, the construction of firing tables, and the assessment of target engagement accuracy are based on refined mathematical models, methods of optimal estimation, and forecasting. The universality of this mathematical framework is confirmed by its application in modeling complex dynamic and physicochemical processes, in particular in parameter identification problems, the solution of inverse problems, and the development of approximation models for systems of various physical nature [3–10].

A special place among the means of verifying artillery firing results is occupied by acoustic methods based on the registration and processing of sound signals generated by the shot and the projectile burst. Despite the complex nature of acoustic wave propagation under real conditions, modern signal processing and mathematical modeling techniques make it possible to obtain informative temporal and spatial parameters suitable for estimating burst coordinates and analyzing firing errors [1, 2].

In view of the above, a relevant scientific and applied task is the development and investigation of methods for determining the coordinates of the artillery projectile impact point based on acoustic measurements using simplified yet informative trajectory approximation models. The use of parabolic approximation makes it possible to reduce the computational complexity of the problem, ensure sufficient estimation

accuracy with a limited amount of measurement information, and create prerequisites for the practical implementation of firing result verification methods in a mode close to real time [3, 4].

At the same time, the proposed approach is based on a number of assumptions that define the scope of its applicability. It is assumed that the projectile motion remains supersonic over the observation segment and that the ballistic wave can be reliably registered at spatially distributed measurement points. The method relies on the availability of sufficiently accurate firing tables for estimating the initial projectile velocity and does not explicitly model complex aerodynamic effects beyond integral drag. In addition, the proposed approximation framework is intended for conditions where meteorological parameters vary slowly in space and time and can be treated as quasi-stationary during a single shot.

8.2 General principles of acoustic reconnaissance tasks

A method for determining the coordinate of the artillery projectile impact with the surface by means of acoustic registration of the acoustic field generated by the projectile is considered. The registration of the acoustic field of a projectile that detonates near the target can be regarded as an integral process, the result of which is a reduction in projectile expenditure during mission execution by avoiding computational and measurement errors, as well as by reducing projectile dispersion under compensating actions of external disturbances recorded over a series of shots. The rate of introducing compensating actions into the operation of artillery units is a decisive factor in the conduct of combat operations under modern conditions.

Acoustic reconnaissance is conducted continuously, and the obtained data must be reliable and accurate. Based on the coordinates of acoustic targets, fire for effect may be conducted without prior adjustment. At the same time, based on the coordinates of projectile impact and burst points, adjustment fire should be carried out for non-acoustic and optically undetected targets.

The registration of the acoustic field for the needs of artillery units makes it possible to solve two main tasks. For this purpose, the equipment of a sound-ranging complex is deployed in a specific configuration in the field, consisting of several sound receivers placed at base points, as well as a central point that accommodates information processing equipment, an observation post, and communication facilities [11].

The first task makes it possible to detect firing positions of guns that are not optically observable, regardless of the types of ammunition used, based on a demasking

feature, namely the sound of the shot. Below, a generalized sequence of operations performed during the deployment of acoustic reconnaissance units to ensure fire support of artillery guns against acoustic targets is presented:

Step 1. The acoustic reconnaissance unit is deployed on the basis of an automated sound-ranging complex that includes three sound receivers placed at base points with known coordinates. At the central point, the coordinates of which are also known, information processing equipment is installed, consisting of a central computing unit, a meteorological measurement complex, and observation and communication facilities. The sound receivers and the information processing equipment are connected via internal communication means, while interaction between the artillery unit and the sound-ranging complex is ensured by external communication means.

Step 2. The sound receivers are deployed in the field under identical conditions, preferably on dominant elevations, along a line perpendicular to the expected direction of acoustic wave propagation, at a distance of 500–1000 m from each other.

Step 3. The coordinates of each sound receiver are determined and entered into the information processing equipment of the central computing unit.

Step 4. The meteorological measurement complex records meteorological information (air temperature, wind direction, and wind speed in the near-surface atmospheric layer), which is transmitted to the central point and entered into the information processing equipment of the central computing unit.

Step 5. Adjustment and calibration of the information reception equipment are performed at each base point with connected sound receivers.

Step 6. Separate adjustment of the interaction channels between the equipment located at the base points and the information processing equipment of the central point is carried out.

Step 7. Calibration of the information transmission channels from each sound receiver to the information processing equipment is performed.

Step 8. Astronomical time is entered into the central computing unit, and synchronization and alignment of the unified time of the central point with the time at each base point are carried out.

The second task makes it possible to conduct fire by friendly artillery against non-acoustic and optically undetected targets by determining the projectile impact points based on the sound of their bursts. Below, a sequence of operations performed during the support of artillery gun fire by an acoustic reconnaissance unit based on projectile bursts is presented:

Step 1. The coordinates of the target and the firing position are entered into the central computing unit.

Step 2. A shot is fired from the artillery gun at the firing position. At the moment the projectile collides with a solid obstacle, it detonates, resulting in the generation of a sound wave which propagates through the atmosphere and reaches the sound receivers.

Step 3. Using the sound receivers, the sound wave generated by the projectile burst is recorded, and the acquired information is transmitted via a communication channel to the information processing equipment. As a result of processing, the central computing unit determines the coordinates of the projectile burst point (reference point).

Step 4. The coordinates of the burst point are calculated based on the known positions of the sound receivers, the sound wave propagation velocity with corrections for the current meteorological conditions of the near-surface atmospheric layer, and the differences in sound wave arrival times at the sound receivers.

Step 5. The coordinates of the projectile impact point relative to the firing position are determined.

Artillery gun fire conducted with the support of an acoustic reconnaissance unit according to the above algorithms during the execution of combat tasks has a number of limitations caused by the physical properties of the medium of acoustic wave propagation, the nature of the surface in the projectile burst zone, and the presence of natural or artificial obstacles along the sound signal propagation path [12].

The above factors should be regarded as inherent limitations of acoustic-based methods and define the conditions under which the proposed approach can be effectively applied.

When firing at targets located on soft marshy soil or on ground covered with a thick snow layer, a complete projectile detonation may not occur upon impact with such a surface. Under these conditions, an acoustic wave capable of propagating in the atmosphere and reaching the sound receivers is not formed, which makes it impossible to register the burst moment and, accordingly, to determine the coordinates of the projectile impact point.

When firing at targets located on a water surface, the projectile passes through the water layer and detonates in the underwater environment. In this case, the main part of the explosion energy is absorbed by the water, as a result of which an acoustic wave in the atmosphere is either not formed or has an intensity insufficient for reliable registration by the sound receivers.

Significant attenuation of the acoustic wave is also possible even when a projectile burst occurs, if its propagation path passes through media with a high

absorption coefficient of acoustic oscillations. Such conditions include large forested areas as well as complex terrain with the presence of hills, ravines, and other natural obstacles, which lead to a reduction in signal amplitude and a deterioration in registration accuracy.

The registration of the acoustic wave generated by a projectile explosion is carried out by sound receivers arranged along a line perpendicular to the direction of the expected arrival of the acoustic wave.

The listed limitations may lead to the impossibility of determining the coordinates of the projectile burst or impact point, either due to the absence of an acoustic signal or under conditions of its significant attenuation during atmospheric propagation. These factors must be taken into account when employing acoustic reconnaissance means to support artillery fire.

8.3 Method for registering the coordinate of artillery projectile impact with the surface

The method for determining the coordinate of an artillery projectile impact with the surface is based on an approach in which, through the introduction of new operations and a modification of the execution order of existing ones, it becomes possible to determine the coordinates of unexploded projectiles and to increase the accuracy of determining the projectile impact coordinate. The following features are relevant for the proposed method [13].

Along the firing direction line from the gun, at a presumed distance at which the projectile loses its supersonic velocity, locations for the placement of three measuring microphones or three groups of measuring microphones are determined.

The conditions for placing three measuring microphones or three groups of measuring microphones are specified:

1) at predetermined locations, the first, second, and third measuring microphones, or the first, second, and third groups of measuring microphones, are deployed with a positioning error not exceeding 50% of the specified distances;

2) the coordinates of the three measuring microphones or three groups of measuring microphones located along the firing line are determined;

3) the ballistic and muzzle waves are recorded above the microphones or groups of microphones;

4) the time interval between the registration of the ballistic wave and the registration of the muzzle wave is determined for each measuring microphone or

group of measuring microphones, from the microphone or group closest to the gun to the microphone or group farthest from the gun;

5) the initial projectile velocity at the moment of firing is determined;

6) three types of ballistic curves defined by three points are obtained, based on which the coordinates of the artillery projectile impact with the surface are determined;

7) using the three obtained coordinates, the average coordinate of the artillery projectile impact with the surface is determined.

The causal relationship between the set of presented conditions and the achieved technical result is explained as follows.

At the moment the projectile exits the barrel (the sound source), two sound waves are generated. The ballistic wave is formed when the projectile moves at supersonic velocity and exists over the time interval until it disappears as a result of the projectile transitioning to a subsonic motion regime, where the propagation velocity of the wave is equivalent to the instantaneous velocity of the projectile. The muzzle wave is formed by the outflow of propellant gases after the projectile leaves the barrel. Initially, over a relatively short time interval, it exhibits the properties of a shock-acoustic wave and transforms into an acoustic wave as the pressure of the gases equalizes with atmospheric pressure [14]. Subsequently, its propagation velocity becomes constant and equal to the speed of sound.

Both waves (ballistic and muzzle) are alternately registered by a microphone or a group of microphones located along the firing direction line. Based on the arrival times of the muzzle and ballistic waves at each microphone or group of microphones, the distances from the sound source to the devices registering the sound waves are determined. The velocity of the ballistic wave above a microphone or group of microphones is measured. At the same time, the initial projectile velocity is determined. At a given moment in time and at a known distance, the propagation velocity of the ballistic wave is equal to the projectile velocity. Subsequently, using the data from three points and the characteristics of the projectile motion, an approximating parabola is constructed, which determines the location of the projectile impact with the surface.

The schematic layout of the equipment is identical to that shown in **Fig. 2.6** (Section 2.6).

The detailed step-by-step procedure for determining projectile impact coordinates based on acoustic registration of ballistic and muzzle waves is provided in Section 2.6. In this chapter, the method is applied to compute trajectory approximation coefficients and mean impact coordinates under varying operational conditions.

8.4 Acoustic fields of a shot – the basis of the method for recording the projectile impact coordinate with the surface

Ensuring the required accuracy of artillery fire under modern conditions is directly associated with the capability for prompt assessment of the results of each shot. In this context, the analysis of acoustic fields generated during a shot and the subsequent projectile flight is considered one of the promising information-based approaches to solving the problem of artillery fire verification [2]. Modern means of ensuring the accuracy of artillery fire and its current assessment, as well as guidance and correction methods, can be divided into the following technological directions: (i) preliminary fire preparation [15]; (ii) verification of firing results, i.e., confirmation of projectile impact at the aiming point or assessment of deviation from the aiming point [16].

The technological direction (i) provides comprehensive accounting of possible firing errors, including systematic ones, and encompasses a set of preparatory measures, among which the following main components are distinguished: target reconnaissance and coordinate determination; topogeodetic preparation; meteorological preparation; ballistic preparation; technical preparation; and determination of firing settings. The implementation of these measures is aimed at reducing systematic firing errors prior to the execution of a shot.

Despite continuous improvement of the technological means associated with direction (i), including the use of information technologies, random disturbances may arise during firing. These disturbances are associated with factors that are difficult to assess with sufficient accuracy, such as barrel wear of the artillery system that has occurred since its last measurement; changes in barrel temperature as a result of intensive previous firing; and inaccurate information regarding the propellant charge and its storage conditions. Errors caused by random disturbances must be assessed during the verification process [17], which necessitates the use of additional information means for monitoring firing results.

Technological direction (ii) is associated with establishing informational feedback between successive shots fired from an artillery system [2] and involves estimating the coordinates of projectile bursts during firing. For fire correction, it is necessary to evaluate the coordinates of the projectile burst at the moment of firing, which significantly complicates and prolongs the verification procedure.

The most commonly used technologies within direction (ii) at present include the following:

1. Optical observation, including the use of unmanned aerial vehicles [18]. The disadvantages are demasking of the observation process and vulnerability of the observation assets.

2. Determination of the projectile impact point using artillery radar stations (Radar Stations) [19]. The disadvantage is demasking of the observation process due to radar emission.

3. Processing of acoustic signals from projectile bursts, i.e., the use of artillery sound-ranging means, specifically for "own-fire adjustment" [20]. The disadvantages include the requirement for large, spatially distributed sensor systems and a strong dependence of effectiveness on meteorological conditions.

The means of analyzing artillery acoustic fields are considered in more detail below. During an artillery shot, two types of waves are generated. A sound impulse produced by the propellant gases exiting the barrel immediately behind the projectile forms a wave known as the muzzle wave [18]. A wave with similar acoustic characteristics also arises during a projectile burst. This type of wave constitutes the object of analysis in artillery sound ranging.

Another type of wave generated during a shot is the air wave produced by the projectile moving at supersonic speed, referred to as the ballistic wave [11]. The ballistic wave remains a shock wave throughout the entire period during which the projectile continues to move at supersonic speed, while propagating together with it. The acoustic signal of the ballistic wave has an *N*-shaped impulse with a duration of 2–5 ms; its energy spectrum is broadband and lies within the frequency range from 10 Hz to 500–700 Hz. The ballistic wave can be registered only within the Mach cone formed by a projectile flying at supersonic speed. For more than 100 years in artillery sound ranging, the ballistic wave was considered an interference signal. However, in [1] it was demonstrated that the ballistic wave is a valuable source of useful information, in particular regarding the current level of barrel wear. This study examines the possibility of developing and investigating a promising method for verification of an artillery shot based on registration of the ballistic wave generated by a projectile flying along a trajectory recorded by a spatially distributed system of acoustic sensors.

8.5 Method for shot verification

General description of the shot verification method. **Fig. 8.1** presents the layout of the artillery gun and the measuring equipment employed to record the projectile flight parameters.

The origin of the coordinate system is aligned with the weapon firing position P_0, from which a projectile is fired with an initial velocity vector $\vec{v}_0$ exceeding the speed of sound. The diagram illustrates the projectile motion in the vertical plane. The aiming point P is located at the horizontal range X. It should be noted

that, in this study, the lateral deviation of the projectile caused by spin drift (derivation) is not taken into account. This assumption is introduced in order to focus on the longitudinal component of the projectile motion and to simplify the analysis of the proposed verification method. The influence of derivation can be incorporated into the model using well-known correction techniques if higher accuracy in the lateral plane is required [21].

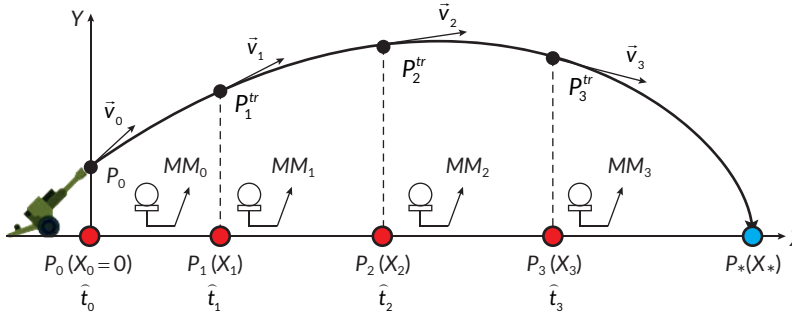

Fig. 8.1 Layout of the artillery gun and measuring equipment

During the projectile flight along a ballistic trajectory at supersonic speed, it is accompanied by a ballistic wave that is observed on the ground surface along the firing line located inside the Mach cone. On the surface, at three observation points with the corresponding coordinates $P_1(X_1)$, $P_2(X_2)$ and $P_3(X_3)$, sets of measuring equipment (Measurement Equipment Set, MES) are deployed. Each MES is intended to record the instants of occurrence of the ballistic wave at the corresponding point $\hat{t}_i, i=1,2,3$, which correspond to the moments when the projectile passes over the observation points. Each MES includes a measuring microphone, an analog-to-digital converter, and a radio communication channel. One additional MES is located at the firing position. All four MES units are synchronized in time.

Objective of the proposed shot verification method. Taking random disturbances into account, the objective of the proposed shot verification method is to estimate the projectile impact coordinates based on the recorded moments of its passage over the observation points and to determine whether the obtained coordinates satisfy the specified accuracy requirements.

Measurement processing method:

Step 1. At the firing point P_0, the projectile velocity is determined using firing tables for the given type of projectile and propellant charge (the firing preparation is assumed to be complete, while possible random disturbances are allowed).

For each observation point P_j ($j=1, 2, 3$), the following calculations are performed based on the data obtained at the preceding points P_i ($i=0, 1, 2$).

Step 2. The segment of the projectile trajectory $P_i^{tr}P_j^{tr}$ is approximated by a straight-line segment $P_i^{tr}P_j^{tr}$ (**Fig. 8.2**).

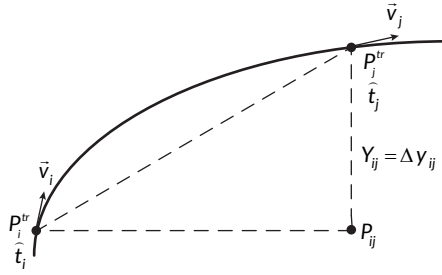

Fig. 8.2 Calculated segment of the trajectory

The air drag force acting on a projectile in flight is described by a quadratic model

$$R=C_x\rho\frac{v^2}{2}SM, \tag{8.1}$$

where C_x is the integral drag coefficient; ρ is the air density; v is the projectile velocity; S is the projectile midsection (reference) area, P_iP_j; $M=v/c$ is the Mach number; c is the speed of sound in air.

The vector $\vec{R}$ is directed opposite to the velocity vector $\vec{v}$; accordingly, the force R imparts a negative acceleration to the projectile

$$a=R/m, \tag{8.2}$$

where m is the projectile mass.

Then, the projectile velocity at point P_j^{tr} is

$$v_j=v_j-C_x\rho\frac{v^2}{2}SM/m. \tag{8.3}$$

The approximate length of the trajectory segment is

$$P_i^{tr}P_j^{tr}=v_j\Delta t_{ij}-C_x\rho\frac{v^2}{2}SM/m\Delta t_{ij}^2, \tag{8.4}$$

where $\Delta t_{ij}=t_j-t_i$.

As a result of performing the computational procedures (8.1)–(8.4), in the right triangle $P_i^{tr}P_j^{tr}P_{ij}$ two sides are known: $P_i^{tr}P_j^{tr}$ and $P_i^{tr}P_{ij} = X_j - X_i$. Thus, the elevation of the projectile flight trajectory along the *Y*-axis at point P_j^{tr} relative to point P_i^{tr} is determined

$$\Delta Y_{ij} = \sqrt{(P_i^{tr}P_j^{tr})^2 - (P_i^{tr}P_{ij})^2}. \tag{8.5}$$

The projectile flight height over point P_j is

$$Y_j = Y_j + \Delta Y_{ij}. \tag{8.6}$$

As a result of performing the described computational procedure, the points of projectile trajectory elevation over the measurement points $P_1^{tr}(X_1, Y_1)$, $P_2^{tr}(X_2, Y_2)$, $P_3^{tr}(X_3, Y_3)$ are obtained, including the firing point P_0 $(X_0 = 0, Y_0 = 0)$.

Step 3. Approximation parabolas are constructed for each triad of points:

$$\begin{aligned}
&(P_0, P_1^{tr}, P_2^{tr}) - Y_1 = A_1X^2 + B_1X,\\
&(P_0, P_2^{tr}, P_3^{tr}) - Y_2 = A_2X^2 + B_2X,\\
&(P_0, P_1^{tr}, P_3^{tr}) - Y_3 = A_3X^2 + B_3X.
\end{aligned} \tag{8.7}$$

One more approximating parabola can be constructed using four points

$$(P_0, P_1^{tr}, P_2^{tr}, P_3^{tr}) - Y_4 = A_4X^2 + B_4X. \tag{8.8}$$

Each of the approximating parabolas represents a model of the projectile motion that, to a certain extent, compensates for random disturbances occurring at the moment of firing. The intersection points of the approximating parabolas with the ground surface (the non-zero roots of the parabolas) $P_*^1, P_*^2, P_*^3, P_*^4$ provide approximate estimates of the projectile impact point. The arithmetic mean of the intersection points with the surface, $X_*^0 = (X_*^1 + X_*^2 + X_*^3 + X_*^4)/4$ is taken as an average estimate of the projectile landing coordinate with partially compensated random disturbances.

It should be noted that, in practice, more than four approximating parabolas are constructed; however, for the evaluation of X_*^0, exactly four are selected, in accordance with the algorithm presented below.

Algorithm for determining the signs of ΔY_{ij}:

In the calculations of relations (8.2)–(8.6), it was assumed that point *j* lies on the trajectory above point *i*. In practice, the *Y*-coordinate of point *i* may be greater than

the *Y*-coordinate of point *j*. This occurs, for example, if point *j* is on the descending branch of the projectile's trajectory. Therefore, when evaluating ΔY_{ij} using expression (8.5) both positive and negative values of ΔY_{ij} should be taken into account. Accordingly, for each point $P_j, (j=1,2,3)$ two values of the projectile's flight height above point P_j must be calculated

$$Y_j^+ = Y_j + \Delta Y_{ij}; Y_j^- = Y_j - \Delta Y_{ij}. \tag{8.9}$$

Next, during the construction of approximating parabolas for each point $P_j, (j=1,2,3)$ included in the triad (8.7) or the tetrad (8.8), two parabolas are built – $Y_j^+ = A_j^+ X^2 + B_j^+ X$ and $Y_j^- = A_j^- X^2 + B_j^- X, (j=1,2,3)$. Then, for each of the two parabolas, the distance from the approximated landing point is determined as $\Delta_j^+ = \left| X_{*j}^+ - X_* \right|, (j=1,2,3)$ and $\Delta_j^- = \left| X_{*j}^- - X_* \right|, (j=1,2,3)$. The parabola with the smaller value of $\Delta_j, (j=1,2,3)$ is selected as the "correct" approximating parabola.

Accounting for the relative positions of points P_j and P_i, as ensured by the proposed algorithm, results in the formation of four "correct" approximating parabolas at Step 3 of the described method.

8.6 Simulation modeling of the shot verification method

The proposed method was validated by means of simulation modeling of firing from an FH70 howitzer using an M107 projectile of 155 mm caliber. In the simulation, it was assumed that the moments of ballistic wave registration can be determined with sufficient accuracy, while random disturbances were introduced only in the temporal parameters of projectile motion. The projectile characteristics [22] are as follows: mass 43 kg, diameter 0.15471 m, initial velocity (full charge No. 8) 684.3 m/s. Firing preparation is assumed to be complete. For the calculations, the following values were adopted: $\rho = 1.2041$ kg/m^3, $c = 341.6$ m/s, and the coordinate of the aiming point $X_* = 25000$ m. The integral drag coefficient C_x was taken from tables [22]. The *X*-coordinates of the measurement points are: $X(P_1) = 4900$ m, $X(P_2) = 10000$ m, $X(P_3) = 16000$ m. The times of projectile passage over the measurement points, taking into account random disturbances $\hat{t}_i, i = 1,2,3$, were generated as follows: 5% random disturbances were introduced into the tabulated passage times

$$\hat{t}_i = t_i^{FT} + \Delta t_i, \Delta t_i \in rand[0.95\Delta t_i; 1.05\Delta t_i] (i=1,2,3).$$

The simulated parameters of the simulation modeling are presented in **Table 8.1**.

Table 8.1 Parameters of simulation modeling of the shot verification method

Simulated parameter	Parameters corresponding to the microphone locations along the firing direction		
	No. 1	No. 2	No. 3
Target coordinate at the aiming point, m	25000	25000	25000
Distance from the gun to the measuring microphone, m	4900	10000	16000
Time of ballistic wave registration, s	10.5	22.2	39.7
Flight height over the measurement point Y_j, m	3634	6163	6686

Using the developed methodology, four approximating parabolas were constructed (**Fig. 8.3**). The results of the simulation modeling are presented in **Table 8.2**.

For clarity of the approximation process, the final segments of the approximating parabolas are shown in **Fig. 8.4**.

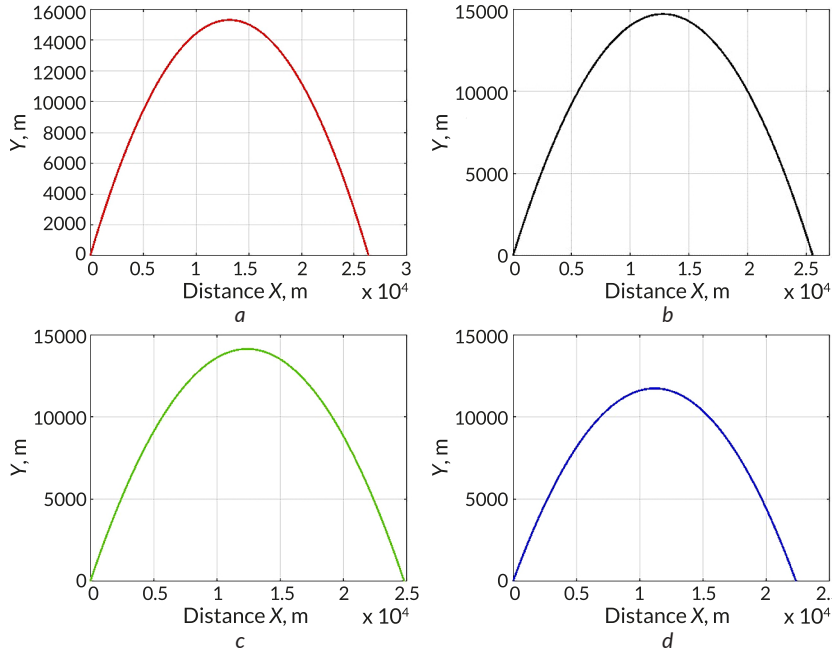

Fig. 8.3 Approximating parabolas: *a* – through points P_0, P_1, P_2; *b* – through points P_0, P_1, P_3; *c* – through points P_0, P_2, P_3; *d* – through points P_0, P_1, P_2, P_3

Table 8.2 Results of simulation modeling of the shot verification method

Simulation results		Approximating parabolas			
		No. 1	No. 2	No. 3	No. 4
Target range X_*, m		25000	25000	25000	25000
Parabola equation coefficients $Y = AX^2 + BX$	A	−0.000092	−0.000090	−0.000090	−0.000088
	B	2.28	2.30	2.11	2.32
X_*^i, m		25070	25060	24610	22850
$\underline{X}_*$, m		24390	24390	24390	24390

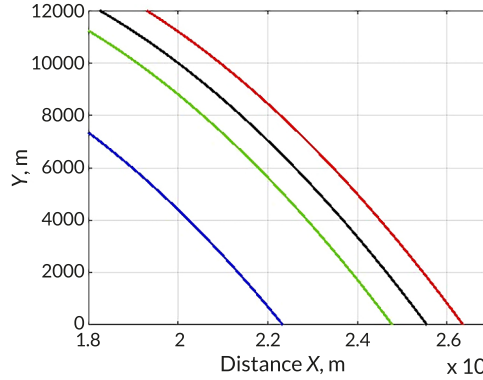

Fig. 8.4 Final sections of the approximating parabolas

Simulation modeling of the proposed shot verification method makes it possible to identify two main results:

1) the verification method, due to the use of a system of approximating parabolas, compensates for random disturbances while maintaining an error of about 0.5% of the firing range;

2) the proposed method allows verification with a single shot, providing results even before the projectile actually lands.

8.7 Comparative analysis of methods

Comparative analysis of the proposed method for registering the coordinates of an artillery projectile's impact with the surface and the method of compensating

random disturbances through successive corrective shots made it possible to identify the main advantages and limitations of each approach.

In order to demonstrate the effectiveness of the proposed method, a model calculation of firing at the same range was carried out using a program for precise trajectory computation based on the NATO standard STANAG 4355 [23]. According to this standard, the projectile flight model describes the projectile as a moving material point with five degrees of freedom. At present, such a model is considered one of the most accurate for describing the trajectories of large-caliber artillery projectiles.

The complete simulation, in accordance with [23], was performed using Matlab software code presented in [24]. To ensure equivalent simulation conditions, random disturbances were taken into account by means of a pseudo-random variation of the projectile's initial velocity

$$v_0^{dist} = v_0^{FT} + \Delta v_0, \Delta v_0 \in rand[0.975 v_0^{FT}; 1.025 v_0^{FT}]. \quad (8.10)$$

After each shot, the deviation of the projectile's impact point was estimated and subsequently compensated using the artillery bracketing method with correction of the aiming angle for the subsequent shots. **Fig. 8.5** presents the calculated projectile flight trajectories for five successive shots. The generalized simulation results are given in **Table 8.3**.

For clarity, **Fig. 8.6** shows the terminal segments of the ballistic trajectories for the specified five shots.

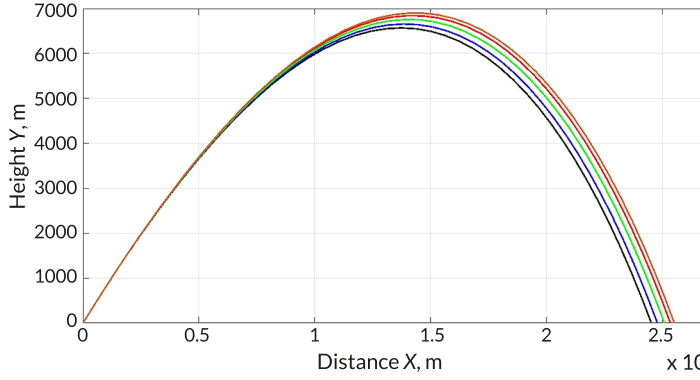

Fig. 8.5 Calculated ballistic trajectories for five shots with subsequent correction

Table 8.3 Results of modeling random disturbance compensation by successive shots using the STANAG 4355 model

Simulation results	Shot numbers				
	No. 1	No. 2	No. 3	No. 4	No. 5
Target range X_*, m	25000	25000	25000	25000	25000
X_i, m	24550	25530	24750	25300	25120
$\underline{X}_*$, m	25120	25120	25120	25120	25120

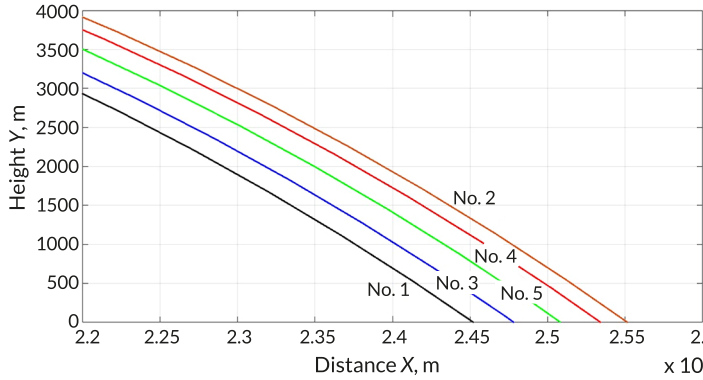

Fig. 8.6 Final segments of ballistic trajectories for five successive shots

The obtained simulation results demonstrated that, in order to compensate for random disturbances down to an error level of approximately 0.5% of the firing range, the traditional adjustment method requires at least five consecutive shots.

For practical verification of the effectiveness of the proposed shot verification method, a full-scale field experiment was conducted with registration of real ballistic wave signals during training firing of a 152 mm towed gun 2A36 "Hyacinth-B". Three sets of measurement equipment were deployed at distances of 5400 m, 7800 m, and 10 000 m from the firing position. Each set included a Rode NT-USB condenser microphone, a 16-bit TASCAM analog-to-digital converter, and radio communication channel equipment with the firing position, where an additional measurement set was installed. All measurement equipment operated in a time-synchronized mode.

Due to the high level of acoustic interference and the low signal-to-noise ratio, the ballistic wave signal was recorded in a distorted form (**Fig. 8.7**). Under such conditions, determining the moment of its onset using threshold-based methods becomes significantly more difficult. Therefore, the determination of the response time

of the measuring microphones to the ballistic wave was carried out by identifying the maximum of the cross-correlation function between the signals recorded at the measurement point and at the firing position. For this purpose, the cross-correlation function of the signal $s_i(t)$ at the measurement point and the signal $s_0(t)$ at the firing position was used [25]

$$\widehat{t}_i = R(s_i(t), s_0(t))\,(i = 1, 2, 3). \tag{8.11}$$

A typical form of the cross-correlation function is shown in **Fig. 8.8**.

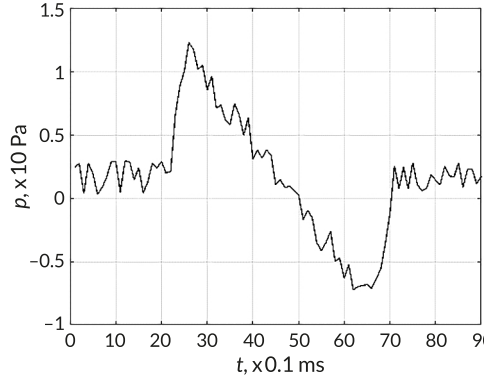

Fig. 8.7 Ballistic wave signal recorded at measurement point No. 1
Source: [26]

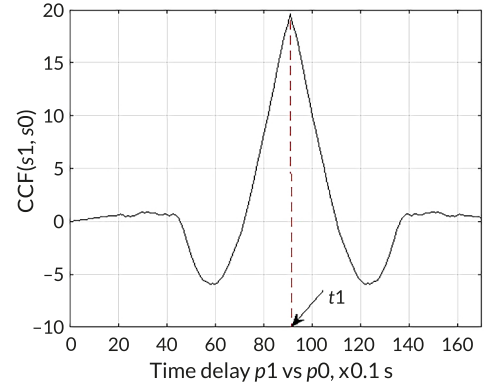

Fig. 8.8 Cross-correlation function of signals at point No. 1 and the firing position
Source: [26]

The results of the field experiment are presented in **Tables 8.4**, **8.5**. It should be noted that in this case only three approximating parabolas were constructed, each defined by three points.

During the field tests, the proposed method provided compensation of random disturbances at the level of 3.5% of the firing range. This value significantly exceeds the result obtained in the simulation experiment. However, considering that it was achieved with a single shot, this result demonstrates a quite acceptable quality of verification.

Let's turn to the identification of the advantages and disadvantages of the proposed shot verification method. The specified verification method based on parabolic approximation, as demonstrated by simulation modeling and full-scale experiments, makes it possible to compensate random disturbances to quite acceptable error levels already with a single shot [16].

Table 8.4 Parameters of the experimental verification of the shot verification method

Parameter	Parameters corresponding to the microphone placement points along the firing line		
	No. 1	No. 2	No. 3
Aimed target coordinate, m	15000	15000	15000
Distance from the gun to the measuring microphone, m	5400	7800	10000
Time of ballistic wave registration, s	8.5	14.8	19.7
Height of projectile over the measurement point Y_j, m	3634	6163	6686

Table 8.5 Results of the experimental verification of the shot verification method

Simulation results		Approximating parabolas		
		No. 1	No. 2	No. 3
Target range X_*, m		15000	15000	15000
Parabola equation coefficients $Y = AX^2 + BX$	A	–0.000096	–0.000088	–0.000080
	B	1.32	1.28	1.19
X_*^i, m		13790	14550	15100
$\underline{X}_*$, m		14480	14480	14480

The computations accompanying the construction of the approximating parabolas are fairly simple and can be performed on an artillery commander's tablet.

The recommended method reduces the time required for fire execution and decreases ammunition expenditure. In this way, it offers new opportunities for preserving weapon survivability in counter-battery operations. The main drawback of the developed verification method is the need for specialized equipment to register acoustic fields and to deploy it along the line of fire. However, information on the development of such equipment and its pilot application is currently available [27].

Based on the results presented in Chapter 4, it can be stated that, for the first time, a method for tracking an artillery shot under the influence of random disturbances has been proposed, relying on the registration of ballistic and muzzle waves generated by the shot and the projectile. This made it possible to verify the state of an artillery gun shot and to determine the point of impact of the projectile with the surface using parabolic approximation of its characteristics.

8.8 Conclusions

In this chapter of the monograph, a method for verifying an artillery shot based on the registration of acoustic fields, in particular ballistic and muzzle waves generated during the shot and the projectile's flight, has been considered and investigated. It is shown that the use of information on the time instants at which the ballistic wave passes over spatially distributed observation points makes it possible to estimate the projectile's impact coordinates even before it collides with the surface.

The proposed method is based on parabolic approximation of segments of the projectile flight trajectory and provides compensation for random disturbances associated with instability of the initial velocity, barrel condition, and other poorly controllable factors. The developed algorithm for determining the signs of trajectory elevation makes it possible to correctly account for the relative positioning of measurement points on the ascending and descending branches of the trajectory.

The results of simulation modeling confirmed the ability of the method to ensure accuracy of impact coordinate estimation at a level of about 0.5% of the firing range using a single shot. A field experiment involving the registration of real ballistic wave signals demonstrated the practical feasibility of the approach and an acceptable quality of verification under conditions of a high level of acoustic interference.

Comparative analysis with traditional adjustment methods showed that the proposed approach makes it possible to significantly reduce the number of corrective shots, decrease ammunition consumption, and shorten the time required for

fire execution, which is critically important in modern counter-battery operations. The obtained results indicate the promise of further development of artillery shot verification methods based on acoustic measurements and their integration into modern artillery information and control systems.

Conflict of interest

The authors declare that they have no conflict of interest in relation to this research, whether financial, personal, authorship or otherwise, that could affect the research and its results presented in this paper.

Use of artificial intelligence statement

The authors declare that they did not use artificial intelligence tools in preparing this manuscript.

Authors' contributions

Pavlo Gultsov: Conceptualization, Methodology, Development of acoustic verification algorithms, Writing – original draft.

Viktor Boltenkov: Simulation modeling, Algorithm implementation, Analysis of projectile flight data.

Yevhenii Dobrynin: Data acquisition, Processing of acoustic signals, Validation of results.

Oleksii Maksymov: Visualization of results, Technical support of field experiments, Writing – review & editing.

References

1. Dobrynin, Y., Volkov, V., Maksymov, M., Boltenkov, V. (2020). Development of physical models for the formation of acoustic waves at artillery shots and study of the possibility of separate registration of waves of various types. Eastern-European Journal of Enterprise Technologies, 4 (5 (106)), 6–15. https://doi.org/10.15587/1729-4061.2020.209847

2. Boltenkov, V., Brunetkin, O., Dobrynin, Y., Maksymova, O., Kuzmenko, V., Gultsov, P. et al. (2021). Devising a method for improving the efficiency of artillery shooting based on the Markov model. Eastern-European Journal of Enterprise Technologies, 6 (3 (114)), 6–17. https://doi.org/10.15587/1729-4061.2021.245854
3. Brunetkin, O., Beglov, K., Brunetkin, V., Maksymov, O., Maksymova, O., Havaliukh, O., Demydenko, V. (2020). Construction of a method for representing an approximation model of an object as a set of linear differential models. Eastern-European Journal of Enterprise Technologies, 6 (2 (108)), 66–73. https://doi.org/10.15587/1729-4061.2020.220326
4. Dobrynin, Y., Brunetkin, O., Maksymov, M., Maksymov, O. (2020). Constructing a method for solving the riccati equations to describe objects parameters in an analytical form. Eastern-European Journal of Enterprise Technologies, 3 (4 (105)), 20–26. https://doi.org/10.15587/1729-4061.2020.205107
5. Maksymov, M. V., Brunetkin, O. I., Beglov, K. V., Alyokhina, S. V., Butenko, O. V. (2022). Automatic Control for the Slow Pyrolysis of Organic Materials with Variable Composition. Advanced Control Systemss: Theory and Applications. Series in Automation, Control and Robotics. River Publishers, 397–434. https://doi.org/10.1201/9781003337010-16
6. Brunetkin, O., Maksymov, M., Dobrynin, Y., Demydenko, V., Sidelnykov, O. (2024). Development of a process model for determining the composition and energy characteristics of a pyrotechnic mixture using the library method. EUREKA: Physics and Engineering, 5, 99–112. https://doi.org/10.21303/2461-4262.2024.003453
7. Brunetkin, O., Dobrynin, Y., Maksymenko, A., Maksymova, O., Alyokhina, S. (2020). Inverse problem of the composition determination of combustion products for gaseous hydrocarbon fuel. Computational Thermal Sciences: An International Journal, 12 (6), 477–489. https://doi.org/10.1615/computthermalscien.2020034878
8. Brunetkin, O. I., Beglov, K. V., Maksymov, M. M., Ulytska, O. O. (2021). Model and method of controlled pyrolysis of organic sub-stances of variable composition. Problems of Control and Informatics, 66 (1), 134–146. https://doi.org/10.34229/1028-0979-2021-1-12
9. Brunetkin, O., Sidelnykov, O., Maksymov, M., Dobrynin, Y. (2025). Improving the model for determining the composition of gunpowder gases during thermal destruction of gunpowder in a limited volume space. Eastern-European Journal of Enterprise Technologies, 3 (6 (135)), 35–45. https://doi.org/10.15587/1729-4061.2025.330654
10. Brunetkin, O., Maksymov, M., Brunetkin, V., Maksymov, O., Dobrynin, Y., Kuzmenko, V., Gultsov, P. (2021). Development of the model and the method for

determining the influence of the temperature of gunpowder gases in the gun barrel for explaining visualize of free carbon at shot. Eastern-European Journal of Enterprise Technologies, 4 (1 (112)), 41–53. https://doi.org/10.15587/1729-4061.2021.239150
11. Damarla, T. (2015). Battlefield Acoustics. Springer International Publishing, Switzerland, 262. https://doi.org/10.1007/978-3-319-16036-8
12. Tarakhtii, O. S., Gultsov, P. S., Maksymov, O. M. (2023). Pat. No. 127193. Sposib vyznachennia koordynaty zustrichi artyleriiskoho snariada z poverkhneiu. declareted: 28.04.2021; published: 31.05.2023, Bul. No. 22.
13. Bolton, J. Q. (2023). The More Things Change … Russia's War in Ukraine Mirrors the Past as Much as It Shows the Future. Military Review, 1–14. Available at: https://www.armyupress.army.mil/Journals/Military-Review/Online-Exclusive/2023-OLE/The-More-Things-Change/
14. Shevtsov, R. (2023). An improved mathematical model of fire damage to enemy artillery units by missile forces and artillery in operations. Social Development and Security, 13 (1), 13–22. https://doi.org/10.33445/sds.2023.13.1.2
15. Sviderok, S. M., Shabatura, U. V., Prokopenko, A. O. (2016). Technique of the fire correction of artillery systems according to modern requiremernts to the data preparation for shooting. Military Technical Collection, 14, 99–103. https://doi.org/10.33577/2312-4458.14.2016.99-103
16. Krzyzanowski, S. (2018). How to assess the accuracy of artillery fire. Scientific Journal of the Military University of Land Forces, 187 (1), 25–39. https://doi.org/10.5604/01.3001.0011.7355
17. Šilinger, K., Brabcová, K., Potužák, L. (2019). Assessment of possibility to conduct fire for effect without adjust fire according to observational distance of a target in artillery automated fire control systems. International Journal of Electrical Engineering and Computer Science, 1, 103–108.
18. Bartulović, V., Trzun, Z., Hoić, M. (2023). Use of unmanned aerial vehicles in support of artillery operations. Strategos, 7 (1), 71–92. Available at: https://www.researchgate.net/publication/372657457_Use_of_Unmanned_Aerial_Vehicles_in_Support_of_Artillery_Operations
19. Khudov, H., Yuzova, I., Lisohorskyi, B., Solomonenko, Y., Mykus, S., Irkha, A. et al. (2021). Development of methods for determining the coordinates of firing positions of roving mortars by a network of counter-battery radars. EUREKA: Physics and Engineering, 3, 140–150. https://doi.org/10.21303/2461-4262.2021.001821
20. Kochan, R., Kochan, O., Trembach, B., Kohut, U., Zawislak, S., Falat, P., Warwas, K. (2019). Theoretical Error of Bearing Method in Artillery Sound Ranging. 2019

10th IEEE International Conference on Intelligent Data Acquisition and Advanced Computing Systems: Technology and Applications (IDAACS), 615–619. https://doi.org/10.1109/idaacs.2019.8924450
21. Zhuravlev, A., Orlov, S., Shuliakov, S. (2020). Mathematical model of the flight path of a projectile of a long-range artillery system. Systems of Arms and Military Equipment, 3 (63), 62–68. https://doi.org/10.30748/soivt.2020.63.09
22. Wessam, M. E., Chen, Z. H. (2015). Firing Precision Evaluation For Unguided Artillery Projectile. Proceedings of the 2015 International Conference on Artificial Intelligence and Industrial Engineering, 123. https://doi.org/10.2991/aiie-15.2015.156
23. STANAG 4355 (2022). The Modified Point Mass and five degrees of freedom trajectory models – AOP-4355 EDITION A. Washington: United States Department of Defense. Available at: https://www.scribd.com/document/492052990/STANAG-4355-The-modified-point-mass-and-five-degrees-of-freedom-trajectory-models-Edition-3
24. Aldoegre, M. (2019). Comparison between trajectory models for firing table application. North-West University. Available at: https://repository.nwu.ac.za/items/cad7cd66-e45d-4da8-aa79-1723e382a549
25. Le Bot, O., Gervaise, C., Mars, J. I. (2016). Time-difference-of-arrival estimation based on cross recurrence plots, with application to underwater acoustic signals. Recurrence Plots and Their Quantifications: Expanding Horizons. Springer, 265–288. https://hal.science/hal-01343668/document
26. Dobrynin, Y. V., Boltenkov, V. O., Kuzmenko, V. V., Maksymov, O. M. (2022). Development of a universal binary classifier of the state of artillery barrels by the physical fields of shots. Applied Aspects of Information Technology, 5 (4), 289–302. https://doi.org/10.15276/aait.05.2022.19
27. Maksymov, M. V., Boltenkov, V. O., Gultsov, P. S., Maksymov, O. M. (2023). Verification of artillery fire under the influence of random disturbances for the computer game ARMA 3. Applied Aspects of Information Technology, 6 (4), 362–375. https://doi.org/10.15276/aait.06.2023.24

CHAPTER 9

Method for determining three acoustic sensors for registering the ballistic wave of an artillery shot

Volodymyr Demydenko
Yevhenii Dobrynin
Maksym Maksymov
Ruslan Riaboshapka

Abstract

The chapter addresses the problem of improving the accuracy of determining the coordinates of the point where an artillery projectile impacts the surface under conditions of random disturbances by means of a rational selection of acoustic sensors for registering the ballistic wave. The factors influencing the effectiveness of acoustic measurements are analyzed, including registration errors, the probability of the sensors being in an operational state, and their spatial arrangement relative to the firing direction line. An approach is proposed for determining three most suitable acoustic measuring devices from the available set, taking into account the combined effect of the specified factors. The obtained results create prerequisites for the practical implementation of the artillery shot verification method and for estimating the coordinates of the projectile impact point in a mode close to real time.

Keywords

Artillery shot, acoustic sensors, ballistic wave, shot verification, random disturbances, trajectory approximation.

9.1 Introduction

In modern conditions of employment of artillery units, operational verification of firing results and estimation of the coordinates of the projectile impact point under uncertainty and random disturbances become particularly important. In practice, the effectiveness of such estimations depends not only on the selected method of processing measurement information, but also on the configuration of the measuring

© The Author(s) of individual chapters, 2026 DOI: 10.21303/978-9908-8450-1-2.ch9

system, in particular on the composition and spatial arrangement of the acoustic sensors used during firing.

One of the promising directions for solving the problem of artillery shot verification is the application of acoustic methods based on the registration of sound signals generated during the shot and the subsequent flight of the projectile. Analysis of the temporal characteristics of the ballistic wave makes it possible to obtain information suitable for estimating the coordinates of the projectile impact point and for analyzing firing accuracy, which is consistent with the results of known studies in this field [1].

At the same time, processing of acoustic information is associated with the need to take into account the complex nature of sound wave generation and propagation, the influence of the external environment, as well as the characteristics of specific munitions and firing conditions. This necessitates the use of mathematical modeling for signal processing, estimation of wave arrival times between sensors, and construction of projectile motion models. The use of simplified but informative models in this case allows computational costs to be reduced and ensures the possibility of practical implementation of verification methods in a mode close to real time.

In a more general context, the problem of firing result verification is considered as a component of combat process modeling aimed at increasing the effectiveness of fire actions through rational use of available resources and reduction of decision-making time. Formalized models in this case make it possible to describe the firing process as a sequence of interconnected states and transitions between them, providing a quantitative assessment of firing results, analysis of probabilistic characteristics of target engagement, as well as consideration of random disturbances and uncertainties of external conditions [2].

The solution of such problems is complicated by the fact that the corresponding systems are characterized by a large number of interrelated parameters and cannot be fully investigated within the framework of full-scale experiments. Under these conditions, mathematical modeling plays a key role, making it possible to analyze a wide range of possible operating modes of the system and to evaluate their characteristics under various application conditions [3, 4]. To describe the complex dynamics of such systems, it is expedient to use universal approximation methods and analytical approaches, in particular models based on the solution of systems of differential equations, which make it possible to reconstruct behavioral characteristics even in cases where certain parameters cannot be measured directly [5, 6].

With an increase in the dimensionality of the parameter space, the computational complexity of the corresponding models increases significantly, which leads to the need to combine numerical methods, approximation algorithms, and optimization procedures. The application of such approaches makes it possible to work with

high-dimensional parameter spaces, solve inverse problems, and analyze the sensitivity of results to variations in initial conditions, which is fundamentally important for estimation and prediction problems under uncertainty [7, 8]. At the same time, consideration of local effects and interactions of parameters in time and space creates the basis for constructing generalized models suitable for further analysis and control of system evolution [9].

Under practical conditions, approaches based on large-scale computational experiments followed by the formation of generalized models or data libraries suitable for rapid analysis and interpretation of results prove to be effective. The use of such generalized representations makes it possible to significantly reduce computational costs at the stage of practical application of models and to ensure decision-making in a mode close to real time, which is especially important for tasks of operational verification of firing results [10].

In view of the above, this chapter addresses the problem of increasing the reliability of determining the coordinates of the point of impact of an artillery projectile with the surface by means of a rational selection of acoustic measuring devices for registering the ballistic wave. It is assumed that a sensor configuration will be formed from the available set of measuring devices, taking into account their geometric arrangement, the probability of an operational state, and random measurement errors. Implementation of such an approach creates prerequisites for building an effective sensor system for verification of artillery shots under conditions of a changing environment and random disturbances.

9.2 Features of constructing a sensor system for shot verification in the artillery firing area

For verification of artillery gun shots in the firing area, a sensor system is deployed, the structure of which is shown in **Fig. 9.1**.

In **Fig. 9.1**, the following notations are adopted:

– AU1, AU2, AU3, …, AU_n are artillery units located in the firing area;

– GS1, GS2, GS3, …, GS_n are sensor groups installed on or near the artillery units;

– AS1, AS2, AS3, …, AS_n are acoustic sensors distributed within the artillery firing area;

– u_{GS1}, u_{GS2}, u_{GS3}, …, u_{GSn} are output signals of sensor groups GS1, GS2, GS3, …, GS_n;

– u_{S1}, u_{S2}, u_{S3}, …, u_{Sn} are output signals of acoustic sensors AS1, AS2, AS3, …, AS_n;

– $\mathbf{U}_S$ is vector of signals transmitted from the intermediate equipment to the computing unit;

– $\mathbf{U}_{CB}$ is vector of signals transmitted from the computing unit to the fire control unit;

– $\mathbf{U}_{SC}$ is vector of signals transmitted from the fire control unit to the computing unit.

The sensor groups GS1, GS2, GS3, ..., GS_n include measuring devices intended for determining projectile motion parameters along the flight trajectory as well as parameters of the external environment that affect the firing process. Each group includes instruments for measuring the initial velocity, elevation and firing direction angles, as well as sensors of meteorological characteristics.

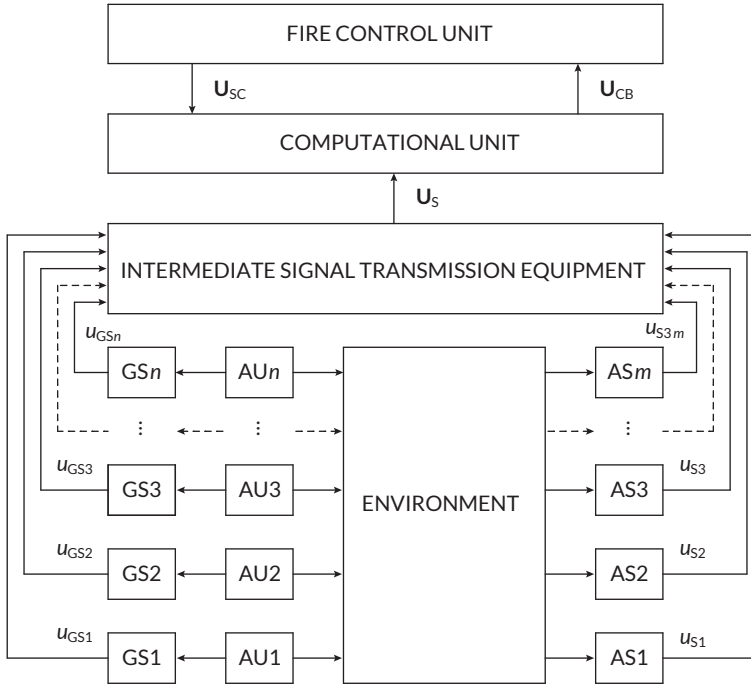

Fig. 9.1 Functional structure of the sensor system for verification of artillery gun shots

Within the firing area, m acoustic sensors register ballistic and muzzle waves generated by artillery shots ($m \gg n$). They are deployed using UAVs or other remote methods, ensuring a uniform spatial distribution and a minimum density that guarantees the required registration accuracy for all n artillery units.

For clarity, **Fig. 9.2** shows a general scheme of acoustic sensor placement in the artillery firing area for the case when the firing direction line forms an angle α

with the *Oy* axis. The following notations are adopted: 1 – artillery unit; 2 – target; 3 – *i*-th acoustic sensor ($I = 1, 2, ..., m$); x_{AU}, y_{AU} are coordinates of the artillery unit; x_t, y_t are coordinates of the target; x_i, y_i are coordinates of the *i*-th acoustic sensor; α is angle between the firing direction line and the *Oy* axis.

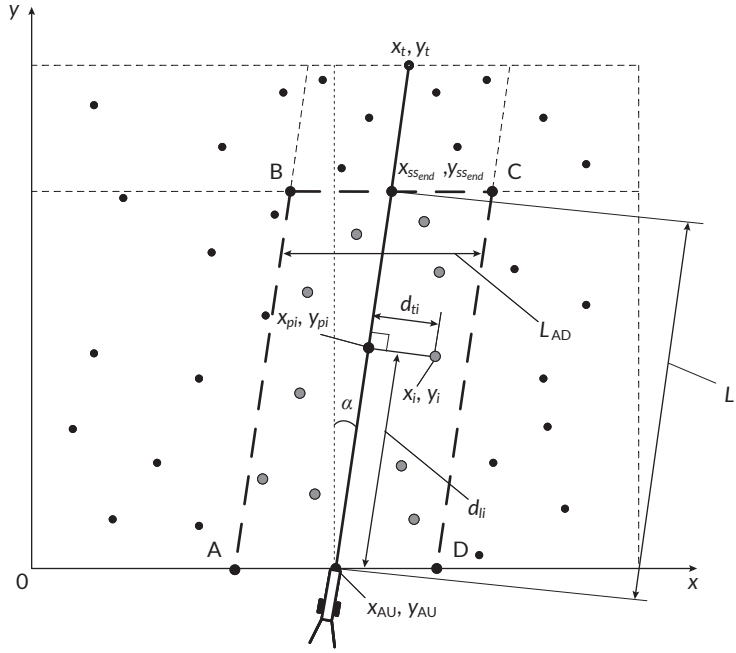

Fig. 9.2 Scheme of acoustic sensor placement in the terrain within the artillery firing area

The accuracy of registering ballistic and muzzle waves depends on the distance between the acoustic sensor and the firing direction line and is determined experimentally. In most practical cases, in order to ensure effective registration of an artillery shot, this distance should not exceed 50 m. Registration of the ballistic wave by acoustic sensors is possible only within the segment of the trajectory where the projectile moves at a supersonic velocity. Under these conditions, the selection of three acoustic sensors for registering shot parameters is carried out from the set of sensors located within parallelogram ABCD, as shown in **Fig. 9.2**.

The following notations are introduced: x_1, y_1, x_2, y_2, x_3, y_3 are the coordinates of the first, second, and third acoustic sensors selected for registering ballistic and

muzzle waves from the set of sensors bounded by parallelogram ABCD; d_1, d_2, d_3 are the distances from the corresponding acoustic sensors to the firing direction line.

In this case, the width of the zone of effective registration of ballistic and muzzle waves by the sensors along AD (**Fig. 9.3**) is 100 m. The length of the ballistic wave action zone AB is preliminarily determined with respect to the specified firing range as the length of the trajectory segment over which the projectile maintains supersonic velocity. The length of this segment is calculated on the basis of mathematical and simulation models of projectile flight [11, 12], developed in accordance with the NATO STANAG 4355 standard.

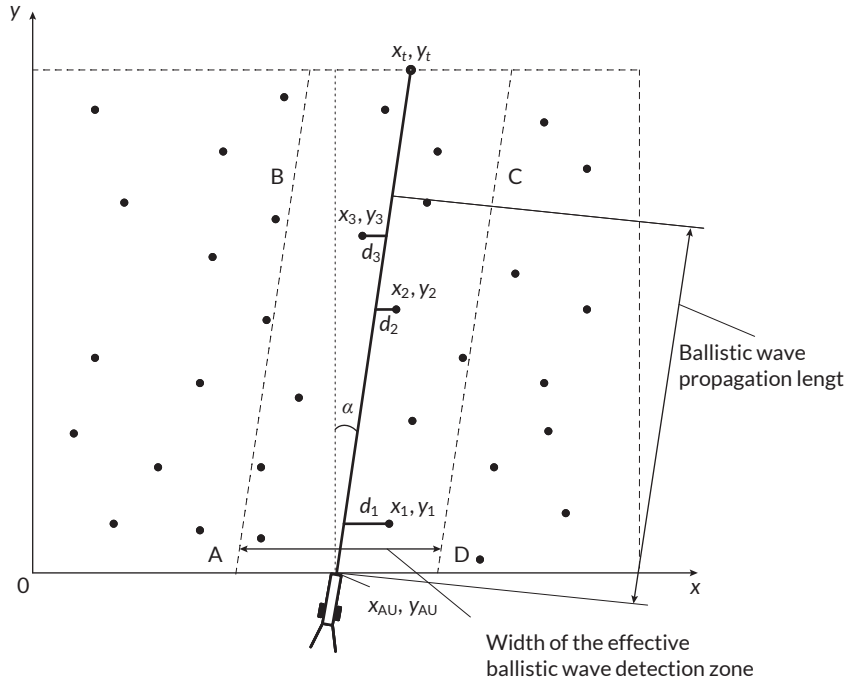

Fig. 9.3 Determination of the sensors closest to the firing direction line

Under the specified configuration, the selection of three acoustic sensors with coordinates x_1, y_1, x_2, y_2, x_3, y_3 from the available set is performed according to the minimum values of distances d_1, d_2, d_3 from the corresponding sensors to the firing direction line.

To reduce the total number of acoustic sensors in the firing area, it is advisable to arrange them in the form of three strips, as shown in **Fig. 9.4**.

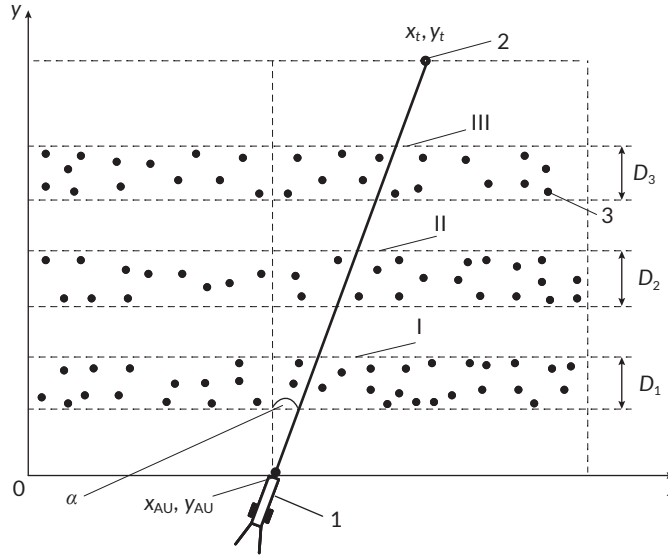

Fig. 9.4 Scheme of acoustic sensor placement in three strips within the artillery firing area

In **Fig. 9.4**, the following notations are adopted: I, II, III are the first, second, and third sensor strips; D_1, D_2, D_3 are the widths of the corresponding strips. The first, second, and third acoustic sensors for registering ballistic and muzzle waves are selected, respectively, from the first, second, and third strips. All three strips must be located within the ballistic wave action zone. Taking into account possible changes in the coordinates of artillery units and targets, the values of D_1, D_2, D_3, as well as the distances between the strips, are determined on the basis of a preliminarily estimated average firing range in the given operational area.

The intermediate equipment intended for transmitting signals from the sensors (vector $\mathbf{U}_S$) to the computing unit includes intermediate nodes and communication channels that form a specialized data transmission network. With a large number of sensors, which may reach several thousand or tens of thousands, direct transmission of signals from the measuring devices to the computing unit becomes significantly complicated. Such a scheme leads to an increase in network complexity, a decrease in its reliability, and, consequently, an increase in the overall system cost.

In order to reduce complexity and increase the reliability of the data transmission network, its structure should be formed according to a hierarchical principle using intermediate information collection nodes. Intermediate nodes of the first hierarchy level perform grouping and preliminary processing of signals from sensors and transmit them to nodes of the second level, and further to the system computing unit. Signal transmission from sensors to network nodes, as well as between individual nodes, is carried out via radio communication, while connections between upper-level nodes and the computing unit may be implemented via wired channels to improve reliability.

The formation of the hierarchical structure of the signal transmission network is carried out as follows. First, a network structure vector S of dimension j_{max} is specified, which corresponds to the total number of hierarchy levels. Each element of the vector S_j ($j = 1, ..., j_{max}$) defines the number of nodes at the j-th hierarchy level. The number of nodes S_j at each level is selected taking into account condition (9.1)

$$S_j \le \text{floor}\left(\frac{S_{j-1}}{2}\right), \tag{9.1}$$

according to which each node must have at least two inputs ($k_j \ge 2$). At the last hierarchy level, the presence of a single main node ($S_{j_{max}} = 1$), directly connected to the computing unit is assumed, while at the penultimate level the number of nodes must be not less than two ($S_{j_{max-1}} \ge 2$).

After determining the number of nodes at each hierarchy level, the number of inputs k_j for the nodes of the corresponding level is calculated on the basis of relation (9.2)

$$k_j = \frac{S_{j-1}}{S_j}. \tag{9.2}$$

If the obtained value of k_j is an integer, all nodes at this level have the same number of inputs. Otherwise, the level contains nodes with a number of inputs equal to the nearest smaller and the nearest larger integers relative to k_j, while the proportion of nodes with the larger number of inputs is determined by the fractional part of the calculated value of k_j.

After determining the number of inputs for the nodes at each hierarchy level, an appropriate hierarchical structure of the sensor signal transmission network is constructed on the basis of the formed vector S. At each j-th level, S_j nodes are created, which are successively interconnected by communication channels from the first level to the final level j_{max}. In this case, nodes of level $j - 1$ are connected exclusively to nodes of level j, taking into account the number of inputs of the latter, and the output

of each node at level (j − 1) may be connected to only one input of a node at level j. After all required connections are established, the construction of the data transmission network structure is considered complete.

For clarity, three variants of signal transmission network structures are presented for the same number of primary sensors $S_0 = 13$. In the structure shown in **Fig. 9.5**, information is transmitted directly from the primary sensors to a single main node connected to the system computing unit.

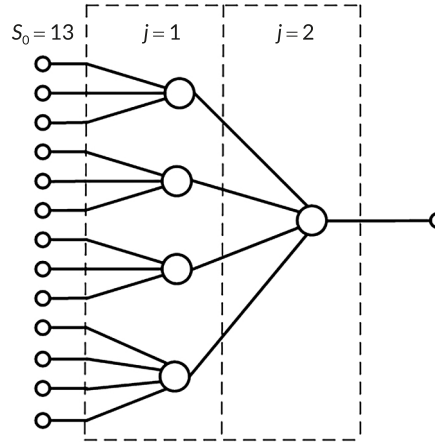

Fig. 9.5 Typical two-level hierarchical structure of sensor signal aggregation

In the limiting case $j_{max} = 1$, the hierarchical structure degenerates into a single-level scheme, where signals from all sensors S_0 are directly transmitted to the main node. As the number of hierarchy levels increases ($j_{max} > 2$), the network structure is expanded in a similar manner by successive grouping of lower-level nodes and connecting them to higher-level nodes.

Thus, the presented scheme reflects a general approach to the formation of hierarchical data transmission structures, within which the specific number of levels is determined by requirements for scalability, transmission delays, and computational load.

For the presented structures, the vectors **S** are defined by expressions (9.3) and (9.4), respectively:

$$\mathbf{S} = \{4,1\}, \tag{9.3}$$

$$\mathbf{S} = \{5,2,1\}. \tag{9.4}$$

Depending on the current fire tasks, the fire control unit transmits to the computing unit the signal vector $\mathbf{U}_{SC}$, which contains the coordinates of the designated targets. Based on the vectors $\mathbf{U}_S$ (from the sensor signal transmission network) and $\mathbf{U}_{SC}$, the computing unit performs verification of artillery shots, taking into account random disturbances, and determines the coordinates of projectile impacts on the surface.

In addition, before each shot, the computing unit identifies three sensors from the available set of measuring devices that are most suitable for registering the ballistic and muzzle waves. The results of these calculations, including the coordinates of projectile impacts and the selected sensors, are transmitted to the fire control unit in the form of the signal vector $\mathbf{U}_{SC}$. The task of selecting the three optimal sensors during artillery shot verification is solved using the method described in the following subsection.

9.3 Method for registering the coordinates of an artillery projectile impact with the surface

The proposed approach makes it possible to determine three acoustic sensors that are the most suitable for registering the ballistic wave during the verification of artillery shots, based on the known current coordinates of the target, the artillery unit, and all functioning acoustic sensors located within the firing area.

The target coordinates are received from the fire control unit in accordance with the assigned fire mission. The current coordinates of the artillery unit and each acoustic sensor are determined using their built-in navigation systems.

At the initial stage, on the basis of the target and artillery unit coordinates, the firing range L_s and the angle α with respect to the *Oy* axis (**Fig. 9.3**) are determined, after which the equation of the firing direction line for the current shot is formed. The values of L_s and α are calculated using relations (9.5) and (9.6), and the equation of the firing direction line in the form of the general equation of a straight line in the plane is written as (9.7) [13–15]:

$$L_s = \sqrt{\left(x_t - x_{\text{AU}}\right)^2 + \left(y_t - y_{\text{AU}}\right)^2}, \tag{9.5}$$

$$\alpha = \arcsin\left(\frac{x_t - x_{\text{AU}}}{L_s}\right), \tag{9.6}$$

$$a_{ls}x + b_{ls}y + c_{ls} = 0, \tag{9.7}$$

where a_{ls}, b_{ls}, c_{ls} are the coefficients of the firing direction line equation.

In this case, the angle α can take values in the range from −90° to 90° and is measured clockwise. The coefficients of the straight-line equation a_{ls}, b_{ls}, c_{ls} are determined using expressions of analytical geometry [13] or on the basis of the least squares method using the known coordinates of the target and the artillery unit [16].

In order to significantly reduce the computational burden when selecting the three most appropriate acoustic sensors, it is expedient at the initial stage to select, from the total number of functioning sensors, only those located within the zone of possible registration of the ballistic and muzzle waves of the current artillery shot. This zone is bounded by parallelogram ABCD (**Fig. 9.3**).

The width AD should be specified depending on the accuracy of registration of ballistic and muzzle waves by acoustic sensors and, as a rule, should not exceed 100 m. The length AB is defined as the length of the projectile flight segment with supersonic velocity (supersonic segment) L_{SS}, which is calculated on the basis of the preliminarily determined firing range L_s using formula (9.5) [11, 12].

To determine the zone of possible registration of ballistic and muzzle waves and for the subsequent selection of sensors located within this zone, it is necessary to determine the coordinates of points A, B, C, and D, as well as the equations of the four straight lines passing through the corresponding pairs of these points.

The coordinates of points A and D are determined on the basis of the current coordinates of the artillery unit AU using expressions (9.8) and (9.9), respectively:

$$x_A = x_{AU} - \frac{L_{AD}}{2}; y_A = y_{AU}, \tag{9.8}$$

$$x_D = x_{AU} + \frac{L_{AD}}{2}; y_D = y_{AU}, \tag{9.9}$$

where L_{AD} is the length of segment AD.

The coordinates of points B and C are determined on the basis of the coordinates of the point on the firing direction line at which the projectile loses its supersonic velocity, using expressions (9.10) and (9.11):

$$x_B = x_{ss_{end}} - \frac{L_{BC}}{2}; y_B = y_{ss_{end}}, \tag{9.10}$$

$$x_C = x_{ss_{end}} + \frac{L_{BC}}{2}; y_C = y_{ss_{end}}, \tag{9.11}$$

where $x_{ss_{end}}$, $y_{ss_{end}}$ are the coordinates of the corresponding point, and $L_{BC} = L_{AD}$.

Thus, the coordinates of the point on the firing direction line at which the projectile loses its supersonic velocity are calculated on the basis of the determined length of the projectile flight segment with supersonic velocity L_{ss}, the angle α, and the current coordinates of the artillery unit using expressions (9.12) and (9.13), respectively:

$$x_{ss_{end}} = x_{AU} + L_{ss} \sin\alpha, \tag{9.12}$$

$$y_{ss_{end}} = y_{AU} + L_{ss} \cos\alpha. \tag{9.13}$$

Next, the equations of the four straight lines passing through the following point pairs are determined: 1) A and B; 2) D and C; 3) A and D; 4) B and C. To simplify the calculations, it is expedient to represent the equations of these lines in the form of straight-line equations with slope coefficients:

$$y = a_{AB}x + b_{AB}, \tag{9.14}$$

$$y = a_{DC}x + b_{DC}, \tag{9.15}$$

$$y = a_{AD}x + b_{AD}, \tag{9.16}$$

$$y = a_{BC}x + b_{BC}, \tag{9.17}$$

where a_{AB}, b_{AB}, a_{DC}, b_{DC}, a_{AD}, b_{AD}, a_{BC}, b_{BC} are the coefficients of the equations of the corresponding straight lines. These coefficients are determined using well-known relations of analytic geometry [13] or by applying the least squares method based on the coordinates of points A, B, C, and D [16].

After that, on the basis of the line equations (9.14)–(9.17) and their determined coefficients, conditions (9.18) are formulated, according to which a sequential verification of all functioning acoustic sensors of the system is carried out using their coordinates. There is:

$$\begin{cases} x_i \geq \dfrac{y_i - b_{AB}}{a_{AB}}; \\ x_i \leq \dfrac{y_i - b_{DC}}{a_{DC}}; \\ y_i \geq a_{AD}x_i + b_{AD}; \\ y_i \leq a_{BC}x_i + b_{BC}. \end{cases} \tag{9.18}$$

If the coordinates of the *i*-th sensor satisfy conditions (9.18), it lies within the zone of possible registration of the ballistic and muzzle waves of an artillery shot and can be selected as one of the three most suitable sensors.

After performing this sorting procedure, all sensors that satisfy conditions (9.18) are numbered and selected for further calculations aimed at determining the three most appropriate measuring devices for registering the ballistic and muzzle waves. Acoustic sensors that do not fall within the region bounded by parallelogram ABCD are not used at subsequent stages of the method.

At the following computational stages of the proposed method, only three sensors are selected from the set of preselected sensors as being the most suitable for registering the ballistic and muzzle waves. To select these three acoustic sensors, all preselected sensors are evaluated according to the following parameters.

The first parameter that significantly affects the suitability of an acoustic sensor for high-quality registration of the ballistic and muzzle waves is its position along the firing direction line. This position is determined by the distance d_l from the artillery unit to the point on the firing direction line that is closest to the given sensor.

For more accurate verification of artillery shots, it is advisable to register the ballistic and muzzle waves over the second half of the projectile flight segment with supersonic velocity and as close as possible to its end [17, 18]. In addition, all three acoustic sensors should be placed uniformly along the firing direction line to ensure reliable registration of the ballistic and muzzle waves at three distinct points. At the same time, the third sensor should not be located too close to the point with coordinates $x_{ss_{end}}$, $y_{ss_{end}}$, at which the projectile loses its supersonic velocity, since the position of this point is determined with a certain error. In such a case, the sensor may be positioned outside the supersonic flight segment of the projectile. Therefore, as optimal distances from the artillery unit to the first, second, and third sensors along the firing direction line, it is reasonable to preliminarily adopt the following values: $d_{l1\text{opt}} = 0.5L_{ss}$; $d_{l2\text{opt}} = 0.7L_{ss}$; $d_{l3\text{opt}} = 0.9L_{ss}$.

Thus, when selecting the most suitable first, second, or third acoustic sensor, it is necessary, for each *i*-th sensor located within the zone of possible registration of the ballistic and muzzle waves (ABCD), to calculate the parameter d_{li} and compare its value with the corresponding predefined optimal value $d_{l1\text{opt}}$, $d_{l2\text{opt}}$ or $d_{l3\text{opt}}$.

At the same time, the distance d_{li} for the *i*-th acoustic sensor is calculated on the basis of the coordinates of this sensor and the obtained general equation of the firing direction line (9.7) as follows. First, the coordinates x_{pi}, y_{pi} of the point on the firing direction line that is closest to the *i*-th sensor are determined using expressions (9.19) and (9.20) [13–15]:

$$x_{pi} = \frac{b_{ls}\left(b_{ls}x_i - a_{ls}y_i\right) - a_{ls}c_{ls}}{a_{ls}^2 + b_{ls}^2}, \tag{9.19}$$

$$y_{pi} = \frac{a_{ls}\left(a_{ls}y_i - b_{ls}x_i\right) - b_{ls}c_{ls}}{a_{ls}^2 + b_{ls}^2}. \tag{9.20}$$

Subsequently, using the obtained coordinates x_{pi}, y_{pi} and the known coordinates of the artillery unit x_{AU}, y_{AU}, the distance d_{li} is directly calculated using formula (9.21)

$$d_{li} = \sqrt{\left(x_{pi} - x_{AU}\right)^2 + \left(y_{pi} - y_{AU}\right)^2}. \tag{9.21}$$

Another equally important parameter used to select the most suitable acoustic sensors is the distance d_t from a sensor to the nearest point on the firing direction line, which is defined as the length of the perpendicular drawn from the sensor location to the firing direction line. The smaller the value of this distance, the higher the accuracy of registering the ballistic and muzzle waves of the shot, and, accordingly, the more suitable the sensor is considered. Therefore, the optimal configuration for all acoustic sensors (first, second, and third) used for shot verification is their placement directly on the firing direction line ($d_{t1opt} = d_{t2opt} = d_{t3opt} = 0$).

The value of this distance d_{ti} for the i-th acoustic sensor can be calculated based on the coordinates of the given sensor x_i, y_i and the obtained general equation of the firing direction line (9.7) using expression (9.22) [13–15]

$$d_{ti} = \frac{\left|a_{ls}x_i + b_{ls}y_i + c_{ls}\right|}{\sqrt{a_{ls}^2 + b_{ls}^2}}. \tag{9.22}$$

The third parameter that must also be taken into account when selecting the three most suitable acoustic sensors is the value of their probability of failure-free operation $P(t)$. Even if the i-th sensor has a sufficiently favorable location (in terms of the parameters d_{li} and d_{ti}) within zone ABCD, but its probability of failure-free operation is low, selecting it for registering ballistic and muzzle waves would be impractical. This is because there is a relatively high risk of sensor malfunction and, consequently, failure to complete the entire verification procedure for the current shot.

In practice, the reliability of any element is determined by two components: the probability of failure-free operation under random failures $P(t)$ and the probability of failures due to wear $P_w(t)$. Random failures are described by an exponential law, according to which the reliability, or probability of failure-free operation $P(t)$, is determined by the expression

$$P(t)=e^{-\lambda t}, \tag{9.23}$$

where λ is the intensity (rate) of random failures.

During the period of normal equipment operation, the failure intensity for the exponential law is a constant value. When wear begins, the failure intensity starts to increase, and in addition to random failures, wear-out failures also occur. These wear-related failures are usually described by a normal distribution

$$P_w(t)=\frac{1}{\sigma\sqrt{2\pi}}\int_t^{\infty} e^{-(t-M)^2/2\sigma^2}\,\mathrm{d}t, \tag{9.24}$$

where M is the mean value of the element lifetime taking wear into account, and σ is the standard deviation of the lifetime from its mean value, which is defined as

$$\sigma=\sqrt{\frac{\sum(t-M)^2}{N}}, \tag{9.25}$$

where N is the number of failures over the time interval t.

Moreover, the combined probability of failure-free operation of an element, taking into account both sudden failures and wear-out failures, over the period from $t = 0$ (when the element is new) to time t, is calculated as

$$P(t)=e^{-\lambda t}P_w(t). \tag{9.26}$$

Thus, in the process of selecting the most suitable sensors for recording the ballistic and muzzle waves of a shot, the probability of failure-free operation $P_i(t)$ for each i-th acoustic sensor is determined using expression (9.26), depending on the operating time t and based on the known values λ_i, M_i, and N_i.

For a comprehensive assessment of the suitability of acoustic sensors for recording ballistic and muzzle waves, it is expedient to formulate an integrated dimensionless suitability criterion J, which properly accounts for all three considered sensor parameters (d_{li}, d_{ti}, and P_i). Accordingly, the suitability criterion J_i for each i-th sensor is defined as

$$J_i=f\left(d_{li},d_{ti},P_i\right). \tag{9.27}$$

Since the considered parameters d_{li}, d_{ti}, and P_i used to assess sensor suitability differ in their physical nature, vary significantly in absolute magnitude, and may be

computed with certain uncertainties, formalizing their interrelation within a single criterion based on strict mathematical dependencies is a rather challenging task. Therefore, to calculate the current value of the criterion J_i with proper consideration of each of the above-mentioned sensor parameters (d_{li}, d_{ti}, and P_i), it is expedient to employ the mathematical apparatus of fuzzy logic theory. This approach enables effective aggregation of expert knowledge and experimental data, approximation of arbitrary nonlinear multidimensional relationships, and construction of linguistic models of complex objects and processes [19–21].

For convenience of calculations, it is reasonable to assume that the acoustic sensor suitability criterion J varies within the range from 0 to 1. The closer the calculated value of the criterion J_i is to 1, the more suitable the i-th sensor is considered.

Since three most suitable sensors must be selected to record the ballistic and muzzle waves of each shot, the criterion J_i for each i-th sensor should be calculated three times (J_{i1}, J_{i2}, J_{i3}), taking into account the role in which the sensor is assumed to be used, namely as the first, second, or third sensor. Subsequently, the maximum of the obtained values (J_{i1}, J_{i2}, or J_{i3}) is used to determine the final suitability of the given sensor J_{if}, with its assignment to a specific role (first, second, or third sensor). Thus,

$$J_{if} = \max\{J_{i1}, J_{i2}, J_{i3}\}. \tag{9.28}$$

After that, based on the value of the final suitability J_{if}, the given i-th acoustic sensor is assigned to one of three groups: potential first, second, or third sensors. For example, for the i-th acoustic sensor the following suitability criterion values were calculated for its use as the first, second, and third sensor: $J_{i1} = 0.791$; $J_{i2} = 0.215$; $J_{i3} = 0.42$. Since the value J_{i1} is the largest among those obtained, this sensor is preliminarily assigned to the group of potential first sensors with the corresponding suitability $J_{if} = 0.791$.

Thus, for all sensors located within the possible ballistic and muzzle wave registration zone ABCD, the suitability criterion J is calculated three times, taking into account their possible use as the first, second, or third sensor. The largest of the obtained values determines the final suitability J_{if}, after which the sensors are distributed among the three corresponding groups.

At the final stage of the method, in the established groups of potential first, second, and third sensors, the most suitable first, second, and third sensors are selected according to the maximum suitability values J_{best1}, J_{best2} and J_{best3}. These acoustic sensors are the three sensors that will be used to register the ballistic and muzzle waves of the current artillery shot.

Based on the above, the steps of the method for determining three acoustic sensors for registering the ballistic and muzzle waves of an artillery shot are presented below:

Step 1. Method initialization. At this stage, all initial data required for the verification of artillery shots are obtained. The number and coordinates of all operational acoustic sensors within the artillery firing zone are determined, and the values of parameters used in subsequent calculations are fixed: the width of the possible ballistic and muzzle wave registration zone L_{AD}; the optimal distances from the artillery unit to the first, second, and third sensors along the firing direction line d_{l1opt}, d_{l2opt}, d_{l3opt}; and the current values of the sensors' probability of failure-free operation $P(t)$.

The width of the zone AD, L_{AD}, should be set according to the accuracy of wave registration (in most practical cases $L_{AD} = 100$ m). The optimal distances d_{l1opt}, d_{l2opt}, d_{l3opt} are specified as functions of the length of the supersonic flight segment. The values of $P(t)$ are determined based on their known parameters λ, M, N and the operating time t. Before starting the calculations, the current coordinates of the target x_t, y_t and the artillery unit x_{AU}, y_{AU} are also recorded.

Step 2. Performing initial calculations. Based on the coordinates of the target x_t, y_t and the artillery unit x_{AU}, y_{AU}, the firing range L_s, the angle α relative to the Oy axis, and the length of the supersonic flight segment L_{SS} are determined. At the same time, the equation of the firing direction line for the current shot is formed, and its coefficients a_{ls}, b_{ls}, c_{ls} are calculated in accordance with (9.5)–(9.7).

Step 3. Determination of the possible registration zone of the ballistic and muzzle waves of the current shot ABCD. At this stage, using expressions (9.8)–(9.13), the coordinates of points A, B, C, D, as well as the point $x_{ss_{end}}$, $y_{ss_{end}}$ at which the projectile loses supersonic velocity, are determined. Then, the equations of the four boundary lines of zone ABCD are constructed according to (9.14)–(9.17).

Step 4. Sorting of sensors within the ABCD zone. From the total set of operational sensors, only those which coordinates satisfy the conditions (9.18) are selected. The selected sensors are numbered and used in subsequent calculations, where as all other sensors are not used in the following stages of the method.

Step 5. Calculation of the parameter d_{li}. For each i-th sensor located within the ABCD zone, the distance d_{li} from the artillery unit to the point on the firing direction line closest to the sensor is calculated using formula (9.21), with the coordinates x_{pi}, y_{pi} determined according to expressions (9.19) and (9.20).

Step 6. Calculation of the parameter d_{ti}. For each selected sensor, the distance d_t from the sensor to the firing direction line is determined using formula (9.22).

Step 7. Determination of the parameter $P_i(t)$. For each i-th sensor within the ABCD zone, the probability of failure-free operation $P_i(t)$ is calculated according to expression (9.26).

Step 8. Calculation of the comprehensive suitability criterion J_i. Based on the parameters d_{li}, d_{ti}, and $P_i(t)$ for each sensor, the criterion J_i is computed three times (J_{i1}, J_{i2}, J_{i3}) according to expression (9.27), taking into account the potential use of the sensor as the first, second, or third. The calculation is performed using the previously developed fuzzy logic model.

Step 9. Assignment of sensors to groups. For each *i*-th sensor, the final suitability J_{if} is determined according to expression (9.28), after which all sensors are classified into three groups of potential first, second, and third sensors.

Step 10. Selection of the best first, second, and third sensors. Within each of the three formed groups, one sensor with the maximum suitability values J_{best1}, J_{best2}, J_{best3} is selected. The selected sensors are used to register the ballistic and muzzle waves of the current artillery shot.

After completion of Step 10, the search for the optimal acoustic sensors is considered complete, and the selected three sensors can be used to verify the current artillery shot and to register the coordinates of the projectile impact point.

9.4 Development of a fuzzy model for calculating the suitability criterion of acoustic sensors for registration of ballistic and muzzle waves of a shot

According to the fuzzy approximation theorem [22], any mathematical relationship can be approximated by a system based on fuzzy logic. This makes it possible to represent complex "input–output" relationships in the form of a set of natural-language rules of the type "IF ..., THEN ...", formalized using the theory of fuzzy sets, without the need to employ complex analytical models, in particular differential and integral equations [19]. Modern fuzzy models, which are characterized by interpretability and logical transparency, can be constructed on the basis of various fuzzy inference mechanisms, enabling effective use of expert knowledge as well as learning based on experimental data sets and objective functions similar to those used in neural networks [20, 21]. These features make fuzzy models and systems flexible, universal, and promising for solving problems related to modeling complex objects and processes.

For the simultaneous calculation of three values of the composite suitability criterion J_{i1}, J_{i2}, and J_{i3} for each *i*-th acoustic sensor, taking into account its possible use as the first, second, or third sensor, a fuzzy model is proposed, which should have the structure shown in **Fig. 9.6**.

In **Fig. 9.6**, the following notations are used: FM denotes the fuzzy model for calculating the suitability criterion; FB is the fuzzification block; FIL is the fuzzy logical

inference block; DB is the defuzzification block; RB is the rule base; K_{d1}, K_{d2}, K_P are normalization coefficients used to convert the input variables of the model d_{li}, d_{ti}, and P_i into relative units with respect to their maximum values; d^*_{li}, d^*_{ti} and P^*_i are the normalized values of the corresponding input variables of the fuzzy model.

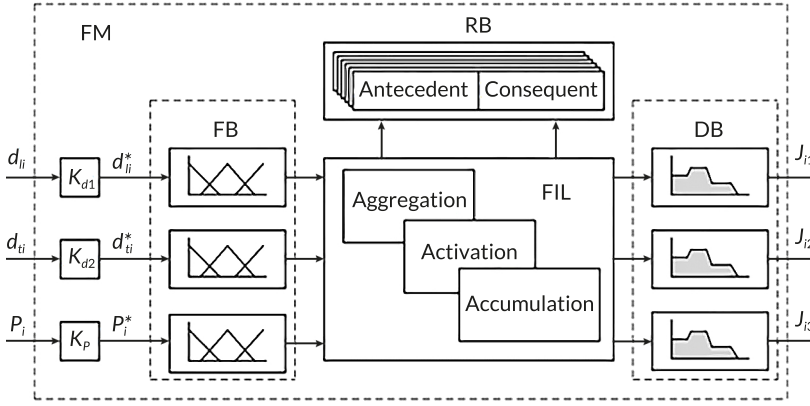

Fig. 9.6 Structure of the fuzzy model for calculating the values of the acoustic sensor suitability criterion

As shown in **Fig. 9.6**, the proposed model has three output variables (J_{i1}, J_{i2}, J_{i3}), each of which represents the suitability of the *i*-th acoustic sensor as the first, second, or third sensor, respectively, depending on the input parameters d_{li}, d_{ti}, and P_i in accordance with the developed rule base.

In this case, for the fuzzy model with the proposed structure (**Fig. 9.6**), it is advisable to choose the Mamdani type of fuzzy logical inference [23], which provides sufficient efficiency with a relatively simple synthesis and tuning procedure [21].

The fuzzification block determines the degrees of membership of the numerical values of the input variables d_{li}, d_{ti}, and P_i to the corresponding fuzzy linguistic terms of the fuzzy model [20]. The fuzzy logical inference block implements aggregation, activation, and accumulation operations based on the rule base. The defuzzification block converts the resulting fuzzy set into a crisp numerical value of the output variable J_i [23].

Next, the main procedures for synthesizing the fuzzy logical model for calculating the suitability criterion of acoustic sensors are considered in detail.

The normalization coefficients of the model K_{d1} and K_{d2} are determined by expressions (9.29) and (9.30):

$$K_{d1} = \frac{1}{L_{ss}}, \tag{9.29}$$

$$K_{d2} = \frac{2}{L_{AD}}. \tag{9.30}$$

This makes it possible to convert the current values of the input variables d_{li} and d_{ti} into relative units with respect to their maximum values ($d_{limax} = L_{ss}$; $d_{timax} = L_{AD}/2$).

Since the probability of failure-free operation P_i for each i-th acoustic sensor varies within the range [0, 1], and the operating range of this variable is assumed to be the interval [0.75, 1], the normalization coefficient K_P in this case is equal to 1. Sensors with a current value of $P_i(t) < 0.75$ are not admitted to further evaluation.

For the input (d_{li}, d_{ti}, P_i) and output (J_{i1}, J_{i2}, J_{i3}) variables of the fuzzy model, sets of linguistic terms have been defined, which are presented in **Table 9.1**.

The triangular membership function of a linguistic term, illustrated here for the variable d_{li}, is defined by expression (9.31):

$$\mu(d_{lj}) = \begin{cases} 0, & \text{when } d_{li} \le a; \\ \dfrac{d_{li} - a}{b - a}, & \text{when } a < d_{li} \le b; \\ \dfrac{c - d_{li}}{c - b}, & \text{when } b < d_{li} < c; \\ 0, & \text{when } d_{li} \ge c, \end{cases} \tag{9.31}$$

where a, b, c are adjustable parameters of the function, subject to the condition $a \le b \le c$. The graphical representation of the linguistic terms for the input and output variables of the fuzzy model with the specified parameters is shown in **Fig. 9.7**.

Table 9.1 Linguistic terms of the fuzzy model for calculating the values of the suitability criterion

Fuzzy model variables	Number of linguistic terms	Selected linguistic terms	Type of membership functions of linguistic terms
d_{li}	5	VS – very short; S – short; M – medium; LN – long; VLN – very long	triangular
d_{ti}	3	S – short; M – medium; LN – long	triangular
P_i	3	L – low; A – average; H – high	triangular
J_{i1}, J_{i2}, J_{i3}	7	VL – very low; L – low; BA – below average; A – average; AA – above average; H – high; VH – very high	triangular

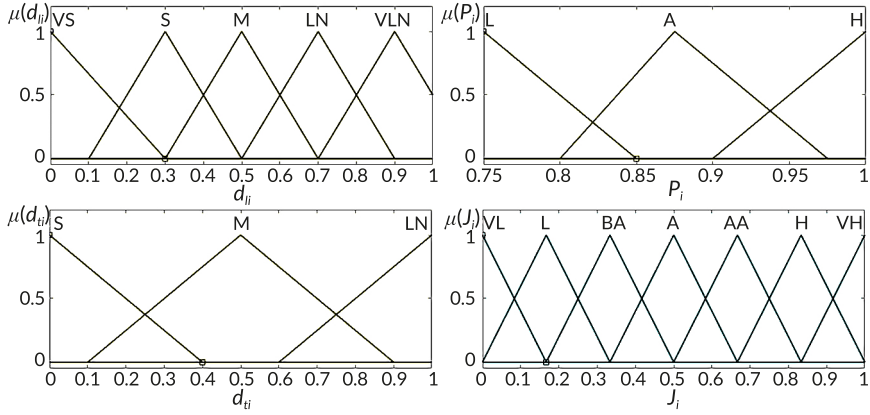

Fig. 9.7 Linguistic terms (with specified parameters) for the input and output variables of the fuzzy model

As can be seen from **Table 9.1** and **Fig. 9.7**, the same sets of linguistic terms are used for the three output variables J_{i1}, J_{i2} and J_{i3}.

The rules of the proposed fuzzy model for calculating the acoustic sensors' suitability criterion are formulated as follows:

$$\begin{aligned}&\text{IF "}d_{li}=LT_{dl}\text{" AND "}d_{ti}=LT_{dt}\text{" AND "}P_i=LT_P\text{"}\\&\text{THEN "}J_{i1}=LT_{J1}\text{" AND "}J_{i2}=LT_{J2}\text{" AND "}J_{i3}=LT_{J3}\text{",}\end{aligned}\tag{9.32}$$

where LT_{dl}, LT_{dt}, LT_P, LT_{J1}, LT_{J2}, LT_{J3} are specific linguistic terms of the input and output variables.

For example, the first rule of RB is expressed as:

$$\begin{aligned}&\text{IF "}d_{li}=\text{VS"}\text{ AND "}d_{ti}=\text{S"}\text{ AND "}P_i=\text{L"}\\&\text{THEN "}J_{i1}=\text{VL"}\text{ AND "}J_{i2}=\text{VL"}\text{ AND "}J_{i3}=\text{VL".}\end{aligned}\tag{9.33}$$

The total number of rules in the rule base is determined by the number of all possible combinations of the linguistic terms of the input variables d_{li}, d_{ti}, and P_i, which equals $5 \cdot 3 \cdot 3 = 45$.

In the proposed fuzzy model, the aggregation and activation procedures are performed using the "min" operation [19]. After these operations, during the accumulation stage, the truncated membership functions are combined to obtain the final fuzzy subset of the output variable. This procedure uses the "max" operation.

The final stage of the calculations is defuzzification, which involves converting the membership function of the output linguistic variable into its precise (numerical) value. In this case, the center of gravity method [20] is chosen as the defuzzification technique for the fuzzy model.

To illustrate the nonlinear relationships realized by the developed fuzzy model, the corresponding characteristic surfaces are shown in **Fig. 9.8**. In particular, **Fig. 9.8** shows the dependencies of the acoustic sensor suitability criterion J_i on the model input variables d_{li} and d_{ti} at a fixed failure-free operation probability $P_i = 0.95$. The resulting surfaces reflect the coordinated influence of the geometric parameters of sensor placement on their suitability as the first, second, or third sensors in the system.

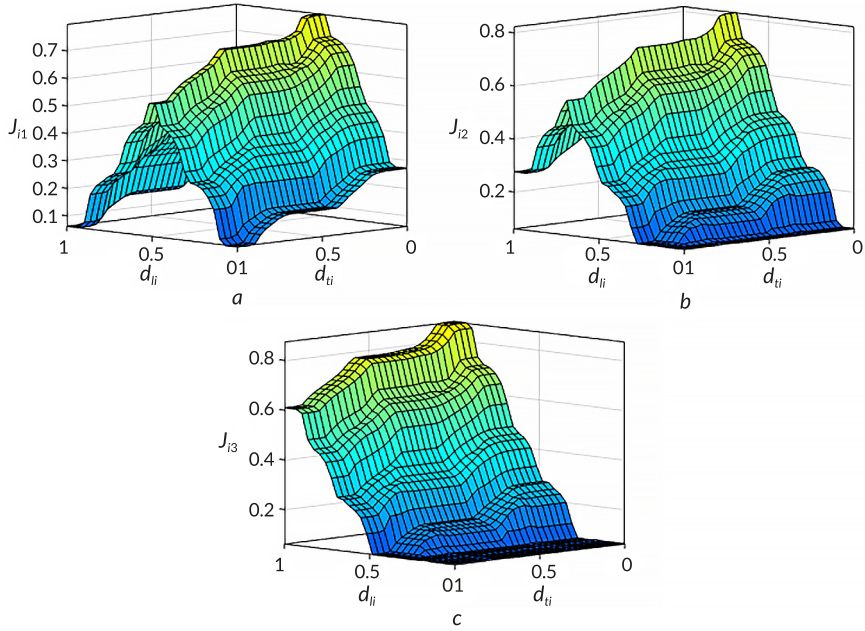

Fig. 9.8 FM characteristic surfaces: *a* – $J_{i1} = f(d_{li}, d_{ti})$; *b* – $J_{i2} = f(d_{li}, d_{ti})$; *c* – $J_{i3} = f(d_{li}, d_{ti})$

Similar characteristic surfaces were also obtained for the pairs of input variables (d_{ti}, P_i) and (P_i, d_{li}) at fixed values of the third variable. In all considered cases, the coordinated nature of the changes in the suitability criterion values is preserved, which confirms the correctness of the formulated rule base and the adequacy of the constructed fuzzy model.

To validate the correct functioning of the proposed fuzzy model, **Table 9.2** presents the results of calculating the suitability criterion of acoustic sensors depending on different values of the input variables d_{li}, d_{ti}, and P_i.

As can be seen from **Table 9.2**, the developed fuzzy model correctly determines the suitability of acoustic sensors as the first, second, and third sensors (J_{i1}, J_{i2}, J_{i3}) depending on the current values of the input variables d_{li}, d_{ti}, and P_i. In the first three rows of **Table 9.2**, the values of d_{li} in relative units are close to the optimal distance from the first sensor to the artillery unit along the firing line ($d_{l1\text{opt}} = 0.5L_{ss}$). Therefore, in these rows, the highest suitability value corresponds to J_{i1}. In turn, in rows 4–6, the highest suitability value corresponds to J_{i2}, as the respective d_{li} values are closest to the optimal distance for the second sensor, $d_{l2\text{opt}} = 0.7L_{ss}$. A similar dependence is observed in rows 7–9 for the third sensor.

Table 9.2 Results of calculating the suitability criterion values of acoustic sensors based on the proposed fuzzy logic model

No.	Input variables			Output variables		
	d_{li}	d_{ti}	P_i	J_{i1}	J_{i2}	J_{i3}
1	0.5	0.5	0.875	0.667	0.333	0.0523
2	0.54	0.133	0.91	0.725	0.591	0.301
3	0.48	0.32	0.86	0.651	0.353	0.0608
4	0.7	0.04	0.93	0.568	0.844	0.568
5	0.71	0.6	0.82	0.237	0.404	0.288
6	0.67	0.1	0.79	0.165	0.296	0.0593
7	0.9	0.03	0.915	0.166	0.536	0.836
8	0.92	0.43	0.95	0.159	0.443	0.776
9	0.86	0.21	0.89	0.274	0.546	0.65
10	0.05	0.98	0.76	0.054	0.054	0.054

The suitability of a given sensor is also significantly influenced by the parameters d_{ti} and P_i, which is reflected in the corresponding changes in the values of J_{i1}, J_{i2}, and J_{i3} in rows 1–9. Moreover, to fully verify the functionality of the developed fuzzy model, the tenth row of **Table 9.2** contains input variable values that are unacceptable for the first, second, and third sensors of the system. In this case, the suitability values J_{i1}, J_{i2}, and J_{i3} calculated by the model are very low, indicating that the corresponding sensors are unsuitable for performing the artillery shot verification process. This also confirms the correct functioning of the developed fuzzy model.

9.5 Conclusions

This chapter has examined an approach for selecting acoustic sensors to register the ballistic and muzzle waves of an artillery shot under conditions of random disturbances. The proposed method is aimed at improving the reliability of acoustic information used in subsequent stages of artillery shot verification and in determining the coordinates of the projectile impact point.

It has been shown that the sensor selection problem is best considered as a multi-criteria task, taking into account the spatial arrangement of measurement points relative to the firing direction line, measurement errors, and the probability of their operational status. To formalize this problem, a fuzzy logic model is employed, which allows for a coordinated consideration of these factors and provides an integrated assessment of the suitability of each sensor.

Computational experiments conducted on two artillery shot examples with different parameters confirmed the effectiveness of the proposed approach. In both cases, three sensors were selected from the available sets of acoustic sensors, providing the most favorable conditions for accurately registering the ballistic and muzzle waves of the current shot. The resulting sensor configurations demonstrate consistency with the physical characteristics of acoustic wave propagation and the geometry of the firing.

Thus, the results presented in this chapter indicate the feasibility of applying the proposed method to form an optimal subsystem of acoustic measurements. This provides a basis for improving the accuracy and robustness of subsequent artillery shot verification procedures under random disturbances and can be used as a component of the corresponding methods and models discussed in the following chapters of the monograph.

Conflict of interest

The authors declare that they have no conflict of interest in relation to this research, whether financial, personal, authorship or otherwise, that could affect the research and its results presented in this paper.

Use of artificial intelligence statement

The authors confirm that they did not use artificial intelligence technologies when creating the current work.

Authors' contributions

Volodymyr Demydenko: Conceptualization, Methodology, Development of sensor selection framework, Writing – original draft.

Yevhenii Dobrynin: Data acquisition, Processing of acoustic signals, Validation of results.

Maksym Maksymov: Computational modeling, Analysis of sensor configurations, Algorithm implementation.

Ruslan Riaboshapka: Visualization of results, Technical support of field experiments, Writing – review & editing.

References

1. Dobrynin, Y., Volkov, V., Maksymov, M., Boltenkov, V. (2020). Development of physical models for the formation of acoustic waves at artillery shots and study of the possibility of separate registration of waves of various types. Eastern-European Journal of Enterprise Technologies, 4 (5 (106)), 6–15. https://doi.org/10.15587/1729-4061.2020.209847
2. Boltenkov, V., Brunetkin, O., Dobrynin, Y., Maksymova, O., Kuzmenko, V., Gultsov, P. et al. (2021). Devising a method for improving the efficiency of artillery shooting based on the Markov model. Eastern-European Journal of Enterprise Technologies, 6 (3 (114)), 6–17. https://doi.org/10.15587/1729-4061.2021.245854
3. Maksymov, M. V., Brunetkin, O. I., Beglov, K. V., Alyokhina, S. V., Butenko, O. V. (2022). Automatic Control for the Slow Pyrolysis of Organic Materials with Variable Composition. Advanced Control Systemss: Theory and Applications. Series in Automation, Control and Robotics. River Publishers, 397–434. https://doi.org/10.1201/9781003337010-16
4. Brunetkin, O. I., Beglov, K. V., Maksymov, M. M., Ulytska, O. O. (2021). Model and method of controlled pyrolysis of organic sub-stances of variable composition. Problems of Control and Informatics, 66 (1), 134–146. https://doi.org/10.34229/1028-0979-2021-1-12
5. Brunetkin, O., Beglov, K., Brunetkin, V., Maksymov, O., Maksymova, O., Havaliukh, O., Demydenko, V. (2020). Construction of a method for representing an approximation model of an object as a set of linear differential models. Eastern-European Journal of Enterprise Technologies, 6 (2 (108)), 66–73. https://doi.org/10.15587/1729-4061.2020.220326

6. Dobrynin, Y., Brunetkin, O., Maksymov, M., Maksymov, O. (2020). Constructing a method for solving the riccati equations to describe objects parameters in an analytical form. Eastern-European Journal of Enterprise Technologies, 3 (4 (105)), 20–26. https://doi.org/10.15587/1729-4061.2020.205107
7. Brunetkin, O., Dobrynin, Y., Maksymenko, A., Maksymova, O., Alyokhina, S. (2020). Inverse problem of the composition determination of combustion products for gaseous hydrocarbon fuel. Computational Thermal Sciences: An International Journal, 12 (6), 477–489. https://doi.org/10.1615/computthermalscien.2020034878
8. Brunetkin, O., Sidelnykov, O., Maksymov, M., Dobrynin, Y. (2025). Improving the model for determining the composition of gunpowder gases during thermal destruction of gunpowder in a limited volume space. Eastern-European Journal of Enterprise Technologies, 3 (6 (135)), 35–45. https://doi.org/10.15587/1729-4061.2025.330654
9. Brunetkin, O., Maksymov, M., Brunetkin, V., Maksymov, O., Dobrynin, Y., Kuzmenko, V., Gultsov, P. (2021). Development of the model and the method for determining the influence of the temperature of gunpowder gases in the gun barrel for explaining visualize of free carbon at shot. Eastern-European Journal of Enterprise Technologies, 4 (1 (112)), 41–53. https://doi.org/10.15587/1729-4061.2021.239150
10. Brunetkin, O., Maksymov, M., Dobrynin, Y., Demydenko, V., Sidelnykov, O. (2024). Development of a process model for d etermining the composition and energy characteristics of a pyrotechnic mixture using the library method. EUREKA: Physics and Engineering, 5, 99–112. https://doi.org/10.21303/2461-4262.2024.003453
11. STANAG 4355 (2022). The Modified Point Mass and five degrees of freedom trajectory models – AOP-4355 EDITION A. Washington: United States Department of Defense. Available at: https://www.scribd.com/document/492052990/STANAG-4355-The-modified-point-mass-and-five-degrees-of-freedom-trajectory-models-Edition-3
12. Aldoegre, M. (2019). Comparison between trajectory models for firing table application. North-West University. Available at: https://repository.nwu.ac.za/items/cad7cd66-e45d-4da8-aa79-1723e382a549
13. Hrinov, B. V., Kyrychenko, I. K. (2008). Analitichna heometriya. Kharkiv: Himnaziya, 340.
14. Kadilnikov, T. M., Kochetkova, I. B., Sushko, L. F., Bilova, O. V. (2012). Analitichna heometriya u prostori. Dnipropetrovsk: NMETAU, 48.
15. Bondarenko, N. V., Otrashevska, V. V. (2022). Analitichna heometriya. Kyiv: KNUBA, 84.

16. Kartashov, M. V. (2008). Imovirnist, protsesy, statystyka. Kyiv: Vydavnychopolihrafichnyi tsentr "Kyivskyi universytet", 494.
17. Maksymov, M. V., Boltenkov, V. O., Gultsov, P. S., Maksymov, O. M. (2023). Verification of artillery fire under the influence of random disturbances for the computer game ARMA 3. Applied Aspects of Information Technology, 6 (4), 362–375. https://doi.org/10.15276/aait.06.2023.24
18. Tarakhtii, O. S., Gultsov, P. S., Maksymov, O. M. (2023). Pat. No. 127193. Sposib vyznachennia koordynaty zustrichi artyleriiskoho snariada z poverkhneiu. Declareted: 28.04.2021; published: 31.05.2023, Bul. No. 22.
19. Hampel, R., Wagenknecht, M., Chaker, N. (2000). Fuzzy control: Theory and practice. New York: Physika-Verlag, Heidelberg, 410. https://doi.org/10.1007/978-3-7908-1841-3
20. Zadeh, L. A., Abbasov, A. M., Yager, R. R., Shahbazova, S. N., Reformat, M. Z. (Eds.) (2014). Recent Developments and New Directions in Soft Computing. Studies in Fuzziness and Soft Computing. Cham: Springer International Publishing. https://doi.org/10.1007/978-3-319-06323-2
21. Jamshidi, M., Kreinovich, V., Kacprzyk, J. (Eds.) (2013). Advance trends in soft computing. Cham: Springer-Verlag, 468. https://doi.org/10.1007/978-3-319-03674-8
22. Kosko, B. (1994). Fuzzy systems as universal approximators. IEEE Transactions on Computers, 43 (11), 1329–1333. https://doi.org/10.1109/12.324566
23. Mamdani, E. H., Assilian, S. (1975). An experiment in linguistic synthesis with a fuzzy logic controller. International Journal of Man-Machine Studies, 7 (1), 1–13. https://doi.org/10.1016/s0020-7373(75)80002-2

Scientific Route OÜ®

We invite you to explore our website.

www.route.ee